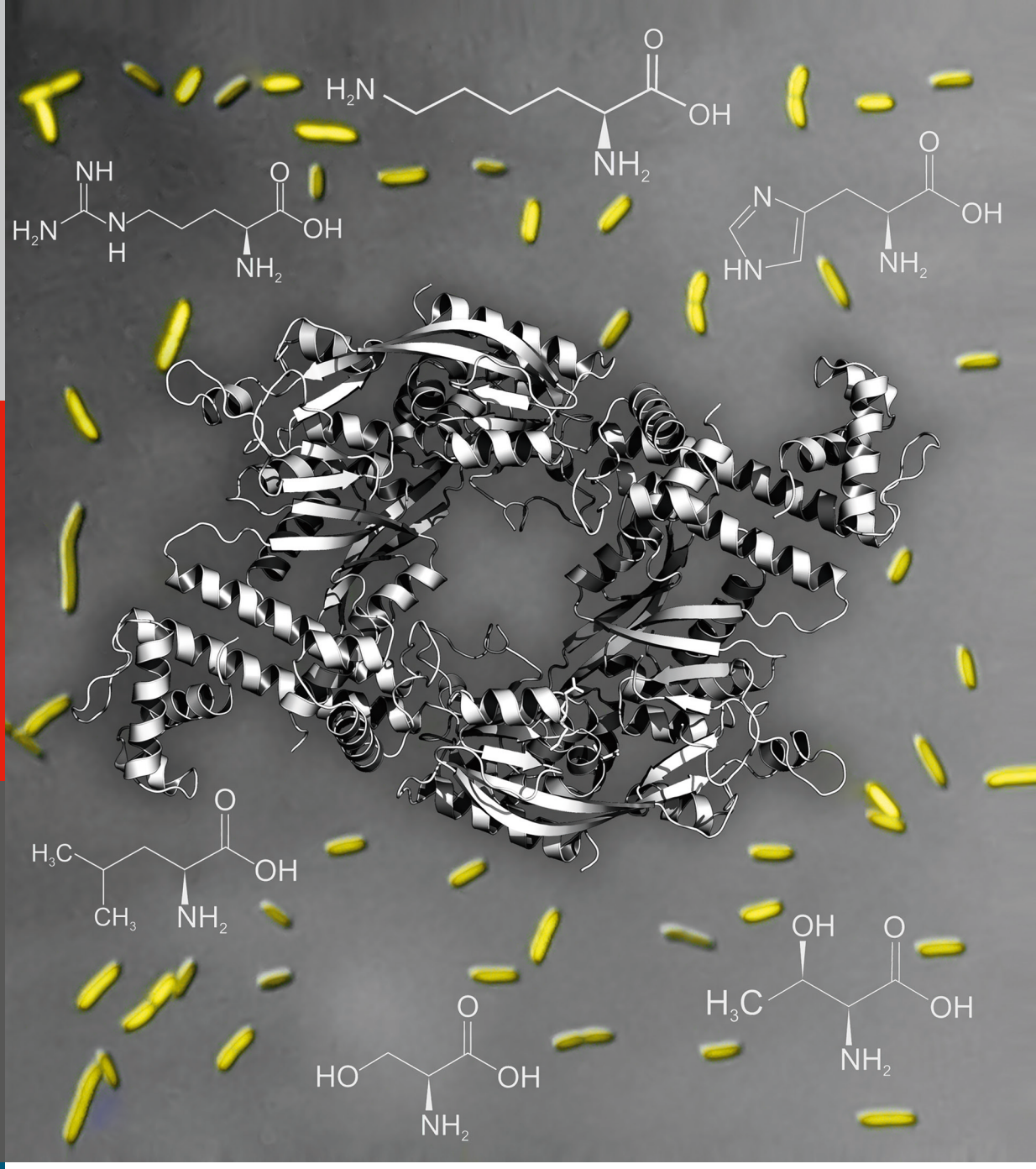

Design and application of metabolite sensors for the FACS-based isolation of feedback-resistant enzyme variants

Georg Schendzielorz

JÜLICH
FORSCHUNGSZENTRUM

Member of the Helmholtz Association

Schriften des Forschungszentrums Jülich
Reihe Gesundheit / Health Band / Volume 71

Forschungszentrum Jülich GmbH
Institute of Bio- and Geosciences (IBG)
Biotechnology (IBG-1)

Design and application of metabolite sensors for the FACS-based isolation of feedback-resistant enzyme variants

Georg Schendzielorz

Schriften des Forschungszentrums Jülich
Reihe Gesundheit / Health

Band / Volume 71

ISSN 1866-1785

ISBN 978-3-89336-955-3

Bibliographic information published by the Deutsche Nationalbibliothek.
The Deutsche Nationalbibliothek lists this publication in the Deutsche Nationalbibliografie; detailed bibliographic data are available in the Internet at http://dnb.d-nb.de.

Publisher and Distributor: Forschungszentrum Jülich GmbH
Zentralbibliothek
52425 Jülich
Tel: +49 2461 61-5368
Fax: +49 2461 61-6103
Email: zb-publikation@fz-juelich.de
www.fz-juelich.de/zb

Cover Design: Grafische Medien, Forschungszentrum Jülich GmbH

Printer: Grafische Medien, Forschungszentrum Jülich GmbH

Schriften des Forschungszentrums Jülich
Reihe Gesundheit / Health, Band / Volume 71

D 61 (Diss. Düsseldorf, Univ., 2013)

ISSN 1866-1785
ISBN 978-3-89336-955-3

The complete volume is freely available on the Internet on the Jülicher Open Access Server (JUWEL) at www.fz-juelich.de/zb/juwel

Summary

Microbes are used since decades for the industrial conversion of sugar feedstock and other renewable carbon sources to important bulk or fine chemicals. Nowadays, food and feed ingredients like amino acids and vitamins are biotechnologically produced in ever increasing quantities. Microorganisms like *Escherichia coli* or *Corynebacterium glutamicum* are used in these production processes, but – except of fermentation products – they are not naturally evolved for profitable metabolite formation. Thus, strain development is an essential prerequisite for the establishment of microbial production processes and can be performed by a number of approaches, such as metabolic engineering or undirected mutagenesis and screening. In the latter approach, large clone libraries are easily generated, but the bottleneck are efficient screening strategies to identify the desired variants with improved metabolite production. Such screening techniques should preferably rely on an optical signal that reflects increased product formation and enables the use of fluorescence activated cell sorting (FACS), which currently allows the highest throughput with more than one billion clones per assay. To generate the desired optical signal, intracellular metabolite sensors have been developed, which transform intracellular product concentrations into a graded optical output. These sensors are based either on RNA sequences or on transcription factors, which bind specifically to small molecules and in response to that, drive transcription of a reporter gene.

In this study, new transcription factor-based metabolite sensors for the monitoring of intracellular concentrations of different amino acids in *C. glutamicum* or *E. coli* were constructed. The sensor pSenLys is based on the transcriptional regulator LysG of *C. glutamicum* and activates transcription of its target gene *lysE* in the presence of elevated intracellular concentrations of L-lysine, L-arginine, and L-histidine. This sensor was used to screen plasmid libraries generated by either undirected or site-directed mutagenesis of ArgB (N-acetylglutamate kinase), HisG (ATP phosphoribosyl transferase) and LysC (aspartate kinase), representing feedback-inhibited key enzymes in arginine, histidine, and lysine biosynthesis. Using FACS, productive variants of these enzymes were isolated and characterized *in vitro* and *in vivo*. *C. glutamicum* strains carrying the best variants secreted up to 45 mM lysine, 34 mM arginine and 17 mM histidine into the medium.

LysG of *C. glutamicum* belongs to family of LysR-type transcriptional regulators (LTTR). As for LysG, transcriptional activation of most LTTRs depends on the presence of a co-inducer, which is often the product or an intermediate of the regulated pathway. To date, no structure of a full-length LTTR co-crystallized with its co-inducer is available. In this study, LysG was crystallized without ligand and co-crystallized with its effector L-arginine and structural models were generated. The overall structure of LysG corresponds to known LTTR structures consisting of an N-terminal DNA-binding domain, an α-helical linker, and two C-terminal effector-binding domains. Four LysG molecules are present in the unit cell, assembled into a tetramer (dimer of dimers). The structural model of the LysG-arginine complex enabled the identification of side-chains in the effector binding domains, which are involved in arginine binding. Structural differences between the models for LysG and LysG-Arg were observed, which disclosed a communication pathway from the effector-binding to the DNA-binding domain, whose binding affinity to DNA could be modulated by effector-interaction.

Zusammenfassung

Mikroorganismen werden seit Jahrzehnten für die Umsetzung nachwachsender Rohstoffe zu industriell genutzten Grund- und Feinchemikalien genutzt. Aminosäuren und Vitamine werden heute als Bestandteil von Nahrungs- und Futtermitteln in immer größeren Mengen biotechnologisch produziert. In diesen Produktionsprozessen werden Mikroorganismen wie *Escherichia coli* oder *Corynebacterium glutamicum* eingesetzt, die - mit Ausnahme von Fermentationsendprodukten - natürlicherweise nicht auf eine effiziente Metabolit-Überproduktion evolviert wurden. Eine essentielle Voraussetzung für die Etablierung mikrobieller Produktionsprozesse ist daher die Stammentwicklung, die durch „metabolic engineering" oder durch ungerichtete Mutagenese und nachfolgendes Screening erfolgen kann. Während die Herstellung großer genetischer Diversität unproblematisch ist, stellt das Screening auf Varianten mit verbesserter Produktbildung in der Regel den limitierenden Schritt dar. Vorzugsweise sollten Screening-Ansätze auf einem optischen Signal basieren, das gesteigerte Produktbildung anzeigt und die Verwendung von Hochdurchsatztechnologien wie z.B. der fluoreszenzaktivierten Zellsortierung (FACS) ermöglicht. FACS bietet mit der Analyse von über einer Milliarde Zellen pro Ansatz derzeit den höchstmöglichen Durchsatz. Um das benötigte optische Signal zu generieren, wurden Metabolitsensoren entwickelt, die intrazelluläre Metabolitkonzentrationen in graduierte optische Signale transformieren. Diese Sensoren basieren entweder auf Transkriptionsfaktoren oder auf RNA-Molekülen, die bei spezifischer Bindung der zu detektierenden Substanz die Transkription eines Reportergens aktivieren.

In dieser Arbeit wurden neue transkriptionsfaktor-basierte Sensoren konstruiert, die verschiedene Aminosäuren in *C. glutamicum* oder *E. coli* detektieren können. Der Sensor pSenLys basiert auf dem Transkriptionsregulator LysG von *C. glutamicum* und aktiviert die Transkription seines Zielgens *lysE* bei erhöhten intrazellulären Konzentrationen von L-Lysin, L-Arginin und L-Histidin. Dieser Sensor wurde eingesetzt, um Plasmidbibliotheken von ungerichtet oder gerichtet mutagenisiertem LysC (Aspartatkinase), ArgB (N-Acetylglutamatkinase) und HisG (ATP-Phosphoribosyltransferase) zu screenen. Es handelt sich dabei um die feedback-inhibierten Schlüsselenzyme der Lysin-, Arginin- und Histidinbiosynthese in *C. glutamicum*. Mittels FACS wurden feedback-resistente Varianten dieser Enzyme isoliert und *in vivo* bzw. *in vitro* charakterisiert. *C. glutamicum*-Stämme mit den besten Varianten akkumulierten im Kulturüberstand bis zu 45 mM Lysin, 34 mM Arginin und 17 mM Histidin.

LysG aus *C. glutamicum* gehört zur Familie der LysR-Typ-Transkriptionsregulatoren (LTTR). Wie im Fall von LysG erfordert die transkriptionsaktivierende Funktion von LTTRs in vielen Fällen die Bindung eines Effektormoleküls. Bis heute ist jedoch keine Proteinstruktur eines mit dem Effektor co-kristallisierten LTTRs bekannt. In dieser Arbeit wurde LysG einerseits ohne Ligand kristallisiert und andererseits im Komplex mit dem Effektor L-Arginin. Für beide Strukturen wurden Modelle generiert. Die Struktur von LysG stimmt grundsätzlich mit bekannten LTTR-Strukturen überein, die sich durch eine N-terminale DNA-Bindedomäne, eine „Linker"-Helix und zwei C-terminale Effektor-Bindedomänen auszeichnen. Vier LysG-Moleküle in der Einheitszelle bilden ein Tetramer (Dimer von Dimeren). Das Strukturmodell des LysG-Arginin-Komplexes ermöglichte die Identifikation der L-Arginin-bindenden Seitenketten in der Effektor-Bindedomäne. Ein Vergleich der Struktur von freiem LysG mit der des LysG-Arginin-Komplexes ergab Unterschiede, die einen Einfluss von Arginin-induzierten strukturellen Veränderungen in der Effektor-Bindedomäne auf die Struktur der DNA-Bindedomäne und auf deren Bindungsaffinität zur DNA ermöglichen könnten.

Content

List of publications and manuscripts

1. **Schendzielorz G**, Dippong M, Grünberger A, Kohlheyer D, Yoshida A, Binder S, Nishiyama C, Nishiyama M, Bott M, Eggeling L. Taking control over control: Use of product sensing in single cells to remove flux control at key enzymes in biosynthesis pathways. *ACS Synthetic Biology 2014,* 3 (1), 21–29. DOI 10.1021/sb400059y

   Impact factor not yet available, own contribution to the work: 80 %
   I had the initial idea for the project, designed the study, performed most of the experiments and wrote the paper together with Lothar Eggeling.

2. **Schendzielorz G**[‡], Syberg F[‡,] Bott M, Eggeling L, Hofmann E. Structure of the transcriptional regulator LysG of *Corynebacterium glutamicum* in complex with its effector L-arginine. *To be submitted to Acta Crystallographica D* (‡ joint first authors)

   Impact factor 14.1, own contribution to the work: 50 %
   I optimized and performed heterologous expression and purification of LysG, set up the crystallization screens, discussed results and interpretation and wrote the paper together with Falk Syberg.

3. Binder S, **Schendzielorz G**, Stäbler N, Krumbach K, Hoffmann K, Bott M, Eggeling L. A high-throughput approach to identify genomic variants of bacterial metabolite producers at the single-cell level. *Genome Biology* 2012, 13 (5), R40. DOI 10.1186/gb-2012-13-5-r40

   Impact factor 10.3, own contribution to the work: 30 %
   I constructed and characterized pSenArg and pSenSer, recorded microscopic pictures together with Alexander Grünberger and prepared all figures in the paper.

4. Siedler S, **Schendzielorz G**, Binder S, Eggeling L, Bringer S, Bott M. SoxR as single-cell biosensor for NADPH-consuming enzymes in *Escherichia coli*. *ACS Synthetic Biology* 2014, 3 (1), 41–47. DOI 10.1021/sb400110j

   Impact factor not yet available, own contribution to the work: 30 %
   I discussed the initial idea with Solvej Siedler, provided plasmid and primer templates for sensor construction, suggested and supported targeted mutagenesis, performed FACS experiments and contributed to the text and figures in the paper.

5. Grünberger A, Paczia N, Probst C, **Schendzielorz G**, Eggeling L, Noack S, Wiechert W, Kohlheyer D. A disposable picolitre bioreactor for cultivation and investigation of industrially relevant bacteria on the single cell level. *Lab on a Chip* 2012, 12: 2060-2068. DOI 10.1039/C2LC40156H

   Impact factor 6.5, own contribution to the work: 20 %
   I optimized strain-specific conditions for picolitre bioreactor cultivations, provided pre-cultures, discussed the results and wrote the corresponding part in the paper.

6. Grünberger A, van Ooyen J, Paczia N, Rohe P, **Schendzielorz G**, Eggeling L, Wiechert W, Noack S. Beyond growth rate 0.6: *Corynebacterium glutamicum* cultivated in highly diluted environments. *Biotechnol Bioeng* 2013*,* 110**:** 220-228. DOI 10.1002/bit.24616

   Impact factor 3.6, own contribution to the work: 20 %
   I introduced and performed FACS based single-cell counting experiments and analyzed the results.

List of patent applications

1. **Schendzielorz G**, Binder S, Bott M, Eggeling L: Verfahren zur Herstellung von Vektoren enthaltend ein für in seiner feedback-Inhibierung gemindertes oder ausgeschaltetes Enzym kodierendes Gen und deren Verwendung für die Herstellung von Aminosäuren und Nukleotiden. *PCT/DE2013/000416*, 22.08.2012.

2. Siedler S, Bringer S, **Schendzielorz G**, Binder S, Eggeling L, Bott M: Sensor für NADP(H) und Entwicklung von Alkoholdehydrogenasen. *PCT/EP2013/002481,* 28.08.2012.

Introduction

The conversion of sugar feedstock and other raw materials to industrial important bulk or fine chemicals by microbes has been used for decades (Adrio and Demain, 2010). Recent progress in metabolic engineering on the one hand, and raising costs as well as ecological drawbacks of fossil resources on the other hand, promote comprehensive growth of the bioeconomy. Nowadays, food and feed ingredients like amino acids and vitamins are biotechnologically produced in ever increasing quantities. For example, the annual production of cobalamine rose to approximately 35 tons, nucleotides to 38,000 tons and amino acids to 5,000,000 tons (Eggeling, L., Pfefferle, W. and Sahm, 2006).

These production processes are based on microorganisms like *Escherichia coli*, *Bacillus subtilis* or *Corynebacterium glutamicum*. The latter one is of particular importance in the amino acid production industry. First isolated as glutamate-producing microorganism in 1958 (Kinoshita et al., 1958), this gram-positive soil bacterium is the most important amino acid producer used today (Eggeling and Bott, 2005). With this bacterium, actually 2,500,000 tons L-glutamate and 1,500, 000 tons L-lysine are produced annually (Becker and Wittmann, 2012). Also other amino acids, including L-serine, L-isoleucine and L-valine, are produced with mutants of *Corynebacterium* strains. L-glutamate occupies a special position, since it is exclusively used in food supplements. In contrast, L-lysine and other amino acids are used as animal-feed additives, a market with notable growth exceeding 6% per year (Kumar, 2012). Additionally, almost all amino acids are used in the pharmaceutical industry for infusions.

However, microorganisms are not naturally designed for profitable metabolite formation and there is an unrelenting need to optimize strains and pathways. This is done by a number of approaches, including metabolic engineering, assisted by the analysis of existing strains or generation of new strains by classical undirected mutagenesis. Frequently, large genotypic libraries are generated and efficient screening strategies are needed to identify desired variants with improved metabolite formation. Therefore, high-throughput (HT) strategies have been developed. These techniques preferably rely on an optical signal, reflecting increased product formation and enabling the use of fluorescence activated cell sorting (FACS) suitable for HT screenings. Natural chromophores like carotenoids are directly detectable (An et al., 1991; Marienhagen and Bott, 2013; Nonomura and Coder, 1988; Ukibe et al., 2008). Also some non-chromogenic substances like gramicidin (Azuma et al., 1992), poly-(β-hydroxybutyrate) (Fouchet et al., 1995) and lipids (Gouveia et al., 2009; Silva et al., 2009) have been optically detected, by coupling their presence to fluorophores.

Unfortunately, this strategy is not yet applicable for most biotechnological products, since they are inconspicuous. More universal detection systems are therefore required as offered by natural cellular detection systems such as regulatory RNAs and transcription factors which enable the sensing of small molecules which are not colored or which cannot easily be converted into a fluorophore.

Regulatory RNA-based metabolite sensors

RNA-based metabolite sensors rely on RNA sequences (aptamers), which bind effectors thereby remodeling the secondary structure of the aptamer. When an aptamer is fused with another RNA sequence (actuator), which has its own structure dependent function, structural changes in the aptamer affect structure and function of the actuator. For example, the actuator could form a transcrip-

tion terminating stem loop, which is destabilized by effector-induced structural changes, thus activating transcription (riboswitch) (Vitreschak et al., 2004). Another example for an actuator is a ribozyme, whose self-cleavage activity is modulated in response to structural changes of the aptamer (allosteric ribozyme) (Hermann and Patel, 2000).

By replacing the natural target gene by a reporter, for example a gene encoding a fluorescent protein (FP), regulatory RNAs can be used as sensors (Benenson, 2012; Liang et al., 2011). This has been done to detect thiamine-pyrophosphate (TPP) (Nomura and Yokobayashi, 2007) and theophylline (Desai and Gallivan, 2004; Suess et al., 2004). A theophylline sensing allosteric ribozyme was constructed by Win et al. (Win and Smolke, 2007, 2008).

Recently, a fluorophore binding aptamer was developed, whose binding affinity is modulated by a ligand-binding aptamer (Paige et al., 2011, 2012). This construction provides an inducible autofluorescent RNA/fluorophore complex, which mimics GFP fluorescence without the need for protein synthesis.

Aptamers for the detection of industrial relevant substances are rare. Engineering of natural aptamers and generation of synthetic ones by the "systematic evolution of ligands by exponential enrichment" (SELEX) method (Ellington and Szostak, 1990; Tuerk and Gold, 1990) was frequently reported to gain access to the detection of the desired molecule (Cho et al., 2009; Stoltenburg et al., 2007). However, current examples are limited to substances like TPP (Nomura and Yokobayashi, 2007), tetracycline (Weigand and Suess, 2007), theophylline and derivatives (Michener and Smolke, 2012; Win and Smolke, 2007), adenosine, S-adenosylmethionine, ADP, guanine and GTP (Paige et al., 2012), which do not include the industrial most relevant molecules. Moreover, many aptamers exhibit binding constants to their effectors in the nanomolar to micromolar range (Stoltenburg et al., 2007), rendering them inapplicable for product detection in metabolic engineering approaches, where the millimolar range is of interest.

Transcription factor-based metabolite sensors

Many natural transcription factors (TFs) interact specifically with small molecules and in response induce or repress transcription of the target genes. This principle has been widely used, to construct whole-cell-biosensors for the detection of environmental pollutants (Gu et al., 2004). In these cases the entire culture fluorescence served as signal.

For screening approaches, TF-induced expression of a reporter gene was first described for the detection of benzoate and 2-hydroxybenzoate in *E. coli* (Fiet et al., 2006). The benzoic acids interact with NahR derived from *Pseudomonas putida*, which induces in consequence transcription of the salicylate promoter. As reporter genes, the α-fragment of β-galactosidase or the *tetA* gene, conferring tetracycline-resistance, were fused to the salicylate promoter, enabling plate-based selection. A similar system, based on BmoR, PcaR and DcuR/DcuS, was described for 1-butanol, adipate and succinate, respectively (Dietrich et al., 2013). Using an auto-fluorescent protein as reporter, small-molecule concentrations can be transformed into an optical output, which is detectable by HT-interfaces like FACS. This approach offers quantitative information on intracellular small-molecule concentrations and in combination with FACS, ideal HT-capability, enabling analyses of up to 10^9 single cells per assay (Becker et al., 2004). The number of small-molecules, which can be detected in this way, is large, given by the existence of many natural transcription factors, with various specificities.

The first approach to link cytosolic concentration of a specific metabolite to FP expression used BenR, an AraC-type transcriptional regulator from *Pseudomonas putida*, to detect benzoate in *E. coli* (Uchiyama and Miyazaki, 2010). BenR activates transcription of *benABCD* genes when benzoate is present as co-inducer. Fusion of P_{benA} to a FP, transforms benzoate concentration into graded optical output. The detection range is 0.01-1 mM with ~35-fold induction as maximal response. The sensor was successfully used to screen fosmid libraries for benzamidase activity. The screening was done in microtiter plates, but given the strong maximal induction of the sensor response, it should be possible to use HT-interfaces like FACS.

In another approach, Tang and Cirino (2011) constructed a mevalonate sensor with an engineered AraC variant and the P_{bad}-promoter, which is fused to GFP. The sensor exhibits a linear detection range from 10-100 mM with half maximal response at 150 mM and a 7-fold induction at maximal response. It was used to screen a library of *E. coli* cells, equipped with mutant MevT-operons, for improved mevalonate production. Further modification of AraC provided variants, which interact with triacetic acid lactone (TAL) as co-inducer. Thus GFP expression is modulated by intracellular TAL concentration with a detection range of 1-10 mM and 12-fold induction at maximal response. β-Galactosidase activity-based assays were used to screen random and saturation libraries of *Gerbera hybrida* 2-pyrone synthase, an enzyme catalyzing condensation reactions of acetyl-CoA and malonyl-CoA to TAL. Also in this case, a screening via FACS should be possible.

The first example for the application of metabolite sensors to screen libraries of mutant cells for productive variants by FACS was given by Binder et al. (2012). The sensor pSenLys, detecting arginine, histidine and lysine, is based on the amino acid exporter LysE from *C. glutamicum*. In previous work it was discovered, that *lysE* expression is modulated by the LTTR-type TF LysG, which becomes active upon binding of arginine, histidine and lysine as co-inducer (Bellmann et al., 2001; Vrljic et al., 1996). Fusion of P_{lysE} with *eyfp* offers co-inducer dependent expression of FP and thus a graded optical output of co-inducer concentration with a detection range for L-lysine of 4-25 mM and a 44-fold maximal induction. The sensor was successfully used to screen libraries of mutant *C. glutamicum* cells for variants with enhanced lysine production. Numerous novel mutants, accumulating up to 37 mM L-lysine in the culture supernatant, were isolated.

A metabolite sensor with specificity for methionine, leucine, isoleucine and valine was constructed by Mustafi et al. (2012). It is based on the transcriptional regulator Lrp, which modulates transcription of the two-component amino acid exporter BrnFE in *C. glutamicum*. On the sensor plasmid, P_{brnF} is fused with eYFP. Linear detection ranges and maximal induction factors are 0.2-23.5/78, 0.2-13.6/22, 0.4-11.5/10, 1.5-23.4/12 for methionine, leucine, isoleucine and valine respectively. The sensor was successfully used to isolate *C. glutamicum* cells with improved valine production after whole-cell mutagenesis.

LysR-type transcriptional regulators

The largest group of one-component TFs in bacteria is represented by LysR-type transcriptional regulators (LTTRs). LTTRs are involved in regulation of diverse cellular processes, including primary and secondary metabolism. Over 40,000 potential members are listed in the protein sequence analysis & classification database (IPR000847), sharing high-sequence similarity and domain organization.

The conserved overall structure includes an N-terminal DNA-binding domain, linked to two C-terminal effector-binding domains via an α-helix. Highest conservation is obtained in the DNA-

binding domain, representing the classical helix-turn-helix (HTH) motif. First discovered in bacteria, the HTH-motif is one of the most abundant DNA-binding motifs in prokaryotes as well as eukaryotes. The HTH-motif of LTTRs consists of three α-helices. Interactions between these helices stabilize their relative orientation in a fixed angle, enabling one of them to fit into the major groove of the DNA-double helix, forming highly specific interactions with the recognized promoter sequence (Aravind et al., 2005; Brennan and Matthews, 1989; Huffman and Brennan, 2002).

As mentioned, transcriptional activation of the LTTRs depends on the presence of a co-inducer (effector), which is often the product or an intermediate of the regulated pathway (Celis, 1999; Keulen et al., 1998; Picossi et al., 2007). Although a putative effector binding cleft is predicted (Stec et al., 2006) and supported by genetic and structural work (Ezezika et al., 2007; Monferrer et al., 2010), a structure of a full-length LTTR, co-crystallized with its effector, is not yet reported.

Aims of this work

(a) Construction and characterization of metabolite sensors for the detection of diverse amino acids in *C. glutamicum* and *E. coli*.

(b) Application of the metabolite sensor pSenLys to isolate mutated variants of ArgB, HisG and LysC with abolished feedback inhibition to enable increased L-arginine, L-histidine and L-lysine synthesis by *C. glutamicum*.

(c) Crystallization of LysG, preferably in complex with its effector, and generation of structural models.

Results

(1) Taking Control over Control: Use of Product Sensing in Single Cells to Remove Flux Control at Key Enzymes in Biosynthesis Pathways

(2) Structure of the transcriptional regulator LysG of *Corynebacterium glutamicum* in complex with its effector L-arginine

(3) A high-throughput approach to identify genomic variants of bacterial metabolite producers at the single-cell level

(4) SoxR as single-cell biosensor for NADPH-consuming enzymes in *Escherichia coli*

(5) A disposable picolitre bioreactor for cultivation and investigation of industrially relevant bacteria on the single cell level

(6) Beyond growth rate 0.6: *Corynebacterium glutamicum* cultivated in highly diluted environments.

ACS SyntheticBiology

Research Article

pubs.acs.org/synthbio

Taking Control over Control: Use of Product Sensing in Single Cells to Remove Flux Control at Key Enzymes in Biosynthesis Pathways

Georg Schendzielorz,[†] Martin Dippong,[†] Alexander Grünberger,[†] Dietrich Kohlheyer,[†] Ayako Yoshida,[‡] Stephan Binder,[†] Chiharu Nishiyama,[‡] Makoto Nishiyama,[‡] Michael Bott,[†] and Lothar Eggeling*[,†]

[†]Institute of Bio- and Geosciences 1: Biotechnology, Forschungszentrum Jülich, D-52428 Jülich, Germany

[‡]Biotechnology Research Center, The University of Tokyo, 1-1-1 Yayoi, Bunkyo-ku, Tokyo 113-8657, Japan

Supporting Information

ABSTRACT: Enzymes initiating the biosynthesis of cellular building blocks are frequently inhibited by the end-product of the respective pathway. Here we present an approach to rapidly generate sets of enzymes overriding this control. It is based on the *in vivo* detection of the desired end-product in single cells using a genetically encoded sensor. The sensor transmits intracellular product concentrations into a graded optical output, thus enabling ultrahigh-throughput screens by FACS. We randomly mutagenized plasmid-encoded ArgB of *Corynebacterium glutamicum* and screened the library in a strain carrying the sensor pSenLys-Spc, which detects L-lysine, L-arginine and L-histidine. Six of the resulting *N*-acetyl-L-glutamate kinase proteins were further developed and characterized and found to be at least 20-fold less sensitive toward L-arginine inhibition than the wild-type enzyme. Overexpression of the mutein ArgB-K47H-V65A in *C. glutamicum*Δ*argR* led to the accumulation of 34 mM L-arginine in the culture medium. We also screened mutant libraries of *lysC*-encoded aspartate kinase and *hisG*-encoded ATP phosphoribosyltransferase. We isolated 11 LysC muteins, enabling up to 45 mM L-lysine accumulation, and 13 HisG muteins, enabling up to 17 mM L-histidine accumulation. These results demonstrate that *in vivo* screening of enzyme libraries by using metabolite sensors is extremely well suited to identify high-performance muteins required for overproduction.

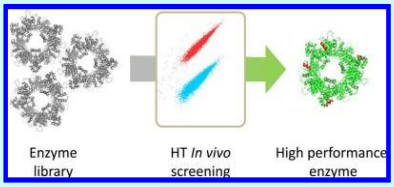

KEYWORDS: *single-cell analysis, metabolite sensor, library screening, flux control, allosteric enzymes, product sensing, fluorescence-activated cell sorting (FACS)*

The potential of microbes to convert inexpensive sugar feedstocks into industrially important products has been used for decades.[1] Vitamins, antibiotics, nucleotides, amino acids and organic acids are produced in ever increasing quantities. This biosynthetic capacity is also increasingly being used for the synthesis of small molecules not naturally made by bacteria, such as pharmaceutical intermediates or biofuels.[2,3] Examples of already established processes include the current annual production of approximately 35 tons of cobalamine, 38 000 tons of nucleotides, or as much as 5 000 000 tons of amino acids.[4] This is done using mutant strains derived from bacteria like *Propionibacterium freudenreichii*, *Escherichia coli*, or *Corynebacterium glutamicum*, for instance.

Microorganisms are not naturally designed for profitable metabolite formation, however, and there is an unrelenting need to optimize strains and pathways. Among others the catalytic activities in the biosynthesis pathway itself have to be increased to enhance and maximize the flux toward the desired metabolite. Key roles are played by enzymes that are controlled by allosteric mechanisms.[5,6] The reason for this is that such enzymes are often inhibited by the final product of the pathway or by intermediates required for its synthesis. Inhibition constants for such enzymes are often in the μM range making them unsuitable for high level production of the desired metabolite.[7] It is therefore a primary goal of many systemic engineering attempts to overcome this limitation. Unfortunately, the accessibility of deregulated enzymes is limited, and most of the engineering approaches rely on the corresponding genes derived from mutants obtained by rounds of random mutation and screening. For example, for a recent construction of a superior L-threonine producer of *E. coli* three such genes (lysC-T432I, thrA-S345F and tdh-S97F) were taken from classical mutants to enable increased flux toward L-threonine.[8] Also an L-lysine producer of *C. glutamicum* generated was based on two genes of this type (pyc-P458S, lysC-T311I) derived from classical mutants,[9] and the construction of a muconic acid producer of *Saccharomyces cerevisiae* required the use of an already available aro4-K229L allele.[10] There are other approaches to overcome allosteric inhibition and the use of the corresponding enzymes, including approaches based on crystal structures, or *in silico* predictions using coevolutionary analysis.[11,12] These latter *in vitro* approaches require plasmid constructions and screens for enzyme activity and control before they can be used. This is not the case for those enzymes obtained from *in vivo* screens, which per se are suitable for

Received: May 20, 2013
Published: July 5, 2013

production. Easier access and a larger choice of such enzymes would be beneficial for metabolic engineering.

We recently used transcription factors and their target promoters as genetic switches to monitor increased concentrations of specific amino acids in single cells of *E. coli* or *C. glutamicum*.[13−15] The sensors developed transmit the inconspicuous phenotype of a metabolite into an easily detectable and highly sensitive optical output. This single-cell technology enables ultrahigh-throughput screens of mutant libraries since it is not restricted to colony color formation or the screening of culture supernatants by chromatography, for instance. It bridges the gap between the numerous and well-developed methods for generating large, diverse genotypic libraries on the one hand,[16] and previous less universal identification procedures for metabolite producers on the other hand. Here we apply the metabolite sensor pSenLys-Spc for the rapid identification of collections of allosterically controlled enzymes of *C. glutamicum* from large plasmid libraries, and we demonstrate their use for product formation.

RESULTS AND DISCUSSION

Monitoring Cytosolic L-Arginine in Single Cells. The metabolite sensor pSenLys-Spc, used in this study, is based on the transcriptional regulator LysG (Figure 1). The regulator

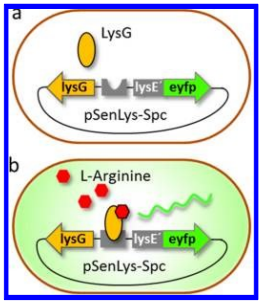

Figure 1. Principle of metabolite sensor pSenLys-Spc. (a) The sensor construct pSenLys-Spc encodes *lysE'* fused to *eyfp*. LysG is the transcriptional activator of *lysE*. (b) LysG senses elevated concentrations of L-arginine, L-lysine or L-histidine and interacts with the target promoter region to drive transcription of *eyfp* resulting in fluorescent cells.

senses increased intracellular concentrations of basic amino acids in *C. glutamicum* and drives at increased cytosolic concentrations the transcription of its target gene *lysE*.[17] In pSenLys-Spc the target promoter is fused to *eyfp*.[13]

We simulated an increased L-arginine concentration by adding the peptide Arg-Ala and followed fluorescence of single cells in a microfluidic chip over time. Peptide addition is a proven method to increase the cytosolic pool of a specific amino acid in *C. glutamicum* or *E. coli*.[18,17] Wild-type cells (WT) carrying pSenLys-Spc received 2 mM Arg-Ala in the medium feed or 2 mM Ala-Ala for control. Already after 1.25 h, cells that received the arginine-containing peptide were well separated from the control. More than 150 cells of the approximately 300 cells analyzed exhibited maximum fluorescence of 50 AU, as given by the red bars (the green bars are the control). As a further control we used *C. glutamicum* with a chromosomal deletion of the basic amino acid exporter region, WTΔlysEG. Such cells are unable to excrete L-arginine or L-lysine from the cell, and L-arginine may increase in the cytosol up to concentrations exceeding 800 mM because of the cell's inability to control the intracellular L-arginine concentration by export.[19] When WTΔlysEG received 2 mM Arg-Ala, cells exhibited the expected strong fluorescence (blue bars). In Figure 2b microscopic snapshots of 2−3 individual cells at each analyzed time point are given. For the purpose of this study it is important that, even with WT, which actively exports basic amino acids, a constant fluorescence signal prevails for Arg-Ala addition, indicating the applicability of pSenLys-Spc to identify cells with increased L-arginine synthesis due to an annulled pathway control. To see Figure 2b in time lapse, watch Video S1 (Supporting Information).

Generation and FACS Screening of ArgB Muteins. In bacteria like *C. glutamicum*, the activity of the *argB*-encoded *N*-acetyl-L-glutamate kinase is strongly inhibited by L-arginine.[20,21] The kinase initiates the L-arginine biosynthesis pathway, and control at this step prevents increased L-arginine formation. The *argB* coding sequence of *C. glutamicum* was amplified using the Diversify PCR Random Mutagenesis Kit (Clontech) to introduce 4.8 mutations per gene. The resulting library of approximately 10^5 clones was established in *E. coli* strain Top10. Transformants were pooled, plasmid DNA was isolated, and the library was introduced into *C. glutamicum*ΔargR carrying the sensor plasmid pSenLys-Spc. This latter strain was chosen since deletion of the transcriptional regulator *argR* favors L-arginine synthesis.[5] Prior to screening via FACS, cells were grown for 4 h on salt medium CGXII-glucose, as were controls containing wild-type *argB* and a control containing a known mutant *argB** allele, which is not inhibited by L-arginine.[5] Samples were gated first by electronic forward and side scatter to exclude debris, and then by fluorescence due to arginine-dependent *eyfp* transcription. The positive control was well separated from the negative control as illustrated by gate P1, which captured 0.057% of the negative control and 80.7% of the positive control (Figure 3). For selection the more stringent gate P2 was used, which captured no cell of the negative control, 0.8% of the positive control, and less than 0.001% of mutant library. About 22^6 cells of the mutant library were analyzed, and 96 positive cells were selected. These were directly spotted into 200 μL of minimal medium CGXII-glucose in a microtiter plate, and 88 of these cells grew up into cultures.

Next, the verification step was performed, and amino acids were determined in culture supernatants. In 41 cultures, L-arginine concentrations ranging from 1 to 18 mM were present, whereas in the remaining cultures up to 3 mM L-lysine was found. With the control neither L-arginine nor L-lysine was present. For unknown reasons from large populations weak L-lysine producers can easily be isolated, which is not the case for L-arginine producers. Since L-lysine elicits response of the reporter system, too, this causes the false positives. Twenty-two clones showing L-arginine accumulation to different degree were chosen, and *argB* was sequenced. Seven singular clones were obtained (Figure 4a and Table S1, Supporting Information). They differ in L-arginine accumulation and mutations in *argB*, with some clones sharing identical mutations as is typical for error-prone PCR.[16]

The significant L-arginine formation achieved by our FACS selection procedure with ArgB-14, ArgB-88, ArgB-79 and ArgB-37 encouraged us to analyze their mutations in more detail. To do so, we applied site-saturation mutagenesis individually to

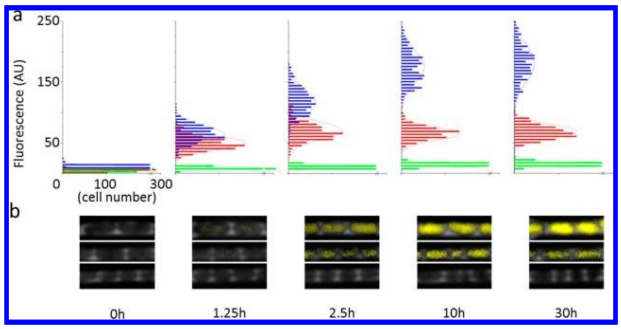

Figure 2. Fluorescence of single *C. glutamicum* cells carrying pSenLys-Spc as triggered by peptide addition. (a) At time 0 h, cells of the wild type received 2 mM Ala-Ala (green bars), or 2 mM Arg-Ala (red bars). Also strain WTΔlysEG deleted of the basic amino acid export carrier that received 2 mM Arg-Ala was used (blue bars). The fluorescence for approximately 300 cells was quantified for each time point (0−30 h). After 1.25 h, cells of the wild type that received Arg-Ala are well separated from cells that received Ala-Ala. The mutant WTΔlysEG with hampered amino acid export developed the strongest fluorescence. (b) Examples of micrographs used for quantification, each showing 2−3 cells of WTΔlysEG + Arg-Ala (top), WT + Arg-Ala (middle), and WT + Ala-Ala (bottom).

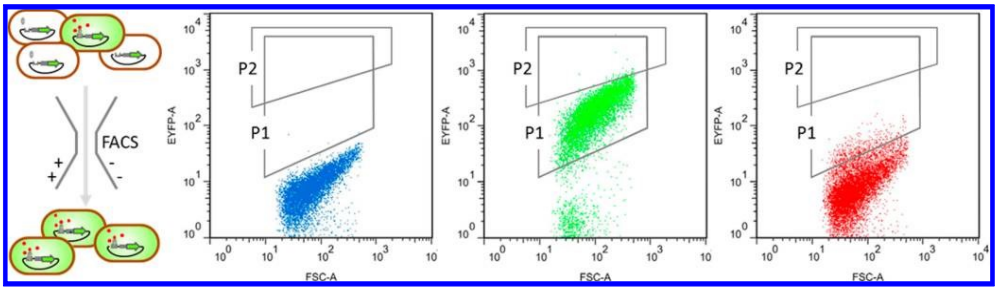

Figure 3. FACS selection of single cells with increased cytosolic L-arginine concentration. On the left, a sketch of the FACS selection procedure is shown. The three FACS plots illustrate, from left to right, the negative control with wild-type *argB*, the positive control with cells expressing the mutant *argB** allele, and cells containing the error-prone PCR library of *argB*. The stringent gate P2 was used for selection.

K47, V65, V110, G122, T180, I189, Y190 (Table S2, Supporting Information) and selected fluorescent cells via FACS from each of the seven libraries as described before. In the case of the G122 library, we isolated a single mutein, ArgB-G122T, and obtained a top L-arginine accumulation of 11.5 ± 0.3 mM (see Table S3, Supporting Information). Moreover, interesting muteins were selected from the assay where K47 was saturated. Strains with ArgB muteins K47E, K47T and K47H produced 1.2, 3.5, and 5.5 mM L-arginine, respectively, whereas with wild-type ArgB, 0.4 mM L-arginine was obtained. Residue K47 of *C. glutamicum* aligns with the corresponding K/R residues of the ArgB proteins of *Mycobacterium tuberculosis*, *Pseudomonas aeruginosa*, *Arabidopsis thaliana*, and *Thermotoga maritima* with known structure (Figure S5, Supporting Information). In these structures, the respective K/R residues are in the αA helix (Figure 4b), which is connected via the β1 strand to the N-terminal helix whose complete deletion abolished L-arginine inhibition of the *P. aeruginosa* enzyme.[23] In the model for the *C. glutamicum* enzyme, K47 is only able to interact with the amide backbone of V42 (3.1 Å). However, K47H is also able to interact with the amide backbone of residues D43 and D44 (<3.5 Å) and the side-chain of Y36 (3.6 Å). These slight alterations might impact on the overall structural organization of the preceding β1 strand and thus affect L-arginine sensitivity via the N-terminal helix. For further development of ArgB we focused on positions K47 and V65 because of the highest production obtained with this mutein. We combined with these mutations a limited set of further mutations by site-directed mutagenesis. In total 6 mutants were generated whose production properties and enzymatic properties were explored in more detail (Table 1). In particular, the combination of K47H with V65A gave rise to an enzyme that caused an exceptionally high L-arginine concentration, whereas further combination with G122T led to a reduction again. Thus upon combining K47H with V65A, an additive effect was present, as occasionally observed for nearby changes in enzyme development.[24]

Kinetic and Physical Characterization of ArgB Muteins. We were also interested in selected biochemical parameters of the obtained ArgB muteins. To this end, the muteins were isolated as His-tagged versions from *E. coli*, and kinetic characteristics were determined. As expected, ArgB-WT was inhibited at low L-arginine concentrations characterized by a K_i of 0.2 mM (Table 2). This agrees with prior work reporting that the enzyme of *C. glutamicum* is inhibited to half its activity by 0.4−2 mM L-arginine.[25,21] All muteins analyzed exhibited an at least 19.5-fold reduced sensitivity toward the allosteric inhibitor L-arginine.

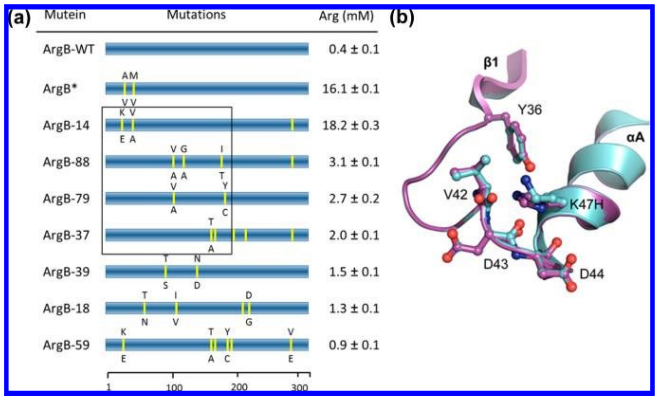

Figure 4. (a) Mutations of the isolated ArgB muteins and the L-arginine accumulation they cause. The yellow bar indicates the approximate location of the mutation. In the case of an amino acid exchange, the WT amino acid is given on top and the mutant amino acid below the yellow bar. The mutant locations that were studied in more detail are framed (see text). (b) Structural overlay of aa 32−53 of ArgB-WT (cyan) and ArgB-K47H (magenta) generated by SWISS-MODEL.[22] The histidine residue in position 47 is able to interact with the amide backbone of residues D43 and D44 and the side-chain of Y36, which results in a slight distortion of the αA helix and the preceding β1 strand, which may influence the degree of L-arginine sensitivity.

Table 1. Influence of Overproduction of Selected ArgB Muteins and Wild-Type ArgB in *C. glutamicum*Δ*argR* on L-Arginine Accumulation in Culture Supernatants[a]

mutation	L-arginine (mM)
No	0.4 ± 0.1
K47H	8.3 ± 0.9
K47H, V65A	34.9 ± 1.2
K47H, V65A, G122T	22.2 ± 2.7
K47H, V65A, T180P	32.5 ± 1.4
K47H, G122T	12.4 ± 0.8
K47H, G122T, T180P	10.1 ± 0.9

[a]Strains were grown for 48 h in minimal medium CGXII-glucose.

ArgB-K47H-V65A is most interesting with respect to its impact on L-arginine production. This enzyme has an intermediate K_i among the isolated muteins, and it retains a reasonable catalytic efficiency of 1.1 s^{-1} mM^{-1} (Table 2). High L-arginine concentrations were also obtained with ArgB-K47H-V65A-T180P and ArgB-K47H-V65A-G122T. The latter protein was obtained from *E. coli* in very low yields only and was not further analyzed. The comparison of ArgB-K47H-G122T and ArgB-K47H-G122T-T180P is informative. These two proteins differ greatly with respect to catalytic efficiency, but perform similarly with respect to product accumulation. This emphasizes the advantage of the *in vivo* selection of productive enzymes, because *in vitro* derived kinetic characterizations apparently do not integrate the total cellular characteristics required for overproduction.

The *N*-acetyl-L-glutamate kinase of *E. coli* is a dimer, and it is not inhibited by L-arginine,[21] whereas the enzyme of *Pseudomonas aeruginosa* and *Thermotoga maritima* is a hexamer and is sensitive toward L-arginine inhibition.[20] For the *P. aeruginosa* enzyme, there are indications that the global structure of the protein displays slight structural alterations during conversion from the relaxed to the tensed state upon interaction with the inhibitor.[26,20] We therefore studied the consequences of L-arginine addition on the *C. glutamicum* enzyme by size exclusion chromatography (Figure 5). As expected from the sequence, the wild-type enzyme eluted with an apparent mass of 231 ± 40 kDa, which indicates that the enzyme is a hexamer (6 × 34.88 kDa = 209 kDa). In the presence of 10 mM L-arginine, the elution profile was almost superimposable (blue line in Figure 5). The elution profiles for the ArgB-K47H-G122T-T180P and ArgB-K47H-V65A enzymes were very different. Without L-arginine present, ArgB-K47H-G122T-T180P eluted in the void volume, which suggests that the mutations promote a high oligomeric state exceeding that of a hexamer. However, in the presence of L-arginine, the protein eluted according to a hexamer (Table S4,

Table 2. Kinetic Characterization of Selected Key Enzymes

protein[a]	K_m (mM)	spec. activity (μmol min^{-1} mg^{-1})	k_{cat} (s^{-1})	efficiency k_{cat}/K_m (s^{-1} mM^{-1})	K_i (mM)
ArgB-WT	3.4 ± 0.3	39.5 ± 0.9	23.0	6.8	0.2
ArgB-A49V-M54V*	2.9 ± 0.3	5.5 ± 0.1	3.2	1.1	7.0
ArgB-K47H	15.7 ± 2.1	71.1 ± 2.9	41.3	2.6	7.4
ArgB-K47H-G122T	25.3 ± 1.2	2.4 ± 0.06	1.4	0.1	3.7
ArgB-K47H-V65A	7.5 ± 0.7	14.0 ± 0.2	8.1	1.1	3.9
ArgB-K47H-G122T-T180P	5.6 ± 0.4	18.4 ± 0.3	10.6	1.9	6.9
ArgB-K47H-V65A-T180P	5.8 ± 0.6	29.5 ± 0.5	17.1	2.9	11.5

[a]The ArgB-A49V-M54V* protein has already been described.[5] The yield of ArgB-K47H-V65A-G122T was too low to enable its detailed analysis.

dx.doi.org/10.1021/sb400059y | ACS Synth. Biol. 2014, 3, 21−29

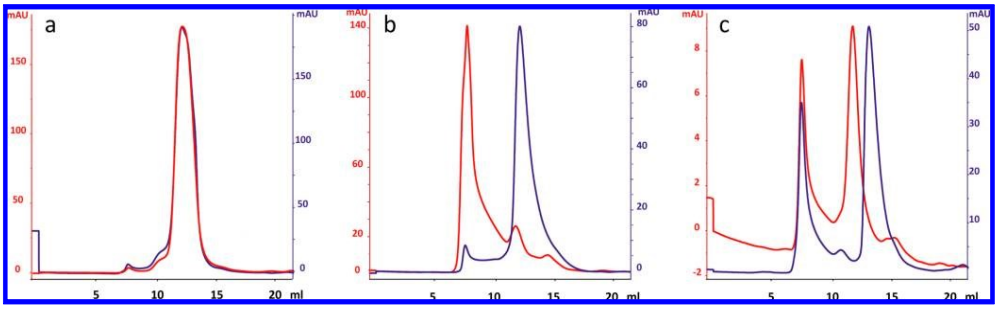

Figure 5. Structural alterations of ArgB proteins in the presence or absence of L-arginine. Three different proteins were subjected to size exclusion chromatography in the absence (red) or presence (blue) of 10 mM L-arginine: (a) ArgB-WT; (b) ArgB-K47H-G122T-T180P; (c) ArgB-K47H-V65A.

Table 3. Overview of LysC and HisG Muteins Obtained by Direct Product Sensing Using Metabolite Sensor Technology[a]

protein							L-lysine (mM)
LysC-WT							1.2 ± 0.1
LysC-77	R20S	N21D	T311I	R399L			44.9 ± 1.5
LysC-88	N21D	T311I					44.8 ± 1.1
LysC-90	N21D	L125L	E278G	A280V			39.0 ± 0.7
LysC-63	L69F	A124P	I211V	L227P	N235D	V350A	32.5 ± 0.7
LysC-56	K141K	V159E	N337S	D341N			30.9 ± 5.3
LysC-57	N21D	M365K	L394L				29.5 ± 0.3
LysC-15	N21D	T311I	R399L				27.1 ± 1.6
LysC-2	N21D	L125L	E278G	A280V	E391G		24.9 ± 2.4
LysC-54	T311I						23.9 ± 2.5
LysC-8	E24G	T311I					23.0 ± 0.1
LysC-42	R20S	N21D	N78S	E123E	I186V	K328E	21.1 ± 1.2
protein							L-histidine (mM)
HisG-WT							0.0
HisG-GT233-3	G233H	T235Q					17.3 ± 1.1
HisG-GT233-8	G233S	T235R					15.3 ± 0.2
HisG-GT233-4	G233V	T235R					14.7 ± 0.1
HisG-GT233-5	G233I	T235V					14.3 ± 0.3
HisG-GT233-1	G233R	T235R					13.4 ± 0.7
HisG-GT233-10	G233L						13.2 ± 0.4
HisG-GT233-6	G233H	T235F					13.1 ± 0.5
HisG-GT233-11	G233P	T235L					11.4 ± 0.5
HisG-GT233-7	G233R						10.7 ± 0.4
HisG-GT233-2	G233S	T235H					9.5 ± 0.5
HisG-N216-1	N216I						12.5 ± 0.2
HisG-N216-3	N216R						12.4 ± 1.2

[a]The *lysC* alleles were derived by epPCR. The *hisG* alleles resulted from applying two saturating primer sets: one targeting codon 233 and codon 235, and the other targeting codon 216. See Tables S6 and S7 (Supporting Information) for nucleotide exchanges.

Supporting Information). For ArgB-K47H-V65A, apparently three different globular structures can be formed: a large one eluting in the void volume, an intermediate one according to a hexamer, and a small one with an elution volume below a hexamer, which could be a tetramer or a dimer. L-arginine shifted the intermediate form to the small form. This shows that exceptional structural alterations of the *N*-acetyl-L-glutamate kinase are possible, which apparently do not result in a substantial loss of activity and efficiency (Table 2), and which are most useful for production purposes (Table 1). The hexameric kinase proteins have an extra N-terminal helix, which interlinks three dimers in the hexamers.[20] As previously mentioned K47 and V65 are located in the αA-helix (Figure 4b), and the observed insensitivity of ArgB-K47H-V65A toward L-arginine is apparently related with the dissociation of the hexamer into active smaller aggregates, as was similarly observed for mutant enzymes of *P. aeruginosa*.[23]

Generation of LysC and HisG Muteins. As mentioned earlier, the metabolite sensor based on the transcriptional regulator LysG detects L-arginine, L-lysine and L-histidine.[13] Its successful use to identify L-arginine-insensitive ArgB muteins prompted us to apply the same approach to screen mutant libraries for deregulated key enzymes of L-lysine and L-histidine synthesis, respectively. The key enzyme of L-lysine synthesis in *C. glutamicum* is the aspartate kinase (LysC), which is inhibited in its activity by L-lysine,[27] whereas the ATP phosphoribosyl-

transferase (HisG) controls L-histidine synthesis and is inhibited by L-histidine.[28] To this end, *lysC* of *C. glutamicum* was amplified by error-prone PCR, and PCR products cloned into pSenLys to give pSenLys-PlysC. Plasmids prepared from *E. coli* were pooled and used to transform *C. glutamicum*. LysC-T311I, encoding a known lysine-insensitive kinase protein,[29] served as a positive control for FACS screenings. In total 3×10^6 cells were screened and as a result, 11 different *lysC* alleles isolated. Among them, alleles with up to seven mutations were found, as was the single *lysC*-T311I mutation (Table 3). These muteins caused L-lysine accumulation up to 44.9 mM in CGXII-glucose medium. Interestingly, each of the muteins carried at least one mutation in the carboxy-terminal part of LysC corresponding to the β-region of the protein known to control kinase activity.[6] Three LysC muteins were also characterized with respect to their inhibition profile by L-lysine (Figure S7, Supporting Information). Whereas the wild type enzyme is inhibited to half of its activity at about 1 mM L-lysine, the three muteins LysC-c77, LysC-c80, and LysC-c90 are virtually uninhibited at a concentration of 10 mM L-lysine.

To mutate HisG of *C. glutamicum*, we used a slightly different approach. The structure of the homologous ATP phosphoribosyltransferase of *Mycobacterium tuberculosis* in complex with the inhibitor L-histidine suggested that specific key residues are involved in histidine binding.[30] We defined equivalent residues in the HisG structure of *C. glutamicum* by homology-modeling using SWISS-MODEL.[22] Five mutagenic primer sets were designed and used for site-saturation mutagenesis of pCLTON2-encoded *hisG* (Table S5, Supporting Information). *C. glutamicum* cells carrying pSenLys were transformed with the saturation libraries. The libraries derived from the five mutagenic primer sets were analyzed separately via FACS, and in two libraries cells with increased fluorescence were present. 48 cells from the two positive libraries were isolated and further analyzed by culture fluorescence and product quantification. Sequencing, retransformation, and product quantification confirmed that 12 different HisG muteins resulted in significant L-histidine accumulation of up to 17 mM (Table 3). Again, three muteins were isolated and assayed for their inhibition by L-histidine (Figure S7, Supporting Information). Whereas the wild type mutein is inhibited to half of its activity at a concentration of 0.2 mM L-histidine, half of the activity is still present with the mutein HisG-GT233HQ at a concentration of 15 mM L-histidine. The muteins HisG-N216R and HisG-N216I retain almost full activity even at 30 mM L-histidine. Thus, our study confirms that selected key residues proposed by Cho et al.[30] interact with the allosteric inhibitor L-histidine on the one hand and provide muteins useful for overproduction on the other hand.

With a few exceptions, so far most of the key enzymes released from feedback control and used for production originate from random mutagenesis of whole cells. Our approach offers rapid access to new alleles, a large choice of which is useful for production purposes. This is of relevance because overriding the control of initial key enzymes may be decisive for product formation, as exemplified for the aspartate kinase of *C. glutamicum*, where different alleles yielded very different L-lysine accumulations.[31,12,32] Also our data on product accumulation obtained with the different allels of *lysC*, *argB* or *hisG* support this view. Of course, our approach on *in vivo* screening using metabolite sensors relies on the availability of appropriate proteins that regulate a promoter's transcriptional output in response to a small-molecule ligand. However, such proteins are naturally at hand because the synthesis of natural products like amino acids, nucleotides, or vitamins, for instance, is controlled by transcription factors. In fact, metabolite sensors for the transformation of cytosolic metabolite concentrations into a graded optical output have already been described for metabolites like L-methionine, L-serine, L-arginine, L-leucine, mevalonate, or *O*-acetyl-serine for *C. glutamicum* and *E. coli*.[13,14,33] The development of new sensor specificities will create more opportunities for isolating enzymes that are ideally suited to the cellular requirements for product formation.

METHODS

Strains, Plasmids, and Growth Conditions. *Corynebacterium glutamicum* was grown at 30 °C either on brain heart infusion medium (Difco) or in the MOPS-buffered minerals salt medium CGXII, which contained 4% glucose as carbon source.[34] When appropriate, media contained 25 μg mL^{-1} of kanamycin or 100 μg mL^{-1} of spectinomycin. Strains and plasmids are shown in Table 4. Genes were cloned as follows:

Table 4. Strains and Plasmids Used

strain/plasmid	relevant characteristics	origin
WT	Wild type, ATCC 13032, biotin-auxotroph	Culture Collection
WTΔlysEG	Wild type deleted of *lysEG*	Vrljic et al.[19]
WTΔargR	Wild type deleted of *argR*	Staebler et al.[35]
pSenLys	Encodes LysG, and its target promoter fused to *eyfp*; KanR	Binder et al.[13]
pSenLys-Spc	Encodes LysG, and its target promoter fused to *eyfp*; SpcR	this work
pAN6	Shuttle vector; KanR	Niebisch et al.[36]
pAN6-ArgB	pAN6 with *argB* (NC_006958.1: 1467889...1468842)	this work
pSenLys-PlysC	pSenLys with *lysC* (NC_006958.1: 268851...270636)	this work
pCLTON2	Shuttle vector; SpcR derived from pCLTON1	Lausberg et al.[37]
pCLTON2-hisG	pCLTON2 with *hisG* (NC_006958.1: 1467889...1468842)	this work
pUC18-argB	pUC18 with *argB* (NC_006958.1: 1467889...1468842)	this work
pUC18-lysC	pUC18 with *lysC* (NC_006958.1: 269371...270636)	this work
pET26b(+)-argB	pET26b(+) with *argB* (NC_006958.1: 1467889...1468842)	this work
pET26b(+)-lysC	pET26b(+) with *lysC* (NC_006958.1: 269371...270636)	this work
pET28b(+)-hisG	pET28b(+) with *hisG* (NC_006958.1: 1467889...1468842)	this work

argB into NdeI/EcoRI cleaved pAN6, *lysC* with its promoter region into XhoI/SalI prepared pSenLys, *hisG* into SmaI/SacI cleaved pCLTON2, *lysC* into BamHI/EcoRI cleaved pUC18, *argB* into NdeI/XhoI prepared pET26b(+), *lysC* into XhoI/NdeI cleaved pET26b(+), and *hisG* into BamHI/EcoRI digested pET28b(+). The correct integration of the inserts and their integrity were verified by sequencing.

Microfluidic Chip Cultivations and Live Cell Imaging. *Corynebacterium glutamicum* cells were inoculated from cryostocks into CGXII-glucose containing 25 μg mL^{-1} of kanamycin and incubated at 30 °C for 16 h.[34] These precultures were used to inoculate fresh cultures to an OD of

2, cultivated for 5 h, and then diluted to an OD of 0.5 for infusion into the chip (for the principle and design of the microfluidic single-cell chemostat, see Figure S3, Supporting Information). Subsequently, fresh CGXII-glucose was infused into the chip device at approximately 100 nL min^{-1} per channel using 1 mL syringes and high-precision syringe pumps for continuous media supply (neMESYS, Cetoni, Germany). After being grown for 20 h, CGXII-glucose supplemented with 2 mM Arg-Ala or Ala-Ala was applied (Bachem AG, Bubendorf, Switzerland).

The chip was mounted onto a motorized inverted microscope (Nikon Eclipse Ti) inside an in-house manufactured incubator for temperature and atmosphere control, as described previously.[15] Furthermore, the microscope was equipped with a focus assistant Nikon PFS compensating for thermal drift during long-term microscopy, and a heated Nikon Apo TIRF 100× Oil DIC N objective (ALA OBJ-Heater, Ala Scientific Instruments, USA). Phase contrast and fluorescence time lapse images of several cell arrays were captured every 15 min. Fluorescence images were recorded using an ANDOR LUCA R DL604 CCD camera with an exposure time of 200 ms. YFP was excited using a 300 W Xenon light source (Lamda DG-4 Sutter Instruments) at maximum intensity and using appropriate optical filters (excitation: HQ 500/20, dichroic: Q515, emission: HQ 535/30; Chroma). The settings were not changed between experiments to allow a direct comparison of fluorescence intensities. The final images were analyzed with the Nikon NIS Elements AR software package to determine cell size and fluorescence intensity. After cell division, one adjacent daughter cell was selected as the next cell of interest.

Error Prone PCR and Plasmid Library Construction. The genes *argB*, *lysC* and *hisG* were derived from genomic DNA of *C. glutamicum* ATCC13032 using KOD-polymerase (Novagen, Merck KGaA, Darmstadt, Germany). PCR products of *argB* and *lysC* were purified, digested with BamHI/EcoRI (Fermentas, Thermo Fisher Scientific, Waltham, MA, USA) and ligated into appropriately prepared pUC18. Error-prone PCR was performed using the Diversify kit (Clonetech, Saint-Germain-en-Laye, France) together with primers annealing 50 bp upstream and downstream of the target gene, respectively. Conditions were chosen to introduce between 2 and 9 mutations per kb, as given in the supplier's manual. Error prone PCR products of *argB* and *lysC* were purified and ligated via NdeI/EcoRI with pAN6 or via XhoI/SalI with pSenLys-PlysC, respectively. *hisG* PCR products were cloned via the SmaI/SacI sites into pCLTON2. Saturation libraries were constructed using QuikChange XL (Agilent, Santa Clara, CA 95051, USA) and saturating primers were ordered with NNK/MNN at the target position (LifeTechnologies GmbH, 64293 Darmstadt, Germany). The plasmids constructed are given in Figure S4 (Supporting Information). For library construction, electrocompetent *E. coli* DH5α cells were used. Cells were regenerated in LB medium and after regeneration inoculated into 15 mL of LB medium containing the appropriate antibiotic. After overnight cultivation, plasmid libraries were isolated from these cultures.

FACS and Library Screening. To enable sorting, *C. glutamicum*ΔargR pSenLys-Spc was transformed with the *argB* library in pAN6. The *lysC* library was directly established in pSenLysPlysC and used to transform *C. glutamicum* WT. The *hisG* library was established in pCLTON2 and used to transform *C. glutamicum* pSenLys. Cells were regenerated in BHI complex medium (Difco Laboratories Inc., Detroit, MI, USA) for 1 h at 30 °C and plated on BHI agar plates containing 25 μg mL^{-1} of kanamycin and 100 μg mL^{-1} of spectinomycin. Plates were incubated for 24 h at 30 °C and swept with 2 mL of CGXII-glucose.[34] The cell suspensions were stored as cryostocks containing 40% glycerol (w/v). Prior to FACS, CGXII-glucose precultures containing the appropriate antibiotics were inoculated from the cryostocks and then grown overnight, before being used to inoculate fresh cultures, which were grown up to OD 2. The culture containing the *argB* library received 1 mM IPTG, and the culture with the *hisG* library 250 ng mL^{-1} of anhydrotetracyclin. Approximately 22 ×10^6, 3 × 10^6, and 1 × 10^5 cells from strains, expressing *argB*, *lysC*, and *hisG* libraries, respectively, were subjected to the FACS analysis 4—6 h later. Cells emitting high fluorescence were spotted directly into 96 well plates, prefilled with 200 μL of CgXII and the appropriate antibiotics. Cultures grown after 48 h were further analyzed.

Immediately prior to FACS analysis, the cell suspensions were diluted to an optical density below 0.1 and analyzed by a FACS ARIA II high-speed cell sorter (BD Biosciences, Franklin Lakes, NJ, USA) using excitation/emission wavelength of 488/530 ± 20 nm and a sample pressure of 70 psi. Data were analyzed using BD DIVA 6.1.3 and FlowJo 7.6.5 software (Tree Star, Inc., Ashland, OR 97520). The electronic signal threshold was defined to exclude nonbacterial particles on the basis of forward versus side scatter areas. Electronic gating in the EYFP channel was set to exclude nonfluorescent cells. Noise level was defined by nonproducing *C. glutamicum* cells, expressing the wild-type allele of the specific target gene.

High-Throughput Cultivation and Analyses. High-throughput cultivation was done in 48-well Flowerplates (FPs; m2p-laboratories GmbH, Baesweiler, Germany) in 0.7 mL of minimal medium CGXII-4% glucose (CGXII-glucose) at 30 °C, 900 rpm and a throw of ø 3 mm. The specific geometry of the FPs ensures high mass-transfer performance and allowed them to be used together with the microcultivation system BioLector allowing online monitoring of growth and fluorescence.[38] For offline cultivations, FPs were cultivated on a Microtron high-capacity micro plate incubator operating at a shaker speed of 900 rpm and a throw of ø 3 mm (Infors AG, CH-4103 Bottmingen, Switzerland). Cells pregrown in CGXII medium were used as inocula for all cultivations. Amino acids were quantified as their *o*-phthaldialdehyde derivatives via high-pressure liquid chromatography as their fluorescent isoindole derivatives, as previously described.[13]

Protein Work. *N*-Acetyl-L-glutamate kinase (*argB*) and aspartate kinase (*lysC*) encoding genes were cloned into pET26b(+) via NdeI/XhoI or BamHI/EcoRI, respectively. Phosphoribosyl transferase encoding genes (*hisG*) were cloned into pET28b(+) via XhoI/NdeI. *E. coli* Bl21(DE3) was transformed with these plasmids and inoculated into 5 mL 2xYT. These precultures were used to inoculate fresh 2xYT (1:100) cultures, which were incubated for 3 h at 37 °C. IPTG was added (1 mM), and they were further incubated for 16 h at 25 °C. Cells were harvested, washed and disrupted in sonication buffer 20 mM Tris-HCl pH7.5, 150 mM NaCl (Branson Ultrasonics Corporation, Danbury, CT, USA). Crude extract supernatants derived from centrifugation (50 000 rpm, 4 °C, 1 h) were applied to Ni-NTA columns, and protein was eluted as recommended by the manufacturer (Qiagen, Hilden, Germany). Elution fractions were analyzed by SDS-PAGE, and concentrated using Amicon Ultra-4 30K centrifugal filters (Millipore Corporation, Billerica, MA01821).

Gel filtrations were performed on an Äkta-P900 System (GE Healthcare, Buckinghamshire, UK) equipped with a Superdex 200 10/300 GL column buffered in 20 mM HEPES, 150 mM NaCl, ± 10 mM L-arginine. UV absorbance was detected with a UPC-900 module, and data were analyzed with the Unicorn 5.01 software (Amersham Biosciences, Amersham, UK). The *N*-acetyl-L-glutamate kinase and aspartate kinase activity was essentially assayed as described by Haas and Leisinger[26] and Black and Wright,[39] respectively. Both are based on complex formation of the synthesized *N*-acetylglutamyl-phosphate or aspartyl-phosphate with Fe^{3+} ions and were scaled down for our purpose to a volume of 100 μL and performed in microtiter plates. Complex formation was determined at 540 nm (ε = 456 M^{-1} cm^{-1}). The phosphoribosyl transferase activity was essentially assayed as described by Ames.[40] Conditions were scaled down to a volume of 150 μL and performed in microtiter plates. Product formation was detected at 290 nm (ε = 3600 M^{-1} cm^{-1}).

Structure Modeling. Structural models of the *C. glutamicum* ArgB and ArgB-K47H were generated with SWISS-MODEL using the structural template of *P. aeruginosa* (PDB ID: 2BUF).

■ ASSOCIATED CONTENT

Supporting Information

A video showing fluorescence development in single cells. Figure S1 gives the dose−response curve of peptide addition. Figure S2 shows the microfluidic device used. Figure S3 shows the plasmids used. Figure S4 gives isothermal titration calorimetry information. Figure S5 shows the sequence alignments of different ArgB genes. Figure S6 gives selected inhibition kinetics for LysC and HisG proteins. Furthermore, tables are included giving the nucleotide exchanges of the alleles obtained and data on gel filtrations. This material is available free of charge via the Internet at http://pubs.acs.org.

■ AUTHOR INFORMATION

Corresponding Author

*E-mail: l.eggeling@fz-juelich.de.

Author Contributions

G.S., M.D., A.G., A.Y., and S.B. performed the experiments, D.K., M.N., C.N., and M.B. provided guidance for experimental set-ups, and L.E. and G.S. wrote the paper.

Notes

The authors declare no competing financial interest.

■ ACKNOWLEDGMENTS

The authors thank Marcus Schallmey for assistance interpretating the ArgB mutations. Support from the BMBF Grant 0315589A "Corynebacterium: improving flexibility and fitness for industrial production" is gratefully acknowledged.

■ REFERENCES

(1) Adrio, J. L., and Demain, A. L. (2010) Recombinant organisms for production of industrial products. *Bioeng. Bugs 1*, 116−131.

(2) Tsuruta, H., Paddon, C. J., Eng, D., Lenihan, J. R., Horning, T., Anthony, L. C., Regentin, R., Keasling, J. D., Renninger, N. S., and Newman, J. D. (2009) High-level production of amorpha-4,11-diene, a precursor of the antimalarial agent artemisinin *Escherichia coli*. *PLoS One 4*, e4489.

(3) Dunlop, M. J., Dossani, Z. Y., Szmidt, H. L., Chu, H. C., Lee, T. S., Keasling, J. D., Hadi, M. Z., and Mukhopadhyay, A. (2011) Engineering microbial biofuel tolerance and export using efflux pumps. *Mol. Syst. Biol. 7*, 487.

(4) Eggeling, L., Pfefferle, W., and Sahm, H. (2006) Amino Acids, in *Basic Biotechnology* (Radledge, C., Kristiansen, B., Eds.) pp 335−398, Cambridge University Press, Cambridge.

(5) Ikeda, M., Mitsuhashi, S., Tanaka, K., and Hayashi, M. (2009) Reengineering of a *Corynebacterium glutamicum* L-arginine and L-citrulline producer. *Appl. Environ. Microbiol. 75*, 1635−1641.

(6) Yoshida, A., Tomita, T., Kuzuyama, T., and Nishiyama, M. (2010) Mechanism of concerted inhibition of alpha2beta2-type hetero-oligomeric aspartate kinase from *Corynebacterium glutamicum*. *J. Biol. Chem. 285*, 27477−27486.

(7) Suter, P., and Rosenbusch, J. P. (1977) Asymmetry of binding and physical assignments of CTP and ATP sites in aspartate transcarbamoylase. *J. Biol. Chem. 252*, 8136−8141.

(8) Lee, K. H., Park, J. H., Kim, T. Y., Kim, H. U., and Lee, S. Y. (2007) Systems metabolic engineering of *Escherichia coli* for L-threonine production. *Mol. Syst. Biol. 3*, 149.

(9) Becker, J., Zelder, O., Hafner, S., Schroder, H., and Wittmann, C. (2011) From zero to hero—design-based systems metabolic engineering of *Corynebacterium glutamicum* for L-lysine production. *Metab. Eng. 13*, 159−168.

(10) Curran, K. A., Leavitt, J. M., Karim, A. S., and Alper, H. S. (2013) Metabolic engineering of muconic acid production in *Saccharomyces cerevisiae*. *Metab. Eng. 15*, 55−66.

(11) Hatley, M. E., Lockless, S. W., Gibson, S. K., Gilman, A. G., and Ranganathan, R. (2003) Allosteric determinants in guanine nucleotide-binding proteins. *Proc. Natl. Acad. Sci. U. S. A. 100*, 14445−14450.

(12) Chen, Z., Meyer, W., Rappert, S., Sun, J., and Zeng, A.-P. (2011) Coevolutionary analysis enabled rational deregulation of allosteric enzyme inhibition in *Corynebacterium glutamicum* for lysine production. *Appl. Environ. Microbiol. 77*, 4352−4360.

(13) Binder, S., Schendzielorz, G., Stabler, N., Krumbach, K., Hoffmann, K., Bott, M., and Eggeling, L. (2012) A high-throughput approach to identify genomic variants of bacterial metabolite producers at the single-cell level. *Genome Biol. 13*, R40.

(14) Mustafi, N., Grünberger, A., Kohlheyer, D., Bott, M., and Frunzke, J. (2012) The development and application of a single-cell biosensor for the detection of L-methionine and branched-chain amino acids. *Metab. Eng. 14*, 449−457.

(15) Grünberger, A., Paczia, N., Probst, C., Schendzielorz, G., Eggeling, L., Noack, S., Wiechert, W., and Kohlheyer, D. (2012) A disposable picolitre bioreactor for cultivation and investigation of industrially relevant bacteria on the single cell level. *Lab Chip 12*, 2060−2068.

(16) Cadwell, R. C., and Joyce, G. F. (2006) Mutagenic PCR. *CSH Protoc.*, DOI: 10.1101/pdb.prot4143 .

(17) Bellmann, A., Vrljic, M., Pátek, M., Sahm, H., Krämer, R., and Eggeling, L. (2001) Expression control and specificity of the basic amino acid exporter LysE of *Corynebacterium glutamicum*. *Microbiology 147*, 1765−1774.

(18) Tavori, H., Kimmel, Y., and Barak, Z. (1981) Toxicity of leucine-containing peptides in *Escherichia coli* caused by circumvention of leucine transport regulation. *J. Bacteriol. 146*, 676−683.

(19) Vrljic, M., Sahm, H., and Eggeling, L. (1996) A new type of transporter with a new type of cellular function: L-lysine export from *Corynebacterium glutamicum*. *Mol. Microbiol. 22*, 815−826.

(20) Ramon-Maiques, S., Fernandez-Murga, M. L., Gil-Ortiz, F., Vagin, A., Fita, I., and Rubio, V. (2006) Structural bases of feed-back control of arginine biosynthesis, revealed by the structures of two hexameric *N*-acetylglutamate kinases, from *Thermotoga maritima* and *Pseudomonas aeruginosa*. *J. Mol. Biol. 356*, 695−713.

(21) Xu, Y., Labedan, B., and Glansdorff, N. (2007) Surprising arginine biosynthesis: a reappraisal of the enzymology and evolution of the pathway in microorganisms. *Microbiol. Mol. Biol. Rev. 71*, 36−47.

(22) Arnold, K., Bordoli, L., Kopp, J., and Schwede, T. (2006) The SWISS-MODEL workspace: a web-based environment for protein structure homology modelling. *Bioinformatics 22*, 195−201.

(23) Fernandez-Murga, M. L., and Rubio, V. (2008) Basis of arginine sensitivity of microbial *N*-acetyl-L-glutamate kinases: mutagenesis and protein engineering study with the *Pseudomonas aeruginosa* and *Escherichia coli* enzymes. *J. Bacteriol. 190*, 3018−3025.
(24) Bornscheuer, U. T., Huisman, G. W., Kazlauskas, R. J., Lutz, S., Moore, J. C., and Robins, K. (2012) Engineering the third wave of biocatalysis. *Nature 485*, 185−194.
(25) Sakanyan, V., Petrosyan, P., Lecocq, M., Boyen, A., Legrain, C., Demarez, M., Hallet, J. N., and Glansdorff, N. (1996) Genes and enzymes of the acetyl cycle of arginine biosynthesis in *Corynebacterium glutamicum*: enzyme evolution in the early steps of the arginine pathway. *Microbiology 142*, 99−108.
(26) Haas, D., and Leisinger, T. (1975) *N*-Acetylglutamate 5-phosphotransferase of *Pseudomonas aeruginosa*. Purification and ligand-directed association-dissociation. *Eur. J. Biochem. 52*, 365−375.
(27) Shiio, I., Miyajima, R., and Sano, K. (1970) Genetically desensitized aspartate kinase to the concerted feedback inhibition in *Brevibacterium flavum*. *J. Biochem. 68*, 701−710.
(28) Mizukami, T., Hamu, A., Ikeda, M., Oka, T., and Katsumata, R. (1994) Cloning of the ATP phosphoribosyl transferase gene of *Corynebacterium glutamicum* and application of the gene to L-histidine production. *Biosci., Biotechnol., Biochem. 58*, 635−638.
(29) Ohnishi, J., Mitsuhashi, S., Hayashi, M., Ando, S., Yokoi, H., Ochiai, K., and Ikeda, M. (2002) A novel methodology employing *Corynebacterium glutamicum* genome information to generate a new L-lysine-producing mutant. *Appl. Microbiol. Biotechnol. 58*, 217−223.
(30) Cho, Y., Sharma, V., and Sacchettini, J. C. (2003) Crystal structure of ATP phosphoribosyltransferase from *Mycobacterium tuberculosis*. *J. Biol. Chem. 278*, 8333−8339.
(31) Cremer, J., Eggeling, L., and Sahm, H. (1991) Control of the lysine biosynthesis sequence in *Corynebacterium glutamicum* as analyzed by overexpression of the individual corresponding genes. *Appl. Environ. Microbiol. 57*, 1746−1752.
(32) Jetten, M. S., Follettie, M. T., and Sinskey, A. J. (1995) Effect of different levels of aspartokinase on the lysine production by *Corynebacterium lactofermentum*. *Appl. Microbiol. Biotechnol. 43*, 76−82.
(33) Tang, S. Y., and Cirino, P. C. (2011) Design and application of a mevalonate-responsive regulatory protein. *Angew. Chem. 50*, 1084−1086.
(34) Eggeling, L., and Bott, M. (2005) *Handbook of Corynebacterium glutamicum*, CRC Press Taylor & Francis Group, Boca Raton, FL.
(35) Stäbler, N., Oikawa, T., Bott, M., and Eggeling, L. (2011) *Corynebacterium glutamicum* as a host for synthesis and export of D-amino acids. *J. Bacteriol. 193*, 1702−1709.
(36) Bott, M., and Niebisch, A. (2005) *Respiratory Energy Metabolism*, CRC Press Taylor & Francis Group, Boca Raton, FL.
(37) Lausberg, F., Chattopadhyay, A. R., Heyer, A., Eggeling, L., and Freudl, R. (2012) A tetracycline inducible expression vector for *Corynebacterium glutamicum* allowing tightly regulable gene expression. *Plasmid 68*, 142−147.
(38) Huber, R., Ritter, D., Hering, T., Hillmer, A.-K., Kensy, F., Müller, C., Wang, L., and Büchs, J. (2009) Robo-Lector—a novel platform for automated high-throughput cultivations in microtiter plates with high information content. *Microb. Cell Fact. 8*, 42.
(39) Black, S., and Wright, N. G. (1955) beta-Aspartokinase and beta-aspartyl phosphate. *J. Biol. Chem. 213*, 27−38.
(40) Ames, G. F., Noel, K. D., Taber, H., Spudich, E. N., Nikaido, K., and Afong, J. (1977) Fine-structure map of the histidine transport genes in *Salmonella typhimurium*. *J. Bacteriol. 129*, 1289−1297.

Acta Crystallographica Section D
Biological Crystallography
ISSN 0907-4449

Structure of the transcriptional regulator LysG of *Corynebacterium glutamicum* in complex with its effector L-arginine

G. Schendzielorz,[a,x] F. Syberg,[b,x] C. Schlicker,[b] M. Bott,[a] L. Eggeling[a]* and E. Hofmann [b]*

[a]Institute for Bio- and Geosciences IBG-1: Biotechnology, Forschungszentrum Juelich GmbH, D-52425 Juelich, and [b]Proteinkristallographie, Lehrstuhl fr Biophysik, Ruhr-Universitt Bochum, D-44780 Bochum. Correspondence e-mail: l.eggeling@fz-juelich.de, eckhard.hofmann@bph.ruhr-uni-bochum.de

LysR type transcriptional regulators represent the largest group of one-component transcriptional regulators in bacteria. With few exceptions, activity is modulated by co-inducers, mostly intermediates of affected metabolic pathways. LysG from *C. glutamicum* modulates transcription of the basic amino acid exporter LysE in response to intracellular arginine, lysine and histidine concentrations. The structures of full-length LysG in the free form (LysG) and together with bound effector L-arginine (LysG+Arg) have been characterized by X-ray diffraction. As shown for other LTTRs, LysG forms a tetramer by two interlaced V-shaped dimers consisting of protomers A+B and X+Y, thereby featuring the "dimer of dimers" conformation. Two different protomer conformations, a compact one and an extended one are present in the asymmetric unit. Helix α_6 of the compact protomer's RD interacts with the linker helix of the same protomer, but helix α_6 of the extended protomer interacts with the "winged part" of the wHTH motif of the compact protomer. In the LysG+Arg structure we discovered one arginine molecule in each inducer binding cleft of the extended protomers, which are mainly coordinated by negatively charged side chains of neighboring residues. Comparing the structure of LysG and LysG+Arg, we observed a tilt of helix α_6 when arginine is bound, which might present a communication pathway from the effector binding to the DNA-binding domain, thereby changing its DNA-binding behavior.

1. Introduction

LysR type transcriptional regulators (LTTRs) represent the largest group of one-component transcriptional regulators in bacteria with over 40.000 potential members, listed in the protein sequence analysis & classification database (IPR000847). Often multiple paralogues exist in one organism, for example 46 members in *Escherichia coli* K-12 strain MG1655, 10 members in *Corynebacterium glutamicum* ATCC13032 (Brinkrolf et al., 2007) and 4 members in *Mycobacterium tuberculosis*. Functional orthologs are found in Archaea and Eukaryota, apparently acquired by horizontal gene transfer (Prez-Rueda et al., 2001).LTTRs are global transcriptional activators or repressors of one or more target genes or operons (Hernndez-Lucas et al., 2008; Heroven et al., 2006). With few exceptions, modulation of activity depends on co-inducers, mostly intermediates of affected metabolic pathways (Celis, 1999; Picossi et al., 2007).

The LysR type transcriptional regulator LysG from *C. glutamicum* controls transcription of the basic amino acid exporter LysE, which is divergently transcribed from the chromosome as typical for many LTTRs. At high intracellular concentrations, lysine, arginine, histidine and citrulline act as co-inducers of LysG and activate transcription of lysE, resulting in export of excess lysine and arginine (Bellmann et al., 2001; Vrljic et al., 1996). This serves under natural conditions to balance the intracellular amino acids concentrations in case where peptides are taken up, and is of particular relevance for producing L-lysine with *C. glutamicum* since mutants of this bacterium are used to produce L-lysine on a scale of more than 1,5 Mill tons/year (Becker et al., 2012). In addition, this apathogenic bacterium serves as a model organism for M. tuberculosis to study its cell wall structure and lipid synthesis (Gande et al., 2004; Mohiman et al., 2012).

Most LTTRs are about 300 amino acids in size and share a conserved overall structure. The N-terminal part (residues 1-60) forms a DNA-binding domain (DBD) with the classical and strongly conserved Helix-turn-Helix (HTH) motif (Brennan, 1993; Brennan et al., 1989). This is linked via a linker helix (residues 60-90) to the effector-binding domains (EBD-I and EBD-II, residues 90-290), which are separated by a hinge region. In this hinge region, composed of two β-strands, the co-inducer binding site is formed, as observed in partial structures of several regulatory domains (Ezezika et al., 2007a; Stec et al., 2006; Tyrrell et al., 1997). In consistence with the broad spectrum of interacting co-inducers, conservation in the hinge region is low. The first full-length structure of a LTTR was solved by Muraoka et al. (2003) for CbnR, which induces transcription of chlorocatechol-degradative genes in *Ralstonia eutropha* (Ogawa et al., 1999). The functionally active form of CbnR is a tetramer, formed by two homodimers. In each dimer two different forms of the monomer, a compact and extended

one, are found, resulting in an asymmetrical ellipsoidal shape of the tetramer. Two other full-length structures for ArgP (Zhou et al., 2010) and TsaR (Monferrer et al., 2010) form tetramers with this general architecture. In contrast, a tetrameric variant with a slightly different architecture was reported for AphB (Taylor et al., 2012) and two octameric structures were reported for CrgA (Sainsbury et al., 2009) and BenM (Ruangprasert et al., 2010).

Commonly LTTRs bind to their target promoter at two adjacent binding sites, located at -35 to +20 bp (regulatory binding site, RBS) and -40 to -20 bp (activation binding site, ABS) (Leveau et al., 1994; McFall et al., 1998; Ogawa et al., 1999; Wang et al., 1995; Wang et al., 1992). In case of the tetramer forming species, each binding site is occupied by one homodimer and interaction of both dimers forms the functional active tetramer. In absence of effectors, binding of one homodimer to the ABS is weak and the tetrameric assembly causes strong DNA bending from 50 to 100 at a region between RBS and ABS (Lochowska et al., 2001; Porra et al., 2007). Interaction with effectors makes binding to the ABS stronger (Monferrer et al., 2010; Tropel et al., 2004), relaxes DNA bending (Hryniewicz et al., 1991; Keulen et al., 1998; Ogawa et al., 1999; Wang et al., 1995) and facilitates binding of RNAP (Lee et al., 1997), thus initiating transcription activation. To date, only one full-length LTTR-structure in complex with soaked co-inducer was solved for TsaR (Monferrer et al., 2010). Given the presence of 11 TSA molecules in the unit cell with at least 2 of them located in the potential co-inducer binding cleft and nearly no structural differences between the model for TSA-bound and unbound form, the nature of LTTR/effector interaction is still a matter of discussion.

2. Materials & Methods

2.1. Cloning, expression and purification of LysG

The lysG encoding sequence (NCgl1215) was amplified from genomic DNA of *Corynebacterium glutamicum* ATCC13032 with primers introducing NdeI/EcoRI sites. After digestion with NdeI/EcoRI, the fragment was cloned into equally cut pET28b(+). The correct integration of the insert and his integrity was verified by sequencing. *E. coli* Bl21(DE3) was transformed with this plasmid and one single colony was inoculated into 5 ml 2xYT, containing 50 g ml-1 kanamycine. This pre-culture was used to inoculate a fresh 2xYTKan50 culture (1:100), which was incubated for 3 h at 37 C. IPTG was added (1 mM), and further incubation was done for 16 h at 25 C. Cells were harvested, washed in buffer (50 mM Sorensen Phosphate pH8, 300 mM NaCl, 10 mM imidazole and 0.3 mM DTT) and disrupted by sonication (Branson Ultrasonics Corporation, Danbury, CT, USA). Crude extract supernatant derived from centrifugation (230.000 xg, 4 C, 1 h) was mixed with 5 ml Ni-NTA beads (Qiagen, Hilden, Germany) and incubated for 1 h at 4 C. This mixture was applied to a gravity-flow column, equilibrated in 50 mM Sorensen Phosphate pH8, 300 mM NaCl, 40 mM imidazole, 0.3 mM DTT. Column was washed with 4 volumes of buffer and Protein was eluted with 50 mM Sorensen Phosphate pH8, 300 mM NaCl, 250 mM imidazole, 0.3 mM DTT. Purest fractions were determined by SDS-PAGE, pooled and dialyzed over night in 20 mM Tris-HCl pH8, 500 mM NaCl, 0.1 mM DTT. The protein was concentrated to 10 mg ml-1 using Amicon Ultra-4 30K centrifugal filters (Millipore Corporation, Billerica, MA01821).

2.2. Gelfiltrations

Gel filtrations were performed on an kta-P900 System (GE Healthcare, Munich) equipped with a Superdex 200 10/300 GL column and a UPC-900 detection unit. The column was buffered in 50 mM Sorensen Phosphate pH8, 150 mM NaCl and calibrated with the Gel Filtration Markers Kit (MWGF200, Sigma-Aldrich, Deisenhofen) as recommended by the manufacturer. Data were analyzed with the Unicorn 5.01 software (GE Healthcare, Munich)

2.3. Crystallization, structure determination and refinement

Initial crystals for LysG were obtained by nanodrop (100 nl+100 nl) crystallization with a Phoenix crystallization robot (Art Robbins Instruments, Sunnyvale) using Nextal crystallization screens (Qiagen, Hilden). Effector-free LysG was crystallized in hanging drop plates by mixing 1l reservoir (17.5% PEG4000, 0.1 M Ammoniumsulfate, 0.1 M Tris-HCl pH8.0) and 1l of LysG (4.5 mg/ml) at 291 K. A crystal with a size of 100 m3 was transferred to reservoir solution supplied with 20% glycerol for cryo protection. A diffraction data set was collected at ESRF (European Synchrotron Radiation Facility) beamline ID29 at wavelength 1.044 Å and 100 K. Co-crystallization of LysG with the effector arginine was facilitated by pre-incubation (15 min, 291 K) of 10 mM effector with 0,34 mM protein solution. A LysG+Arg crystal was harvested directly from the screen MbClass II C2 (0.1 M NaCl, 0.1 M Tris ph8.5, 30% (v/v) PEG400) and was cry protected by addition of 15% saccharose. Diffraction data were collected at ESRF beamline BM30A at wavelength 0.978 Å and 100 K. XDS (Kabsch2010) and XSCALE (Kabsch2010) were used for data processing and scaling. For the calculation of Rfree, 5% of the data were randomly assigned. The crystal structure of ArgP from *Mycobacterium tuberculosis* (PDB ID: 3ISP) was used as search model for molecular replacement using Phaser (Adams et al., 2010). The structure of LysG was used as search model for LysG+Arg. The structures were manually improved in Coot (Emsley et al., 2004) and automatically refined in Phenix (Adams et al., 2010). Models were deposited at the PDB with accession codes XXXX for LysG wt XXXX and for LysG+Arg. The interaction interfaces were calculated using the PISA server (Krissinel et al., 2007).

3. Results and discussion

3.1. Structure of LysG and LysG+L-Arginine

We were able to solve the structure of full length LysG both in the free form (LysG) and together with bound effector L-Arginine (LysG+Arg) at 2.9 Å and 3.3 Å respectively. Several side chains, especially in flexible loop regions and water molecules, could not be assigned due to missing electron den-

sity. Table 1 summarizes the crystallographic data and refinement statistics for both structures (table 1). Several side chains, especially in flexible loop regions and water molecules, could not be assigned due to missing electron density.

3.2. Protomer structure

LysG shows the typical features of LTTRs (figure 1). The highly conserved N-terminal DNA-binding domain consists of 3 α-helices and 2 β-sheets. Helices α_2 and α_3 and β-sheets β_1 and β_2 compose a winged helix-turn-helix (wHTH) motif (amino acid residues 18-58). Helix α_3, the so-called recognition helix (amino acid residues 29-43), is responsible for DNA-interaction by binding into the major groove of the DNA double helix (Aravind et al., 2005). The "β-sheet wing" is constructed by the amino acid residues 44-58. The residues Leu 9, Ile 12, Phe 18, Val 31 and Val 36 form a hydrophobic core of the three α-helices. The DNA-Binding domain is connected to the regulatory domain via a linker helix (amino acid residues 59-82 / 59-86 with respect to the protomer conformation). C-terminally of the linker helix lies the regulatory domain. It is about 200 amino acid long and is composed of the regulatory domains I and II (RDI, RDII), which display a Rossmann fold topology. Two antiparallel β-strands form the hinge region which connects RDI and RDII. This cavity was shown to exhibit the effector binding pocket (Ezezika et al., 2007a; Monferrer et al., 2010).

3.3. Different protomers in the asymmetric unit

Two different protomer conformations can be found in the asymmetric unit (figure 2). They are defined by a hinge region (amino acid residues 55-58) between the N-terminal DNA-binding domain and the C-terminal regulatory domain, right above the linker helix. The linker helix (59-82) of the compact protomer is slightly shorter than the linker helix (59-86) of the extended protomer. The angle between the regulatory domain and the linker helix, measured between helix $\alpha_1$0 in the RD and the linker helix, is 80 in the compact and 198 in the extended protomer. A similar dimer asymmetry has been reported for the other known LTTR structures (Monferrer et al., 2010; Muraoka et al., 2003; Ruangprasert et al., 2010; Sainsbury et al., 2009; Taylor et al., 2012; Zhou et al., 2010). In our LysG-Arg structure, only the effector-binding pocket of the extended monomer is occupied by an arginine molecules, whereas the pocket of the compact monomer is empty. The interaction surface area of the two protomers is 1698 Å^2. One part of this contact area is created by helix α_3 and the "wing" motif of the DNA-binding domain of the compact protomer and the lower part of RDI of the extended protomer (319 Å^2). The main contact is formed by a hydrophobic interface of 1379 Å^2 between the antiparallel linker helices of the compact and extended protomers, involving Val 62, Leu 63 and Met 70. This tail to tail arrangement of the dimeric DNA-binding domain leads to a V-shaped dimer, in which the recognition helices are separated by 28 Å. The regulatory domains of the compact and extended dimer superpose very well with an rms deviation of 0.59 Å. The structures of the compact and extended regulatory domain differ slightly in the flexible loop region from amino acid residue 191-196. Furthermore the orientation of helix α_6, second helix of the regulatory domain, varies in the compact and extended protomers RDs. It is tilted 8 towards its RDs inducer binding cavity, with respect to the orientation of helix α_6 of the compact protomer (figure 3). Helix α_6 of the compact protomer's RD interacts with the linker helix of the same protomer, but helix α_6 of the extended protomer interacts with the winged part of the wHTH motif of the compact protomer via a 240 Å big interaction interface (figure 4). This arrangement could represent a communication between the IBC and the DNA-Binding motif via the interaction of helix α_6 of the extended protomer and the wHTH of the compact protomer.

3.4. Tetramer structure

In size exclusion chromatography, LysG elutes as a peak of molecular mass of 158 kDa. Based on the mass of 34 kDa deduced from the sequence, this indicates a tetrameric assembly of LysG in solution. The tetramer is formed by two interlaced V-shaped dimers consisting of protomers A+B and X+Y, thereby featuring the "dimer of dimers" conformation, shown for other LTTRs, like CbnR, TsaR or the PA01-protein, a putative LTTR from Pseudomonas aeruginosa (Knapik AA, n/a; Monferrer et al., 2010; Muraoka et al., 2003). The tetramer dimensions are 120 Å x 80 Å x 50 Å. Protomers A and X, respectively B and Y are symmetric copies of the compact protomer and the extended protomer with bound L-arginine. The dimers facing in the opposite direction. Therefore the RDI and RDII of the compact and extended protomer of the two opposing dimers contact each other in a head-to-tail arrangement. Contact is made via two hydrophobic patches, resulting in a total dimer-dimer interface area of 1450 Å^2 (figure 5). One hydrophobic patch in the RDI of the compact protomer A (amino acid residues Leu 99-Leu 122) contacts a hydrophobic patch in the RDII of the extended protomer Y (Val 213-Leu 230), exhibiting an interface area of 375 Å^2.The second hydrophobic interaction is constructed via a hydrophobic patch in the RDII of the compact protomer A (amino acid residues Val 186-Pro 192 and Val 213-Val 16) and an hydrophobic patch at the RDI of the extended protomer Y (Leu 99, Val 106-Val 110 and Leu 118-Leu 122), creating an interface area of 350 Å^2. The interface area of opposing protomers therefore is 725 Å^2. The compact protomers A and X exhibit two small interfaces with a total area of 173 Å^2 because of an interleaved design of the tetramer. This typical ellipsoidal LTTR conformation enables the tetramer to expose all four DBD on one side of the tetramer, thereby facilitating one dimer to bind the DNA's Recognition Binding Site (RBS), whereas the other dimer binds the Activation Binding Site (ABS). The crystallographic two fold axis of the dimer of dimers tetramer is located at the central cavity of the tetramer. Additionally there is a local rotational symmetry of the linker helices and the DNA-Binding domain in the dimer of the compact and extended protomer.

3.5. Comparison of LysG+Arg with LysG

Beneath the co-crystallization experiments which lead to the structure of LysG with L-arginine coordinated in the IBC, we furthermore were successful in solving the structure of LysG without bound effector molecule. The structure of LysG without L-arginine is essentially the same as the LysG+Arg structure described above. The rms deviation of the LysG and the LysG+Arg structure is 0.907 Å (figure 6). In 3.3 we described different angles of α-helix 6 in the compact and extended protomers. This difference also occurs in comparison of the extended protomers of the arginine-free and the arginine-bound LysG structure. In the arginine-free structure the side chains of amino acid residues Asp 124 and Glu 125 of the extended protomer point away from the inducer binding pocket. In the LysG+Arg structure, the side chains of Asp 124 and Glu 125 are pointing towards the inducer binding pocket, thereby coordinating the amide group of the effector L-arginine (figure 7). As a result the extended protomers α-helix 6 of the effector-bound structure is tilted 8 in comparison with the extended protomers α-helix 6 of the effector-free structure. Figure 8 shows a superposition of all four types of protomers observed in our two crystal structures. The movement of helix 6 is observed only in the extended protomer with bound effector. The induced fit movement seems to be the only significant structural change, which communicates effector-binding to the DNA-Binding domain of its dimers compact protomer.

3.6. Comparison of the tetrameric TsaR, ArgP , CbnR and PA-01 with LysG

Although CbnR, PA-01, TsaR and ArgP exhibit the same ellipsoidal tetrameric "dimer of dimers" conformation as LysG, there are differences in the arrangement of the protomers. This affects the whole tetrameric structure. PA-01 is the most compact tetramer, thereby displaying the biggest distance between the dimeric DNA-Binding domains (135 Å), resulting in a relatively small central cavity. Opposing protomers contact each others RDs in a head to tail manner. Each protomer contacts the other three protomers. The dimeric V shows the smallest opening angle of the discussed LTTRs. The linker helices interface is relatively small. As a consequence of the tight dimeric V-conformation the RD of the compact and opposing extended protomer exhibit a big interaction interface of 781 Å^2. In contrast, the LysG tetramer is more loose. Its dimeric DNA-Binding domains are 119 Å apart, thereby the central cavity is widened. The compact protomers contact the three other protomers, but as a result of the "opening" the extended protomers show no contact interface comparable to the PA-01 tetramer. RDI of the compact protomer interacts with RDII of the extended protomer and vice versa, but the interaction interfaces of the compact protomers are drastically reduced to 173 Å^2. The dimeric DNA-Binding domains of the tetrameric CbnR are 116 Å apart. The central cavity has nearly the same dimension as in LysG. Like LysG the extended protomers have no contact interface to each other. The compact protomers contact each other mostly over their RDII creating a contact interface of 840 Å^2. The TsaR and the ArgP tetramer (**Zhou2009**) show the smallest distance between the dimeric DNA-Binding domains (both 110 Å). Especially the TsaR dimer looks more like a "check mark" than a "V", as a result the TsaR central cavity is a large tunnel, the tetrameric structure is quite loose and the compact protomers have no interacting interface. Each protomer contacts just the two conformationally different protomers (figure 9).

3.7. Arginine coordination

By using relatively low effector concentrations (10 mM) we were able to solve the structure with just one effector molecule bound within each of the inducer binding sites (IBC) of the two extended protomers in the asymmetric unit. No electron density for arginine was observed in the IBC of the compact protomer, pointing towards a lower effector affinity. This is in contrast to the situation of the only other known full length LTTR structure with effector, TsaR (3FXU) (Monferrer2010). In this structure, eleven molecules of p-Toluenesulfonate (TSA) were identified within each TsaR dimer, two of which are found in both IBCs of the extended and compact protomer. The very high effector concentration used in this study could have masked the IBC affinity differences and lead to the probably artificially high number of binding sites (Monferrer et al., 2010). In our LysG+Arg structure, the arginine molecule is mainly coordinated by negatively charged side chains of neighboring residues. (figure 10) Asp 193 forms a H-bond to the arginine amide group. On the other side the side chain nitrogen atom ND1 of His 161 is in close contact (3.37 Å) with arginine carboxy group. The guanidinium group of arginine is coordinated mostly by salt-bridges. Oxygen atom OD2 of Asp 97 forms a H-bond 2.23 Å with the arginine side chain secondary amine NE and is also within salt-bridge distance (3.0 Å) of the arginine primary amine NH1. Furthermore NH1 is coordinated by the side chain oxygen OE2 of Glu 125 which is located 3.78 Å aside. The side chain oxygen OD1 of Asp 124 forms a salt-bridge with the arginine side chain primary amine NH2 (3.78 Å). The positively charged amide group is coordinated by the three negatively charged side chains of amino acid residues Asp 91, Asp 124 and Glu 125. Given this effector coordination, the IBC should be also accessible for lysine and histidine, which are proven to act as effectors of LysG in physiological experiments (Bellmann et al., 2001; Vrljic et al., 1996). Due to the high pK value, arginine has a more positive partial charge than the side chains of lysine and histidine, and thereby may display a higher binding affinity to the negatively charged binding pocket.

4. Conclusion

We did not detect major differences in tetramer assembly upon binding of the effector L-arginine. Both LysG and LysG+Arg tetramers can be superposed with an rms deviation of 0.907 Å (1160 Cα atoms). Similarly, for TsaR nearly identical tetramer structures have been found for both effector-bound and effector-free structures (Monferrer2010). The fact that we do not see any changes upon effector binding does not support the proposed models of conformational changes for LTTR activation (Ezezika et al., 2007b; Monferrer et al., 2010). These models predict a modulation of tetramer packing upon effector bind-

ing, resulting in modification of the distance between the DNA-binding motifs. Most likely, the observed large differences the distance of the DNA binding domains reflect the structural variability of different LTTR proteins, rather than dynamic variations upon activation of a single LTTR. Instead, the observed tilt of Helix 6 might present a communication pathway from the effector binding to the DNA-binding domain. Effector-binding could be signaled to the DNA-binding domain, thereby changing its DNA-binding behavior. Ultimately, a complete model of LTTR activation will most likely require structural information on the ternary complex of LTTR, effector and target DNA. Experiments in this direction are underway in our laboratories.

5. References

Adams, Paul D. et al. (2010). "PHENIX: a comprehensive Python-based system for macromolecular structure solution." eng. In: *Acta Crystallogr D Biol Crystallogr* 66.Pt 2, pp. 213–221 (cit. on p. 2).

Aravind, L., Vivek Anantharaman, Santhanam Balaji, M. Mohan Babu, and Lakshminarayan M Iyer (2005). "The many faces of the helix-turn-helix domain: transcription regulation and beyond." eng. In: *FEMS Microbiol Rev* 29.2, pp. 231–262 (cit. on p. 3).

Becker, Judith and Christoph Wittmann (2012). "Bio-based production of chemicals, materials and fuels -Corynebacterium glutamicum as versatile cell factory." eng. In: *Curr Opin Biotechnol* 23.4, pp. 631–640 (cit. on p. 1).

Bellmann, A., M. Vrljic, M. Ptek, H. Sahm, R. Krmer, and L. Eggeling (2001). "Expression control and specificity of the basic amino acid exporter LysE of Corynebacterium glutamicum." eng. In: *Microbiology* 147.Pt 7, pp. 1765–1774 (cit. on pp. 1, 4).

Brennan, R. G. (1993). "The winged-helix DNA-binding motif: another helix-turn-helix takeoff." eng. In: *Cell* 74.5, pp. 773–776 (cit. on p. 1).

Brennan, R. G. and B. W. Matthews (1989). "The helix-turn-helix DNA binding motif." eng. In: *J Biol Chem* 264.4, pp. 1903–1906 (cit. on p. 1).

Brinkrolf, Karina, Iris Brune, and Andreas Tauch (2007). "The transcriptional regulatory network of the amino acid producer Corynebacterium glutamicum." eng. In: *J Biotechnol* 129.2, pp. 191–211 (cit. on p. 1).

Celis, R. T. (1999). "Repression and activation of arginine transport genes in Escherichia coli K 12 by the ArgP protein." eng. In: *J Mol Biol* 294.5, pp. 1087–1095 (cit. on p. 1).

Emsley, Paul and Kevin Cowtan (2004). "*Coot*: model-building tools for molecular graphics". In: *Acta Crystallographica Section D* 60.12 Part 1, pp. 2126–2132 (cit. on p. 2).

Ezezika, Obidimma C., Sandra Haddad, Todd J. Clark, Ellen L. Neidle, and Cory Momany (2007a). "Distinct effector-binding sites enable synergistic transcriptional activation by BenM, a LysR-type regulator." eng. In: *J Mol Biol* 367.3, pp. 616–629 (cit. on pp. 1, 3).

Ezezika, Obidimma C., Sandra Haddad, Ellen L. Neidle, and Cory Momany (2007b). "Oligomerization of BenM, a LysR-type transcriptional regulator: structural basis for the aggregation of proteins in this family." eng. In: *Acta Crystallogr Sect F Struct Biol Cryst Commun* 63.Pt 5, pp. 361–368 (cit. on p. 4).

Gande, Roland, Kevin J C Gibson, Alistair K Brown, Karin Krumbach, Lynn G Dover, Hermann Sahm, Susumu Shioyama, Tadao Oikawa, Gurdyal S Besra, and Lothar Eggeling (2004). "Acyl-CoA carboxylases (accD2 and accD3), together with a unique polyketide synthase (Cg-pks), are key to mycolic acid biosynthesis in Corynebacterianeae such as Corynebacterium glutamicum and Mycobacterium tuberculosis." eng. In: *J Biol Chem* 279.43, pp. 44847–44857 (cit. on p. 1).

Hernndez-Lucas, I., A. L. Gallego-Hernndez, S. Encarnacin, M. Fernndez-Mora, A. G. Martnez-Batallar, H. Salgado, R. Oropeza, and E. Calva (2008). "The LysR-type transcriptional regulator LeuO controls expression of several genes in Salmonella enterica serovar Typhi." eng. In: *J Bacteriol* 190.5, pp. 1658–1670 (cit. on p. 1).

Heroven, Ann Kathrin and Petra Dersch (2006). "RovM, a novel LysR-type regulator of the virulence activator gene rovA, controls cell invasion, virulence and motility of Yersinia pseudotuberculosis." eng. In: *Mol Microbiol* 62.5, pp. 1469–1483 (cit. on p. 1).

Hryniewicz, M. M. and N. M. Kredich (1991). "The cysP promoter of Salmonella typhimurium: characterization of two binding sites for CysB protein, studies of in vivo transcription initiation, and demonstration of the anti-inducer effects of thiosulfate." eng. In: *J Bacteriol* 173.18, pp. 5876–5886 (cit. on p. 2).

Keulen, G. van, L. Girbal, E. R. van den Bergh, L. Dijkhuizen, and W. G. Meijer (1998). "The LysR-type transcriptional regulator CbbR controlling autotrophic CO2 fixation by Xanthobacter flavus is an NADPH sensor." eng. In: *J Bacteriol* 180.6, pp. 1411–1417 (cit. on p. 2).

Knapik AA Tkaczuk KL, Chruszcz M Wang S Zimmerman MD Cymborowski M Skarina T Kagan O Savchenko A Edwards AM Joachimiak A Bujnicki JM Minor W (n/a). "Crystal structure of pa01 protein, putative lysr family transcriptional regulator from pseudomonas aeruginosa." In: *No recorded citation in PubMed* n/a, n/a (cit. on p. 3).

Krissinel, Evgeny and Kim Henrick (2007). "Inference of Macromolecular Assemblies from Crystalline State". In: *Journal of Molecular Biology* 372.3, pp. 774 –797 (cit. on p. 2).

Lee, Y., H. Lee, J. Yim, and D. Hwang (1997). "The binding of two dimers of IciA protein to the dnaA promoter 1P element enhances the binding of RNA polymerase to the dnaA promoter 1P." eng. In: *Nucleic Acids Res* 25.17, pp. 3486–3489 (cit. on p. 2).

Leveau, J. H., W. M. de Vos, and J. R. van der Meer (1994). "Analysis of the binding site of the LysR-type transcriptional activator TcbR on the tcbR and tcbC divergent promoter sequences." eng. In: *J Bacteriol* 176.7, pp. 1850–1856 (cit. on p. 2).

Lochowska, A., R. Iwanicka-Nowicka, D. Plochocka, and M. M. Hryniewicz (2001). "Functional dissection of the LysR-type CysB transcriptional regulator. Regions important for

DNA binding, inducer response, oligomerization, and positive control." eng. In: *J Biol Chem* 276.3, pp. 2098–2107 (cit. on p. 2).

McFall, S. M., S. A. Chugani, and A. M. Chakrabarty (1998). "Transcriptional activation of the catechol and chlorocatechol operons: variations on a theme." eng. In: *Gene* 223.1-2, pp. 257–267 (cit. on p. 2).

Mohiman, Niloofar, Manuela Argentini, Sarah M Batt, David Cornu, Muriel Masi, Lothar Eggeling, Gurdyal Besra, and Nicolas Bayan (2012). "The ppm operon is essential for acylation and glycosylation of lipoproteins in Corynebacterium glutamicum." eng. In: *PLoS One* 7.9, e46225 (cit. on p. 1).

Monferrer, Dominique, Tewes Tralau, Michael A Kertesz, Ina Dix, Maria Sol, and Isabel Usn (2010). "Structural studies on the full-length LysR-type regulator TsaR from Comamonas testosteroni T-2 reveal a novel open conformation of the tetrameric LTTR fold." eng. In: *Mol Microbiol* 75.5, pp. 1199–1214 (cit. on pp. 2–4).

Muraoka, Shin, Rumi Okumura, Naoto Ogawa, Takamasa Nonaka, Kiyotaka Miyashita, and Toshiya Senda (2003). "Crystal structure of a full-length LysR-type transcriptional regulator, CbnR: unusual combination of two subunit forms and molecular bases for causing and changing DNA bend." eng. In: *J Mol Biol* 328.3, pp. 555–566 (cit. on pp. 1, 3).

Ogawa, N., S. M. McFall, T. J. Klem, K. Miyashita, and A. M. Chakrabarty (1999). "Transcriptional activation of the chlorocatechol degradative genes of Ralstonia eutropha NH9." eng. In: *J Bacteriol* 181.21, pp. 6697–6705 (cit. on pp. 1, 2).

Picossi, Silvia, Boris R Belitsky, and Abraham L Sonenshein (2007). "Molecular mechanism of the regulation of Bacillus subtilis gltAB expression by GltC." eng. In: *J Mol Biol* 365.5, pp. 1298–1313 (cit. on p. 1).

Porra, Odil, Manuel Garca-Jaramillo, Eduardo Santero, and Fernando Govantes (2007). "The LysR-type regulator AtzR binding site: DNA sequences involved in activation, repression and cyanuric acid-dependent repositioning." eng. In: *Mol Microbiol* 66.2, pp. 410–427 (cit. on p. 2).

Prez-Rueda, E. and J. Collado-Vides (2001). "Common history at the origin of the position-function correlation in transcriptional regulators in archaea and bacteria." eng. In: *J Mol Evol* 53.3, pp. 172–179 (cit. on p. 1).

Ruangprasert, Ajchareeya, Sarah H Craven, Ellen L Neidle, and Cory Momany (2010). "Full-length structures of BenM and two variants reveal different oligomerization schemes for LysR-type transcriptional regulators." eng. In: *J Mol Biol* 404.4, pp. 568–586 (cit. on pp. 2, 3).

Sainsbury, Sarah, Laura A Lane, Jingshan Ren, Robert J Gilbert, Nigel J Saunders, Carol V Robinson, David I Stuart, and Raymond J Owens (2009). "The structure of CrgA from Neisseria meningitidis reveals a new octameric assembly state for LysR transcriptional regulators." eng. In: *Nucleic Acids Res* 37.14, pp. 4545–4558 (cit. on pp. 2, 3).

Stec, Emilia, Malgorzata Witkowska-Zimny, Monika M Hryniewicz, Piotr Neumann, Anthony J Wilkinson, Andrzej M Brzozowski, Chandra S Verma, Jolanta Zaim, Stanislaw Wysocki, and Grzegorz D Bujacz (2006). "Structural basis of the sulphate starvation response in E. coli: crystal structure and mutational analysis of the cofactor-binding domain of the Cbl transcriptional regulator." eng. In: *J Mol Biol* 364.3, pp. 309–322 (cit. on p. 1).

Taylor, Jennifer L, Rukman S De Silva, Gabriela Kovacikova, Wei Lin, Ronald K Taylor, Karen Skorupski, and F. Jon Kull (2012). "The crystal structure of AphB, a virulence gene activator from Vibrio cholerae, reveals residues that influence its response to oxygen and pH." eng. In: *Mol Microbiol* 83.3, pp. 457–470 (cit. on pp. 2, 3).

Tropel, David and Jan Roelof van der Meer (2004). "Bacterial transcriptional regulators for degradation pathways of aromatic compounds." eng. In: *Microbiol Mol Biol Rev* 68.3, 474–500, table of contents (cit. on p. 2).

Tyrrell, R., K. H. Verschueren, E. J. Dodson, G. N. Murshudov, C. Addy, and A. J. Wilkinson (1997). "The structure of the cofactor-binding fragment of the LysR family member, CysB: a familiar fold with a surprising subunit arrangement." eng. In: *Structure* 5.8, pp. 1017–1032 (cit. on p. 1).

Vrljic, M., H. Sahm, and L. Eggeling (1996). "A new type of transporter with a new type of cellular function: L-lysine export from Corynebacterium glutamicum." eng. In: *Mol Microbiol* 22.5, pp. 815–826 (cit. on pp. 1, 4).

Wang, L. and S. C. Winans (1995). "High angle and ligand-induced low angle DNA bends incited by OccR lie in the same plane with OccR bound to the interior angle." eng. In: *J Mol Biol* 253.1, pp. 32–38 (cit. on p. 2).

Wang, Lu, John D. Helmann, and Stephen C. Winans (1992). "The A. tumefaciens transcriptional activator OccR causes a bend at a target promoter, which is partially relaxed by a plant tumor metabolite". In: *Cell* 69.4, pp. 659 –667 (cit. on p. 2).

Zhou, Xiaohong, Zhiyong Lou, Sheng Fu, Anqi Yang, Hongbo Shen, Zexuan Li, Yingji Feng, Mark Bartlam, Honghai Wang, and Zihe Rao (2010). "Crystal structure of ArgP from Mycobacterium tuberculosis confirms two distinct conformations of full-length LysR transcriptional regulators and reveals its function in DNA binding and transcriptional regulation." eng. In: *J Mol Biol* 396.4, pp. 1012–1024 (cit. on pp. 2, 3).

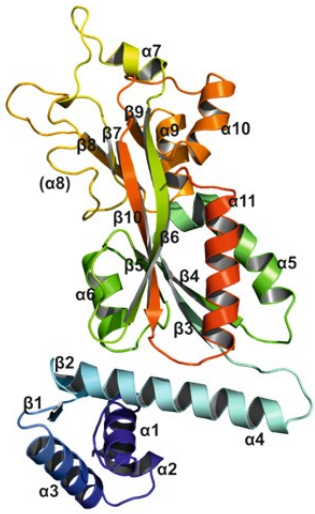

Figure 1
LysG protomer: Secondary structure elements are numbered consecutively, beginning at the blue N-terminal DNA-binding domain, ending at the red C-terminus. Helix α_8 is not ordered, due to high flexibility.

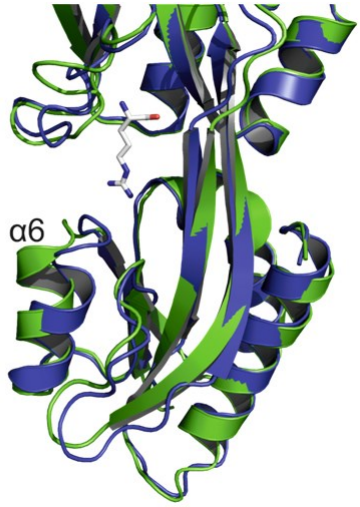

Figure 3
Comparison of helix 6 of the compact and extended protomer: Alignment of the EBD of the compact (green) and extended (blue) protomer. The extended protomer's Helix 6 is tilted 8 toward its inducer-binding cavity. The Effector molecule L-arginine is shown in white sticks, Oxygen atoms (red), nitrogen atoms (blue).

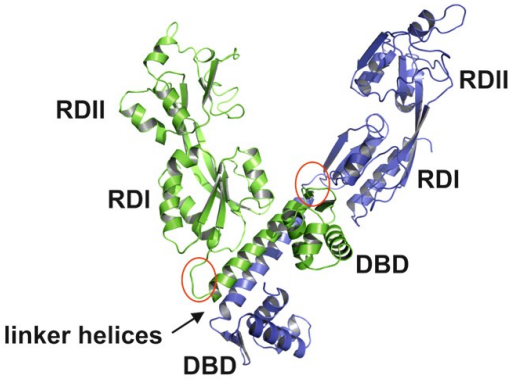

Figure 2
LysG dimer: Cartoon representation of the compact (green) and extended (blue) LysG protomers. One protomer consists of the N-terminal DNA-Binding domain (DBD), the linker helix and the C-terminal effector-binding domain (EBD), consisting of regulatory domain RDI and RDII. The angle between the linker helix and the EBD is 80 in the compact and 198 in the extended protomer. The hinge regions are highlighted with red circles.

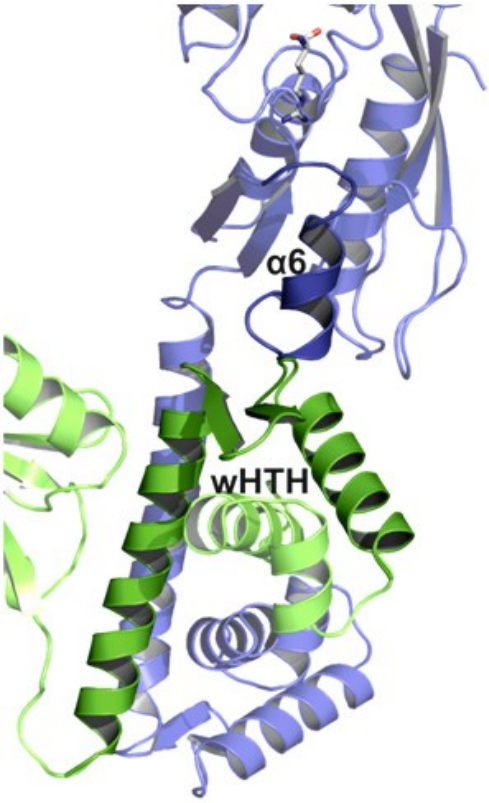

Figure 4
Helix 6 winged Helix-turn-Helix (wHTH) motif interactions: The compact protomer is shown in green the extended protomer is shown in blue. Helix 6 of the extended protomer is in close contact with the wHTH motif off the compact protomer. Effector molecule L-arginine is shown in white, Oxygen atoms (red), nitrogen atoms (blue).

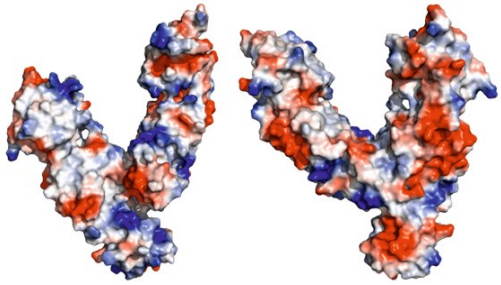

Figure 5
Electrostatic interactions of the dimers: The figure shows a surface representation of both sides of a LysG dimer. The surface is colored according to its charge distribution. Red color indicates negative charge, blue color indicates positive charge. Dimer-dimer contact is facilitated over highlighted patches.

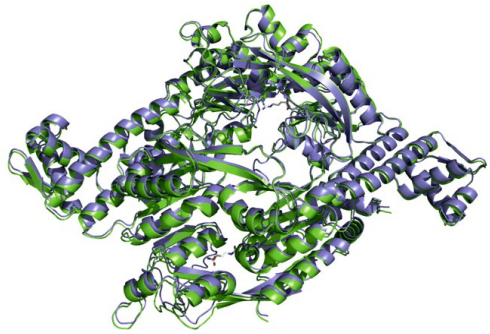

Figure 6
Comparison of L-arginine bound and L-arginine free LysG structure: Structural alignment of L-arginine bound (blue) and L-arginine free (green) LysG tetramer. The rms deviation of the alignment is 0.907 Å. Effector molecule L-arginine is shown in white, Oxygen atoms (red), nitrogen atoms (blue).

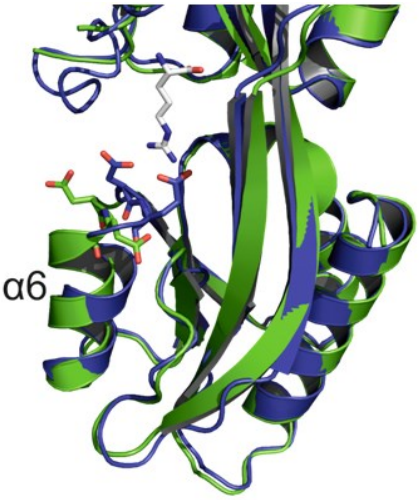

Figure 7
Arginine coordinators of L-arginine bound and L-arginine free LysG structure: Alignment of the extended protomer's EBD. The L-arginine free structure is shown in green, the L-arginine bound structure is shown in blue. Amino acid residues Asp 124 and Glu 125 and effector L-arginine (white) are illustrated in sticks. Oxygen atoms are shown in red, nitrogen atoms are shown in blue. In the L-arginine bound structure Asp 124 and Glu 125 are pointing towards the IBC, thereby coordinating L-arginine.

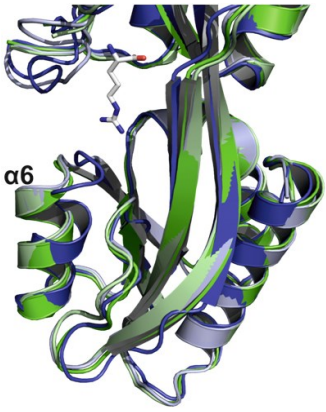

Figure 8
Alignment of the compact and extended protomers' EBD of L-arginine bound and L-arginine free LysG structure: The L-arginine bound protomers are shown blue (extended) and light blue (compact). The L-arginine free protomers are shown green (extended) and light green (compact). The effector molecule L-arginine is shown in white sticks, oxygen atoms (red), nitrogen atoms (blue). Only helix 6 of the extended L-arginine bound protomer is tilted towards the inducer-binding cavity.

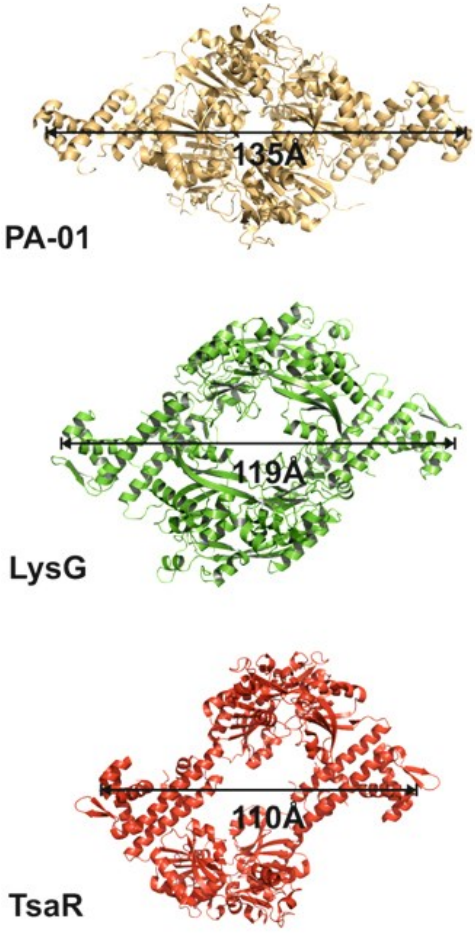

Figure 9
Tetrameric structures of PA-01, LysG and TsaR: PA-01 (PDB ID: 3FZV) exhibits a very tight tetrameric architecture (gold). Only a small inner cavity is visible and the dimeric DBDs are 135 Å apart. The LysG tetramer (green) is looser. Its dimeric DBDs are 119 Å apart. The red TsaR tetramer (PDB ID: 3FXU) shows a big central cavity and its dimeric DBDs are 110 Å apart.

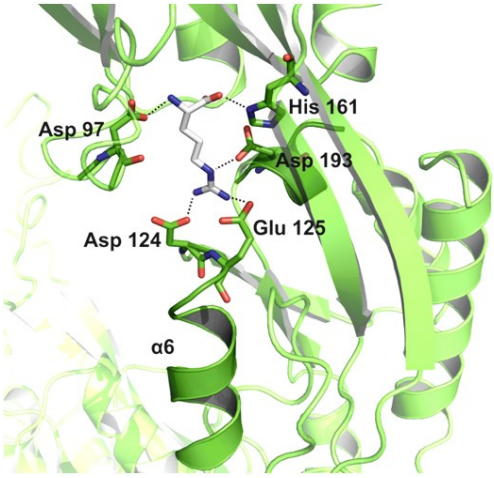

Figure 10
L-arginine coordination: Cartoon presentation of the extended protomer's inducer-binding cavity of the LysG with bound L-arginine. L-arginine and its coordinating amino acids are shown in sticks, oxygen atoms in red, nitrogen atoms in blue. Coordinating atoms are connected by dotted lines.

	LysG		
Space group	C2 2 2 (1)	Refinement resolution	43.8 – 3.3 Å
Unit cell constants	A = 175.18 Å,	Reflections used for refinement	25536
	b = 175.25 Å,	Protein atoms	8868
	c = 111.3 Å,	Ligand atoms	0
	α, β, γ = 90°	Solvent atoms	0
Resolution (Å)	43.8 – 3.3 (3.39 – 3.30)	R.m.s.d. bond lengths	0.008
Unique reflections	25576	R.m.s.d. bond angles	1.398
<I / σ>	14.77 (2.17)	Average B-factor	
Completeness[a]	97.8 % (99.3 %)	Protein	18.88
R_{merge}[a][b]	8.8 % (67.8 %)	Effector	19.27
CC (1/2)	99.8 (67.4)	Final R_{cryst} / R_{free}[d][e]	21.2 % / 27.2 %

Figure 11
Data collection and refinement statistics

Binder et al. Genome Biology 2012, 13:R40
http://genomebiology.com/2012/13/5/R40

Genome Biology

METHOD Open Access

A high-throughput approach to identify genomic variants of bacterial metabolite producers at the single-cell level

Stephan Binder, Georg Schendzielorz, Norma Stäbler, Karin Krumbach, Kristina Hoffmann, Michael Bott and Lothar Eggeling*

Abstract

We present a novel method for visualizing intracellular metabolite concentrations within single cells of *Escherichia coli* and *Corynebacterium glutamicum* that expedites the screening process of producers. It is based on transcription factors and we used it to isolate new L-lysine producing mutants of *C. glutamicum* from a large library of mutagenized cells using fluorescence-activated cell sorting (FACS). This high-throughput method fills the gap between existing high-throughput methods for mutant generation and genome analysis. The technology has diverse applications in the analysis of producer populations and screening of mutant libraries that carry mutations in plasmids or genomes.

Background

Since the first demonstration of microbial product formation more than a century ago [1], vitamins, antibiotics, nucleotides, amino acids and organic acids have been produced in ever increasing quantities. For example, about three million tonnes of sodium glutamate are produced each year as a small microbial molecule. Bacterial synthesis is increasingly also used for the production of small molecules not naturally made by bacteria, such as pharmaceutical intermediates [2,3] or biofuels [4]. The combination of the successful application of microbial synthesis, progress in synthetic biology and changes in the global economy that necessitate intensified use of renewable raw materials indicates that microbial metabolite production will continue to expand.

Microorganisms are not naturally designed for profitable metabolite formation, however, and there is an unrelenting need to optimize strains and pathways. Current strain improvement strategies make use of a variety of methods for engineering and isolating microbial variants with the desired traits. These techniques fall into two major categories: 'rational' methods, which involve the targeted alteration of known genetic information; and 'random' approaches, which are typically based on the creation of mutant libraries containing nondirected changes in genotype with subsequent screening for phenotypes of interest. Both approaches have been successful but the use of mutant libraries has proven to have distinct advantages. The reason is that the exact genomic mutations necessary to adapt the cellular metabolism for increased product synthesis are often difficult to predict, and that 'rational' methods are restricted to known targets. Random approaches with subsequent screening for the phenotype of interest enable us to overcome these difficulties. They have made possible the commercial-scale production of a variety of compounds, such as the unrivaled formation of succinate by *Escherichia coli* [5] or riboflavin by *Bacillus subtilis* [6]. Random and combinatorial approaches were also profitably used for the development of plasmid-encoded targets for the optimization of pathway flux in *E. coli*. This has been demonstrated with amorpha-4,11-diene production [2], which is an artemisinin precursor that is effective for the treatment of malaria, or with taxadiene production [3], an intermediate of the anticancer compound taxol.

However, with few exceptions, the evaluation of methods that utilize random approaches currently requires the cultivation of individual clones to determine production properties. This presents an obstacle. While high-throughput

* Correspondence: l.eggeling@fz-juelich.de
Institut für Bio- und Geowissenschaften, IBG-1: Biotechnologie, Forschungszentrum Jülich GmbH, D-52425 Jülich, Germany

(HT) techniques for introducing genetic diversity and for product analysis or sequencing are well developed [7], comparable strategies for the identification and isolation of high-producer bacterial cells are still lacking. The opportunity to directly monitor product formation within single cells *in vivo* would add a new dimension to the characterization and development of microbial producers.

Here, we present examples of the monitoring of intracellular metabolite concentrations in single bacterial cells and demonstrate in an HT screen the isolation of new bacterial producer cells, as well as the identification of novel mutations based on whole-genome sequencing. The sensors we use are based on transcription factors (TFs) that regulate the transcriptional output of a target promoter in response to a cytosolic metabolite. Whereas the use of TFs to construct whole-culture biosensors for the detection of environmental small-molecule pollutants has long been established [8], this same approach has remained largely untranslated with respect to single-cell analysis and library screening. TFs are naturally targeted to a variety of small ligands, ranging from amino acids to sugars, sugar phosphates, vitamins, antibiotics, oxoacids and lipids [9]. They can also be engineered to obtain altered specificity [10,11], as recently summarized in a comprehensive review [12]. Coupling transcription of the target gene to a reporter protein provides a molecular device for recognition. This has already been successfully applied for screening in plate-based assays using colony color or colony size [10,13], for instance. Here we make full use of intracellular recognition of a specific metabolite in single cells by applying an autofluorescent protein as reporter and also fluorescence-activated cell sorting (FACS). This enables the isolation in HT screens of new bacterial small-molecule producers with random mutations introduced into the genome that enhance production of the molecule of interest, and we present an example of this.

Results

Schematic of approach

The workflow for HT selection of genomic variants of metabolite producers consists of the following steps: a) design of a suitable metabolite sensor, b) generation of genetic diversity in genomes of cells carrying the sensor, c) screening of the mutant library and selection of single producer cells via FACS, d) verification and characterization of mutants, and e) sequencing for target identification. We developed sensors for intracellular detection of basic amino acids, as well as of L-serine and O-acetyl-serine, and demonstrated the feasibility of the approach by isolating bacteria producing L-lysine from a library of randomly mutagenized wild-type (WT) cells, culminating in the identification of new useful mutations by whole-genome sequencing.

Design of L-lysine sensor

To develop a sensor suitable for intracellular L-lysine detection, we focused on the LysR-type transcriptional regulator (LTTR) LysG of *Corynebacterium glutamicum*. This protein senses elevated concentrations of basic amino acids, causing transcription of its target gene *lysE*, which encodes a basic amino acid exporter [14]. To explore the application of this native regulatory device to the conversion of an intracellular metabolite concentration into an optical output, we characterized the interaction of LysG with its target region upstream of *lysE* in a series of electrophoretic mobility shift assays (Figure S1 in Additional file 1). These data were used to construct the metabolite sensor pSenLys shown in Figure S2 in Additional file 1. It contained *lysG*, together with the LysG-binding site in front of the *lysE* promoter driving transcription of *eyfp* coding for enhanced yellow fluorescent protein (EYFP). In addition, P_{tac}-driven *crimson* was incorporated as a second fluorescence protein in the vector backbone. All strains and plasmids are listed in Table S1 in Additional file 1.

Characterization of L-lysine sensor

The WT of *C. glutamicum* does not excrete L-lysine but there is a genealogy of defined mutants that exhibit increased L-lysine productivity [15]. We determined the cytosolic L-lysine concentration by silicone oil centrifugation and the response of pSenLys in these strains. The WT had a cytosolic L-lysine concentration below 5 mM, while the defined producers had steady-state concentrations ranging from roughly 8 to 25 mM (Figure 1a). A clear increase in specific EYFP fluorescence in cultures is seen with increasing cytosolic L-lysine concentration. As evident from microscopic inspection (insets in Figure 1a), pSenLys is a tool for visualizing cytosolic L-lysine concentrations also within single cells. The range of the cytosolic L-lysine concentration covered translates into a dynamic range of signal output of 8.3-fold.

The fluorescence signal from the pSenLys sensor also correlates with the extracellular L-lysine concentration that accumulates after glucose is consumed (Figure 1b). One instructive exception to this is strain DM1920, which accumulates extracellular L-lysine at concentrations comparable to that of DM1919 despite displaying lower fluorescence due to lower cytosolic concentrations of L-lysine. This is due to altered L-lysine export: Strain DM1919 has one copy of the exporter gene *lysE* and an export rate of 10.1 ± 0.4 nmol $minute^{-1}$ mg(dry weight) $^{-1}$ (Figure 1c), whereas strain DM1920 has two copies of *lysE* (Table S1 in Additional file 1), which results in an increased rate of export of L-lysine of 12.1 ± 0.6 nmol $minute^{-1}$ mg(dry weight) $^{-1}$, and thus reduced cytosolic concentration. This observation provides an opportunity of influencing the read-out properties of a sensor that

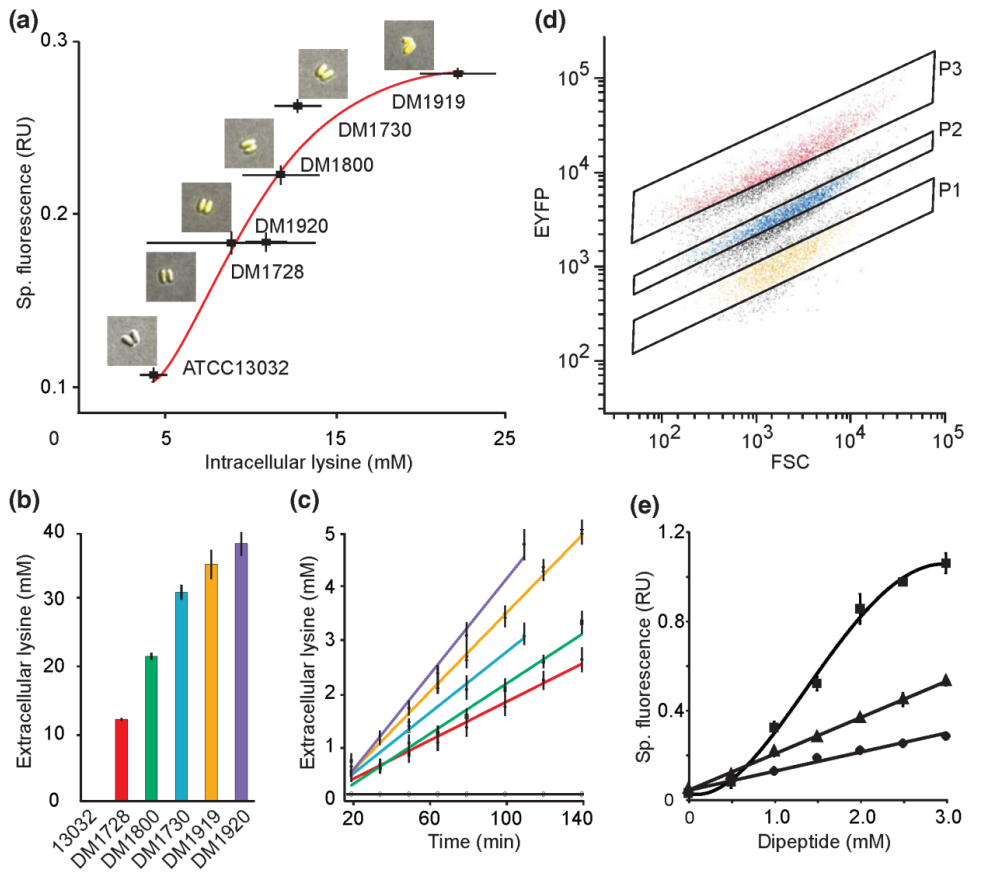

Figure 1 Characterization of lysine sensor and lysine-producing recombinant cells. (**a**) Cytosolic L-lysine concentration in *C. glutamicum* WT and five defined lysine producer strains, all carrying pSenLys, and specific fluorescence (Sp. fluorescence) of the cultures. Error bars give the means of three independent cultures for each strain. Fitting the data to the Hill equation describes the signal transfer function by an n_{app} of 3.19 ± 1.45 and this is shown as the red curve. (**b**) Extracellular accumulation of lysine after 48 h by the strains used in (a). (**c**) Lysine excretion rates of the same strains showing that strains with increased final lysine accumulation have increased excretion rates. Strain DM1920 has two copies of the lysine exporter gene *lysE* present in its chromosome and shows the highest excretion rate, but an intermediate cytosolic lysine concentration (color code as in (b)). (**d**) Differentiation of an equal mixture of cells of ATCC13032, DM1728 and DM1919 each carrying pSenLys by flow cytometry. The success of strain-specific sorting using gates P1 to P3 was over 90%. (**e**) Influence of dipeptide addition on specific fluorescence of *C. glutamicum* WT carrying pSenLys. The peptides Lys-Ala (circle), Arg-Ala (triangle) and His-Ala (square) were added to the cultures at the indicated concentrations. Additionally, Ala-Ala was added to give a total dipeptide concentration of 3 mM. The specific fluorescence was measured 1.5 h after dipeptide addition. FSC, forward scatter; RU, relative units.

had not previously been taken into consideration. As demonstrated for the production of antibiotics [16], amino acids [17], and biofuels [4], small-molecule production depends on export proteins. The ability to manipulate export activities permits cytosolic concentration of the substrate to be increased or decreased, which may be helpful, for example, when using strains that display high productivity and high cytosolic concentrations of substrate.

To isolate single cell producers by HT flow cytometry, it is essential that the cells can be separated according to their fluorescent properties. To demonstrate that this is the case with pSenLys, sensor-carrying cells of WT, DM1728, and DM1919 grown in glucose minimal medium

were mixed in a 1:1:1 ratio to give a total of 4×10^7 cells ml^{-1}. This cell population was analyzed via FACS at a rate of 10^3 events per second. Clear differentiation of the population was achieved on the basis of intensity of the EYFP signal (Figure 1d). Three further qualities were assessed (Table S2 in Additional file 1): 1) the sorting specificity achieved using gates P1 to P3 resulted in the selection of ≥ 89% of the L-lysine producer expected within the respective gate; 2) the recovery of viable single cells for each gate was ≥ 84%; 3) when DM1728 was mixed with a 10,000-fold excess of WT cells and then re-isolated, 92% of the prepared cells were DM1728.

LysG recognizes L-arginine and L-histidine in addition to L-lysine [14]. Peptide addition is a proven method to increase the cytosolic pool of a specific amino acid in *C. glutamicum* or *E. coli* [18,19]. The fluorescence response of *C. glutamicum* carrying pSenLys to exogenously applied Lys-Ala is similar to endogenously synthesized L-lysine (Figure 1e). The fluorescence response due to Arg-Ala supply was substantially greater, and that to His-Ala was greater still, which may indicate a higher affinity of these ligands for LysG.

Further metabolite sensors

To assess the general utility of TFs for reporting on small-molecules at the single-cell level, we constructed pSenArg based on ArgP of *E. coli* controlling *argO* transcription as a function of cytosolic L-arginine [20]. When pSenArg was assayed for dipeptide responsiveness, the addition of Arg-Ala resulted in fluorescent *E. coli* cells (Figure 2, left), with fluorescence increasing in proportion to the dose of dipeptide (Figure S3 in Additional file 1). As additional metabolite sensors, pSenSer and pSenOAS were constructed (Table S1 in Additional file 1), suitable for L-serine (Figure 2, middle), and *O*-acetyl-L-serine detection in *C. glutamicum* (Figure 2, right), respectively.

Generation of genetic diversity and library screening

To demonstrate the feasibility of metabolite sensors for HT screening of mutant libraries, we introduced chromosomal mutations into the WT of *C. glutamicum* carrying pSenLys by treatment with MNNG (N-methyl-N'-nitro-N-nitrosoguanidine), one of the most effective chemical mutagens for creating genetic diversity [21]. While the separation of mixtures of defined producers could be achieved using FACS (Figure 1d), direct processing of the mutagenized library with FACS was not successful. We used a liquid culture recovery and enrichment step taking into account that metabolically active cells require 2 h for Crimson synthesis (Figure S4 in Additional file 1), and that cells derived from the glycerol stock have to be incubated for 6 h on minimal medium to establish host-specific EYFP fluorescence. The suspension of mutagenized cells from glycerol stock (200 µl) was diluted into minimal medium containing IPTG (isopropyl-β-D-thiogalactopyranoside and, after 2 h, 6.5×10^6 Crimson-positive cells were sorted in minimal medium. After cultivation for a further 22 h, 350 EYFP positive cells were spotted onto minimal medium plates. Of these, 270 grew into colonies within 48 h.

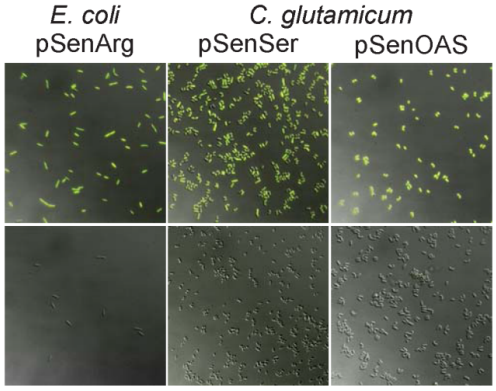

Figure 2 Metabolite sensors reporting on cytosolic arginine, serine, and *O*-acetyl-serine. Cells of *E. coli* DH5α (left) carrying pSenArg fluoresce when Arg-Ala was added (top), but not following supplementation with Ala-Ala (bottom). The peptide-dose response curves for Arg-Ala, Lys-Ala and His-Ala are shown in Figure S3 of Additional file 1. The serine-producing strain *C. glutamicum*-Ser4 (middle) [45] with pSenSer is fluorescent (top), but the WT carrying pSenSer is not (bottom). (**c**) Fluorescence is seen with the L-cysteine producer *C. glutamicum*-Cys3 carrying pSenOAS (top right), but not with the control strain (bottom right). Epifluorescence microscopic analysis was done at λ_{ex} = 490 to 510 nm and λ_{em} = 520 to 550 nm.

Producer verification

The 270 colonies were used to inoculate microtiter plates, to enable HT screening of cultures using 0.75 ml minimal medium. L-lysine was detected in culture supernatants of 185 clones. Re-cultivation of 120 clones (Figure 3a) revealed that the L-lysine concentration ranged from 0.2 to 37 mM. Four clones accumulated 3.6 to 5 mM L-lysine plus 0.6 to 0.8 mM L-arginine and one clone 24.9 mM L-lysine plus 0.6 mM L-arginine. None of the mutants accumulated L-histidine, possibly due to the length of this pathway and its tight regulation.

Of the 120 mutants, 40 were selected randomly, and their culture fluorescence and growth recorded (Figure S5 in Additional file 1). Using an expectation maximization algorithm [22], two clusters relating specific fluorescence to L-lysine accumulation were apparent (Figure 3b). The cluster represented by the lower curve showed characteristics similar to the defined recombinant strains used in Figure 1a, which are included in Figure 3b as gray dots and numbered in parentheses. This cluster includes the mutants of main interest. Mutants in the other cluster show in part extreme fluorescence at a comparatively low extracellular L-lysine accumulation. Since we screened for high fluorescence, it is possible that mutants with reduced L-lysine export activity - and therefore increased intracellular L-lysine concentration - accumulated. This finding warrants further exploration. Cellular export activity is influenced by a number of parameters, including the lipid environment of carriers and the composition of the outer membrane [4,16], which may cause mutants to excrete metabolites at different rates than the WT does.

Gene analysis in 40 mutants

We sequenced *lysC*, which encodes aspartate kinase in the 40 mutants described above (Figures 4 and 5a). To date, all L-lysine producers described have a mutation in *lysC*, preventing feedback inhibition of aspartate kinase activity by the concerted action of L-lysine plus L-threonine [23]. In 15 of the mutants that we found, *lysC* was mutated, including seven cases of the known mutation *lysC*-T308I, which is located in the regulatory β-subunit of the aspartate kinase [23]. New mutations - *lysC*-H357Y, *lysC*-T313I, *lysC*-G277D, and *lysC*-G277S - that also affect the regulatory subunit (Figure S6 in additional file 1) were

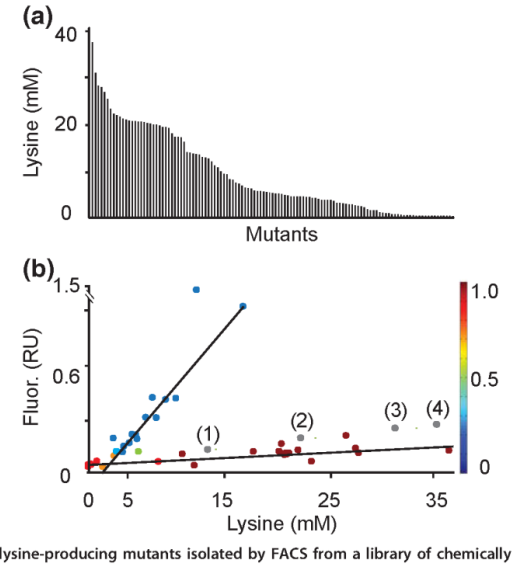

Figure 3 Characterization of L-lysine-producing mutants isolated by FACS from a library of chemically mutagenized wild type cells. (**a**) The spectrum of L-lysine accumulation in the culture supernatant of 120 mutants obtained using FACS selection. Mutants were grown in minimal medium with 4% (w/v) glucose and lysine concentrations determined after 48 h. (**b**) Specific culture fluorescence was determined for 40 arbitrarily chosen mutants. Two clusters are apparent after applying an expectation maximization (EM) algorithm to construct a distribution containing maximum likelihood estimates of the parameters in a Gaussian mixture model with two components for data in the 40-by-2 data matrix [22]. The heat bar on the right gives the probability of clones belonging to cluster one, which corresponds to that with the flat curve. The probability of clones belonging to cluster two, corresponding to that with the steep curve, uses the same heat bar with the highest probability in blue and lowest in red. The four gray circles marked (1) to (4) give lysine accumulation and specific fluorescence for the defined recombinants DM1728 (1), DM1800 (2), DM1730 (3), and DM1919 (4) used in Figure 1a. RU, relative units.

Strain	Lys(mM)	$\mu(h^{-1})$	Mutation	Strain	Lys(mM)	$\mu(h^{-1})$	Mutation
K015	36.9	0.34	*lysC* A279T	K042	4.2	0.12	*hom* T233I
K037	27.4	0.33	*lysC* A279T	K039	10.9	0.24	*hom* V211F
K053	19.8	0.39	*lysC* A279V	K016	0.1	0.11	*thrB* S102F
K008	7.2	0.36	*lysC* G277D	K055	2.7	0.18	*murE* L121F
K106	19.6	0.39	*lysC* G277S	K051	15.9	0.23	*murE* G81E
K096	0.9	0.25	*lysC* H357Y				
K035	21.5	0.35	*lysC* T308I				
K100	20.6	0.29	*lysC* T308I				
K047	20.3	0.27	*lysC* T308I	K117	7.0	0.34	
K065	20.2	0.30	*lysC* T308I	K005	6.6	0.38	
K019	20.1	0.23	*lysC* T308I	K021	5.9	0.37	
K090	19.8	0.34	*lysC* T308I	K079	5.2	0.30	
K078	0.3	0.18	*lysC* T308I	K093	5.0	0.39	
K101	26.4	0.23	*lysC* T311I	K013	4.9	0.38	
K115	1.5	0.25	*lysC* T313I	K048	4.5	0.38	
K002	27.7	0.30	*hom* A328V	K062	3.7	0.26	
K049	9.6	0.15	*hom* A364V	K107	3.6	0.36	
K074	2.9	0.14	*hom* G241S	K023	16.9	0.17	
			thrC A372V	K120	2.6	0.37	
K052	0.2	0.18	*hom* G241S	K046	0.1	0.39	
			thrC A372V	K118	10.5	0.36	
K032	22.9	0.26	*hom* R158C	K063	9.0	0.37	
			hom T351I	K112	7.9	0.38	

Figure 4 Genetic characterization of mutants. In 40 mutants, targeted sequencing revealed mutations in *lysC*, *hom*, *thrC* and *thrB*, with some of the mutations already known from prior work (see text). Mutations that resulted in amino acid exchanges are indicated, along with growth rates and final external lysine titers. The mutation *murE*-G81E in strain K051 was identified by whole-genome sequencing. The second *murE* mutation, *murE*-L121F, was identified by subsequent targeted sequencing. In 15 mutants (plus K051), it was not possible to identify any mutation by site-directed mutagenesis.

found. We also sequenced *hom* in all 40 mutants, since reduced homoserine dehydrogenase activity reduces L-threonine availability in cells and thus also reduces kinase activity (Figure 5a). Current approaches to engineering L-lysine synthesis rely on just a single *hom* mutation [15]. Seven of the mutants isolated in this study carry novel mutations in *hom* (Figure 4).

In the remaining 18 mutants, neither *lysC* nor *hom* was mutated. We therefore sequenced *thrB* and *thrC* as further genes of L-threonine synthesis (Figure 5a). In strain K016 the mutation *thrB*-S102F was identified and in strain K074 the mutation *thrC*-A342V was found (Figure 4). The introduction of four selected mutations into the WT chromosome resulted in significant L-lysine concentrations (Table S3 in Additional file 1), demonstrating that these new mutations cause increased L-lysine formation.

Genome sequence of mutant K051

We performed whole-genome sequencing on strain K051, which has no mutation in *lysC*, *hom*, *thrB*, or *thrC* yet accumulates L-lysine up to a concentration of 15.9 mM. Paired-end sequencing on an Illumina HiSeq 2000 provided more than 20 million reads. Trimming and mapping to the WT genome (NC_000913) [15] resulted in a 260-fold coverage (Table S4 in Additional file 1). The genome sequence of strain K051 has been deposited at the European Nucleotide Archive under accession number HE802067. Within K051, 268 SNPs are manifest. They are unevenly distributed in the genome (Figure 5b). The number of SNPs is within the range observed for *E. coli* treated with MNNG [24]. All of the SNPs identified are transitions, as expected with this mutagen, the majority of them resulting in amino acid exchanges (Figure 5b; Table S1 in Additional file 2). In addition, NCgl0863, which carries the amino acid exchange G54D, was partially duplicated, with the variant copy placed 6,108 bp distant from NCgl0863 in an intergenic region.

We searched the mutations in K051 for genes known to increase L-lysine production and to participate in the pathway from glucose uptake up to L-lysine excretion

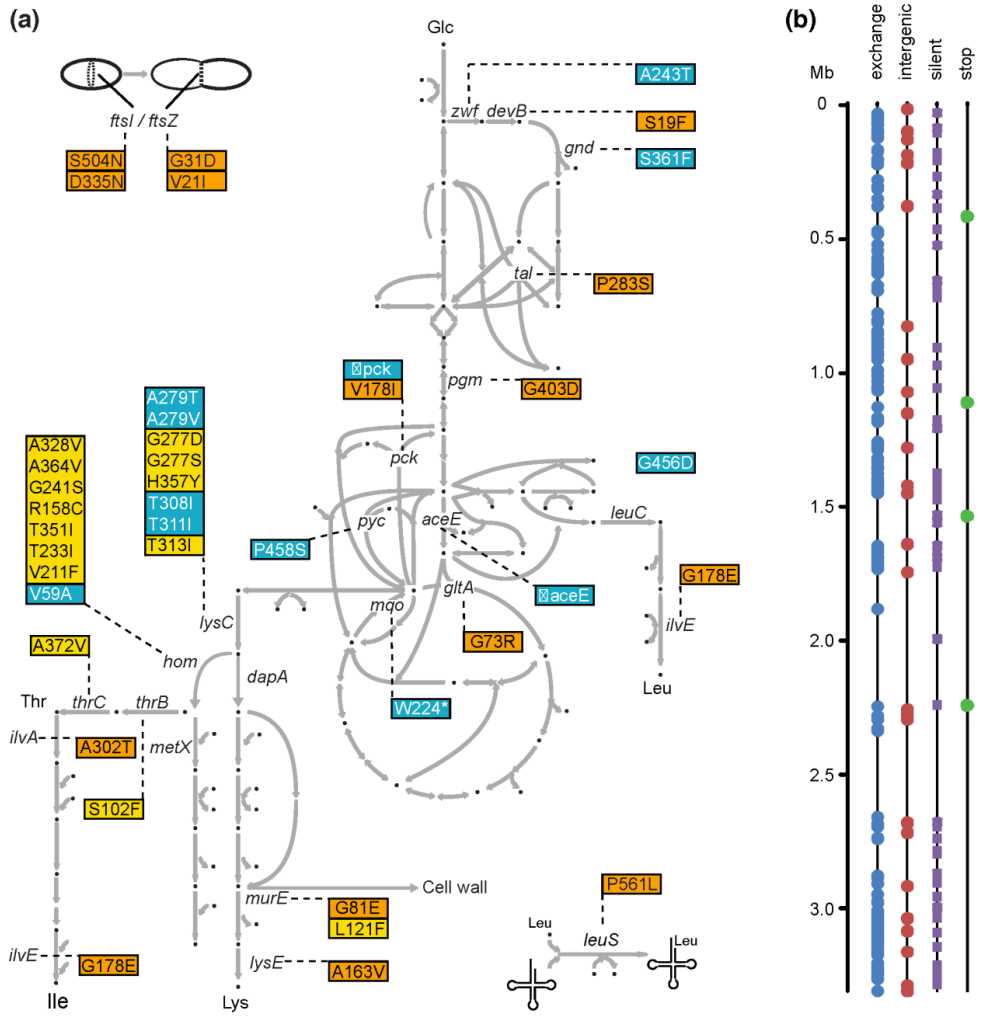

Figure 5 Sketch of the central metabolism and localization of mutations in *C. glutamicum* together with whole-genome sequencing results of the mutant K051. (**a**) Pathways and reactions required for and related to lysine synthesis. Genes that carry mutations leading to amino acid exchanges are indicated as follows: blue box, mutations known previously; yellow box, new mutations identified by targeted sequencing in 40 mutants; orange box, new mutations derived from the K051 genome. (**b**) Localization of the 268 SNPs in the genome of strain K051 determined by whole-genome sequencing. The size of the genome is 3.28 Mb, scale on the left. The mutations are classified into those causing an amino acid exchange, those that are silent, those leading to a stop codon, and those located in non-coding regions. The genome sequence of strain K051 is deposited at the European Nucleotide Archive under the accession number HE802067.

(Figure 5a). Specific mutations in *zwf* and *gnd* in the pentose phosphate pathway are known to increase L-lysine formation due to an increased supply of NADPH [25]; K051 has mutations in *devB* and *tal* that could also be effective. K051 also has mutations in *pck* and *gltA*, genes encoding phosphoenolpyruvate carboxykinase and citrate synthase, where reduced activities are known to increase the supply of pyruvate and oxaloacetate for L-lysine

synthesis [26,27]. Also, mutations of branched-chain amino acid metabolism have been demonstrated to increase lysine formation, and K051 carries a mutation in *ilvE*, as well as in the Leu-tRNA synthetase LeuS. Of particular interest was the *murE* mutation (*murE*-G81E) in K051. This gene encodes UDP-N-acetylmuramyl-tripeptide synthetase, an enzyme that utilizes D, L-diaminopimelate as a substrate, as does the D, L-diaminopimelate decarboxylase, in L-lysine synthesis.

Influence of *murE* mutations on L-lysine synthesis

To determine whether the *murE*-G81E mutation identified could generate increased L-lysine formation, we introduced it by allelic replacement into DM1132, DM1728, DM1730, DM1800, and DM1933. The new strains were cultivated in parallel to their ancestor strains in shake flask cultivations and final L-lysine concentrations were determined after 48 h. As shown in Figure 6, the mutation caused strong L-lysine accumulation when introduced into the WT DM1132 and also DM1728, the strains that have few mutations and which form comparatively little L-lysine. Yet even with the best producer available, strain DM1933, a significant increase in L-lysine accumulation was determined. Given this finding, we sequenced *murE* in the remaining mutants isolated by our HT technology that had no identified mutation (Figure 4), and found *murE*-L121F in strain K055. Introduction of this specific mutation into the five defined L-lysine producers yielded increased L-lysine accumulation, too (Figure 6). Whether the increases with the two *murE* mutations identified were due to increased availability of D, L-diaminopimelate for L-lysine synthesis, or whether a global regulatory effect pushes synthesis of D, L-diaminopimelate remains to be studied.

Discussion

The key requirement for visualization of single cells with elevated concentrations of a small molecule of interest is the availability of suitable *in vivo* sensor systems with sufficient sensitivity and specificity. There are a large number of options for developing customized reporters sensing intracellular metabolites. They are based on natural molecular recognition, allosteric switching, and gene regulation behavior of proteins and RNA. Every system has its own specific advantages and disadvantages, and the reader is referred to recent reviews on the numerous ideas and ongoing developments in the field [12,28-33]. Whereas protein sensors based on periplasmic binding proteins and Förster resonance energy transfer (FRET) in principle enable concentration determinations in real time, use of TFs relies on expression of the reporter gene. This delay between ligand binding and the corresponding phenotypic change is not a disadvantage in developing or characterizing recombinant cells since stable genetically encoded genotypes are sought. With respect to the use of TFs in metabolite sensing for screening purposes, the present work based on LysR of *C. glutamicum* is the first example where the responsiveness of the optical output to an existing intracellular metabolite concentration is given, and where a TF-based sensor is used in an HT screen applying FACS for the isolation of new bacterial small-molecule producers.

The responsiveness of TFs previously characterized is deduced from the external addition of the effector molecule and whole culture response. Although this may only be of limited significance for screening, it is disadvantageous for precise characterization since various processes such as active uptake, active export, diffusion and degradation of effector might result in a different cytosolic concentration than that present extracellularly. In the case of LysG-based pSenLys, we determined a detection range of 4 to 25 mM intracellular L-lysine. Sensor responsiveness is characterized by an analog-like response that, when fitted to the Hill equation, is described by n_{app} of 3.19 ± 1.45. It enables the differentiation of WT from medium- and high-level producer cells (Table S2 in Additional file 1). As our intracellular determinations and the comparison of the isogenic strains with one copy and two copies of *lysE* revealed, the effective range of detection may be extended by altering export activity. This could be of relevance for further improvement of good producers. Sensor response and its usefulness will depend on the interplay between the cytosolic concentration of the small-molecule and export activity, as well as on the affinity of the sensor to the effector and target promoter site.

Three of the small-molecule sensors described in the present work are based on a LysR-type TF, and one on a ROK-type TF. Fortunately, the range of small molecules detectable by TFs is large. *E. coli* has more than 230 TFs, with many of them detecting small molecules. In bacteria, TFs have been found to sense sugars, sugar phosphates, vitamins, 2-oxoacids, ions, antibiotics, and acyl-CoA derivatives [9]. Moreover, TFs with new specificities can be generated [11]. An example is AraC, which has been switched from a natural L-arabinose sensor to a sensor detecting D-arabinose [34] or mevalonate [10], and the latter effector specificity has been used in a plate-based assay to screen for improved mevalonate producers. Other sensors that were given new specificities were developed from NahR or XylR for the detection of benzoic acid-related compounds [35], or TetR for structural derivatives of tetracycline [36]. Advances in the design of microbial-based molecular reporters and customizing ligand dependence derived from natural TFs have recently been reviewed [12].

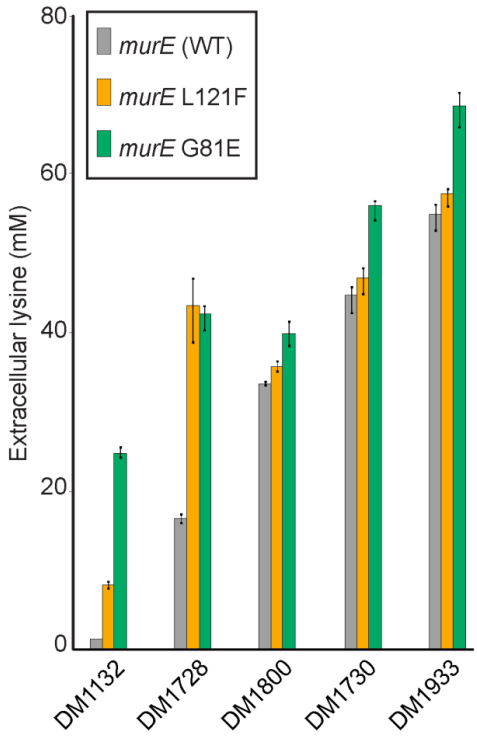

Figure 6 Effect of *murE* mutations on lysine accumulation. Lysine production by different strains modified to carry a chromosomal *murE* mutation. Color code: gray, ancestor strains; orange, strains carrying the amino acid exchange L121F in MurE; green, strains carrying the amino acid exchange G81E in MurE.

Thus, sensors for a significant number of small molecules of biotechnological or pharmaceutical importance are within reach.

Whereas the WT of *C. glutamicum* does not excrete L-lysine, cytosolic sensing and FACS as an efficient screen enabled the rapid isolation of 185 new mutants accumulating L-lysine in the culture supernatant. The current number of genes where mutations cause increased L-lysine synthesis is about 12 [37,38]. These mutations serve to increase flux through the L-lysine pathway itself, or to increase the pyruvate and oxaloacetate pool, or the NADPH supply. However, there are still unknown mutations to be discovered, since it is known that in an L-lysine-producing mutant developed over decades in classical screenings, many genes of biosynthesis pathways exhibit increased expression [39], and in a similarly derived L-arginine producer, arginine biosynthesis genes are highly expressed in a manner not achievable by plasmid-encoded expression [40]. Our approach provided alleles of known genes, and this is very useful for genomic reconstruction of producers where advantageous mutations are combined, and alleles may result in different productivity [2,41]. The number of 268 SNPs present in K051 is too great to study their individual impact on product formation, but new possibilities might be offered when more genome sequences become available. Striking was the *murE* mutation present in K051. We suggest that the catalytic activity of UDP-N-acetylmuramoyl-L-alanyl-D-glutamate:meso-diaminopimelate ligase in MurE-G81E is reduced, with the consequence that more D, L-diaminopimelate is available for L-lysine synthesis. MurE of *C. glutamicum* is similar to MurE of *Mycobacterium tuberculosis* and *E. coli*, the crystal structures of which are known [42]. From these, it can be deduced that G81E is close to the nucleoside part of UDP-MurNAc-L-Ala-D-Glu, and L121F in the second mutant identified is close to the ATP-binding site. Thus, a reduced activity is meaningful, and in line with the increased L-lysine

formation obtained with all strains when the *murE* mutations were introduced in their genomes. It is also in line with the reduced growth rates of these new recombinants (Table S5 in Additional file 1), since less D, L-diaminopimelate is channeled towards cell wall synthesis. An alternative to simple mass balance effects is that a lack of cell wall building blocks initiates a global response that has a positive effect on biosynthesis.

We applied one of our transcriptional sensors for HT screening of a mutant library with chromosomal mutations, but the same principle may also be explored for HT screening of cells carrying plasmid libraries. This is attractive, since many pharmaceuticals currently produced microbially, such as amorpha-4,11-diene, taxadiene and lycopene, use plasmid-encoded biosynthesis pathways, for example, in *E. coli* [2,3,13]. Use of an appropriate sensor combined with FACS-assisted screening may significantly accelerate the development of producers for such small molecules, too. The HT selection routine for mutant isolation closes the gap between HT generation of mutant libraries and HT sequencing technologies, and further applications of sensing small molecules in single cells are in progress, such as the verification of producer population homogeneity and time-lapse microscopy of *C. glutamicum* in microfluidic chips [43].

Conclusions

This work examines visualization of the intracellular concentration of small molecules at the single cell level by the use of specific TFs. It opens up various possibilities to characterize and analyze single cells in populations with respect to their cytosolic small molecule concentration. We have demonstrated that the visualization of L-lysine combined with HT sorting of genomic mutant libraries via FACS enables the isolation of new mutants. Together with whole-genome sequencing, this therefore establishes rapid access to new mutations to achieve more efficient product formation. In addition to the screening of cells with genomic mutations, the system is also suitable for screening cells with plasmid libraries to identify more efficient product accumulation.

Materials and methods

Sensor plasmid construction

The regulatory units were synthesized (LifeTechnologies GmbH, 64293 Darmstadt, Germany) and cloned into pJC1 using the restriction sites *Bam*HI and *Sal*I. An overview of the sensor plasmids is shown in Figure S2 in Additional file 1. The entire plasmid sequences were deposited at EMBL under the accession numbers HE583184 (pSenLys), HE583185 (pSenArg), HE583186 (pSenSer), and HE583187 (pSenOAS1).

FACS analysis and cell sorting

Cells were diluted to an optical density below 0.1 and immediately analyzed by a FACS ARIA II high-speed cell sorter (BD Biosciences, Franklin Lakes, NJ USA 07417) using excitation lines at 488 and 633 nm and detecting fluorescence at 530 ± 15 nm and 660 ± 10 nm at a sample pressure of 70 psi. Data were analyzed using BD DIVA 6.1.3 software. The sheath fluid was sterile filtered phosphate-buffered saline. Electronic gating was set to exclude non-bacterial particles on the basis of forward versus side scatter area. For sorting of Crimson- or EYFP-positive cells the next level of electronic gating was set to exclude non-fluorescent cells. Background was estimated using non-induced *C. glutamicum* for sorting of Crimson-positive cells. When sorting EYFP-positive cells, non-producing *C. glutamicum* cells were used.

Mutagenesis and library screening

C. glutamicum ATCC13032 carrying pSenLys was grown in 5 ml BHI complex medium (Difco Laboratories Inc., Detroit, MI 48201, USA) containing 25 μg ml^{-1} kanamycin to an optical density of 5 to ensure exponential growth. Whole-cell mutagenesis was done by the addition of MNNG dissolved in dimethyl sulfoxide (DMSO) to a final concentration of 0.1 mg ml^{-1} and incubation for 15 mintes at 30°C. The treated cells were washed twice with 45 ml NaCl, 0.9% (w/v), resuspended in 10 ml BHI and regenerated for 3 h at 30°C and 180 rpm. Mutant cells were stored at -30°C as cryostocks in BHI containing 40% glycerol (w/v). Of the initial cells, 46.2% survived the MNNG treatment and among the surviving cells approximately 16% were auxotrophs. For FACS screening, the mutant stock population containing 7.5×10^8 viable cells per ml was diluted 1:100 in 20 ml minimal medium containing 0.1 mM IPTG to induce expression of the far-red fluorescent protein Crimson, which was taken as an indicator of metabolically active cells. After 2 h of cultivation, 6.5×10^6 cells were analyzed by FACS and 2×10^6 Crimson-positive cells collected in fresh 20 ml minimal medium without IPTG. After cultivation for a further 22 h, 1.8×10^7 cells were screened and 350 EYFP-positive cells spotted on Petri dishes containing minimal medium. Colonies grown after 48 h at 30°C were further analyzed.

HT cultivation and culture fluorescence analysis

HT cultivation was done in 48-well Flowerplates (FPs; m2p-labs GmbH, 52499 Baesweiler, Germany) at 30°C, 990 rpm and a throw of ø 3 mm. The specific geometry of the FPs ensures high mass transfer performance and can be used together with the microcultivation system BioLector [44], allowing online monitoring of growth

and fluorescence. The medium used for FP cultivations was the MOPS-buffered salt medium CGXII [45], with 4% glucose as substrate and 25 μg ml^{-1} kanamycin to select for maintenance of pSenLys. For offline cultivations, FPs were cultivated on a Microtron high-capacity microplate incubator operating at a shaker speed of 990 rpm, throw ø 3 mm (Infors AG, CH-4103 Bottmingen, Switzerland). Shake flask cultivations were used to compare the consequences of the *murE* mutations for L-lysine accumulation (Figure 4b); these were done in 500 ml baffled Erlenmeyer flasks with 50 ml medium. The medium was the same as used in FP cultivations, except that the phosphate concentration was reduced by half. Cells pregrown in CGXII medium were used as inocula for all cultivations.

Amino acid quantification

Amino acids were quantified as their *o*-phthaldialdehyde derivatives via high-pressure liquid chromatography using a uHPLC 1290 Infinity system (Agilent, Santa Clara, CA 95051, USA) equipped with a Zorbax Eclipse AAA C18 3.5 micron 4.6 × 75 mm and a fluorescence detector. As eluent, a gradient of 0.01 M Na-borate buffer pH 8.2 with increasing concentrations of methanol was used, and detection of the fluorescent isoindole derivatives was at λ_{ex} = 230 nm and λ_{em} = 450 nm.

Determination of cytosolic amino acid concentrations and amino acid export rates

Cells were pregrown as for FP cultivations for 24 h. They were washed once with fresh CGXII medium at room temperature and transferred into new medium in FPs to give an initial optical density of 10, which corresponds to 3.0 mg (dry weight) ml^{-1}. Cultures were incubated at 30°C on the Microtron high-capacity microplate incubator as above. Samples were processed at regular intervals to separate extra- and intracellular fluid by silicone oil centrifugation [46]. For the resulting fractions, amino acids were quantified as described above. The intracellular volume used to calculate the internal amino acid concentration was 1.6 μl mg (dry weight)$^{-1}$. When peptides were added (Figure 1e; Figure S3 in Additional file 1) mixtures of dipeptides at a final concentration of 3 mM were used, such as 1 mM Arg-Ala plus 2 mM Ala-Ala, to ensure that a constant supply of Arg-Ala-derived Arg is present over time in the cytosol at the lower Arg-Ala concentrations.

Epifluorescence microscopic analysis

Fluorescence imaging was performed using a fully motorized inverted microscope (Nikon Eclipse Ti) equipped with a focus assistant (Nikon PFS), Apo TIRF 100× Oil DIC N objective, NIKON DS-Vi1 color camera, ANDOR LUCA R DL604 camera, Xenon fluorescence light source and standard filters for EYFP detection (λ_{ex} = 490 to 510 nm; λ_{em} = 520 to 550 nm). Differential interference contrast (DIC) microscopy images as well as fluorescence images were captured and analyzed using the Nikon NIS Elements AR software package. Prior to analysis, cells were fixed on soft agarose-covered glass slides.

Additional material

Additional file 1: Supplementary Tables S1 to S4 and Figures S1 to S6. Table S1: strains used. Table S2: quality assessment of sorting cells carrying pSenLys. Table S3: L-lysine formation with mutations introduced by reverse engineering. Table S4: statistics on whole-genome sequencing of strain K051. Table S5: growth rates of *murE* mutants. Figure S1: isolation of LysG and characterization of the LysG binding site. Figure S2: the vector pSenLys and general configuration of sensor plasmids. Figure S3: peptide-dose response curves with sensor-carrying *E. coli* and *C. glutamicum*. Figure S4: development of Crimson and EYFP signals in mixtures of ATCC13032 with DM1728 over time. Figure S5: growth curves and fluorescence of 40 mutant cultures. Figure S6: structural presentation of LysC and localization of mutations identified.

Additional file 2: All mutations of *C. glutamicum* strain K051.

Abbreviations

bp: base pair; EYFP: enhanced yellow fluorescent protein; FACS: fluorescence-activated cell sorting; FP: Flowerplate; HT: high throughput; IPTG: isopropyl-β-D-thiogalactopyranoside; MNNG: N-methyl-N'-nitro-N-nitrosoguanidine; SNP: single nucleotide polymorphism; TF: transcription factor; WT: wild type.

Acknowledgements

This work was funded by the German Federal Ministry of Education and Research, FlexFit project, support code 0315589A. We thank Jessica Schneider, Thomas Bekel and Stephan Hans for support in genome analysis, Peter Droste for his introduction to the Omix software, Katharina Nöh for statistical analyses, Jan Marienhagen for useful discussions, Alexander Grünberger for preparation of microscopic pictures, and Tino Polen for help with data analysis.

Authors' contributions

SB performed experimental studies and the FACS analyses. GS constructed sensors and did the graphic work. NS and KH contributed to sensor construction. The determination of pool concentrations and export rates was done by KK, MB contributed to manuscript writing, and LE designed the project and wrote the paper. All authors have read and approved the manuscript for publication.

Competing interests

The authors declare that they have no competing interests.

Received: 2 April 2012 Revised: 16 May 2012 Accepted: 28 May 2012
Published: 28 May 2012

References

1. Demain AL, Adrio JL: **Strain improvement for production of pharmaceuticals and other microbial metabolites by fermentation.** *Prog Drug Res* 2008, **65**:253-289.
2. Tsuruta H, Paddon CJ, Eng D, Lenihan JR, Horning T, Anthony LC, Regentin R, Keasling JD, Renninger NS, Newman JD: **High-level production of amorpha-4,11-diene, a precursor of the antimalarial agent artemisinin, in *Escherichia coli*.** *PLoS One* 2009, **4**:e4489.
3. Ajikumar PK, Xiao W-H, Tyo KEJ, Wang Y, Simeon F, Leonard E, Mucha O, Phon TH, Pfeifer B, Stephanopoulos G: **Isoprenoid pathway optimization for Taxol precursor overproduction in *Escherichia coli*.** *Science* 2010, **330**:70-74.

4. Dunlop MJ, Dossani ZY, Szmidt HL, Chu HC, Lee TS, Keasling JD, Hadi MZ, Mukhopadhyay A: **Engineering microbial biofuel tolerance and export using efflux pumps.** *Mol Syst Biol* 2011, **7**:487.
5. Zhang X, Jantama K, Moore JC, Jarboe LR, Shanmugam KT, Ingram LO: **Metabolic evolution of energy-conserving pathways for succinate production in *Escherichia coli*.** *Proc Natl Acad Sci USA* 2009, **106**:20180-20185.
6. Abbas CA, Sibirny AA: **Genetic control of biosynthesis and transport of riboflavin and flavin nucleotides and construction of robust biotechnological producers.** *Microbiol Mol Biol Rev* 2011, **75**:321-360.
7. Mardis ER: **A decade's perspective on DNA sequencing technology.** *Nature* 2011, **470**:198-203.
8. Gu MB, Mitchell RJ, Kim BC: **Whole-cell-based biosensors for environmental biomonitoring and application.** *Adv Biochem Eng* 2004, **87**:269-305.
9. Binder S, Mustafi N, Frunzke J, Bott M, Eggeling L: **Sensors for the detection of intracellular metabolites. WIPO Patent Application WO/2011/138006.** [http://patentscope.wipo.int/search/en/detail.jsf?docId=WO2011138006&recNum=37&docAn=EP2011002196&queryString=ALL:nmr%2520AND%2520DP:2011&maxRec=7293].
10. Tang S-Y, Cirino PC: **Design and application of a mevalonate-responsive regulatory protein.** *Angew Chem Int Ed Engl* 2010, **50**:1084-1086.
11. Galvão TC, de Lorenzo V: **Transcriptional regulators à la carte: engineering new effector specificities in bacterial regulatory proteins.** *Curr Opin Biotechnol* 2006, **17**:34-42.
12. Gredell JA, Frei CS, Cirino PC: **Protein and RNA engineering to customize microbial molecular reporting.** *Biotechnol J* 2011, **7**:477-499.
13. Klein-Marcuschamer D, Ajikumar PK, Stephanopoulos G: **Engineering microbial cell factories for biosynthesis of isoprenoid molecules: beyond lycopene.** *Trends Biotechnol* 2007, **25**:417-424.
14. Bellmann A, Vrljic M, Pátek M, Sahm H, Krämer R, Eggeling L: **Expression control and specificity of the basic amino acid exporter LysE of *Corynebacterium glutamicum*.** *Microbiology* 2001, **147**:1765-1774.
15. Ohnishi J, Mitsuhashi S, Hayashi M, Ando S, Yokoi H, Ochiai K, Ikeda M: **A novel methodology employing *Corynebacterium glutamicum* genome information to generate a new L-lysine-producing mutant.** *Appl Microbiol Biotechnol* 2002, **58**:217-223.
16. Nikaido H: **Molecular basis of bacterial outer membrane permeability revisited.** *Microbiol Mol Biol Rev* 2003, **67**:593-656.
17. Eggeling L: **Microbial Metabolite Export in Biotechnology.** *Encyclopedia of Industrial Biotechnology: Bioprocess, Bioseparation, and Cell Technology* Hoboken, NJ: John Wiley & Sons, Inc.; 2009.
18. Tavori H, Kimmel Y, Barak Z: **Toxicity of leucine-containing peptides in *Escherichia coli* caused by circumvention of leucine transport regulation.** *J Bacteriol* 1981, **146**:676-683.
19. Bellmann A, Vrljic M, Patek M, Sahm H, Kramer R, Eggeling L: **Expression control and specificity of the basic amino acid exporter LysE of *Corynebacterium glutamicum*.** *Microbiology-Sgm* 2001, **147**:1765-1774.
20. Nandineni MR, Gowrishankar J: **Evidence for an arginine exporter encoded by yggA (argO) that is regulated by the LysR-type transcriptional regulator ArgP in *Escherichia coli*.** *J Bacteriol* 2004, **186**:3539-3546.
21. Adelberg EA, Mandel M, Ching Chen GC: **Optimal conditions for mutagenesis by N-methyl-N'-nitro-N-nitrosoguanidine in K12.** *Biochem Biophys Res Commun* 1965, **18**:788-795.
22. Geoffrey McLachlan DP: *Finite Mixture Models* Hoboken, NJ: John Wiley & Sons, Inc.; 2000.
23. Yoshida A, Tomita T, Kuzuyama T, Nishiyama M: **Mechanism of concerted inhibition of $\alpha_2\beta_2$-type hetero-oligomeric aspartate kinase from *Corynebacterium glutamicum*.** *J Biol Chem* 2010, **285**:27477-27486.
24. Studier FW, Daegelen P, Lenski RE, Maslov S, Kim JF: **Understanding the differences between genome sequences of *Escherichia coli* B strains REL606 and BL21(DE3) and comparison of the *E. coli* B and K-12 genomes.** *J Mol Biol* 2009, **394**:653-680.
25. Ikeda M, Ohnishi J, Hayashi M, Mitsuhashi S: **A genome-based approach to create a minimally mutated *Corynebacterium glutamicum* strain for efficient L-lysine production.** *J Ind Microbiol Biotechnol* 2006, **33**:610-615.
26. Petersen S, de Graaf AA, Eggeling L, Möllney M, Wiechert W, Sahm H: **In vivo quantification of parallel and bidirectional fluxes in the anaplerosis of *Corynebacterium glutamicum*.** *J Biol Chem* 2000, **275**:35932-35941.
27. van Ooyen J, Noack S, Bott M, Reth A, Eggeling L: **Improved L-lysine production with *Corynebacterium glutamicum* and systemic insight into citrate synthase flux and activity.** *Biotechnol Bioeng* 2012, **109**:2070-2081.
28. Zhang J, Lau MW, Ferré-D'Amaré AR: **Ribozymes and riboswitches: modulation of RNA function by small molecules.** *Biochemistry* 2010, **49**:9123-9131.
29. East AK, Mauchline TH, Poole PS: **Biosensors for ligand detection.** *Adv Appl Microbiol* 2008, **64**:137-166.
30. van der Meer JR, Belkin S: **Where microbiology meets microengineering: design and applications of reporter bacteria.** *Nat Rev Microbiol* 2010, **8**:511-522.
31. Tracy BP, Gaida SM, Papoutsakis ET: **Flow cytometry for bacteria: enabling metabolic engineering, synthetic biology and the elucidation of complex phenotypes.** *Curr Opin Biotechnol* 2010, **21**:85-99.
32. Zhang F, Keasling J: **Biosensors and their applications in microbial metabolic engineering.** *Trends Microbiol* 2011, **19**:323-329.
33. Liang JC, Bloom RJ, Smolke CD: **Engineering biological systems with synthetic RNA molecules.** *Mol Cell* 2011, **43**:915-926.
34. Tang S-Y, Fazelinia H, Cirino PC: **AraC regulatory protein mutants with altered effector specificity.** *J Am Chem Soc* 2008, **130**:5267-5271.
35. de Las Heras A, de Lorenzo V: **Cooperative amino acid changes shift the response of the sigma-dependent regulator XylR from natural m-xylene towards xenobiotic 2,4-dinitrotoluene.** *Mol Microbiol* 2011, **79**:1248-1259.
36. Krueger M, Scholz O, Wisshak S, Hillen W: **Engineered Tet repressors with recognition specificity for the tetO-4C5G operator variant.** *Gene* 2007, **404**:93-100.
37. Kelle R, Hermann T, Bathe B: **L-lysine production.** In *Handbook of Corynebacterium glutamicum*. Edited by: Eggeling L, Bott M. Boca Raton, FL: CRC Press, Taylor 2005:465-488.
38. Becker J, Zelder O, Hafner S, Schroder H, Wittmann C: **From zero to hero - design-based systems metabolic engineering of Corynebacterium glutamicum for L-lysine production.** *Metab Eng* 2011, **13**:159-168.
39. Hayashi M, Ohnishi J, Mitsuhashi S, Yonetani Y, Hashimoto S-I, Ikeda M: **Transcriptome analysis reveals global expression changes in an industrial L-lysine producer of *Corynebacterium glutamicum*.** *Biosci Biotechnol Biochem* 2006, **70**:546-550.
40. Ikeda M, Mitsuhashi S, Tanaka K, Hayashi M: **Reengineering of a *Corynebacterium glutamicum* L-arginine and L-citrulline producer.** *Appl Environ Microbiol* 2009, **75**:1635-1641.
41. Mockel B, Eggeling L, Sahm H: **Threonine dehydratases of *Corynebacterium glutamicum* with altered allosteric control: their generation and biochemical and structural analysis.** *Mol Microbiol* 1994, **13**:833-842.
42. Bertrand JA, Auger G, Fanchon E, Martin L, Blanot D, van Heijenoort J, Dideberg O: **Crystal structure of UDP-N-acetylmuramoyl-L-alanine:D-glutamate ligase from *Escherichia coli*.** *EMBO J* 1997, **16**:3416-3425.
43. Grunberger A, Paczia N, Probst C, Schendzielorz G, Eggeling L, Noack S, Wiechert W, Kohlheyer D: **A disposable picolitre bioreactor for cultivation and investigation of industrially relevant bacteria on the single cell level.** *Lab Chip* 2012, **12**:2060-2068.
44. Huber R, Ritter D, Hering T, Hillmer A-K, Kensy F, Müller C, Wang L, Büchs J: **Robo-Lector - a novel platform for automated high-throughput cultivations in microtiter plates with high information content.** *Microb Cell Fact* 2009, **8**:42.
45. Stolz M, Peters-Wendisch P, Etterich H, Gerharz T, Faurie R, Sahm H, Fersterra H, Eggeling L: **Reduced folate supply as a key to enhanced L-serine production by *Corynebacterium glutamicum*.** *Appl Environ Microbiol* 2007, **73**:750-755.
46. Klingenberg M, Pfaff E: **Means of terminating reactions.** In *Oxidation and Phosphorylation. Volume 10*. Edited by: Ronald W. Estabrook MEP: Academic Press; 1967:680-684.

doi:10.1186/gb-2012-13-5-r40
Cite this article as: Binder *et al.*: A high-throughput approach to identify genomic variants of bacterial metabolite producers at the single-cell level. *Genome Biology* 2012 **13**:R40.

ACS SyntheticBiology

Research Article

pubs.acs.org/synthbio

SoxR as a Single-Cell Biosensor for NADPH-Consuming Enzymes in *Escherichia coli*

Solvej Siedler,† Georg Schendzielorz, Stephan Binder, Lothar Eggeling, Stephanie Bringer, and Michael Bott*

IBG-1: Biotechnology, Institute of Bio- and Geosciences, Forschungszentrum Jülich, D-52425 Jülich, Germany

Supporting Information

ABSTRACT: An ultra-high-throughput screening system for NADPH-dependent enzymes, such as stereospecific alcohol dehydrogenases, was established. It is based on the [2Fe−2S] cluster-containing transcriptional regulator SoxR of *Escherichia coli* that activates expression of *soxS* in the oxidized but not in the reduced state of the cluster. As SoxR is kept in its reduced state by NADPH-dependent reductases, an increased NADPH demand of the cell counteracts SoxR reduction and increases *soxS* expression. We have taken advantage of these properties by placing the *eyfp* gene under the control of the *soxS* promoter and analyzed the response of *E. coli* cells expressing an NADPH-dependent alcohol dehydrogenase from *Lactobacillus brevis* (*Lb*Adh), which reduces methyl acetoacetate to (*R*)-methyl 3-hydroxybutyrate. Under suitable conditions, the specific fluorescence of the cells correlated with the substrate concentration added and with *Lb*Adh enzyme activity, supporting the NADPH responsiveness of the sensor. These properties enabled sorting of single cells harboring wild-type *Lb*Adh from those with lowered or without *Lb*Adh activity by fluorescence-activated cell sorting (FACS). In a proof-of-principle application, the system was used successfully to screen a mutant *Lb*Adh library for variants showing improved activity with the substrate 4-methyl-2-pentanone.

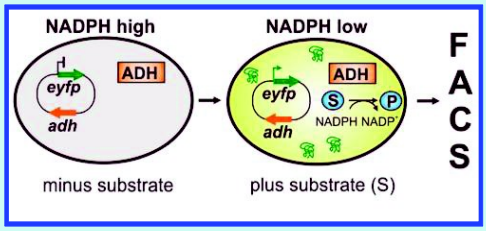

KEYWORDS: *NADPH biosensor, alcohol dehydrogenases, enzyme evolution, single-cell analysis, FACS*

Redox reactions are at the core of cellular metabolic processes, and about one-quarter of known enzymes are oxidoreductases.[1] A feature of many of these enzymes is their stereo- and regiospecificity. The pharmaceutical industry takes advantage of these properties as well as the mild and environmentally friendly conditions under which enzyme-catalyzed reactions proceed. Among such processes, alcohol dehydrogenases are of particular interest.[2,3] They are employed in the reduction of various ketones to produce enantiopure secondary alcohols. These enzymes are frequently NADPH-dependent, and there is a need for a continuous supply of the reduced cofactor for the reaction to proceed.[2,4,5] This applies both for isolated enzymes and for whole-cell processes.[6,7]

In our studies with *Escherichia coli* on the reductive biotransformation of methyl acetoacetate (MAA) to (*R*)-methyl 3-hydroxybutyrate (MHB) by a strictly NADPH-dependent alcohol dehydrogenase from *Lactobacillus brevis* (*Lb*Adh),[6,8,9] we noticed a significantly increased mRNA level of the *soxS* gene in cells catalyzing MAA reduction. SoxS is a transcription factor whose expression is activated under conditions of oxidative stress by SoxR.[10−13] The genes of the SoxRS regulon mediate the cellular response to superoxide, to diverse redox-cycling drugs like paraquat, or to nitric oxide.[14,15] SoxR is a homodimer with each subunit containing an [2Fe−2S] cluster.[16,17] Only when the cluster is oxidized to $[2Fe-2S]^{2+}$ is transcriptional activity conferred to SoxR, which in turn results in the expression of *soxS*.[18,19] SoxS then activates expression of the SoxRS regulon, which includes, for example, the genes for superoxide dismutase (*sodA*), glucose 6-phosphate dehydrogenase (*zwf*), or fumarase C (*fumC*).[20] Inactivation of SoxR involves its NADPH-dependent reduction catalyzed by the *rsxABCDGE* and *rseC* products.[21]

The nature of the cellular signal sensed by SoxR is still a matter of debate.[22−24] Besides direct oxidation of the iron−sulfur centers by superoxide[25] and redox cycling drugs,[23] Liochev and Fridovich first suggested that the SoxRS regulon is responsive to the NADPH/$NADP^+$ ratio,[26] which was supported by several studies. Krapp et al.[27] showed that introduction of a heterologous $NADP^+$-reducing enzyme, the nonphosphorylating glyceraldehyde 3-phosphate dehydrogenase from wheat, into *E. coli* led to an increased NADPH/$NADP^+$ ratio, inhibition of the SoxR-mediated response, and enhanced sensitivity to the superoxide propagator methyl viologen (MV) and vice versa: overproduction of pea ferredoxin, which stimulates NADPH oxidation via ferredoxin-NADP(H) reductase, led to a decreased NADPH/$NADP^+$ ratio, triggering of the SoxR response and a higher tolerance to MV. Kobayashi and Tagawa[28] isolated an 84 kDa enzyme that catalyzed the NADPH-dependent reduction of oxidized SoxR.

Received: August 14, 2013
Published: November 27, 2013

In our previous work, we showed that after starting the NADPH-dependent reductive biotransformation of MAA to MHB the NADPH/NADP$^+$ ratio of the cells decreased, whereas the NADH/NAD$^+$ ratio (and the *soxS* mRNA level) increased.[29] These results favor NADPH and disfavor NADH as a SoxR reductant. In the present work, we provide further evidence that SoxR can sense NADPH availability, and we utilized this finding to develop a sensor for the in vivo analysis of NADPH-dependent reactions, offering a number of exciting possibilities for high-throughput analysis and the development of NADPH-dependent enzymes.

RESULTS AND DISCUSSION

SoxR as an NADPH Sensor. Our previous studies indicated that the transcriptional regulator SoxR of *E. coli* activates expression of its target gene *soxS* during reductive biotransformations with a high demand of NADPH because of a reduced capability of the cell for NADPH-dependent reduction and inactivation of SoxR. On the basis of this correlation, SoxR might be used as an NADPH sensor. To evaluate and apply such a function of SoxR, we constructed plasmid pSenSox in which *soxR* of *E. coli* DH5α together with the *soxR*–*soxS* intergenic region and a small part of the *soxS* coding region followed by a stop codon were cloned in front of *eyfp*, thereby placing synthesis of the autofluorescent protein eYFP under transcriptional control of the *soxS* promoter (Figure 1). The sensor plasmid also encodes the NADPH-dependent alcohol dehydrogenase of *L. brevis*, *Lb*Adh, under the control of an isopropyl β-D-thiogalactoside-inducible promoter. *Lb*Adh was previously shown by us and others to convert efficiently MAA stoichiometrically to MHB.[6,8,29,30]

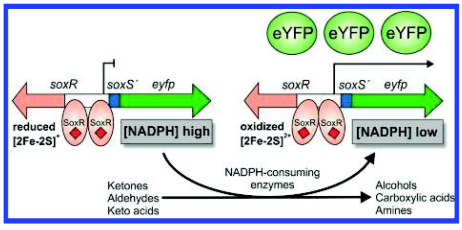

Figure 1. NADPH biosensor based on the transcriptional regulator SoxR of *E. coli*. Dimeric SoxR with two Fe–S clusters binds to the *soxR*–*soxS* intergenic region. At sufficient NADPH levels, the Fe–S clusters are kept in the reduced state, and SoxR is inactive. The enhanced activity of NADPH-consuming enzymes impedes SoxR reduction, and the oxidized Fe–S clusters trigger a conformational change of SoxR, causing transcription of its target gene *soxS*. In the NADPH biosensor pSenSox, *soxS* has been replaced by *eyfp* coding for the fluorescent protein eYFP, which allows for the identification of cells with a low NADPH level by their increased fluorescence.

E. coli BL21(DE3) was transformed with plasmid pSenSox and used for whole-cell biotransformation assays in 2× TY medium with 10–70 mM MAA as an *Lb*Adh substrate. Complex medium was used to enable eYFP synthesis. In these assays, NADPH is provided by the metabolism of components present in yeast extract and tryptone. For online recording of eYFP fluorescence and growth, a BioLector system was used. Under the chosen conditions, at best doubling of the cells was observed (Figure S1). Upon addition of MAA, the cultures started to emit fluorescence with the initial slope of the fluorescence increase being independent of the MAA concentration added (Figure 2a). As recently discussed by us,[30] in the biotransformation system used here with a high activity of wild-type *Lb*Adh, the enzyme is saturated with the substrate MAA, and metabolic NADPH generation is likely the limiting step. Increasing concentrations of MAA led to higher fluorescence maxima, and the time period required to reach these maxima also increased (Figure 2a). The maximal fluorescence intensity obtained for different initial MAA concentrations remained constant for several hours because of the marginal growth of the cells, the slow maturation kinetics of the eYFP chromophore, and the high stability of eYFP. When the specific fluorescence achieved after 10 h was plotted against the initial MAA concentration, an almost linear

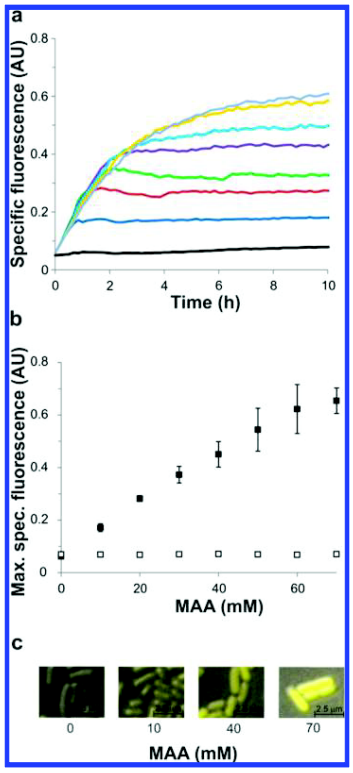

Figure 2. (a) Specific fluorescence (485 nm excitation, 520 nm emission) of *E. coli* carrying the NADPH biosensor pSenSox during biotransformation of 10 (dark blue), 20 (brown), 30 (green), 40 (purple), 50 (light blue), 60 (yellow), and 70 mM (gray) MAA to MHB via the NADPH-dependent alcohol dehydrogenase *Lb*Adh. A control without MAA is shown in black. (b) Specific fluorescence of cells (■) measured after 10 h of biotransformation plotted against the initial MAA concentration. Mean values and standard deviations of three independent replicates are shown. The empty squares (□) show the values obtained with the control plasmid, pSenNeg, encoding an inactive *Lb*Adh fragment. (c) Epifluorescence of cells from biotransformations with 0, 10, 40, or 70 mM MAA.

dx.doi.org/10.1021/sb400110j | ACS Synth. Biol. 2014, 3, 41–47

Table 1. Dependence of the Maximal Specific Fluorescence from the Specific *Lb*Adh Activity of Cells

plasmids carried in *E. coli* BL21(DE3)	IPTG[a]	*Lb*Adh activity (μmol min^{-1} (mg protein)$^{-1}$)[b]	maximal specific fluorescence[b,c]
pSenNeg	−	0.03 ± 0.01	0.07 ± 0.01
pSenSox pET28a[d]	−	0.5 ± 0.1	0.09 ± 0.01
pSen-L194S	−	0.7 ± 0.3	0.11 ± 0.01
pSen-L194A	−	2.7 ± 0.6	0.18 ± 0.04
pSenSox	−	6.3 ± 0.6	0.38 ± 0.02
pSenSox	+	15.2 ± 2.0	0.46 ± 0.04

[a]IPTG was added at 1 mM. To allow reproducible expression, plasmid pSenSox carries no *lacI* gene, but *E. coli* BL21(DE3) contains a chromosomal copy of *lacI*. IPTG was used to maximize expression. [b]Mean values and standard deviations from three replicates are given. [c]Values were measured after 19 h of biotransformation with 40 mM MAA. [d]Vector pET28a provided an additional copy of *lacI* for stronger repression of *Lbadh*.

relationship was obtained for MAA concentrations up to 60 mM (Figure 2b). In the absence of MAA, constant background fluorescence was observed. Similarly, in biotransformation experiments with cells carrying plasmid pSenNeg encoding an inactive *Lb*Adh fragment, only background fluorescence was detectable independent of the MAA concentration added. These controls confirm that the fluorescence increase was strictly dependent on the NADPH-dependent reduction of MAA to MHB. The increased fluorescence obtained with increased MAA concentrations was also visible at the single-cell level by epifluorescence microscopy (Figure 2c) and flow cytometry (see below).

The results reported above support the view that SoxR of *E. coli* is active under conditions of high NADPH demand, as obtained by the reduction of MAA to MHB by *Lb*Adh. By measuring SoxR activity via *eyfp* expression under control of the *soxS* promoter, we showed that the maximal specific fluorescence of cells correlates with the concentration of MAA reduced to MHB (Figure 2). To explain the observed correlation, we propose that SoxR is subject to permanent oxidation under aerobic conditions (e.g., by superoxide ions, which were reported to be formed at a rate of 5 μM s^{-1}),[15,31] but it is kept in its reduced form by NADPH-dependent reduction via the *rsxABCDGE* and *rseC* gene products. Under conditions of high NADPH demand, SoxR reduction is hampered, thus favoring the presence of oxidized, active SoxR. Regarding the discussion on the nature of the signal sensed by SoxR, our data support the concept of Liochev and Fridovich[26] that there are multiple ways to induce the SoxRS regulon, which ultimately shift the equilibrium of oxidized and reduced SoxR to the oxidized form. This can either happen by increasing the oxidation of reduced SoxR or by decreasing the reduction of oxidized SoxR, as exemplified in our study.

Correlation between Fluorescence and *Lb*Adh Activity. In the next series of experiments, the influence of varying *Lb*Adh activities on the fluorescence output was tested (Table 1). For this purpose, six cultures with a specific *Lb*Adh activity between 0.03 U (mg protein)$^{-1}$ (background activity) and 15.2 U (mg protein)$^{-1}$ were used in biotransformations with a set of different MAA concentrations. The different *Lb*Adh activities were achieved either by varying the expression level of the wild-type enzyme via induction with IPTG or repression with LacI or by using mutant *Lb*Adh proteins with amino acid exchanges Leu194Ser or Leu194Ala. The time course of specific fluorescence for these cultures when incubated with different MAA concentrations is shown in Figure S2. Higher *Lb*Adh activities led to higher maximal specific fluorescence, and this is shown exemplarily for 40 mM MAA in Table 1. Thus, the pSenSox system in the living cell offers the possibility to distinguish NADPH-dependent enzymes with varying specific activity.

Application of SoxR for High-Throughput Screening of NADPH-Dependent Enzymes. Recently, metabolite-activated transcription factors controlling *eypf* expression were used to monitor the cytosolic concentration of the respective metabolites in single bacterial cells, which allowed high-throughput screening and isolation of single producer cells using fluorescence-activated cell sorting (FACS).[32−34] On the basis of these results, we tested whether single cells differing in their specific *Lb*Adh activity also can be analyzed and sorted via FACS. For this purpose, *E. coli* cells carrying either pSenSox (6.2 U mg^{-1} *Lb*Adh activity), pSen-L194A (2.7 U mg^{-1}), or pSenNeg (0.03 U mg^{-}1) were used for biotransformation of 70 mM MAA for 19 h and then subjected to FACS. The resulting combined histogram (Figure 3a) shows three well-resolved peaks of eYFP fluorescence, indicating that the three strains differing in their specific *Lb*Adh activities form homogeneous populations. Using an appropriate gate, P1, to exclude cells with background fluorescence (carrying pSenNeg), 80.8% of the population of cells with high fluorescence (carrying pSenSox) and 1.5% of the cells with lower fluorescence (carrying pSen-L194A) could be isolated.

These results encouraged us to test the suitability of pSenSox for high-throughput screening of alcohol dehydrogenase mutant libraries. To do this, we introduced mutations in *Lb*Adh both randomly by error-prone PCR and by individual site-directed mutagenesis at positions Ala93, Leu152, and Val195, which are known to be involved in substrate binding.[9] The cells of the four mutant libraries were pooled and used for reductive biotransformation of 20 mM 4-methyl-2-pentanone (4M2P). This prochiral ketone was chosen because the reduced product (*R*)-4-methyl-2-pentanol is of economic interest and because wild-type *Lb*Adh has only ∼12% activity with this substrate as compared to MAA (15.5 μmol min^{-1} (mg protein)$^{-1}$). Analysis of cells containing wild-type *Lb*Adh showed that the maximal specific fluorescence obtained with 20 mM 4M2P was obtained already after 2 to 3 h of biotransformation. Therefore, the cells of the mutant libraries were subjected to FACS after approximately 3 h of biotransformation.

We performed a sort on the library in which wild-type *Lb*Adh after biotransformation of 4M2P was used to define the lower bound of the sorting gate. This bound was set close to the maximal fluorescence of cells containing wild-type *Lb*Adh, which enhances the chances for identifying even slightly improved Adh variants but also for sorting false positives. The wild-type *Lb*Adh-containing strain served as a positive control after biotransformation of MAA instead of 4M2P (Figure 3b). In the scatter plots of wild-type *Lb*Adh with either 4M2P or

dx.doi.org/10.1021/sb400110j | ACS Synth. Biol. 2014, 3, 41−47

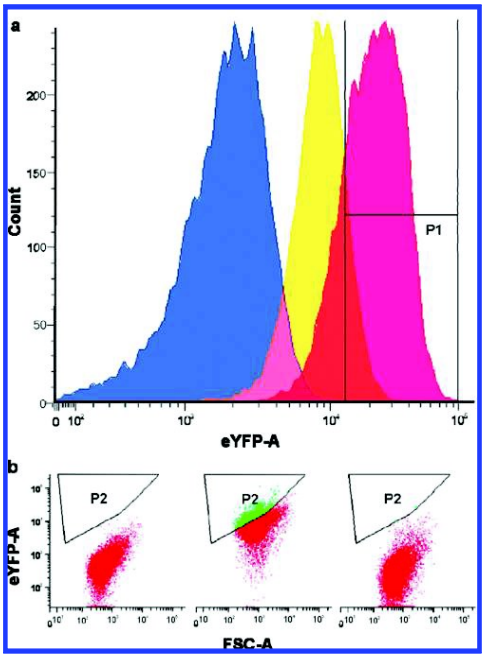

Figure 3. Flow cytometric analysis of *E. coli* cells with the *soxR*–*soxS*-based NADPH sensor and different NADPH-dependent *Lb*Adh activities. (a) Combined fluorescence histograms of three *E. coli* strains carrying either pSenNeg (blue, 0.03 U mg^{-1} *Lb*Adh acitivity), pSen-L194A (yellow, 2.7 U mg^{-1} *Lb*Adh activity), or pSenSox (red, 6.28 U mg^{-1} *Lb*Adh activity) after biotransformation for 19 h with 70 mM MAA. Gate P1 was used for differentiation of pSenNeg and mutant or wild-type populations. (b) FACS-generated scatter plots displaying the forward scatter signal (FSC) and the eYFP signal of *E. coli* cells carrying pSenSox after reductive biotransformation of 20 mM 4M2P (left side) or 20 mM MAA (middle). On the right side, the library of mutant *Lb*Adhs was used for biotransformation of 20 mM 4M2P and then subjected to FACS. Gate P2 was used for mutant screening.

MAA as a substrate, a relatively broad distribution of the cells was observed. Similar observations were made for yeast cells with a theophylline sensor,[35] and the authors speculated that individual gene expression noise was responsible for this heterogeneity, arising from cell-specific differences in cell cycle stage, fluctuations in plasmid copy numbers, and other parameters.[36] Such heterogeneity may distort the quantitative output of a metabolite sensor to some extent and enhance the background signal, thereby increasing the rate of false positives. In a single screen, 10^6 cells of the *Lb*Adh mutant library were analyzed, and 250 cells showing slightly enhanced fluorescence were selected and spotted on plates, of which 123 grew to form colonies. Ninety six of these clones were analyzed in a microtiter plate for fluorescence intensity after a 2 to 3 h incubation with 4M2P (Figure S3). From six selected clones with high specific fluorescence at the selected time point, the specific *Lb*Adh activity was determined (Table S1), and one clone was identified that had a 36% increased activity with the substrate 4M2P accompanied by an 8-fold increased K_m value (Table 2). The plasmid of this mutant clone was fully sequenced and found to contain a single mutation in the *Lbadh* gene that led to an Ala93Met exchange.

Table 2. Properties of Wild-Type *Lb*Adh and Variant *Lb*Adh-A93M for the Substrate 4-Methyl-2-pentanone

enzyme[a]	V_{max} (μmol min^{-1} mg^{-1})[b]	K_m (mM)[b]
*Lb*Adh	1.94 ± 0.02	0.11 ± 0.01
*Lb*Adh-A93M	2.62 ± 0.03	0.88 ± 0.07

[a]Enzyme activities were determined with crude extracts of the respective strains carrying either pSenSox or pSen-A93M. [b]Mean values and standard deviation from three replicates are given.

In conclusion, the correlation between NADPH consumption and fluorescence was visible at the single-cell level and suitable for FACS analysis, allowing the highest throughput assays currently possible. Because we could identify conditions leading to a good correlation between the specific activity of the NADPH-consuming enzyme and the specific fluorescence of the cells, the SoxR sensor provides a generalized high-throughput screening system for this type of enzymes. We demonstrated this potential by the rapid isolation of an *Lb*Adh variant via FACS with an improved activity toward the substrate 4M2P (Table 2). To reduce the number of false positives, suitable enrichments steps have to be identified and included in future applications of the SoxR-based sensor, as reported for other high-throughput screening systems.[35,37−39] As long as educts and products can enter and leave the sensor-containing cells, libraries of NADPH-dependent enzymes can now be assayed in a high-throughput format without the development of specific assays. This novel technology has the potential to expedite the availability of new enzymes for the synthesis of chiral compounds significantly.

METHODS

Bacterial Strains, Media, and Growth Conditions. Bacterial strains and plasmids are listed in Table 3. *E. coli* strains were transformed by the method described by Hanahan[40] and cultivated in LB medium[41] or in 2× YT medium (16 g L^{-1} of tryptone, 10 g L^{-1} of yeast extract, and 5 g L^{-1} of sodium chloride). *E. coli* DH5α[40] was used for cloning and screening purposes, and *E. coli* BL21 Star (DE3) (Invitrogen, Karlsruhe, Germany) and derivatives were used for gene expression and whole-cell biotransformation for sensor establishment. Plasmids were selected by adding antibiotics to the medium at a final concentration of 100 μg mL^{-1} of ampicillin (pSenSox and derivatives) and 50 μg mL^{-1} of kanamycin (pET28a).

Recombinant DNA Work. Standard methods, including PCR and DNA restriction or ligation, were carried out according to standard protocols.[42] Oligonucleotides were synthesized by Biolegio eV (Nijmegen, The Netherlands) and are listed in Table 3. For construction of the plasmid-based biosensor pSenSox, the *E. coli* DNA region encompassing the *soxR* open reading frame, the *soxR*–*soxS* intergenic region, and the first 21 codons of *soxS* were amplified with Phusion DNA polymerase (Thermo Scientific) from chromosomal DNA of *E. coli* BL21(DE3) by PCR using oligonucleotides SoxS_for_*SphI* and SoxR_rev_*SalI*, which introduce *SphI* and *SalI* restriction sites as well as a stop codon after codon 21 of *soxS*. Additionally, the *eyfp* gene was amplified by PCR with

dx.doi.org/10.1021/sb400110j | ACS Synth. Biol. 2014, 3, 41−47

Table 3. Strains, Plasmids, and Oligonucleotides Used in This Work

strains, plasmids, and oligonucleotides	relevant characteristics or 5′−3′ sequence	ref or restriction site
Strains		
Escherichia coli BL21 Star (DE3)	F⁻ *ompT* $hsdS_B(r_B^-, m_B^-)$ *gal dcm rne*131 (DE3)	Invitrogen
Escherichia coli DH5α	F⁻ Φ 80Δ*lacZ*ΔM15 Δ(*lacZYA-argF*) U169 *deoR recA*1 *endA*1 *hsdR*17 (rk^-, mk^+) *phoA supE*44 λ^- *thi*-1 *gyrA*96 *relA*1	Hanahan[40]
Plasmids		
pBTac-*Lbadh*	Amp^R; pBtac1 derivative with *adh* gene from *Lactobacillus brevis*	Ernst et al.[8]
pSenSox	Amp^R; pBtac-*Lbadh* derivative containing *soxRS*-based biosensor	this study
pSenNeg	Amp^R; pSenSox derivative encoding an inactive *Lb*Adh fragment	this study
pSen-L194S	Amp^R; pSenSox derivative encoding *Lb*Adh-L194S	this study
pSenL194A	Amp^R; pSenSox derivative encoding *Lb*Adh-L194A	this study
pSenA93M	Amp^R; pSenSox derivative encoding *Lb*Adh-A93M	this study
pET28a	Kan^R; plasmid used for provision of IPTG-inducible *lacI* gene	Novagen
pSenLys	Kan^R; pJC1 derivative containing *lysGE*-based biosensor	Binder et al.[32]
Oligonucleotides[a]		
SoxS_for_*SphI*	ATCTGCATGC*TTACGGCTGGTCAATATGCTCGTC*	*SphI*
SoxR_rev_*SalI*	GCTAGTCGAC*CAAACTAAAGCGCCCTTGTG*	*SalI*
EYFP_for_*SphI*	AGAGGCATGC*AAGGAGAATTAC**ATG**GTGAGCAAGGGCGAGG*	*SphI*
EYFP_rev_*ClaI*	GCGCATCGAT*TTATTACTTGTACAGCTCGTCCATG*	*ClaI*
ADH_negK_for	ACAAGAATTC*GCTAAGAGTGTCGGCACTCC*	*Eco*RI
ADH_negK_rev	GGCCAAGCTT*CCGAAGAAGACACCATCAAG*	*Hin*dIII
Ala93_for	GTTAATAACGCTGGGATCNNKGTTAACAAGAGTGTC	
Ala93_rev	GACACTCTTGTTAACMNNGATCCCAGCGTTATTAAC	
Leu152_for	GATCCTAGCTTAGGGGCNNKCAACGCATC	
Leu152_rev	GATGCGTTGMNNGCCCCTAAGCTAGGATC	
Val195_for	GACACCATTGGNNKATGACCTACCAGGGGC	
Val195_rev	GCCCCTGGTAGGTCATCAACMNNTGGTGTC	
ADH_mut_for	ATACGAATTC*ATGTCTAACCGTTTGGATGG*	*Eco*RI
ADH_mut_rev	GTGTGAAGCTT*ACTATTGAGCAGTGTAG*	*Hin*dIII

[a]Restriction sites are underlined, coding sequences are shown in italics, and start or stop codons are shown in bold.

oligonucleotides EYFP_for_*SphI*, containing a ribosome binding site, and EYFP_rev_*ClaI* using the vector pSenLys[32] as template, thereby introducing restriction sites for *SphI* and *ClaI* digestion. Both PCR products were cloned into the plasmid pBtac*Lbadh*,[8] resulting in plasmid pSenSox. For the construction of pSenNeg, a 221 bp region of the *adh* gene of *L. brevis* was amplified with the oligonucleotides ADH_negK_for and ADH_negK_rev, introducing *Eco*RI and *Hin*dIII restriction sites. The PCR product was cut with *Eco*RI and *Hin*dIII and used to replace the functional *adh* gene in plasmid pSenSox by a nonfunctional *adh* fragment. For individual saturation mutagenesis of codons Ala93, Leu152, and Val195 within the intact *adh* gene, the oligonucleotide pairs Ala93_for/Ala93_rev, Leu152_for/Leu152_rev, and Val195_for/Val195_rev were used according to the Stratagene site-directed mutagenesis kit with the following modifications: *Dpn*I (Fermentas) and PFX polymerase (Invitrogen) were used. For random mutagenesis of the entire *adh* gene, error-prone PCR (ep-PCR) was performed using the oligonucleotide pair ADH_mut_for/ADH_mut_rev, plasmid pSenSox as template, and Phusion DNA polymerase using the protocol described by Wilson and Keefe.[43] The PCR products were cut with *Eco*RI and *Hin*dIII and used to replace the native *adh* gene in pSenSox.

Whole-Cell Biotransformation in Microtiter Plates. For biotransformation experiments with *E. coli* cells harboring pSenSox or a derivative, 5 mL of 2× YT medium containing the appropriate antibiotic(s) was inoculated with a single colony of the respective strain and incubated overnight at 37 °C and 130 rpm. These precultures were used for inoculation of the main cultures to an optical density at 600 nm (OD_{600}) of 0.05. Main cultures were grown in 50 mL of 2× YT medium in the presence of the appropriate selection marker at 37 °C and 130 rpm to an OD_{600} of 0.3, induced with 1 mM IPTG when required, and incubated for another 3 h to an OD_{600} between 5 and 6. For online monitoring of fluorescence during biotransformation, 900 μL portions of the cultures were transferred into 48-well microtiter Flowerplates, and the cultures were supplemented with 100 μL of the biotransformation substrate dissolved in water and incubated in a BioLector cultivation system (m2plabs GmbH, Aachen, Germany) at 30 °C and 1200 rpm (shaking diameter 3 mm). During cultivation, biomass was measured as scattered light intensity (620 nm, signal gain factor of 15). The eYFP fluorescence of the cultures was measured at an excitation wavelength of 485 nm and an emission wavelength of 520 nm (signal gain factor of 70). The specific fluorescence was calculated as the ratio of eYFP fluorescence/scattered light intensity (given in a.u.).[44]

Ninety-Six-Well Screening System. For screening ADH activity, *E. coli* DH5α was transformed with the pSenSox derivatives subjected to site-directed mutagenesis and plated on LB agar plates containing 100 μg mL^{-1} of ampicillin. Single colonies were inoculated into 200 μL of 2× YT medium in a 96-well plate and grown overnight at 37 °C and 800 rpm. For the main culture, 5 μL of the preculture was inoculated into 145 μL of 2× YT medium in a 96-well plate. After 5 h, 40 mM methyl acetoacetate (MAA) or 40 mM 4M2P was added to the cells, and the fluorescence and the OD_{600} was measured every hour for 4 h using a plate reader (TECAN, Infinite 200 PRO). The specific fluorescence was defined as the fluorescence per OD_{600}.

dx.doi.org/10.1021/sb400110j | ACS Synth. Biol. 2014, 3, 41−47

Fluorescence Microscopy. Fluorescence microscopy was performed according to Mustafi et al.[33] Samples were placed on a microscope slide coated with a thin aqueous 0.1% (w/v) poly-L-lysine solution (Sigma-Aldrich GmbH, Munich, Germany) and covered by a coverslip. Images were taken on a Zeiss Axioplan 2 imaging microscope equipped with an AxioCam MRm camera and a Plan-Apochromat 100×, 1.40 Oil DIC oil-immersion objective. The exposure time was 500 ms. Digital images were acquired and analyzed with AxioVision 4.6 software (Zeiss, Göttingen, Germany).

Fluorescence-Activated Cell Sorting. Flow cytometric measurements were performed with a FACSAria II (Becton Dickinson, San Jose, USA) with 488 nm excitation (blue solid-state laser). Forward-scatter characteristics (FSC) and side-scatter characteristics (SSC) were detected as small-angle and large-angle scatters of the 488 nm laser, respectively. eYFP fluorescence was detected using a 502 nm long-pass and a 530/30 nm band-pass filter set. Data were analyzed using BD DIVA 6.1.3 software. The sheath fluid was sterile-filtered phosphate-buffered saline (137 mM NaCl, 2.7 mM KCl, 10 mM Na_2HPO_4, and 1.8 mM KH_2PO_4). Electronic gating was set to exclude nonbacterial particles on the basis of forward- versus side-scatter area. For sorting eYFP-positive cells, the next level of electronic gating was set to exclude nonfluorescent cells. Background was estimated using cells with pSenSox (wild-type *Lb*Adh) for sorting eYFP-positive cells. For screening cells having increased Adh activity with the substrate 4M2P, *E. coli* DH5*α* was transformed with a pSenSox library containing either site-directed or randomly mutagenized, via ep-PCR, *Lbadh*. After transformation, plating on LB agar plates containing ampicillin, and incubation for 18 h at 37 °C, the colonies were resuspended in 10 mL of 2× YT medium and diluted by a factor of 10 using 2× YT medium. Cells containing nonmutagenized pSenSox were used as background control. After 4 h of growth at 37 °C and 130 rpm, 20 mM 4M2P was added to the cells, and incubation was continued for 2.5 h, after which the cells were subjected to FACS.

Determination of Alcohol Dehydrogenase Activity. *E. coli* strains carrying the desired plasmids were cultured for 5 h at 37 °C and 130 rpm in 50 mL of 2× YT medium. Cells were harvested by centrifugation for 5 min at 10 000*g* and 4 °C. The cells were resuspended in 100 mM potassium phosphate buffer, pH 6.5, with 1 mM dithiothreitol and 1 mM $MgCl_2$. Cells were disrupted at 4 °C by 3 × 15 s bead-beating with glass beads (diameter 0.1 mm) using a Silamat S5 (Ivoclar Vivadent GmbH, Germany), and crude extracts were centrifuged for 20 min at 16 000*g* and 4 °C to remove intact cells and cell debris. The supernatants were used as cell-free extracts. Adh activity was measured photometrically at 340 nm using different dilutions of the cell-free extract using a mixture of 10 mM MAA, 250 μM NADPH, and 1 mM $MgCl_2$ in 100 mM potassium phosphate buffer, pH 6.5. Reactions were started by addition of cell-free extract. One unit of enzyme activity was defined as the amount of enzyme catalyzing the oxidation of 1 μmol min^{-1} NADPH at 30 °C under the specified conditions. Protein concentrations were determined by the method of Bradford[45] using bovine serum albumin as the standard. For the determination of the K_m values, substrate 4M2P was used at concentrations of 0.1−10 mM. K_m and V_{max} values were calculated using Lineweaver−Burk plots of the experimental data.[46]

■ ASSOCIATED CONTENT

Supporting Information

This material is available free of charge via the Internet at http://pubs.acs.org.

■ AUTHOR INFORMATION

Corresponding Author

*Phone: +49 2461 613294; Fax: +49 2461 612710; E-mail: m.bott@fz-juelich.de.

Present Address

†Technical University of Denmark, Novo Nordisk Foundation Center for Biosustainability, Kogle Allé 6, DK-2970 Hørsholm, Denmark.

Author Contributions

S.S., G.S., and S.Bi. performed the experiments, S.Br., L.E., and M.B. provided guidance for the experimental setups, and S.Br., L.E., and M.B. wrote the paper.

Notes

The authors declare no competing financial interest.

■ ACKNOWLEDGMENTS

We thank Alexander Grünberger for taking the epifluorescence pictures of the cells. This work was supported by the Ministry of Innovation, Science, Research and Technology of North Rhine-Westphalia (BioNRW, Technology Platform Biocatalysis, RedoxCell, support code W0805wb001b).

■ REFERENCES

(1) McDonald, A. G., Boyce, S., and Tipton, K. F. (2009) ExplorEnz: The primary source of the IUBMB enzyme list. *Nucleic Acids Res. 37*, D593−D597.

(2) Hall, M., and Bommarius, A. S. (2011) Enantioenriched compounds via enzyme-catalyzed redox reactions. *Chem. Rev. 111*, 4088−4110.

(3) Bornscheuer, U. T., Huisman, G. W., Kazlauskas, R. J., Lutz, S., Moore, J. C., and Robins, K. (2012) Engineering the third wave of biocatalysis. *Nature 485*, 185−194.

(4) Reetz, M. T. (2011) Laboratory evolution of stereoselective enzymes: A prolific source of catalysts for asymmetric reactions. *Angew. Chem., Int. Ed. 50*, 138−174.

(5) Huisman, G. W., Liang, J., and Krebber, A. (2010) Practical chiral alcohol manufacture using ketoreductases. *Curr. Opin. Chem. Biol. 14*, 122−129.

(6) Schroer, K., Mackfeld, U., Tan, I. A., Wandrey, C., Heuser, F., Bringer-Meyer, S., Weckbecker, A., Hummel, W., Daussmann, T., Pfaller, R., Liese, A., and Lütz, S. (2007) Continuous asymmetric ketone reduction processes with recombinant *Escherichia coli*. *J. Biotechnol. 132*, 438−444.

(7) Hummel, W. (1999) Large-scale applications of NAD(P)-dependent oxidoreductases: Recent developments. *Trends Biotechnol. 17*, 487−492.

(8) Ernst, M., Kaup, B., Müller, M., Bringer-Meyer, S., and Sahm, H. (2005) Enantioselective reduction of carbonyl compounds by whole-cell biotransformation, combining a formate dehydrogenase and a (*R*)-specific alcohol dehydrogenase. *Appl. Microbiol. Biotechnol. 66*, 629−634.

(9) Schlieben, N. H., Niefind, K., Müller, J., Riebel, B., Hummel, W., and Schomburg, D. (2005) Atomic resolution structures of *R*-specific alcohol dehydrogenase from *Lactobacillus brevis* provide the structural bases of its substrate and cosubstrate specificity. *J. Mol. Biol. 349*, 801−813.

(10) Greenberg, J. T., Monach, P., Chou, J. H., Josephy, P. D., and Demple, B. (1990) Positive control of a global antioxidant defense regulon activated by superoxide-generating agents in *Escherichia coli*. *Proc. Natl. Acad. Sci. U.S.A. 87*, 6181−6185.

(11) Tsaneva, I. R., and Weiss, B. (1990) *soxR*, a locus governing a superoxide response regulon in *Escherichia coli* K-12. *J. Bacteriol. 172*, 4197−41205.
(12) Wu, J., and Weiss, B. (1991) Two divergently transcribed genes, *soxR* and *soxS*, control a superoxide response regulon of *Escherichia coli*. *J. Bacteriol. 173*, 2864−2871.
(13) Amabile-Cuevas, C. F., and Demple, B. (1991) Molecular characterization of the *soxRS* genes of *Escherichia coli*: Two genes control a superoxide stress regulon. *Nucleic Acids Res. 19*, 4479−4484.
(14) Chiang, S. M., and Schellhorn, H. E. (2012) Regulators of oxidative stress response genes in *Escherichia coli* and their functional conservation in bacteria. *Arch. Biochem. Biophys. 525*, 161−169.
(15) Imlay, J. A. (2013) The molecular mechanisms and physiological consequences of oxidative stress: Lessons from a model bacterium. *Nat. Rev. Microbiol. 11*, 443−454.
(16) Watanabe, S., Kita, A., Kobayashi, K., and Miki, K. (2008) Crystal structure of the [2Fe-2S] oxidative-stress sensor SoxR bound to DNA. *Proc. Natl. Acad. Sci. U.S.A. 105*, 4121−4126.
(17) Hidalgo, E., and Demple, B. (1994) An iron-sulfur center essential for transcriptional activation by the redox-sensing SoxR protein. *EMBO J. 13*, 138−146.
(18) Ding, H., Hidalgo, E., and Demple, B. (1996) The redox state of the [2Fe-2S] clusters in SoxR protein regulates its activity as a transcription factor. *J. Biol. Chem. 271*, 33173−33175.
(19) Gaudu, P., and Weiss, B. (1996) SoxR, a [2Fe-2S] transcription factor, is active only in its oxidized form. *Proc. Natl. Acad. Sci. U.S.A. 93*, 10094−10098.
(20) Blanchard, J. L., Wholey, W. Y., Conlon, E. M., and Pomposiello, P. J. (2007) Rapid changes in gene expression dynamics in response to superoxide reveal SoxRS-dependent and independent transcriptional networks. *PLoS One 2*, e1186-1−e1186-13.
(21) Koo, M. S., Lee, J. H., Rah, S. Y., Yeo, W. S., Lee, J. W., Lee, K. L., Koh, Y. S., Kang, S. O., and Roe, J. H. (2003) A reducing system of the superoxide sensor SoxR in *Escherichia coli*. *EMBO J. 22*, 2614−2622.
(22) Liochev, S. I., Benov, L., Touati, D., and Fridovich, I. (1999) Induction of the *soxRS* regulon of *Escherichia coli* by superoxide. *J. Biol. Chem. 274*, 9479−9481.
(23) Gu, M., and Imlay, J. A. (2011) The SoxRS response of *Escherichia coli* is directly activated by redox-cycling drugs rather than by superoxide. *Mol. Microbiol. 79*, 1136−1150.
(24) Liochev, S. I., and Fridovich, I. (2011) Is superoxide able to induce SoxRS? *Free Radical Biol. Med. 50*, 1813.
(25) Fujikawa, M., Kobayashi, K., and Kozawa, T. (2012) Direct oxidation of the [2Fe-2S] cluster in SoxR protein by superoxide: Distinct differential sensitivity to superoxide-mediated signal transduction. *J. Biol. Chem. 287*, 35702−35708.
(26) Liochev, S. I., and Fridovich, I. (1992) Fumarase C, the stable fumarase of *Escherichia coli*, is controlled by the *soxRS* regulon. *Proc. Natl. Acad. Sci. U.S.A. 89*, 5892−5896.
(27) Krapp, A. R., Humbert, M. V., and Carrillo, N. (2011) The *soxRS* response of *Escherichia coli* can be induced in the absence of oxidative stress and oxygen by modulation of NADPH content. *Microbiology 157*, 957−965.
(28) Kobayashi, K., and Tagawa, S. (1999) Isolation of reductase for SoxR that governs an oxidative response regulon from *Escherichia coli*. *FEBS Lett. 451*, 227−230.
(29) Siedler, S., Bringer, S., and Bott, M. (2011) Increased NADPH availability in *Escherichia coli*: Improvement of the product per glucose ratio in reductive whole-cell biotransformation. *Appl. Microbiol. Biotechnol. 92*, 929−937.
(30) Siedler, S., Bringer, S., Blank, L. M., and Bott, M. (2012) Engineering yield and rate of reductive biotransformation in *Escherichia coli* by partial cyclization of the pentose phosphate pathway and PTS-independent glucose transport. *Appl. Microbiol. Biotechnol. 93*, 1459−1467.
(31) Imlay, J. A., and Fridovich, I. (1991) Assay of metabolic superoxide production in *Escherichia coli*. *J. Biol. Chem. 266*, 6957−6965.
(32) Binder, S., Schendzielorz, G., Stäbler, N., Krumbach, K., Hoffmann, K., Bott, M., and Eggeling, L. (2012) A high-throughput approach to identify genomic variants of bacterial metabolite producers at the single-cell level. *Genome Biol 13*, R40-1−R40-12.
(33) Mustafi, N., Grünberger, A., Kohlheyer, D., Bott, M., and Frunzke, J. (2012) The development and application of a single-cell biosensor for the detection of L-methionine and branched-chain amino acids. *Metab. Eng. 14*, 449−457.
(34) Schendzielorz, G., Dippong, M., Grünberger, A., Kohlheyer, D., Yoshida, A., Binder, S., Nishiyama, C., Nishiyama, M., Bott, M., Eggeling, L. (2013) Taking control over control: Use of product sensing in single cells to remove flux control at key enzymes in biosynthesis pathways. *ACS Synth. Biol.* [Online early access], DOI: 10.1021/sb400059y, Published Online: July 5, 2013.
(35) Liang, J. C., Chang, A. L., Kennedy, A. B., and Smolke, C. D. (2012) A high-throughput, quantitative cell-based screen for efficient tailoring of RNA device activity. *Nucleic Acids Res. 40*, e154.
(36) Raser, J. M., and O'Shea, E. K. (2004) Control of stochasticity in eukaryotic gene expression. *Science 304*, 1811−1814.
(37) Tang, S. Y., Fazelinia, H., and Cirino, P. C. (2008) AraC regulatory protein mutants with altered effector specificity. *J. Am. Chem. Soc. 130*, 5267−5271.
(38) Tang, S. Y., and Cirino, P. C. (2011) Design and application of a mevalonate-responsive regulatory protein. *Angew. Chem., Int. Ed. 50*, 1084−1086.
(39) Binder, S., Siedler, S., Marienhagen, J., Bott, M., and Eggeling, L. (2013) Recombineering in *Corynebacterium glutamicum* combined with optical nanosensors: A general strategy for fast producer strain generation. *Nucleic Acids Res. 41*, 6360−6369.
(40) Hanahan, D. (1983) Studies on transformation of *Escherichia coli* with plasmids. *J. Mol. Biol. 166*, 557−580.
(41) Miller, J. (1972) *Experiments in Molecular Genetics*, pp 352−355, Cold Spring Harbor Laboratory, Cold Spring Harbor, NY.
(42) Sambrook, J., and Russell, D. W. (2001) *Molecular Cloning: A Laboratory Manual*, 3rd ed., Cold Spring Harbor Laboratory Press, Cold Spring Harbor, NY.
(43) Wilson, D. S., and Keefe, A. D. (2001) Random mutagenesis by PCR, in *Current Protocols in Molecular Biology*, Chapter 8, Unit 8.3, Wiley, New York.
(44) Funke, M., Diederichs, S., Kensy, F., Müller, C., and Büchs, J. (2009) The baffled microtiter plate: Increased oxygen transfer and improved online monitoring in small scale fermentations. *Biotechnol. Bioeng. 103*, 1118−1128.
(45) Bradford, M. M. (1976) A rapid and sensitive method for the quantitation of microgram quantities of protein utilizing the principle of protein-dye binding. *Anal. Biochem. 72*, 248−254.
(46) Lineweaver, H., and Burk, D. (1934) The determination of enzyme dissociation constants. *J. Am. Chem. Soc. 56*, 658−666.

Lab on a Chip

Cite this: *Lab Chip*, 2012, **12**, 2060–2068

www.rsc.org/loc

PAPER

A disposable picolitre bioreactor for cultivation and investigation of industrially relevant bacteria on the single cell level†

Alexander Grünberger, Nicole Paczia, Christopher Probst, Georg Schendzielorz, Lothar Eggeling, Stephan Noack, Wolfgang Wiechert and Dietrich Kohlheyer*

Received 13th February 2012, Accepted 13th March 2012
DOI: 10.1039/c2lc40156h

In the continuously growing field of industrial biotechnology the scale-up from lab to industrial scale is still a major hurdle to develop competitive bioprocesses. During scale-up the productivity of single cells might be affected by bioreactor inhomogeneity and population heterogeneity. Currently, these complex interactions are difficult to investigate. In this report, design, fabrication and operation of a disposable picolitre cultivation system is described, in which environmental conditions can be well controlled on a short time scale and bacterial microcolony growth experiments can be observed by time-lapse microscopy. Three exemplary investigations will be discussed emphasizing the applicability and versatility of the device. Growth and analysis of industrially relevant bacteria with single cell resolution (in particular *Escherichia coli* and *Corynebacterium glutamicum*) starting from one single mother cell to densely packed cultures is demonstrated. Applying the picolitre bioreactor, 1.5-fold increased growth rates of *C. glutamicum* wild type cells were observed compared to typical 1 litre lab-scale batch cultivation. Moreover, the device was used to analyse and quantify the morphological changes of an industrially relevant L-lysine producer *C. glutamicum* after artificially inducing starvation conditions. Instead of a one week lab-scale experiment, only 1 h was sufficient to reveal the same information. Furthermore, time lapse microscopy during 24 h picolitre cultivation of an arginine producing strain containing a genetically encoded fluorescence sensor disclosed time dependent single cell productivity and growth, which was not possible with conventional methods.

Introduction

Industrial biotechnology is concerned with the production of chemicals, pharmaceuticals and proteins by using microorganisms growing on sustainable resources. Growth and production are the two key factors in biotechnological production processes which typically underlie continuous optimization. Assuming isogenic starting populations, optimal reactor control and mixing, uniform cell behaviour during growth might be expected. However, it has emerged in recent years that isogenic bacterial populations can be physiologically heterogeneous,[1–6] *e.g.*, comprising producing and non-producing cells. Hence there is strong demand to gain knowledge on population heterogeneity impacting industrial-scale cultivation.

Population heterogeneity may have two reasons: firstly, cellular heterogeneity, caused by either (a) emerged genetic differences,[7] (b) generally stochastic effects,[8] and (c) population based phenomena like quorum sensing,[9] and secondly, environmental heterogeneities at the microscale level, caused by insufficient process control and mixing. Particularly, cells are continuously exposed to fluctuating conditions as they travel through the various zones of bioreactors. Clearly, such heterogeneity directly affects cell metabolism.[10,11] Typically, cellular as well as environmental heterogeneities occur at the same time, leading to the problem that phenotypic screening and characterization is hard to accomplish. Until now, mainly due to missing experimental and analytical techniques, detailed knowledge on population heterogeneity and its impact on production processes is not available.[12,13]

To date, most of the heterogeneity studies are based on large cell populations, containing several billions of cells to collect statistically reliable data. To investigate the behaviour of individual cells of such populations, a well-established method is fluorescence activated cell sorting (FACS).[14] FACS is an ideal high throughput tool for screening and sorting of populations up to 80 000 cells per second.[15] However, FACS as well as other cytometric methods like Coulter counters are offline methods implying elaborate sampling routines prior to analytics. Furthermore, FACS is a snapshot analysis device and possibilities for investigating time dependent processes on the single cell level are limited. For example, FACS does not facilitate individual cell tracking, to determine proliferation, cell cycle events, growth rates and time dependent production.

Institute of Bio- and Geosciences, IBG-1: Biotechnology, Forschungszentrum Jülich GmbH (Juelich Research Center), 52428 Jülich, Germany. E-mail: d.kohlheyer@fz-juelich.de
† Electronic supplementary information (ESI) available. See DOI: 10.1039/c2lc40156h

Due to its simplicity and applicability with conventional microscopes, cell culturing on small agar pads is frequently applied. It enables time-lapse investigations of microcolonies with single cell resolution, however, at very low throughput and minimal environmental control.[16] To overcome some of these limitations, automated microscopy and image recognition software have been applied to analyse multiple bacteria microcolonies on a single agar pad.[17] Nevertheless, lack of environmental and spatial cell growth control remain major drawbacks.

In contrast to FACS and agar pads, microfluidics and lab-on-a-chip devices do allow for long term cell analysis with the possibility to perform environmental and cell growth control.[18] Microfluidics offers homogeneous and well controllable microscale environments due to laminar flow and diffusion based mixing. Furthermore, due to massive parallelization of micrometre sized components, microfluidics has the potential for high-throughput bacterial cell analysis.

Two approaches have been described in the literature so far: Firstly, miniaturization of common bioreactor technology down to nanolitre volumes with integrated sensors for various process parameters. These microfluidic bioreactors allow environmental control but do not facilitate single cell resolution for longer time periods.[19] Secondly, microfluidic devices for biotechnological single cell studies including, *e.g.*, phenotypic population heterogeneity[20] and single cell growth.[20,21] Our intention is a combination of both approaches, to be specific, a microfluidic device allowing environmental reactor control at a defined culture volume and continuous single cell observation simultaneously.

To accomplish single cell analysis in microfluidic devices, cell trapping is essential. Different methods for single cell trapping have been applied so far, including contactless and contact based methods.[22,23] However, most methods were applied to eukaryotic cells.[24] Evidently, the typically 10–100 times smaller prokaryotic cells used in industrial biotechnology necessitate more precise microfabrication and well device control. Hence, only a few microfluidic methods for single bacteria analysis have been demonstrated till now. Keymer *et al.* and Mannik *et al.* developed microfluidic systems to investigate growth and motility of bacteria populations.[25,26] Wang *et al.* applied hundreds of 1 μm wide dead-end channels to determine the growth rate of individual *E. coli* cells over more than 200 generations, but no investigations on complete colonies were possible.[27] Kortmann *et al.* used elaborate dielectrophoretic (DEP) trapping to determine growth rates of single yeast cells and bacteria cells.[21] Walden *et al.* developed parallel trapping regions for bacteria cultivation of up to 300 cells in a monolayer.[28] The latter allows for population heterogeneity analysis of larger bacterial microcolonies. Unfortunately, the layout does not allow controlled spatial cell growth and could result in inaccurate growth rate quantification.

In this study a novel microfluidic bioreactor is presented allowing parallel analysis not only of individual bacteria but also of multiple microcolonies of up to 500 cells inside 1 pL sized bioreactors (PLBRs). The system was developed for single use with a focus on simplicity. In contrast to previously reported systems, single cells simply remain trapped inside the shallow bioreactor, not relying on sophisticated cell trapping mechanisms, and cells grow in a monolayer ideal for time-lapse microscopy. Analysis can be performed on many PLBRs in parallel by automated and image based microscopy. An innovative reactor design with overflow capability allows for continuous and non-restricted cell cultivation and observation, ideal for bioprocess investigations. Furthermore, it allows for steady medium infusion maintaining constant environmental conditions as well as defined medium switches within seconds to induce various cell reactions. Moreover, the high potential for parallelization makes the system an ideal tool to collect statistically trustworthy data.

This paper covers device principle, design, basic fabrication aspects and focuses on typical applications in biotechnological research, where other methods reach their technological limits. Three exemplary biotechnological investigations are presented indicating the versatility of the device. Firstly, as a proof of principle, the cultivation of two industrially relevant organisms, *E. coli* and *C. glutamicum*, was performed under constant conditions. By determining growth rates of three picolitre bioreactor cultivations, biocompatibility and reproducibility was investigated as a necessary step for further experiments. Secondly, defined short time medium changes were applied, to assess the biological response of the growing bacteria colony under starving conditions. Thirdly, a first example of combined growth and production studies with genetically encoded fluorescence reporters for *C. glutamicum* is shown. Utilizing one microfluidic system, we could investigate important bioprocess parameters, *e.g.*, cell growth, morphology, and productivity, at the same time.

Device principle and design

The presented microfluidic device is intended for the analysis of bacteria cells on the single cell level. We aim for the investigation of microcolonies of up to 500 cells. In contrast to previously reported systems, the device shown in this report has been designed for non-motile bacteria. For this purpose, novel picolitre sized bioreactors, in this paper referred to as PLBR, were designed and implemented into a microfluidic chip. The device can incorporate up to several hundred PLBRs connected to various inlet and outlet channels for supplying growth medium and waste removal. To minimize hydrodynamic resistance but enforce cells to grow in a monolayer, two different channel heights were included: The supply and waste channels have an approx. height of 10 μm, whereas the shallow cell cultivation region is approx. 1 μm high. This 1 μm culturing region restricts cell growth to a monolayer, ideal for image based live-cell and time-lapse microscopy. As illustrated in Fig. 1, each PLBR consists of a circular plateau with radially arranged channels. The front channel is elongated thereby forming the cell seeding inlet. The PLBR is located inside the centre of the supply channel, enabling a medium flow around the trap and reduced flow through the cultivation region (as evident from Fig. S1, ESI†).

As illustrated in Fig. 1 the experiment can be divided into three phases:

(a) During the "seeding phase", the device is infused with a cell suspension as shown in Fig. 1A. Cells are randomly seeded into the PLBRs with the fluid flow dragging cells through the seeding inlet into the circular reactors. Cells simply remain trapped in between the glass cover and reactor plateau, not relying on sophisticated trapping methods. Ideally each reactor is seeded

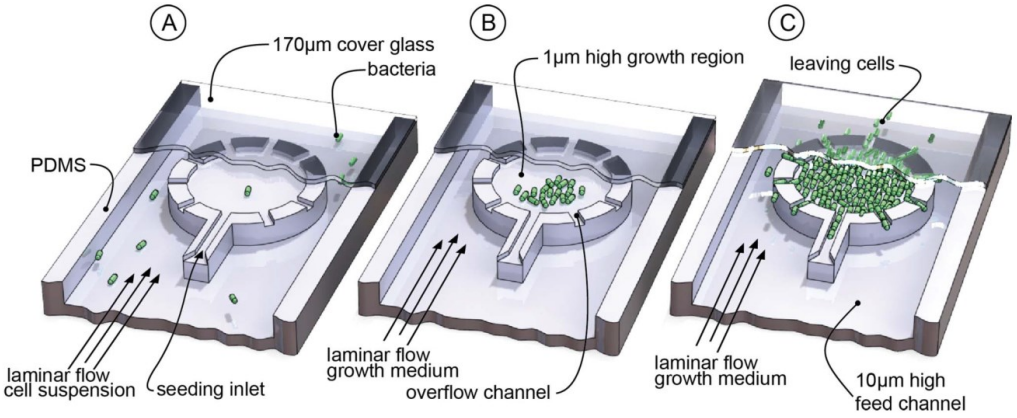

Fig. 1 Illustration of the picolitre bioreactor (PLBR) for cultivation of bacteria. The shallow circular PLBR has radially arranged channels and is placed inside a deeper supply channel. (A) During the "seeding phase" single cells are seeded into the PLBR. (B) Once a single cell is seeded, growth medium is infused initiating the "growth phase". (C) As soon as the reactor is fully packed, cells are pushed out of the overflow channels during the "overflow phase". Illustration is not to scale.

with one single mother cell, leading to isogenic microcolonies during cultivation.

(b) As soon as a single cell is seeded into the reactor, fresh growth medium is infused. This initiates the "growth phase", as illustrated in Fig. 1B. During this phase the growth of each microcolony can be followed over several generations by image based time-lapse microscopy.

(c) Depending on the size and shape of the cultivated organism, a maximum capacity of approx. 500 cells can be reached, until geometric constraints lead to the "overflow phase" of the PLBR. Excess cells are pushed out of the reactor chamber *via* the overflow channels and are continuously dragged away by the medium stream (Fig. 1C). This design allows for continuous cultivation and analysis.

Each device consists of a microfabricated polydimethylsiloxane (PDMS) chip bonded onto a 170 µm thick glass slide suitable for high resolution microscopy. Total processing time, including lithography for the mask as well as the chip fabrication, is usually accomplished within several days allowing for short innovation cycles. Since PDMS chips can be fabricated rapidly the system is designed for single use only and to be discarded after application. Hence elaborate cleaning and extensive autoclaving procedures can be omitted. A successfully fabricated device is shown in Fig. 2A. Each chip is 4 mm thick, 15 mm wide and 20 mm long. The total interior fluid volume is approximately 200 nL. As depicted, dispensing needles are connected to the device inlets and waste outlet. Six interconnected channel arrays (Fig. 2B) containing 5 PLBRs each (30 PLBRs in total) can be flushed with specific medium simultaneously. A gradient generator channel network was implemented, however, it was not utilized during this project and is intended for further studies. To verify structure resolution of the moulded PDMS chips, scanning electron microscopy (SEM) was performed prior to chip bonding with an SEM image of one PLBR shown in Fig. 2C.

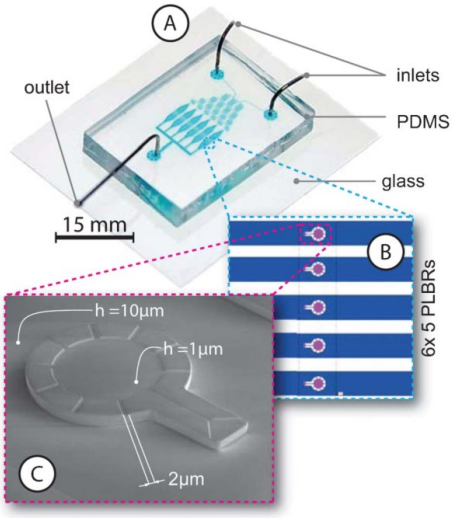

Fig. 2 Images showing the fabricated microfluidic chip device. (A) The PDMS microfluidic chip was bonded to a 170 µm glass slide and connected to silicone tubing. For purpose of illustration, the chip was filled with ink. Each chip is 4 mm × 15 mm × 20 mm (height × width × length) in size. The device consists of two inlets, one outlet, a microfluidic gradient generator for future studies and 6 linear arrays containing 5 PLBRs each (30 PLBRs in total). (B) CAD image of one PLBR array, containing 5 PLBRs in parallel. (C) SEM of a single PLBR with 1 pL cultivation volume. The height of the PLBR is approx. 1 µm and the supply channel height is approx. 10 µm. Seeding and overflow channels have a width of 2 µm.

Material and methods

Chip fabrication

To fabricate the mould for PDMS casting, a two layer SU8 process was carried out on a silicon wafer. For typical processing parameters the reader is referred to the literature.[29] In this report, only major processing steps and parameters are given.

Processing was performed under class 100 cleanroom conditions. A 4 inch silicon wafer was thoroughly cleaned in piranha solution, deionized water and eventually spin dried. Prior to resist spinning, a 30 min dehydration bake at 150 °C was performed. A 1200 nm thick layer of negative photoresist SU8 (SU8 2000.5/2010 mixture = 12 : 100, MicroChem Corp.) was spincoated onto the wafer. This layer was pre-baked for 1 min at 90 °C. To achieve the desired structure resolution, an electron beam written 5″ lithography mask was fabricated and applied during wafer exposure. Exposure time was optimized with respect to SU8 thickness, structure resolution and mask aligner lamp intensity (SÜSS MicroTec AG, Garching, Germany), and was typically below 4 s carried out in vacuum contact mode. After a 1 min post exposure bake at 90 °C the wafer was developed in resist developer (mrdev 600, Micro Resist Technology GmbH, Germany) and eventually hard baked at 120 °C. A second SU8 layer (10 μm, SU8 2010) was spin coated onto the wafer. Lithography was carried out similar to the first layer and in accordance with the manufacturer's specifications. Processing resulted in a two layer relief structure ready for PDMS casting.

Moulding was carried out under conventional lab conditions. Polydimethylsiloxane (PDMS) (Sylgard 184 Silicone Elastomer, Dow Corning Corporation, Midland, USA) was mixed with cross linker in a 10 : 1 ratio and degassed under slight vacuum. The liquid PDMS was cast over the mould and thermally cured for 3 h at 65 °C. The cured PDMS slab was cut into several chips. Uncured PDMS monomer residue was removed by washing the PDMS chips in pentane, acetone and eventually followed by a drying step overnight in accordance with Wang and co-workers.[27] Holes for the inlets and outlet were manually punched into the chip using sharp dispensing needles. The PDMS chip and a 170 μm thin glass plate (D263 T eco, 30 mm × 25 mm × 0.17 mm, Schott AG, Germany) were thoroughly rinsed with isopropanol ensuring sterile culturing conditions after assembly. After drying with nitrogen the PDMS chip and the glass plate were placed in oxygen plasma for 25 s at 50 watts (Femto Plasma Cleaner, Diener Electronics, Germany) and permanently bonded to the glass slide. Bonding was strengthened through two minute incubation at 65 °C. The inlet and outlet of the microfluidic chip were connected to silicone tubing (Tygon S-54-HL, ID = 0.25 mm, OD = 0.76 mm, VWR International) *via* dispensing needles (ID = 0.2 mm, OD = 0.42 mm). Chips were immediately used for microfluidic cultivation after fabrication.

Experimental setup, procedure and analysis

1 mL sterile glass syringes (ILS Innovative Labor Systeme GmbH, Germany) were used for medium supply. Medium flow control was realized with high precision syringe pumps (neMESYS, Cetoni, Germany). The chip was placed inside an in-house fabricated incubator for temperature and atmosphere control. The incubator was placed on a fully motorized inverted microscope (Nikon Eclipse Ti) suitable for time-lapse live cell imaging. In detail, the setup was equipped with a focus assistant (Nikon PFS) compensating for thermal drift during long term microscopy, Apo TIRF 100× Oil DIC N objective, NIKON DS-Vi1 colour camera, ANDOR LUCA R DL604 camera, xenon fluorescence light source for fluorescence excitation and high quality filters for the proper excitation of the chromophore EYFP and detection of its emission. Additionally, the objective was heated with an objective heater (ALA OBJ-Heater, Ala Scientific Instruments, USA).

The microfluidic device was flushed with fresh medium for 30 min prior to each cell seeding phase. A cell suspension with an optical density between 1 and 3, just transferred from a pre-culture at exponential growth phase, was infused to the system. Flow was stopped when satisfying amounts of PLBRs were seeded with a single cell. After seeding the flow was switched from bacteria suspension to growth medium, with a flow rate of approx. 10 nL min^{-1} per PLBR device (300 nL min^{-1} in total), to initiate the growth experiment. This flow rate was optimized to ensure stable trapping of the seeded mother cells inside the PLBRs. Medium switching was done manual as soon as the desired colony size was observed.

Time lapse images of individual PLBRs were typically acquired in 10 min time intervals. DIC microscopy images as well as fluorescence images were captured and analysed using the Nikon NIS Elements AR software package. Image analysis and data acquisition for the growth experiments was done as follows: the number of bacteria in each reactor chamber was counted and cell size measured manually at different time steps.

Additional methods and protocols for microfluidic experiments, bacteria sample preparation and bench-scale cultivation can be found in the ESI material and methods.†

Results and discussion

The *E. coli* strain BL21 is one of the most frequently used microbial hosts for recombinant protein production.[30] This strain is genetically modified to disable flagella functionality, and thus unable to move or migrate during cultivation. Likewise, *C. glutamicum* is one of the most important hosts for industrial amino acid production.[31–33] This bacterium is naturally non-motile. Therefore, both bacteria are suited for our PLBR single cell seeding principle, where cell migration is undesirable. Motile bacteria might actively leave the PLBR zone, and prevent proper cell counting studies.

Picolitre cultivation of *E. coli* BL21

A proof of principle experiment was performed to demonstrate the device functionality. During our microfluidic experiments *E. coli* BL21 was cultivated in complex LB-medium at 37 °C (± 0.2 °C) under aerobic conditions. We expect variations in oxygen to be minor in our device because of the high gas permeability of the PDMS, large surface area to volume ratio and the continuous influx of fresh growth medium. Recent studies suggest that even with bigger reactor chambers and more bacteria sufficient oxygen supply is guaranteed.[34,35] As expected we observed the three phases as explained in the device principle section.

(a) As depicted in Fig. 3A, the suspension of *E. coli* BL21 pre-grown in LB-medium was infused and within minutes the PLBRs were seeded with bacterial cells. Since filling was performed randomly, roughly 25% of the PLBRs were seeded with one single cell as desired. Since each device incorporates many PLBRs, enough PLBRs were available for microscopy and analysis. Chip designs with hundreds of PLBRs and improved seeding efficiency are currently under development. After switching to growth medium, a short adaption phase was observed and then the single mother cells started to grow. In Fig. 3D the first division event is resolved in more detail.

(b) During the growth phase (Fig. 3B) the microcolony could be analysed with respect to, *e.g.*, cell morphology, division rate, fluorescence related productivity, stress reactions and population heterogeneities on a single cell level. The constant environmental conditions and the possibility to induce instantaneous changes make this microfluidic system ideal for single cell analysis and bioprocess characterization. Performing image analysis, cell division was followed over several generations until the reactor was filled and eventually the overflow started, as shown in Fig. 3C.

(c) During the overflow phase cells were continuously pushed out of the reactor and eventually dragged away with the medium stream. If culture growth and cell removal are in balance, a nearly constant cell density can be maintained inside the PLBR, suitable for bioprocess studies (for a time lapse movie conforming to Fig. 3 watch Video S1, ESI†). However, depending on the organism's growth rate an ongoing increase in cell density inside the PLBR can be observed instead. Hence, in contrast to the relatively low cell density during the growth phase, the overflow phase can result in extremely high cell densities. At these high densities, individual cells are difficult to analyse. However, due to rapid chip production the overflow channels and reactor size can be easily tailored to specific requirements.

Growth quantification of *C. glutamicum*

For long-term growth rate experiments, defined constant and non-toxic environmental conditions have to be guaranteed. Therefore, it was essential to investigate the influence of our system on the physiological state of the cells, in this report indirectly measured by the growth rate. PLBR cultivation was performed with the wild type of *C. glutamicum* in minimal medium CGXII at 30 °C. For comparison the growth rates of three PLBR colonies on one chip were derived from time-lapse microscopy images by single cell counting. It can be seen in Fig. 4 that colonies grew exponentially with equivalent growth rates. It appeared that the growth curves are slightly shifted. This is potentially due to initially different cell-division cycle states of the captured "mother" cells and the adaption to the new environment. The maximum growth rate determined during our experiments was $\mu_{max} = 0.63 \pm 0.02\ h^{-1}$ ($n = 3$).

To the best of our knowledge this is the first study investigating growth of *C. glutamicum* on a single cell level in microfluidic devices. Literature values derived during typical shake flask cultivations are in the range of $\mu_{max} = 0.40\ h^{-1}$.[36] Applying a sophisticated continuously infused turbidostat bioreactor system only Baumchen *et al.* observed a nearly comparable growth rate of $\mu_{max} = 0.58\ h^{-1}$ using similar medium composition.[37]

The high PLBR growth rate of $\mu_{max} = 0.63 \pm 0.02\ h^{-1}$ supports our assumption that bacteria remain in good physiological state in

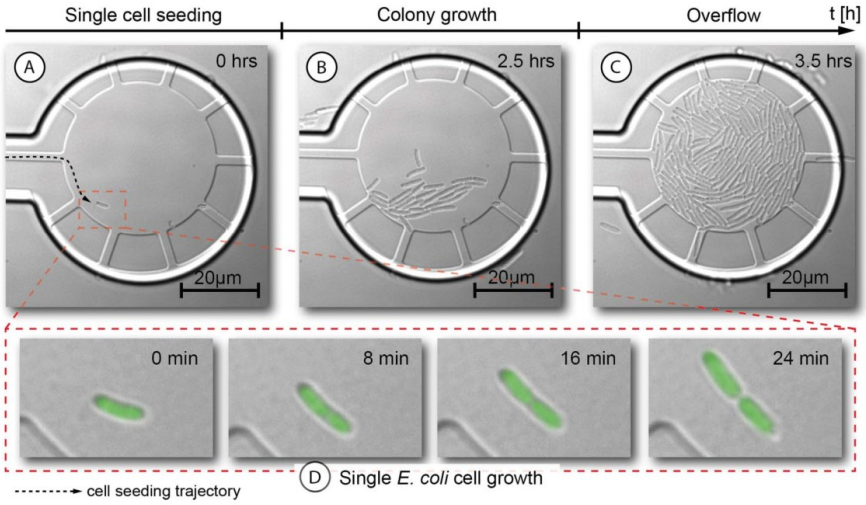

Fig. 3 Time lapse microscopy images showing the cultivation of *E. coli* BL21 inside a PLBR (see also Video S1, ESI†). (A) A single *E. coli* cell was seeded into the PLBR and complex LB growth medium was infused. (B) After 2.5 h of cultivation at $T = 37$ °C a microcolony of approx. 30 cells was formed. (C) After 3.5 h of cultivation the overflow phase was reached. Cells were pushed continuously out of the PLBR maintaining a constant density. (D) Time lapse image series showing the growth of the single mother cell after initiating the growth phase (for purpose of illustration the dividing *E. coli* cell was artificially coloured afterwards by image processing software). (A)–(C) The overflow channels have different lengths due to a slight misalignment during the two layer photolithography process. The functionality was not affected by this misalignment.

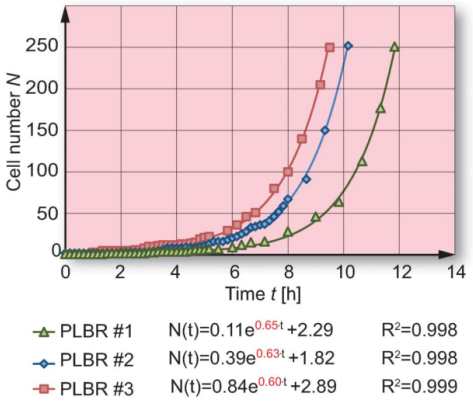

Fig. 4 Growth curves of *C. glutamicum* wild type microcolonies cultivated in three different PLBRs on one chip. Growth was followed by single cell counting of time-lapse microscopy images. The average maximal growth rate (μ_{max}) and corresponding doubling time (t_d) was determined by exponential data fitting as $\mu_{max} = 0.63 \pm 0.02\ h^{-1}$ ($n = 3$) and $t_d = 66$ min.

our microfluidic system. Actually, it also suggests that the microfluidic system offers better growth conditions than in typical lab-scale experiments. This is probably due to the continuous medium flow leading to more homogeneous conditions and the removal of secreted by-products. This aspect will be further investigated in more detailed future experiments.

Induced stationary phase during PLBR cultivation of *C. glutamicum* DM1800

In the following section, a comparison of a typical batch cultivation (1 litre) with our PLBR (10^{-12} litre) is shown. Results obtained during 1 litre cultivation will be discussed first, followed by our PLBR results.

A batch cultivation can be characterized by three phases, as illustrated in Fig. 5A. The process starts with the lag phase, in which freshly seeded cells adapt to the new environmental conditions. The lag phase is followed by the exponential growth phase where typically the maximum growth rate under the applied conditions is derived. Eventually, available nutrients are consumed and metabolic side products have increased, inducing the stationary phase. During this phase negligible growth is normally measured followed by cell degradation and cell death. Morphological variability of *C. glutamicum* has been known from prior microscopic observations, but no systematic process and time dependent investigations have been done so far.[33]

In a lab-scale batch cultivation (1 litre cultivation: for details see materials and methods in the ESI†) of the L-lysine producing strain *C. glutamicum* DM1800, cellular heterogeneity during the stationary and late stationary phase was observed (Fig. 5B). Two different sub-populations were seen as determined by the applied Coulter counter system, namely: cells larger than 1.3 μm and cells smaller than 1.3 μm in length. As depicted in Fig. 5B, over the entire cultivation time single cells larger than 1.3 μm and cells smaller than 1.3 μm in length can be observed. There is a pronounced change in the ratio of these two cell classes, with a clear predominance of small cells in the stationary phase. Similar results were obtained using *C. glutamicum* wild type (data not shown). The quantitative assessment of population heterogeneity required elaborate lab-scale cultivation, sample preparation and Coulter counter based cell counting. As can be seen in Fig. 5B, samples were taken, prepared and analysed during more than 160 h of cultivation. Despite the high relevance and interest in the observed population heterogeneity and its possible impact on industrial-scale cultivation, it becomes clear that processing time and effort is inappropriate for more detailed studies at lab-scale.

At this stage the developed microfluidic PLBR was applied to perform the same investigations during the late stationary phase. Obviously, our chip device that is continuously infused with fresh medium cannot be directly compared to a batch cultivation process. However, it can be used to artificially induce different environmental conditions within seconds simply by changing the medium and for instance mimic the stationary growth phase.

The chip was infused with the *C. glutamicum* DM1800 cells and PLBRs were seeded with single cells. The growth phase was initiated with fresh minimal medium CGXII at 30 °C. During the growth phase the measured maximal growth rate $\mu_{max\_PLBR} = 0.56 \pm 0.02\ h^{-1}$ was again significantly higher than the growth rate of $\mu_{max\_LS} = 0.37\ h^{-1}$, which was experimentally derived during the lab-scale batch cultivation described above. These findings are in accordance with previous PLBR cultivations and prove that better growth conditions can be maintained not only for the *C. glutamicum* wild type but also for the industrially utilized L-lysine producing strain DM1800. After reaching approx. 50 cells inside the PLBR, the medium was changed to a medium lacking glucose thereby artificially inducing the stationary phase. Time-lapse microscopy images revealed the same phenotypic differentiation as observed during the 1 litre lab-scale cultivation. Although no carbon source was available, the absolute cell number increased. Whereas one part of the culture almost stopped growing, the other part still continued to divide but into remarkable smaller cells, as exemplarily shown in Fig. 5C. A possible reason could be the formation of carbon storage pools like, *e.g.*, glycogen in some cells during the growth period under carbon excess. These storage pools are then used under carbon limiting conditions to continue growth for several generations. The amount of cells larger than 1.3 μm dropped notably after inducing the stationary phase, as shown in Fig. 5D. It can be seen that our PLBR system reduced the required experimental time drastically. Within 45 min of chip cultivation after inducing the stationary phase, the amount of cells smaller 1.3 μm equalled the quantity of cells larger than 1.3 μm. In contrast to that, 120 h of sheer experimental time were needed to obtain the same results at lab-scale batch cultivation. In particular the experimental time was reduced 160 fold. The slight increase of cells larger than 1.3 μm after approx. 8 h could be due to inaccurate cell measurement, as it became difficult to measure accurately 1.3 μm at densely packed colonies, as evident from Fig. 5C (12 h). Growth inside the PLBR completely stopped beyond 14 h of cultivation, which was comparable to the results obtained during the 1 litre cultivation.

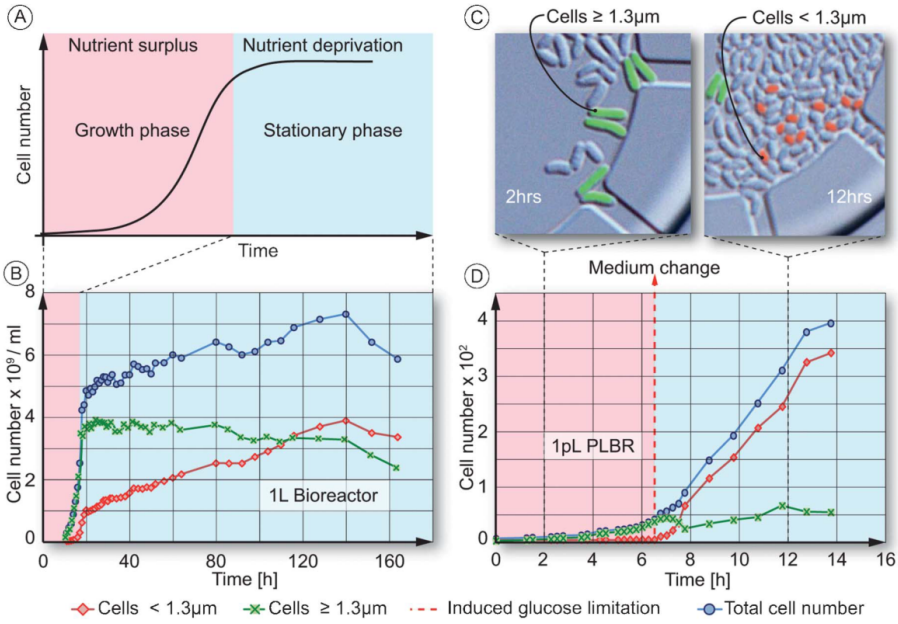

Fig. 5 Growth and morphology analysis of *C. glutamicum* DM1800 during 1 litre lab-scale batch cultivation and under PLBR cultivation after inducing an artificial stationary phase: (A) Typical growth curve during batch cultivation. (B) Experimentally derived growth curve of a 1 litre batch cultivation of *C. glutamicum* DM1800 following the exponential and late stationary growth phase. The number of small cells exceeded the number of larger cells approx. 100 h after reaching the stationary phase. (C) Time-lapse microscopy images showing the cell population at 2 h and after 12 h experimental time inside the PLBR. A few cells were artificially coloured exemplarily for purpose of illustration. (D) Experimentally derived growth curve of an isogenic microcolony inside the PLBR; The number of small cells exceeded the number of larger cells in approx. 45 min after artificially inducing the stationary phase.

Fluorescence based production studies

As described in the introduction, FACS is an ideal high-throughput system to sort and analyse microorganisms based on a fluorescence signal. However, FACS is limited to snap-shot analysis and time dependent analysis is impossible. In contrast, our microfluidic system allows fluorescence based productivity analysis on a single cell level for long time periods (here over 30 h) and tracking of individual cells is possible by image analysis.

As a proof of principle we cultivated the L-arginine producing *C. glutamicum* pSenLysTKP-argB(fbr) strain in our PLBR device. This wild type derivative contains a plasmid-encoded metabolite sensor, enabling yellow fluorescence protein (EYFP) expression in response to enhanced intracellular L-arginine concentration.[38] The plasmid contains in addition a feedback resistant acetylglutamate kinase, resulting in weak extracellular L-arginine accumulation as observed in shake flask cultivations. Using PLBR, constant environmental conditions were applied to analyse the characteristics of this strain with respect to the growth and EYFP signal. Fig. 6 shows a time-lapse image series of the isogenic microcolony inside the PLBR (see also Video S2, ESI†). Clearly an interesting change in cellular fluorescence and cell growth can be observed. It can be realized that the two cells in focus start to emit fluorescence after an adaptation phase apparently required to synthesize sufficient endogenous L-arginine to induce expression of the genetically encoded L-arginine sensor. EYFP emission continues up to 22 h, although some heterogeneity with respect to fluorescence intensity becomes apparent. With significant growth (μ_{max} = 0.46 h^{-1}) beginning after 22 h the number of fluorescent cells decreases, and at 30 h no single cell is fluorescent. A similar behaviour of fluorescence and growth was observed in additional PLBR cultivations, too, but not observed with a control carrying a vector devoid of argB(fbr). Currently, we cannot explain conclusively the time dependent fluorescence observed. One reason could be the rather weak production of the strain available. However, the experiment demonstrates the applicability of our system to investigate more complex biological phenomena such as time dependent production processes which was not possible before.

Conclusions

This report demonstrates an innovative microfluidic device for cultivation of bacteria on single cell level. A PDMS device was designed and fabricated for trapping of single bacteria cells in picolitre volume bioreactors (PLBR). The PLBR has a few important key characteristics: The system is a disposable low cost product, no intensive cleaning is required and the risk of

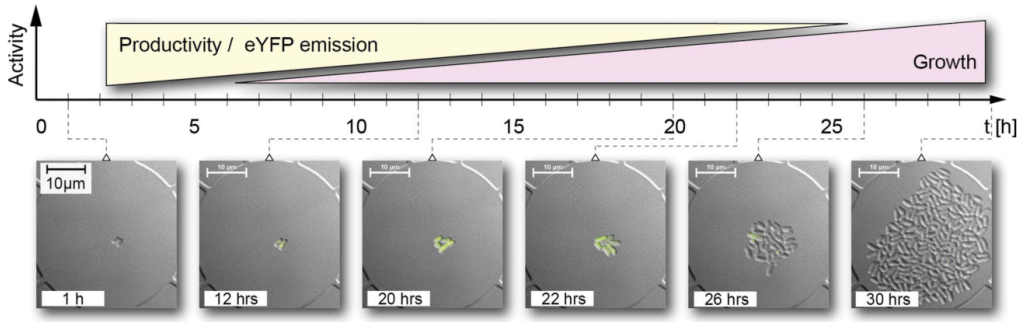

Fig. 6 Time-lapse image series showing growth and production of *C. glutamicum* pSenLysTKP-argB(fbr) during PLBR cultivation. The strain contains a metabolite sensor enabling EYFP expression in response to enhanced intracellular L-arginine concentration. The seeded mother cell starts to emit fluorescence after 12 h indicating production of L-arginine. While undergoing a change to maximum cell growth EYFP emission declined.

contamination is minimal. Due to an innovative design, bacteria are being trapped simply by the shallow bioreactor region, not relying on sophisticated technical cell trapping methods, and grow inside confined reactor regions allowing continuous analysis. Once the bioreactor is filled, radially arranged overflow channels provide well controlled cell removal not limiting experimental time. Moreover, fast medium changes facilitate to mimic every desired environmental situation of a lab-scale process. Due to picolitre volumes, low cell numbers and short response time, a fraction of experimental time is required for otherwise elaborate and time-consuming investigations. Furthermore, the high potential for parallelization makes the system an ideal tool to collect statistically trustworthy data.

The presented system is not limited to the analysis of cell growth under standard conditions, but could be applied to investigate many environmental changes, *e.g.*, medium composition, pH changes, temperature fluctuations and flow rates. Furthermore, if time-lapse images are recorded at appropriate time intervals, also division events of individual cells could be analysed in detail, rather than just counting cell populations. In-depth studies are planned to investigate population heterogeneity effects in more detail.

Additionally, the device carries great potential if combined with appropriate analytical techniques, for analysing substrate consumption and (by)-product formation of resulting micro-colonies. Hence future studies will also concentrate on quantifying the PLBR upstream regarding the cells exometabolome by untargeted (GC-TOF-MS) and targeted (LC-MS/MS) approaches as well as protein secretion by fluorescence labelling techniques.

As a final conclusion, our microfluidic PLBR is well suited for population heterogeneity studies on the single cell level and future bioprocess optimization strategies.

Acknowledgements

This work was partly performed at Helmholtz Nanoelectronic Facility (HNF) of Forschungszentrum Jülich GmbH. The authors would like to thank for their help and support.

References

1 M. E. Lidstrom and D. R. Meldrum, *Nat. Rev. Microbiol.*, 2003, **1**, 158–164.
2 N. Q. Balaban, J. Merrin, R. Chait, L. Kowalik and S. Leibler, *Science*, 2004, **305**, 1622–1625.
3 D. Di Carlo and L. P. Lee, *Anal. Chem.*, 2006, **78**, 7918–7925.
4 J. W. Veening, W. K. Smits and O. P. Kuipers, *Annu. Rev. Microbiol.*, 2008, **62**, 193–210.
5 D. Dubnau and R. Losick, *Mol. Microbiol.*, 2006, **61**, 564–572.
6 W. K. Smits, O. P. Kuipers and J. W. Veening, *Nat. Rev. Microbiol.*, 2006, **4**, 259–271.
7 M. Blot, D. Papadopoulos, D. Schneider, J. Meier-Eiss, W. Arber and R. E. Lenski, *Proc. Natl. Acad. Sci. U. S. A.*, 1999, **96**, 3807–3812.
8 D. Huh and J. Paulsson, *Nat. Genet.*, 2011, **43**, 95.
9 A. Prindle, P. Samayoa, I. Razinkov, T. Danino, L. S. Tsimring and J. Hasty, *Nature*, 2012, **481**, 39–44.
10 A. R. Lara, E. Galindo, O. T. Ramirez and L. A. Palomares, *Mol. Biotechnol.*, 2006, **34**, 355–381.
11 S. O. Enfors, M. Jahic, A. Rozkov, B. Xu, M. Hecker, B. Jurgen, E. Kruger, T. Schweder, G. Hamer, D. O'Beirne, N. Noisommit-Rizzi, M. Reuss, L. Boone, C. Hewitt, C. McFarlane, A. Nienow, T. Kovacs, C. Tragardh, L. Fuchs, J. Revstedt, P. C. Friberg, B. Hjertager, G. Blomsten, H. Skogman, S. Hjort, F. Hoeks, H. Y. Lin, P. Neubauer, R. van der Lans, K. Luyben, P. Vrabel and A. Manelius, *J. Biotechnol.*, 2001, **85**, 175–185.
12 M. E. Lidstrom and M. C. Konopka, *Nat. Chem. Biol.*, 2010, **6**, 705–712.
13 R. L. Fernandes, *et al.*, *Biotechnol. Adv.*, 2011, **29**, 575–599.
14 B. F. Brehm-Stecher and E. A. Johnson, *Microbiol. Mol. Biol. Rev.*, 2004, **68**, 538.
15 H. M. Davey and D. B. Kell, *Microbiol. Rev.*, 1996, **60**, 641.
16 J. W. Young, J. C. W. Locke, A. Altinok, N. Rosenfeld, T. Bacarian, P. S. Swain, E. Mjolsness and M. B. Elowitz, *Nat. Protoc.*, 2012, **7**, 80–88.
17 J. C. W. Locke, J. W. Young, M. Fontes, M. J. H. Jimenez and M. B. Elowitz, *Science*, 2011, **334**, 366–369.
18 J. El-Ali, P. K. Sorger and K. F. Jensen, *Nature*, 2006, **442**, 403–411.
19 K. S. Lee, P. Boccazzi, A. J. Sinskey and R. J. Ram, *Lab Chip*, 2011, **11**, 1730–1739.
20 P. Sun, Y. Liu, J. Sha, Z. Y. Zhang, Q. Tu, P. Chen and J. Y. Wang, *Biosens. Bioelectron.*, 2011, **26**, 1993–1999.
21 H. Kortmann, P. Chasanis, L. M. Blank, J. Franzke, E. Y. Kenig and A. Schmid, *Lab Chip*, 2009, **9**, 576–585.
22 R. M. Johann, *Anal. Bioanal. Chem.*, 2006, **385**, 408–412.
23 J. Nilsson, M. Evander, B. Hammarstrom and T. Laurell, *Anal. Chim. Acta*, 2009, **649**, 141–157.
24 D. Di Carlo, L. Y. Wu and L. P. Lee, *Lab Chip*, 2006, **6**, 1445–1449.
25 J. E. Keymer, P. Galajda, C. Muldoon, S. Park and R. H. Austin, *Proc. Natl. Acad. Sci. U. S. A.*, 2006, **103**, 17290–17295.
26 J. Mannik, R. Driessen, P. Galajda, J. E. Keymer and C. Dekker, *Proc. Natl. Acad. Sci. U. S. A.*, 2009, **106**, 14861–14866.

27 P. Wang, L. Robert, J. Pelletier, W. L. Dang, F. Taddei, A. Wright and S. Jun, *Curr. Biol.*, 2010, **20**, 1099–1103.
28 M. Walden and J. Elf, *Curr. Opin. Biotechnol.*, 2011, **22**, 81–86.
29 Y. N. Xia and G. M. Whitesides, *Angew. Chem., Int. Ed.*, 1998, **37**, 551–575.
30 F. W. Studier, P. Daegelen, R. E. Lenski, S. Maslov and J. F. Kim, *J. Mol. Biol.*, 2009, **394**, 653–680.
31 J. Becker and C. Wittmann, *Curr. Opin. Biotechnol.*, 2012, DOI: 10.1016/j.copbio.2011.11.012.
32 A. Burkovski, *Corynebacteria: Genomics and molecular biology*, Caister Academic Press, Norfolk UK, 2008.
33 L. Eggeling and M. Bott, *Handbook of Corynebacterium glutamicum*, Academic Press, Inc., Boca Raton, FL, 2005.
34 F. K. Balagadde, L. C. You, C. L. Hansen, F. H. Arnold and S. R. Quake, *Science*, 2005, **309**, 137–140.
35 A. Zanzotto, N. Szita, P. Boccazzi, P. Lessard, A. J. Sinskey and K. F. Jensen, *Biotechnol. Bioeng.*, 2004, **87**, 243–254.
36 J. van Ooyen, D. Emer, M. Bussmann, M. Bott, B. J. Eikmanns and L. Eggeling, *J. Biotechnol.*, 2011, **154**, 140–148.
37 C. Baumchen, A. Knoll, B. Husemann, J. Seletzky, B. Maier, C. Dietrich, G. Amoabediny and J. Buchs, *J. Biotechnol.*, 2007, **128**, 868–874.
38 S. Binder, G. Schendzielorz, N. Stäbler, K. Krumbach, K. Hoffmann, M. Bott and L. Eggeling, A high-throughput approach to identify genomic variants of bacterial metabolite producers at the single-cell level, *Genome Biology*, 2012, under review.

ARTICLE

BIOTECHNOLOGY and BIOENGINEERING

Beyond Growth Rate 0.6: *Corynebacterium glutamicum* Cultivated in Highly Diluted Environments

Alexander Grünberger,[1] Jan van Ooyen,[2] Nicole Paczia,[1] Peter Rohe,[1] Georg Schiendzielorz,[2] Lothar Eggeling,[2] Wolfgang Wiechert,[1] Dietrich Kohlheyer,[1] Stephan Noack[1]

[1]Institute of Bio- and Geosciences, IBG-1: Biotechnology, Systems Biotechnology, Forschungszentrum Jülich, Jülich 52425, Germany; telephone: +49-2461-61-6044; fax: +49-2461-61-3870; e-mail: s.noack@fz-juelich.de

[2]Systemic Microbiology, Forschungszentrum Jülich, Jülich 52425, Germany

ABSTRACT: Fast growth of industrial microorganisms, such as *Corynebacterium glutamicum*, is a direct amplifier for the productivity of any growth coupled or decoupled production process. Recently, it has been shown that *C. glutamicum* when grown in a novel picoliter bioreactor (PLBR) exhibits a 50% higher growth rate compared to a 1 L batch cultivation [Grünberger et al. (2012) Lab Chip]. We here compare growth of *C. glutamicum* with glucose as substrate at different scales covering batch cultivations in the liter range down to single cell cultivations in the picoliter range. The maximum growth rate of standard batch cultures as estimated from different biomass quantification methods is $\hat{\mu} = 0.42 \pm 0.03\,h^{-1}$ even for microtiter scale cultivations. In contrast, growth in a microfluidic perfusion system enabling analysis of single cells reproducibly reveals a higher growth rate of $\hat{\mu} = 0.62 \pm 0.02\,h^{-1}$. When in the same perfusion system cell-free supernatant from exponentially grown shake flask cultures is used the growth rate of single cells is reduced to $\hat{\mu} = 0.47 \pm 0.02\,h^{-1}$. Likewise, when fresh medium is additionally supplied with 5 mM acetate, a growth rate of $\hat{\mu} = 0.51 \pm 0.01\,h^{-1}$ is determined. These results prove that higher growth rates of *C. glutamicum* than known from typical batch cultivations are possible, and that growth is definitely impaired by very low concentrations of byproducts such as acetate.

Biotechnol. Bioeng. 2013;110: 220–228.

KEYWORDS: growth rate; *C. glutamicum*; microfluidics; single cell; acetate

Correspondence to: S. Noack

Contract grant sponsor: Bundesministerium für Bildung und Forschung (BMBF)
Contract grant number: 0316017B
Additional supporting information may be found in the online version of this article.
Received 17 May 2012; Revision received 17 July 2012; Accepted 18 July 2012
Article first published online 13 August 2012 in Wiley Online Library (http://onlinelibrary.wiley.com/doi/10.1002/bit.24616/abstract)
DOI 10.1002/bit.24616

Introduction

Importance of Maximum Growth Rate

The maximum growth rate (μ_{max}) is the key characteristic for describing the phenotype of a microbial cell population. The knowledge of μ_{max} for a certain microorganism and cultivation condition builds the basis for optimizing media compositions for growth and production (Khanna and Srivastava, 2005; Mandenius and Brundin, 2008), characterizing the effect of genetic manipulations by metabolic engineering tasks (Fong and Palsson, 2004), and describing cellular metabolism by kinetic models (Wiechert and Noack, 2011).

Moreover, μ_{max} is one of the most important parameters for industrial production processes utilizing microorganisms. On the one hand this directly relates to all processes, which are known to work well in a growth-coupled manner, for example, the production of amino and organic acids (Feist et al., 2010) as well as recombinant proteins (San et al., 1994). On the other hand it is also of great interest for all processes where the growth and production phase is decoupled and hence fast generation of high cell densities have a high impact on the overall economic feasibility of a certain production process. In fact, this holds true for all processes based on biotransformations using whole cells or cell extracts, which are in competition with cell-free synthetic approaches in the near future (Zhang, 2010).

However, until now, it is impossible to precisely predict μ_{max} for a given media composition in a typical batch process. This is simply due to the fact that growth under batch conditions is usually greatly affected by a combination of substrate excess, higher cell densities, heterogeneities caused by insufficient mixing and accumulation of possible toxic side-products (Luli and Strohl, 1990).

Clearly, if the growth rate of an organism can be raised in a production process, this has an immediate impact on its

overall productivity. It will be shown below that maximum growth rates published for common production organisms might not be the upper limit.

Single Cell Investigation Versus Classical Culture

Nowadays, in order to gain more insight into the mechanism of microbial growth microfluidic tools are being developed that also allow investigations on the single cell level (Groisman et al., 2005; Kortmann et al., 2009; Lee et al., 2011). In a recent study we reported on the development of a novel picoliter bioreactor (PLBR) for cultivation of single bacterial cells (Grünberger et al., 2012). Surprisingly, the application of the PLBR for cultivation of the *Corynebacterium glutamicum* wild type, a model organism of white biotechnology, showed a 1.5-fold higher exponential growth rate compared to a 1 L batch cultivation. Higher growth rates in microfluidic systems compared to typical lab-scale batch approaches were also reported for *E. coli* (Wang et al., 2010) and support the hypothesis of faster cell growth under constant environmental conditions.

In general, it can be argued that the overall culture conditions in a microfluidic system are more optimal for fast growth compared to the conventional approaches, for example, bioreactor or shake flask. It is already known for a long time that several inhomogeneity factors including gradients in chemical and physical properties (e.g., media and gas supply) have a major impact on cell population growth. This is most pronounced in cultivations applying high cell densities where growth of distinct cells is likely to be impaired by short-term limitations of substrate or oxygen supply leading to a decrease in the overall growth rate of the cell population. For more details the reader is referred to (Kensy et al., 2009; Lara et al., 2006; Suresh et al., 2009; Takors, 2011).

Interestingly, detailed studies of the impact of cultivation modes as well as biomass measurements on the maximum growth rate estimation have not been systematically performed so far.

Estimation of Maximum Growth Rate

In the following we provide some definitions related to the estimation of μ_{max} to allow a precise formulation of the major questions that we will address within this article.

The time dependent specific growth rate $\mu(t)$ of a bacterial cell population X in a closed system (batch culture) is calculated as:

$$\mu(t) = \frac{\dot{X}}{X} \tag{1}$$

From Equation (1) the "true" maximum growth rate in the time interval $0 \leq t \leq T$ of cultivation is derived as:

$$\mu_{max} \overset{def}{=} \max_{0 \leq t \leq T} \mu(t) \tag{2}$$

Clearly, μ_{max} is not accessible as the underlying biomass quantification methods are not accurate enough to allow for a statistical trustworthy calculation of the time-derivatives in Equation (1).

Nevertheless, an estimation of μ_{max} can be realized by assuming a constant exponential growth behavior over some time interval $T_1 \leq t \leq T_2$. Integration of Equation (1) then leads to an average growth rate $\overline{\mu}$ that is, *per definition*, a lower boundary for μ_{max}. Since from Equation (1) it follows

$$\ln(X_2) = \ln(X_1) + \int_{T_1}^{T_2} \mu(t)\, dt$$

the exact solution of Equation (1) at time T_2 is given by

$$X_2(T_2) = X_1(T_1)\, e^{\overline{\mu}(T_2 - T_1)} \tag{3}$$

with the average growth rate

$$\overline{\mu} = \frac{1}{T_2 - T_1} \int_{T_1}^{T_2} \mu(t)\, dt \leq \mu_{max}$$

As an alternative, the exponential growth rate μ can be directly estimated when the growth rate is constant over the time interval $T_1 \leq t \leq T_2$ as is, for example, the case in the exponential growth phase of a batch culture. In that case Equation (3) reads:

$$X_2(t) = X_1(T_1) e^{\mu(t - T_1)} \tag{4}$$

with

$$\mu = \mu(t) = \text{const.}$$

Thus fitting this exponential function to the biomass measurements $X(t_i)$ by applying the well-known method of least squares

$$\hat{\mu} = \arg_{\mu} \min \kappa(\mu) \leq \mu_{max}$$

with

$$\kappa(\mu) = \sum_{i=1}^{n} \left\| X(t_i) - \hat{X}(t_i) \right\|^2_{\sum_{X(t_i)}} \tag{5}$$

a reliable estimate $\hat{\mu}$ of the exponential growth rate is obtained if the constant growth assumption is correct. Fortunately, this assumption can be checked by inspecting the goodness of fit. This method has the main advantage that multiple biomass measurements including its randomly distributed errors $\sum_{X(t_i)}$ are utilized to give a more robust estimation of μ_{max}.

Assuming that the average size and volume of single cells grown in a population does not change during the time of investigation, the increase in cell density is proportional to the increase in cell concentration. In that case an

under-estimation of μ_{max} in terms of one or the other variable leads to the same results. However, as already shown in several studies with different microorganism, the average size and volume of cells can vary considerably in dependence of the cultivation conditions (Guillouet and Engasser, 1996; Petelenz-Kurdziel et al., 2011; Volkmer and Heinemann, 2011). In turn, this has a direct influence on the estimation of μ_{max} based on cell density, which is then different from the maximum rate estimate from cell concentration measurements.

Aims of This Study

In this study we comprehensively compare the growth of *C. glutamicum* wild type on CGXII glucose applying well-defined cultivation experiments at different cultivation scales. Moreover, several biomass quantification methods related to cell concentration and bacterial cell density are applied to safely answer the following two questions:

(1) Has the cultivation scale and underlying technical devices a direct influence on the estimation of the maximum growth rate?
(2) Is the constant growth rate in the exponential phase of a batch culture equal to the maximum possible growth rate under the pre-defined conditions?

Furthermore, we show how miniaturized batch systems such as microtiter plates in combination with microfluidic systems can be used to test the influence of selected medium components onto growth and production formation of industrially relevant microorganism.

Materials and Methods

Cultivation Media

CGXII was used as standard mineral medium for *C. glutamicum* consisting of (per liter): 20 g $(NH_4)_2SO_4$, 5 g urea, 0.5 g K_2HPO_4, 0.25 g $MgSO_4 \cdot 7H_2O$, 42 g 3-morpholinopropanesulfonic acid, 10 mg $CaCl_2$, 10 mg $FeSO_4 \cdot 7H_2O$, 10 mg $MnSO_4 \cdot H_2O$, 1 mg $ZnSO_4 \cdot 7H_2O$, 0.2 mg $CuSO_4$, 0.02 mg $NiCl_2 \cdot 6H_2O$, 0.2 mg biotin, 0.03 mg of protocatechuic acid adjusted to pH 7, and 4% glucose as carbon and energy source. To prevent any medium related influences, the same batch of CGXII was used for all cultivations. First, the mineral medium was prepared and sterile filtered without 3-morpholinopropanesulfonic acid and aliquots for bioreactor experiments were taken. For shake flask, BioLector and microfluidic chip experiments sterile 3-morpholinopropanesulfonic acid was added.

Shake Flask Cultivations

Prior to all main cultures, cells were pre-cultured as 50 mL cultures in 500 mL baffled Erlenmeyer flasks on a rotary shaker at 120 rpm with orbital shaking at a diameter of 25 cm at 30°C. A first pre-culture in LB complex medium was inoculated to a second pre-culture in CGXII mineral medium, which was then inoculated to an OD_{600} of 1 to the main cultures of shake flask, bioreactor, microtiter plates, and microfluidic chip experiments.

For main cultures in shake flasks *C. glutamicum* was grown as 50 mL cultures in 500 mL baffled Erlenmeyer flasks on buffered CGXII medium.

Bioreactor Cultivations

The 1.4 L bioreactors (Multifors Multi-Fermenter System with 4 independently controllable bioreactors, Infors, Einsbach, Germany) contained 600 mL CGXII medium with 4% (w/v) glucose, but without the buffer substance 3-morpholinopropanesulfonic acid. The bioreactors were sparged with 0.9 L min^{-1} air. Oxygen saturation was measured online with a polarimetric oxygen electrode (Mettler Toledo, Giessen, Germany) and was held permanently over 30% by gradually increasing stirrer speed from 600 rpm up to 1,000 rpm. The pH was determined online using a standard pH electrode (Mettler Toledo) and adjusted to pH 7 with 3 M sodium hydroxide and 3 M hydrochloric acid. Foam formation was suppressed automatically by titration of 25% (v/v) Antifoam 204/water suspension (Sigma–Aldrich, Steinheim, Germany).

Microtiter Plate (MTP) Cultivations

MTP cultivations were carried out in 48 well Flowerplates (m2p-labs, Aachen, Germany) incubated in a BioLector (m2p-labs), each well filled with 1 mL with the same inoculated CGXII medium as in shake flasks. Wells with not inoculated media were analyzed as negative controls in the same MTP. MTPs were incubated at 30°C with a relative humidity above 80% avoiding evaporation. In addition, MTPs were shaken at 1,200 rpm with a shaking diameter of 3 mm. To minimize evaporation but allow feasible gas transfer MTPs were sealed with gas permeable films (m2p-labs). Biomass was monitored online with backscatter measurement at 600 nm and gain 20. The two cultivation parameters pO_2 and pH were measured with immobilized indicator substances, so-called optodes, inside each flowerplate well.

Microfluidic Chip Cultivations

To investigate single cell growth behavior of *C. glutamicum* at different culturing parameters, the previously reported PLBR was used (Grünberger et al., 2012). The microfluidic device is intended for the analysis of bacteria on single cell level. Starting from one single "mother" cell, microcolonies of up to 500 cells can be investigated. The device is continuously infused with fresh media, resulting in constant environmental conditions over the whole experimental

time. The device can incorporate up to several hundred PLBRs connected to various inlet and outlet channels for supplying growth medium and waste removal. The 1 μm culturing region restricts cell growth to a monolayer, ideal for image based live-cell and time-lapse microscopy. For fabrication and detailed device principle, the reader is referred to (Grünberger et al., 2012).

The chip was placed inside an in-house manufactured incubator for temperature and atmosphere control and connected to 1 mL sterile glass syringes (ILS Innovative Labor Systeme GmbH, Stützerbach, Germany) for continuous media supply. Media flow was controlled with high precision syringe pumps (neMESYS, Cetoni, Korbussen, Germany). The incubator was mounted onto a fully motorized inverted microscope (Nikon Eclipse Ti, Nikon GmbH, Düsseldorf, Germany) suitable for time-lapse live cell imaging. In detail, the setup was equipped with a focus assistant (Nikon PFS, Nikon GmbH) compensating for thermal drift during long term microscopy, Apo TIRF 100x Oil DIC N objective, NIKON DS-Vi1 color camera and ANDOR LUCA R DL604 camera. Additionally, the objective was heated with an objective heater (ALA OBJ-Heater, Ala Scientific Instruments, Farmingdale, NY).

The microfluidic device was purged with buffered CGXII-medium for 30 min prior to each cell seeding phase. A cell suspension with an optical density between 1 and 3, transferred from a pre-culture at exponential growth phase, was infused to the system. Flow was stopped when satisfying amounts of PLBRs were seeded with a single cell. After successful cell seeding with bacteria suspension, the growth medium was infused at approx. 10 nL min^{-1} per PLBR to initiate the cultivation.

DIC microscopy images of individual PLBRs were captured in 10 min time intervals and resulting time lapse images were recorded as well as analyzed employing the Nikon NIS Elements AR software package. To derive growth rates, the number of bacteria was counted and the area of evolving microcolony was measured for each PLBR and corresponding time-lapse images, respectively.

Offline Analytics

Optical density (OD_{600}) was measured at 600 nm (PharmaSpec UV 1700, Schimadzu, Kyoto, Japan) against 0.9% (w/v) NaCl. Glucose was measured using an enzymatic analysis system (EBIO compact, Eppendorf AG, Hamburg, Germany). Cell count and cell size were monitored offline via a Coulter counter equipped with a 45 μm capillary (CASY 1 Modell TT, Roche Diagnostics, Mannheim, Germany).

For fluorescence activated cell sorting (FACS) analytics cells were carefully diluted to an optical density below 0.1 and immediately analyzed by a FACS ARIA II high-speed cell sorter (BD Biosciences, San Jose, CA) using excitation lines at 488 and 633 nm and detecting fluorescence at 660 ± 10 nm at a sample pressure of 70 psi. Data were analyzed using BD DIVA 6.1.3 software. The sheath fluid was sterile filtered PBS. Non-bacterial particles were excluded by electronic gating on the basis of forward versus side scatter area. To obtain precise cell numbers an exact number of fluorescent beads (BD TruCOUNT Tubes, BD Biosciences) was added to the samples for internal calibration. In one experiment targeted and untargeted analysis of the culture supernatant was performed by HPLC (Litsanov et al., 2012) and GC-ToF-MS (Sisignano et al., 2010) measurements, respectively.

Results and Discussion

Maximum Growth Rates at Different Cultivation Scales

Growth of *C. glutamicum* wild type on CGXII glucose was followed by applying a series of experiments at different cultivation scales. A special device is the single cell cultivation system PLBR. In this system single cells are trapped in a microfluidic channel (Fig. 1), allowing for constant perfusion with fresh medium and microscopic inspection of growth. An example of a time lapse video is included as supplemental video S1, which served to derive the triplicate growth rate data of these first experiments. Starting from one identical CGXII glucose pre-culture cultivations of *C. glutamicum* were done as outlined in Figure 2, ranging

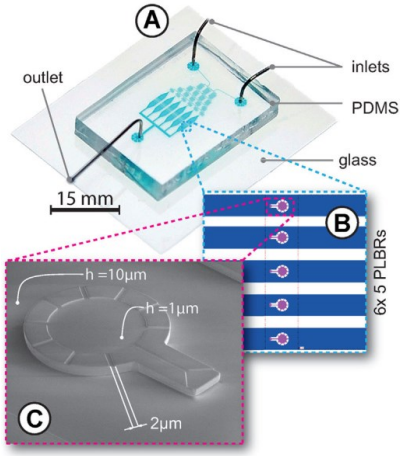

Figure 1. Picoliter bioreactor system (PLBR) used for perfusion growth studies. **A:** Fabricated microfluidic chip device. **B:** Magnification of one growth array containing 5 PLBRs in parallel. **C:** Scanning electron microscopy image of a single PLBR with 1 pL cultivation volume. The height of the PLBR is approximately 1 μm and the supply channel height is approximately 10 μm. Seeding and overflow channels have a width of 2 μm. Figure is taken from Grünberger et al. (2012). Reproduced with permission of the Royal Society of Chemistry.

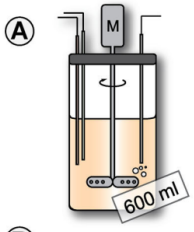

Cultivation specification	Analytical method	Biomass related quantity	Max. growth rate [h^{-1}]
Multifors multi-fermenter ▫ 4x 1.4 liter bioreactor volume ▫ 4x 600 ml cultivation volume ▫ Stirrer rotation at 1000 rpm ▫ 0.9 l min^{-1} air	VIS Spectrometry (VS)	Optical density (OD)	$\hat{\mu}_{OD(VS)}$ = 0.40 ± 0.00
	Coulter counter (CC)	Cell number (N)	$\hat{\mu}_{N(CC)}$ = 0.39 ± 0.03
		Cell volume (V)	$\hat{\mu}_{V(CC)}$ = 0.39 ± 0.02
	FACS	Cell number (N)	$\hat{\mu}_{N(FACS)}$ = 0.38 ± 0.01

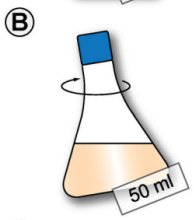

Cultivation specification	Analytical method	Biomass related quantity	Max. growth rate [h^{-1}]
Shake flask ▫ 500 ml Erlenmeyer flask ▫ 50 ml cultivation volume ▫ Orbital shaking freq. 120 rpm	VIS Spectrometry (VS)	Optical density (OD)	$\hat{\mu}_{OD(VS)}$ = 0.41 ± 0.00
	Coulter counter (CC)	Cell number (N)	$\hat{\mu}_{N(CC)}$ = 0.48 ± 0.02
		Cell volume (V)	$\hat{\mu}_{V(CC)}$ = 0.42 ± 0.01
	FACS	Cell number (N)	$\hat{\mu}_{N(FACS)}$ = 0.43 ± 0.01

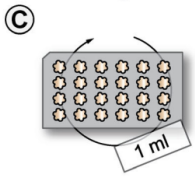

Cultivation specification	Analytical method	Biomass related quantity	Max. growth rate [h^{-1}]
m2p labs BioLector ▫ 48 well Flowerplate ▫ 48x 1ml cultivation volume ▫ Shaking diameter 3 mm ▫ Shaking at 1200 rpm ▫ Rel. humidity >80%	VIS Spectrometry (VS)	Optical density (OD)	$\hat{\mu}_{OD(VS)}$ = 0.41 ± 0.02
		Backscatter (BS)	$\hat{\mu}_{BS(VS)}$ = 0.48 ± 0.03
	Coulter counter (CC)	Cell number (N)	$\hat{\mu}_{N(CC)}$ = 0.44 ± 0.01
		Cell volume (V)	$\hat{\mu}_{V(CC)}$ = 0.41 ± 0.02

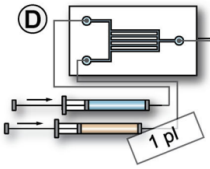

Cultivation specification	Analytical method	Biomass related quantity	Max. growth rate [h^{-1}]
Microfluidics ▫ 30x 1 pL cultivation volume ▫ Continuous media infusion ▫ Flow rate = 10 nl min^{-1} / PLBR	Microscopy image based (MI)	Cell number (N)	$\hat{\mu}_{N(MI)}$ = 0.64 ± 0.02
		Microcolony area (A)	$\hat{\mu}_{A(MI)}$ = 0.61 ± 0.02

Figure 2. Growth of *C. glutamicum* wild type at different cultivation scales on CGXII glucose medium. **A–D:** In each case maximum growth rates were estimated during the exponential phase and based on different methods for biomass determination. Mean values and standard deviations are calculated from at least triplicate cultures.

from 600 mL bioreactor scale over 50 mL shake flask scale and 1 mL microtiter plate scale down to 1 pL PLBR scale. Most importantly, each cultivation experiment was performed in at least three biological replicates.

In order to test and reproduce possible effects on the estimation of μ_{max} when based on different measurements of either cell concentration or cell density we applied different quantification methods including cell number, optical density, backscatter, cell volume, and colony area. Values for μ_{max} were then estimated for each culture and quantification method by fitting an exponential function to the measurement data in the time window of exponential growth (cf. Equations 4 and 5).

The maximum growth rate during the exponential phase of bioreactor cultivations is estimated in an overall range of $0.37\,h^{-1} \leq \hat{\mu} \leq 0.41\,h^{-1}$ if all rate estimates from the different measurements are covered by one standard confidence interval (Fig. 2A and Supplementary Fig. S1). The determined exponential growth rate from the shake flask experiments lies within a range of $0.40\,h^{-1} \leq \hat{\mu} \leq 0.47\,h^{-1}$, showing some tendency to higher growth rates (Fig. 2B and Supplementary Fig. S2). The volume reduction in microtiter plates as compared to the bioreactor is by a factor of 10^3. However, no significant influence on exponential growth is observed in the microtiter plates and the growth rate determined is identical to the shake flask experiment (Fig. 2C and Supplementary Fig. S3). Most interestingly, growth in the microfluidic chip is much faster as compared to all other experiments showing a rate between $0.60\,h^{-1} \leq \hat{\mu} \leq 0.65\,h^{-1}$ (Fig. 2D and Supplementary Fig. S4). In that case the working volume is reduced by a factor of 10^{12}.

Reproducibility of Maximum Growth Rate Estimation

To the best of our knowledge this is also the first report which uses biological replicate cultivations and several biomass measurements techniques to prove the reproducibility of maximum growth rate estimations for a model organism in industrial biotechnology. Depending on the measurement method and cultivation condition the relative standard deviation from at least triplicates varies between $1\% \leq \sigma_{rel} \leq 10\%$ (cf. Fig. 1). Moreover, our results clearly demonstrate that under the conditions tested, there are no significant differences between the maximum growth rate estimates based on cell concentration and bacterial cell density measurements, respectively. Although there is no superior biomass quantification method regarding reproducibility it has to be pointed out that the microscopy image based method in combination with the microfluidic chip is currently the only direct quantification method for cell concentration and bacterial cell density.

General Impact of the Micro-Environment

The surprising result of a 50% increase in the maximum growth rate of *C. glutamicum* when cultivated under the PLBR conditions consequently asks for a rational explanation behind this observation. Clearly, cells cultivated in the PLBR are not growing under batch conditions. Due to the specific design of the PLBR, cells are growing in a monolayer with continuous supply of fresh media (Grünberger et al., 2012). Hence all growth essential nutrients are provided in excess for each cell of the micro-colony. This also holds true for the essential gas components oxygen and carbon dioxide, which are instantaneously supplied by direct diffusion through the gas permeable PDMS layer and taken up by the cells monolayer via a large cell surface area. Regarding the cells micro-environment, the conditions are comparable to a continuously operated bioreactor at high dilution rates (e.g., chemostat or turbidostat).

In a recent study the effect of increased dissolved carbon dioxide concentrations (p_{CO_2}) on the maximum growth rate of *C. glutamicum* in a 1.5 L bioreactor under turbidostat conditions with glucose or lactate as single carbon sources was investigated (Bäumchen et al., 2007). In that case the growth rate was derived indirectly by calculating the mean dilution rate from the glucose consumption rate, which was necessary to hold a constant biomass concentration of $2\,g\,L^{-1}$ inside the bioreactor. Most interestingly, a comparable high maximum growth rate of $\mu_{max} = 0.58\,h^{-1}$ on glucose was reported under standard p_{CO_2}-levels (corresponding to atmospheric pressure) as shown here for the PLBR cultivations. However, no growth accelerating effect of higher p_{CO_2}-levels was detectable during growth on defined glucose media.

In fact there is a common striking feature between the turbidostat and our PLBR, which relies on a continuous removal of secreted by-products via the dilution with fresh media solution. Moreover, in all other experimental setups tested here, the classical batch-mode was applied, which is known to provoke pyruvate overflow metabolism under conditions of carbon excess resulting in typical by-products like acetate or pyruvate in prokaryotes like *C. glutamicum* (Eggeling and Bott, 2005). Hence it can be readily concluded that the formation of by-products and/or its re-uptake somehow directly impairs growth through toxicity effects or on the other hand is much more energy demanding than currently believed.

In order to test for a negative effect of growth due to by-product formation we conducted experiments in the microtiterplate scale as well as in the microfluidic scale.

Influence of By-Product Dilution on Growth

In one experiment we investigated the potential impact of "by-product dilution" on the maximum growth rate in microtiter plates, starting from the same pre-culture as mentioned above and performing a log-dilution series, each in threefold biological replicates. The resulting growth curves show a direct dependency on the initial cell concentration (Fig. 3A). By comparing the cultivation times needed to reach a certain threshold backscatter signal, a shift towards lower initial cell densities is found where growth accelerates faster within the first hours of cultivation.

Since the backscatter measurements in the diluted cultures are below the upper limit of quantification at the beginning of the cultivation the data cannot be directly used for a maximum growth rate estimation following the standard procedure as stated above. For that reason we applied Equation (3) to estimate average growth rates $\overline{\mu}_i$ for each diluted culture i. Here the variable $X_{2,i} = BS_{60}$ is set to a threshold backscatter signal of BS = 60. The initial biomass values $X_{1,i} = BS_{ref,0} \cdot v_i$ are estimated from the backscatter signal of the undiluted reference cultures $BS_{ref,0} = BS_{ref,0}$ $(t = 0)$ of each replicate series and the dilution factor v_i.

Following this approach, the calculated average growth rates show a clear increase along the dilution series (Fig. 3B). Most interestingly, starting with only few cells an average growth rate of $\overline{\mu}_7 = 0.66 \pm 0.33\,h^{-1}$ is reached, which resembles the maximum growth rate of the PLBR cultivation experiment (cf. Fig. 1D). Obviously, the final dilution $(v_7 = 10^{-7})$ is in the range of only a few single cells and possible effects of less active or dead cells are much more pronounced. Eventually, this leads to a higher variation in the obtained growth curves (cf. Supplementary Fig. S5) and therefore the estimated growth rate shows a higher standard deviation. Nevertheless, is has to be kept in mind that the calculated average growth rates always represent underestimations of the true maximum growth rate (cf. Equation 3) and hence the true μ_{max}-value is likely to be higher in the first phase of the cultivation.

In contrast, no systematic effect on the maximum growth rate is observed in the later exponential phase providing in each case a sufficiently high biomass concentration and hence signal to noise ratio for rate estimation according to

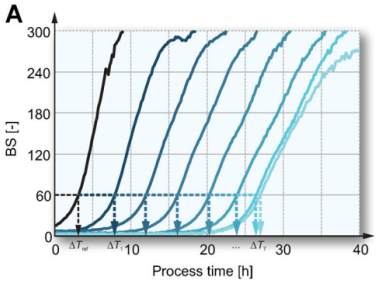

B

Dilution factor [-]	Time interval [h]	Av. growth rate [h^{-1}]
$v_{ref} = 1$	$\Delta T_{ref} = 3.12 \pm 0.10$	$\bar{\mu}_{ref} = 0.46 \pm 0.03$
$v_1 = 10^{-1}$	$\Delta T_1 = 07.88 \pm 0.00$	$\bar{\mu}_1 = 0.47 \pm 0.01$
$v_2 = 10^{-2}$	$\Delta T_2 = 11.99 \pm 0.39$	$\bar{\mu}_2 = 0.49 \pm 0.02$
$v_3 = 10^{-3}$	$\Delta T_3 = 16.11 \pm 0.10$	$\bar{\mu}_3 = 0.52 \pm 0.01$
$v_4 = 10^{-4}$	$\Delta T_4 = 20.33 \pm 0.39$	$\bar{\mu}_4 = 0.53 \pm 0.01$
$v_5 = 10^{-5}$	$\Delta T_5 = 24.00 \pm 0.75$	$\bar{\mu}_5 = 0.54 \pm 0.01$
$v_6 = 10^{-6}$	$\Delta T_6 = 26.55 \pm 0.73$	$\bar{\mu}_6 = 0.58 \pm 0.01$
$v_7 = 10^{-7}$	$\Delta T_7 = 27.16 \pm 1.23$	$\bar{\mu}_7 = 0.66 \pm 0.03$

Figure 3. Influence of by-product dilution on growth of *C. glutamicum* wild type in microtiter plates on CGXII glucose medium. A: Log-dilution series were generated from three reference cultures and grown in parallel. For each cultivation mean backscatter signals are shown. B: Corresponding time intervals after reaching the threshold backscatter signal of BS = 60 were determined and used for the estimation of average growth rates according to Equation (3). Standard deviations are calculated from the triplicate cultures.

Equations (4) and (5). This observation can be again explained by the fact, that at low cell density the possible growth impairing by-products are greatly diluted in the cell's surrounding, while at higher cell density, proportional to biomass, the secreted by-product concentration is much higher.

Influence of Secreted By-Products on Growth

In two further experiments we directly addressed the question whether secreted by-products negatively influence the growth of *C. glutamicum* under PLBR conditions. For that purpose *C. glutamicum* cells were fed with either undefined cell-free supernatant from exponentially grown shake flask cultures (OD = 5) or CGXII glucose medium supplemented with 5 mM acetate, a well-known by-product of glucose grown *C. glutamicum* cells (Han et al., 2008) (Fig. 4 and Supplementary Figs. S6 and S7). In both cases growth is significantly slower compared to the reference cultivation (cf. Fig. 2D). Moreover in the cell-free supernatant medium the estimated growth rate lies within the range of the standard batch-approaches (cf. Fig. 2A–C), whereas in the acetate media the rate is still significantly higher.

The acetate concentration in the cell free supernatant was detectable (>0.05 mM) by HPLC analytics, but below the upper limit of quantification (<0.5 mM). Additionally, untargeted GC–ToF-MS analyses was performed to identify possible other by-products in the cell-free supernatant, but no further differences were found in comparison to non-inoculated medium (data not shown). Interestingly, when *C. glutamicum* cells are grown in defined media with glucose and acetate as carbon sources the glucose consumption rate decreases to 50% compared to cells grown with glucose as sole carbon source (Wendisch et al., 2000). The effect on growth can thus partly be explained with accumulation of by-products or even autoinducers (Shin et al., 2011) in the culture supernatant.

Macroscopic View of Batch Growth

To sketch up a qualitative picture on how by-product formation possibly effects the specific growth rate in a batch culture we formulated a simple unstructured model allowing for by-product formation, inhibition as well as its coutilization. For more details on the model structure see the Appendix.

The model is applied to simulate the time dependent changes in all process variables and the resulting dynamics are shown in Figure 5. The cells initially grow very fast on the primary substrate with a significantly higher maximum growth rate. However, with an increasing by-product concentration also growth on the primary substrate is inhibited and the resulting specific growth rate greatly decreases until a steady-state is reached where by-product formation and coutilization are balanced. Consequently, the following exponential growth phase is determined by a specific growth rate that does not equal the maximum growth rate from the beginning, but a constant rate resulting from coutilization of substrate and by-product as well as constant by-product inhibition. Noteworthy, the model simulations also reflect the current understanding of glucose induced acetate metabolism in *C. glutamicum* from the macroscopic point of view.

Conclusions and Outlook

From our results we can conclude that the exponential growth rate of *C. glutamicum* wild type on CGXII glucose medium is not directly depending on the cultivation scale and underlying technical devices (e.g., stirred-tank bioreactor, shake flask, and microtiter plate). In fact, it is a function

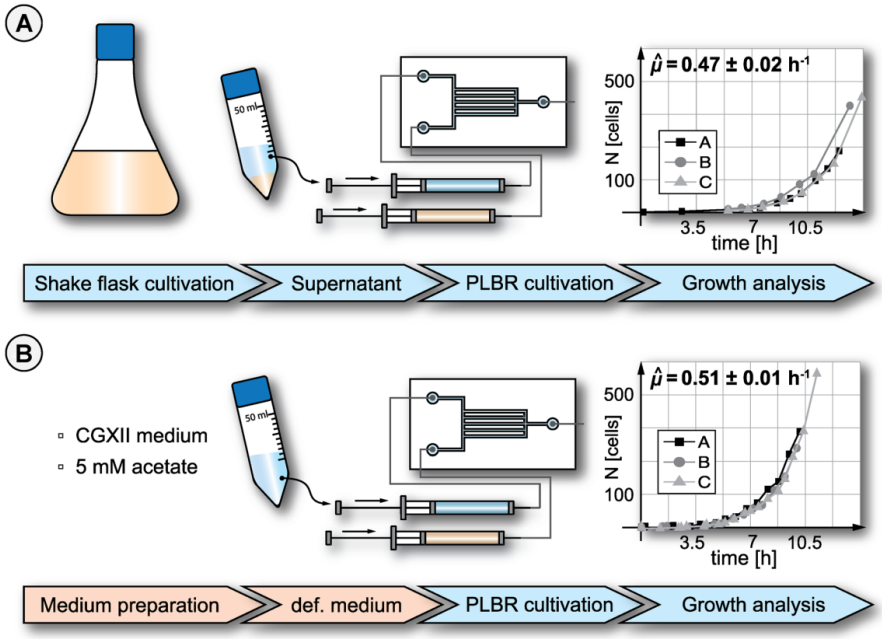

Figure 4. Influence of secreted by-products on growth of *C. glutamicum* wild type cultivated under PLBR conditions. A: Cells are grown on undefined cell-free supernatant from exponentially grown shake flask cultures. B: Cells are grown on CGXII glucose medium supplemented with 5 mM acetate. Cell counts from microscopic images are used for exponential growth rate estimation. Mean values and standard deviations are calculated from triplicate cultures.

of the pre-defined (start medium and mode of operation) and resulting (medium with by-products) cultivation conditions. On the one hand, in all tested conventional approaches, the chosen mode of operation was batch where

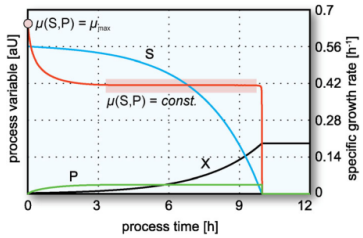

Figure 5. Dynamics of a batch process as a function of cell (X), substrate (S) and by-product concentrations (P). Cell population growth is determined by a balance of by-product formation and cutilization of the primary substrate and the by-product. The following model parameter values are used for simulation: $X_0 = 0.1$ g L^{-1}, $S_0 = 20$ g L^{-1}, $P_0 = 0$ g L^{-1}, $\pi_P = 0.75$ g g^{-1} h^{-1}, $\mu_{max,S} = 0.85$ h^{-1}, $\mu_{max,P} = 0.28$ h^{-1}, $K_S = K_P = 0.01$ g L^{-1}, $Y_{X/S} = 0.41$ g g^{-1}, $Y_{X/P} = 0.29$ g g^{-1}, $k_i = 0.015$ g L^{-1}.

at a certain threshold cell density the concentration of specific by-products (e.g., acetate) is high enough to exert a growth impairing effect. On the other hand, under conditions of low by-product concentrations as a result of cell washing in the PLBR (comparable to a continuously operated bioreactor) or very low cell densities at the initial batch phase (e.g., BioLector), growth is not impaired and hence most likely maximal for the specific medium composition under investigation.

The results show, that the PLBR as well as the BioLector approach can be used to unravel "true" maximum growth rates. Hence both setups can be used in future screening studies for determining growth influencing factors focusing mainly on medium components. The main advantage of the PLBR compared to classical lab-scale approaches relies in the instantaneous observation of the cell's response to specific environmental stimuli. Hence experiments can be carried out to directly relate a strain's genotype and its growth phenotype (including morphology) in dependence of underlying nutritional conditions. These studies can then be combined with experiments in microtiter plates to test and optimize candidate factors in a high-throughput manner.

Appendix: Unstructured Model of Batch Growth

To model the negative effect of a by-product on batch growth an unstructured model is formulated using well-known Monod Kinetics (Monod, 1949):

$$\dot{X} = r_X$$
$$\dot{S} = r_S$$
$$\dot{P} = r_P$$

with

$$r_X = \mu(S,P) \cdot X, \quad r_S = -\left(\frac{\mu(S,I)}{Y_{X/S}} + \pi_P\right) \cdot X,$$
$$r_P = -\left(\frac{\mu(P)}{Y_{X/P}} - \pi_P\right) \cdot X$$

and

$$\mu(S,P) = \mu(S,I) + \mu(P)$$
$$\mu(P) = \mu_{max,P} \cdot \frac{P}{K_P + P}$$
$$\mu(S,I) = \mu_{max,S} \cdot \frac{S}{K_S + S} \cdot \frac{k_I}{k_I + P}$$

Here S denotes the primary substrate that is converted to biomass X and the by-product P with a constant rate π_P. The by-product is allowed to be coutilized in parallel and hence the resulting specific growth rate $\mu(S, P)$ is a sum of the substrate specific growth rates $\mu(P)$ and $\mu(S, I)$. The latter is further modulated by a multiplicative term representing a non-competitive inhibition by P.

The model parameters $\mu_{max,S}$ and $\mu_{max,P}$ denote the "true" maximum growth rates on the primary substrate and by-product, respectively (cf. Equation 2). The respective half-saturation constants, yield coefficients and the inhibition constant are denoted as K_S, K_P, $Y_{X/S}$, $Y_{X/P}$, and k_I, respectively.

References

Bäumchen C, Knoll A, Husemann B, Seletzky J, Maier B, Dietrich C, Amoabediny G, Büchs J. 2007. Effect of elevated dissolved carbon dioxide concentrations on growth of Corynebacterium glutamicum on D-glucose and L-lactate. J Biotechnol 128(4):868–874.

Eggeling L, Bott M. 2005. Handbook of Corynebacterium glutamicum. Boca Raton, Florida: CRC Press, Tailor and Francis Group.

Feist AM, Zielinski DC, Orth JD, Schellenberger J, Herrgard MJ, Palsson B. 2010. Model-driven evaluation of the production potential for growth-coupled products of *Escherichia coli*. Metab Eng 12(3):173–186.

Fong SS, Palsson B. 2004. Metabolic gene-deletion strains of *Escherichia coli* evolve to computationally predicted growth phenotypes. Nat Genet 36(10):1056–1058.

Groisman A, Lobo C, Cho H, Campbell JK, Dufour YS, Stevens AM, Levchenko A. 2005. A microfluidic chemostat for experiments with bacterial and yeast cells. Nat Methods 2(9):685–689.

Grünberger A, Paczia N, Probst C, Schendzielorz G, Eggeling L, Noack S, Wiechert W, Kohlheyer D. 2012. A disposable picoliter bioreactor for cultivation and investigation of industrially relevant bacteria on single cell level. Lab Chip 12(11):2060–2068.

Guillouet S, Engasser JM. 1996. Kinetics of volume variation of Corynebacterium glutamicum following saline osmotic upshifts. Biotechnol Lett 18(2):145–148.

Han SO, Inui M, Yukawa H. 2008. Effect of carbon source availability and growth phase on expression of Corynebacterium glutamicum genes involved in the tricarboxylic acid cycle and glyoxylate bypass. Microbiology 154(Pt 10):3073–3083.

Kensy F, Zang E, Faulhammer C, Tan RK, Büchs J. 2009. Validation of a high-throughput fermentation system based on online monitoring of biomass and fluorescence in continuously shaken microtiter plates. Microb Cell Fact 8:31.

Khanna S, Srivastava AK. 2005. Statistical media optimization studies for growth and PHB production by Ralstonia eutropha. Process Biochemistry 40(6):2173–2182.

Kortmann H, Chasanis P, Blank LM, Franzke J, Kenig EY, Schmid A. 2009. The Envirostat—A new bioreactor concept. Lab Chip 9(4):576–585.

Lara AR, Galindo E, Ramírez OT, Palomares LA. 2006. Living with heterogeneities in bioreactors: Understanding the effects of environmental gradients on cells. Mol Biotechnol 34(3):355–381.

Lee KS, Boccazzi P, Sinskey AJ, Ram RJ. 2011. Microfluidic chemostat and turbidostat with flow rate, oxygen, and temperature control for dynamic continuous culture. Lab Chip 11(10):1730–1739.

Litsanov B, Kabus A, Brocker M, Bott M. 2012. Efficient aerobic succinate production from glucose in minimal medium with Corynebacterium glutamicum. Microb Biotechnol 5(1):116–128.

Luli GW, Strohl WR. 1990. Comparison of growth, acetate production, and acetate inhibition of *Escherichia coli* strains in batch and fed-batch fermentations. Appl Environ Microbiol 56(4):1004–1011.

Mandenius CF, Brundin A. 2008. Bioprocess optimization using design-of-experiments methodology. Biotechnol Prog 24(6):1191–1203.

Monod J. 1949. The growth of bacterial cultures. Annu Rev Microbiol 3:371–394.

Petelenz-Kurdziel E, Eriksson E, Smedh M, Beck C, Hohmann S, Goksör M. 2011. Quantification of cell volume changes upon hyperosmotic stress in Saccharomyces cerevisiae. Integr Biol (Camb) 3(11):1120–1126.

San KY, Bennett GN, Aristidou AA, Chou CH. 1994. Strategies in high-level expression of recombinant protein in *Escherichia coli*. Ann NY Acad Sci 721:257–267.

Shin HS, Kim YJ, Yoo IH, Lee HS, Jin S, Ha UH. 2011. Autoinduction of a genetic locus encoding putative acyltransferase in Corynebacterium glutamicum. Biotechnol Lett 33(1):97–102.

Sisignano M, Morbitzer D, Gätgens J, Oldiges M, Soppa J. 2010. A 2-oxoacid dehydrogenase complex of Haloferax volcanii is essential for growth on isoleucine but not on other branched-chain amino acids. Microbiology 156(Pt 2):521–529.

Suresh S, Srivastava VC, Mishra IM. 2009. Critical analysis of engineering aspects of shaken flask bioreactors. Crit Rev Biotechnol 29(4):255–278.

Takors R. 2011. Scale-up of microbial processes: Impacts, tools and open questions. J Biotechnol

Volkmer B, Heinemann M. 2011. Condition-dependent cell volume and concentration of *Escherichia coli* to facilitate data conversion for systems biology modeling. PLoS ONE 6(7):e 23126.

Wang P, Robert L, Pelletier J, Dang WL, Taddei F, Wright A, Jun S. 2010. Robust growth of *Escherichia coli*. Curr Biol 20(12):1099–1103.

Wendisch VF, de Graaf AA, Sahm H, Eikmanns BJ. 2000. Quantitative determination of metabolic fluxes during coutilization of two carbon sources: Comparative analyses with Corynebacterium glutamicum during growth on acetate and/or glucose. J Bacteriol 182(11):3088–3096.

Wiechert W, Noack S. 2011. Mechanistic pathway modeling for industrial biotechnology: Challenging but worthwhile. Curr Opin Biotechnol 22(5):604–610.

Zhang YH. 2010. Production of biocommodities and bioelectricity by cell-free synthetic enzymatic pathway biotransformations: Challenges and opportunities. Biotechnol Bioeng 105(4):663–677.

Discussion

Construction of metabolite sensors

As outlined in the introduction, the current number of transcription factor-based metabolite sensors, suitable for bacterial HT screenings, is very limited. The combined use of such sensors with FACS is reported so far for LysG and Lrp of *C. glutamicum* in screenings of new L-lysine producers (Binder et al., 2012) and L-valine producers (Mustafi et al., 2012), respectively.

Metabolite sensors constructed in this study

In this work 18 new metabolite sensors were constructed, in order to broaden the utility of amino acid sensors for *E. coli* and *C. glutamicum*. Eight of them used regulatory devices from *C. glutamicum* and twelve those from *E. coli*. Details are summarized in Table 1 which reports on only eleven of the sensors, since eight are covered by an industrial cooperation and thus confidential. In all cases *eyfp* was fused to the promoter of a gene, which is thought to be controlled by an effector-inducible regulator. In several cases, this gene encodes a putative or verified amino acid exporter, which maybe induced by high intracellular amino acid concentrations. To include all potential TF-binding sites in the promoter regions, the first 30-60 codons of the selected native target genes were included in the fusion construct. A stop-codon followed by a ribosomal binding site is placed upstream of *eyfp* to enable its expression without the initial N-terminal amino acids of the natural target. If known, the corresponding TF is also encoded in the sensor plasmid; otherwise sensor function relies on chromosomal encoded TF.

All metabolite sensors were introduced into their host-organism, *C. glutamicum* or *E. coli*, and fluorescence in response to peptide-addition was assayed. Addition of peptides is a proven method to increase the cytosolic pool of a specific amino acid in *C. glutamicum* or *E. coli* (Bellmann et al., 2001; Kennerknecht et al., 2002; Simic et al., 2001; Tavori et al., 1981; Trötschel et al., 2005; Zittrich and Krämer, 1994). Peptides were always added to give a final concentration of 5mM and as the negative control water was used. Data were recorded using a BioLector microbioreactor system (Kensy et al., 2009) with eYFP-filter gain set to 60, and backscatter gain set to 10. The specific fluorescence (eYFP/backscatter) is used as benchmark.

Functional constructions

Nine sensors responded specifically to externally added peptide. Whereas six of them belong to those covered by an industrial cooperation, the other three detect serine in *C. glutamicum*, leucine in *E. coli*, and arginine in *E. coli*, respectively.

The serine sensor (pSenSer) is based on a putative serine exporter, encoded by cg0701. cg0702 is divergently transcribed and encodes an LTTR-type transcriptional regulator. This co-localization on the chromosome, the predicted function and experiments by N. Stäbler (unpublished data) led to the assumption, that Cg0702 regulates expression of cg0701 in response to intracellular serine concentration and thus could be suitable to construct a sensor. As in case of LysE (Vrljic et al., 1996), Cg0701 could naturally serve as a valve for exporting excess serine that might be harmful to the cell. Cells carrying pSenSer emitted enhanced fluorescence, when Ser-tripeptide was added, which was not the case with Thr-tripeptide or Ala-Ala dipeptide. In these experiments a 1.6-fold maximal induction was observed. When the serine producer strain Ser4 (Stolz et al., 2007), which accumulates up to 81 mM serine, was transformed with pSenSer, a 33.3-fold maximal induction was observed. This difference

in fluorescence between peptide feeding of wild-type cells and producer strain points to a general problem of *in vivo* sensor characterization. When no producer strain is available, peptide addition is the only option to increase the cytosolic pool of a specific amino acid. But peptide uptake rate, peptide hydrolyzation and amino acid use may vary significantly, as known from the use of different L-isoleucine or L-threonine containing peptides and determinations of intracellular amino acid concentrations (Kennerknecht et al., 2002; Simic et al., 2001; Zittrich and Krämer, 1994). In addition, stability of the intracellular concentration over time is not ensured (Diesveld et al., 2008), since the peptide is consumed. Thus data obtained with this method rather give qualitative information than to enable a quantitative assessment of sensor parameters. The selective increase of a specific small molecule in the cytosol is a major problem for the evaluation and characterization of sensors, except for studies with *C. glutamicum* and with amino acids, where intracellular concentrations have been determined (Bellmann et al., 2001; Kennerknecht et al., 2002; Simic et al., 2001; Trötschel et al., 2005; Zittrich and Krämer, 1994). In all other cases simply the dose response to externally added metabolite concentrations or inducer concentrations are given (Dietrich et al., 2010).

pSenArg is constructed from the arginine exporter ArgO of *E. coli* and its LTTR-type transcriptional regulator ArgP. It was reported, that the transcription of *argO* is ArgP dependent and induced by arginine (Nandineni and Gowrishankar, 2004). Therefore, we expected the arginine-induced expression of the P_{argO}-eyfp fusion construct. Indeed, the maximal sensor induction was 8.1-fold with this amino acid. Interestingly, ArgP interacts with both, arginine and lysine, as known for LysG in *C. glutamicum*, which shares high sequence similarity with ArgP (35% identity, 53% similarity). Also recruitment of RNA polymerase to the *argO* promoter is mediated by arginine- as well as lysine-bound ArgP. But in the final steps of transcription initiation, arginine-bound ArgP initiates *argO* transcription only, while lysine-bound ArgP restrains RNA polymerase at the promoter (Laishram and Gowrishankar, 2007). Thus, the specificity for arginine is achieved on a higher level than that of the co-inducer/transcription factor interaction.

pSenLeu is based on RhtC from *E. coli*. Overexpression of *rhtC* in *E. coli* provides increased resistance to high threonine concentrations, which inhibit growth due to intracellular perturbations (Kruse et al., 2002; Zakataeva et al., 1999). Therefore it was annotated as probable threonine efflux transporter. Further experiments supported this view by demonstrating enhanced threonine secretion of *C. glutamicum* cells, expressing *rhtC* from *E. coli* (Diesveld et al., 2008). However, expression of the P_{rhtC}-eyfp fusion in *E. coli* cells carrying pSenLeu was induced 3.5-fold by Gly-Leu and Ala-Leu dipeptides and only 1.4-fold by Thr-Ala dipeptide. But these observations are not contradictory, since resistance to high leucine concentrations was not tested by Zakataeva et al. and Thr-Ala dipeptide does induce P_{rhtC} transcription. It is unknown, whether there is a TF activating *rhtC* transcription in response to threonine or leucine. Nonetheless, Gly-Leu and Ala-Leu-dipeptide induced transcription of the P_{rthC}-eyfp fusion argues for the presence of an activating transcription factor present in the chromosome of *E. coli*.

Non-functional constructions

The threonine sensor pSenThrE is based on the threonine efflux protein ThrE of *C. glutamicum*. Simic et al. determined export rates for threonine in *C. glutamicum* wild-type cells, ThrE-overexpressing cells and a ThrE-deletion mutant to be 2.7, 3.8 and 1.1 nmol min^{-1} mg of dry $weight^{-1}$ (Simic et al., 2001). Aside from ThrE mediated export, additional active export and passive diffusion contribute to total threonine export. In the sensor construct pSenThrE made in this work, P_{thrE} is fused with *eyfp* and in addition the open reading frame (cg2904) upstream of *thrE* is included in the sensor plasmid.

Cg2904 includes a HTH-motif and thus could be the transcriptional regulator of thrE. When *C. glutamicum* cells carrying pSenThrE were incubated with Thr-tripeptide, eYFP-fluorescence increased by factor 1.6, compared to cells incubated with Ala-Ala dipeptide. Based on this weak induction, differentiation of cell populations by FACS was hardly possible. There are several reasons to explain this. Possibly, transcriptional activation of *thrE* expression by threonine is weak. The known rather slight increase of threonine export in *thrE* overexpressing cells from 2.7 to 3.8 nmol min^{-1} mg of dry $weight^{-1}$ might be an indication for this. Moreover, it is not ensured that the putative regulator included in pSenThrE influences *thrE* expression. At least a failure to load the cells with threonine by Thr-tripeptide addition is unlikely, since much related procedures were used in previous works to obtain intracellular threonine concentrations of 160 mM (Diesveld et al., 2008; Palmieri et al., 1996; Simic et al., 2001).

With six sensor constructs made, no specific response to any of the assayed peptide additions was observed. One of these cases was pSenThr1, based on Cg2941, annotated as putative threonine efflux pump by sequence similarity prediction. The divergently transcribed cg2942 belongs to the AsnC type family of transcriptional regulators. This gene organization and prediction of function was the reason to construct pSenThr1. However, with all tested peptides as well as water as a negative control, only basal fluorescence was observed, representing a very low constitutive expression of eYFP. There are a number of reasons to explain this fact. Among them it could be, that Cg2941 is defect or not expressed. However, it is more likely that Cg2941 does not export an amino acid but another unknown small molecule. Whereas the polarity of transport direction (i.e. outward versus inward) is largely retained within a transporter family (Saier, 2000), the substrates for transporters can hardly be predicted.

Another example of a non-functional construct is pSenHis, based on *hutH* and *hutG* from *Corynebacterium resistens*. The hut (*histidine utilization*) gene cluster contains four transcriptional units, whose transcription is controlled by the HutR protein, an IclR-type regulator, and is activated, when histidine is used as sole nitrogen source (Schröder et al., 2012). Strongest induction of the operon by histidine was observed for *hutH*, followed by *hutG*. Promoters of both genes were used to construct pSenHis with a P_{hutG}-*eyfp* and a P_{hutH}-*crimson* fusion and *hutR* on the plasmid. Unfortunately, *C. glutamicum* pSenHis cells grown in presence of various peptides, including His-Ala, did not emit any fluorescence. *C. glutamicum* does not possess genes for histidine utilization and does not grow with histidine as sole nitrogen source (Kulis-Horn et al., 2013). In a BLAST search with the HutR protein sequence as template no ortholog of HutR in *C. glutamicum* was found. To test, whether an induction of hut genes is possible in *C. glutamicum* under nitrogen-limitation, cells were cultivated in CgXII medium containing glutamine instead of urea and ammonium. Again, no sensor response was detectable. These observations indicate that HutR/histidine induced transcription of *hutH* and *hutG* genes is not transferable to *C. glutamicum*. There are again several reasons to explain the failure of a His-dependent induction of fluorescence. One could speculate that environmental condition-specific activation of the responsible sigma factor differs between *C. glutamicum* and *C. resistens*. Also the fact, that in many cases of histidine utilization imidazole acrylic acid is the inducer of the hut operon (Zhang and Rainey, 2007), may explain malfunction of pSenHis.

Table 1: Overview of metabolite sensors constructed in this study. [1](Simic et al., 2001), [2](Brune et al., 2007), [3](Schröder et al., 2012), [4](Celis, 1999; Laishram and Gowrishankar, 2007; Nandineni and Gowrishankar, 2004; Peeters et al., 2009), [5](Kruse et al., 2002; Livshits et al., 2003; Zakataeva et al., 1999), [6](Tsyrenzhapova et al., 2009)

Plasmid	Sensor induced by	Regulator	Regulator family	Putative effector	Controlled gene	Annotated protein function	Organism	Ref.
pSenSer(Cg)	D/L-Ser	Cg0702	LTTR	Ser	*cg0701*	DMT family permease	*C. glutamicum*	
pSen3413(Cg)	-	Lrp	AsnC	Leu, Met, Val	*cg3413*	Putative branched-chain amino acid permease	*C. glutamicum*	
pSen2941(Cg)	-	Cg2942	AsnC	Thr	*cg2941*	Putative threonine efflux protein	*C. glutamicum*	
pSenThrE(Cg)	L-Thr	Cg2904	Xre	Thr	*thrE*	Putative threonine exporter	*C. glutamicum*	1
pSen2546(Cg)	-	Cg1486	IclR	Leu	*cg2546*	Putative secondary C4-dicarboxylate transporter	*C. glutamicum*	2
pSenHutGH(Cg)	-	HutR	IclR	His	*hutG , hutH*	Formiminoglutamase / Histidine ammonia-lyase	*C. resistens*	3
pSenArg(Ec)	L-Arg	ArgP	LTTR	Arg	*argO*	Arginine transporter	*E. coli*	4
pSenLeu(Ec)	L-Leu	Unknown		Thr	*rhtC*	Threonine efflux pump	*E. coli*	5
pSenYddG(Ec)	-	Unknown		Phe	*yddG*	Aromatic amino acid exporter	*E. coli*	6
pSenYfeH(Ec)	-	YfeR	LTTR	Cys, OAS	*yfeH*	Inner membrane protein	*E. coli*	

Desirable characteristics of metabolite sensors for HT-screening approaches

Based on literature data and own experiments, some specific features of metabolite sensors might be desirable for screening purposes.

(1) In metabolic engineering approaches, presumably sensors with a **detection range** in the millimolar range will be required. Many TFs meet this requirement, for example AraC variants, detecting mevalonate at concentrations ranging from 10-100 mM or TAL concentrations from 1-10 mM (Tang and Cirino, 2011; Tang et al., 2013). LysG senses L-lysine from 4-25 mM and Lrp responds to L-methionine concentrations ranging from 0.2-23.5 mM (Binder et al., 2012; Mustafi et al., 2012). In some metabolic engineering approaches less sensitive variants of a specific sensor could be of particular interest, in order to discriminate highly productive strains and already productive ones. To meet those needs, the sensitivity of TF-based metabolite sensors can be modified, as demonstrated for variants of AraC (Tang and Cirino, 2011; Tang et al., 2013).

(2) Preferably, there is a **strong signal induction** in response to effectors to facilitate clear discrimination of cells with induced and un-induced sensor. Many TF-based sensors provide these characteristics, for example the Lrp based methionine sensor (Mustafi et al., 2012), pSenLys (Binder et al., 2012), the BenR based benzoate sensor (Uchiyama and Miyazaki, 2010) and pSenSer (Binder et al., 2012) with a maximal induction of 78-fold, 44-fold, 35-fold and 33-fold respectively.

    Comparing the fluorescence of single cells, individual gene expression noise can be a relevant factor by enhancing the strength of background signal. This might be a problem, when screening approaches are based on small differences in signal strength, for example when strains with slightly different productivity should be distinguished. Gene expression noise arises from cell-specific differences in cell cycle stage, fluctuations in plasmid copy numbers and physiologic adaption to individual micro-environments (Raser and O'Shea, 2004; Tang, 2008). For example, different copy numbers of the sensor plasmid within different cells could result in different FP expression, even if sensed product concentrations are equal or provoking the opposite relation. Thus, gene expression noise may distort the quantitative output of a metabolite sensor, as reported for an allosteric ribozyme, detecting theophylline (Liang et al., 2012). To reduce gene expression noise in this example, the theophylline responsive fluorescence signal was normalized to another fluorescence signal, controlled by a constitutive promoter, whose activity may correspond to cell-specific conditions. Plotting one signal against the other in FACS experiments facilitated discrimination of different populations, which was impossible without the constitutive signal. This principle could also be beneficial for TF-based sensors.

(3) The **total signal strength** appears to be less critical for many screening approaches, because the sensitivity of detection machinery, for example plate-readers or FACS, is rarely limiting. However, there are several aspects, which are relevant for signal-intensity, for example the copy number of the TF, copy number of the sensor plasmid, maturation of eYFP and half-life of eYFP. To investigate the influence of TF-copy-numbers on sensor function, derivatives of pSenLys with or without plasmid encoded LysG were constructed. Lysine overproducing *C.*

glutamicum cells, carrying pSenLys without *lysG*, emitted 30% less eYFP-fluorescence than cells carrying pSenLys with *lysG* present. This may indicate, that the number of LysG molecules limits P_{lysE}-controlled eYFP expression and that a higher copy number of *lysG* leads to a higher concentration of LysG enabling stronger eYFP expression. Stronger fluorescent cells were also observed by Baumgart et al. with the same basic sensor construct in different plasmid backgrounds (Baumgart et al., 2013). In this case, increased fluorescence correlates with an increased plasmid copy number. However, a total increase in fluorescence by such means does not solve the problem of weak sensitivity, since also the background fluorescence is expected to increase.

Protein folding and chromophore formation of GFP and its derivatives are a time- and oxygen-dependent process. Cells in an exponentially growing culture are often limited by oxygen supply, which results in delayed chromophore maturation and thus delayed sensor signal, represented by a temporary decline in culture fluorescence prior to the stationary growth-phase (Hentschel et al., 2013; Shaner et al., 2005; Tsien, 1998). This could be avoided by using Flavin Mononucleotide-binding fluorescent proteins (FbFPs), which are oxygen-independent and emit fluorescence immediately after gene expression (Drepper et al., 2010).

In addition, the stability of GFP derivatives influences the total signal intensity due to an extremely long half-life of up to several days (Tombolini et al., 1997). This leads to an accumulation of the protein within the cell, thereby increasing fluorescence over time. The attachment of C-terminal tags, which render the protein accessible for tail-specific proteases, reduces the half-life dramatically (Allen et al., 2007; Andersen et al., 1998; Blokpoel et al., 2003; Triccas et al., 2002). This was also done for eYFP in *C. glutamicum* and results in reduced overall signal intensity (Hentschel et al., 2013).

(4) Requirements on **sensor specificity** depend on individual screening applications. Many TFs do not solely interact with one effector, but with several related ones. This is no disadvantage, as long as the substance of interest does not compete with an alternative effector, which is frequently present at higher concentrations. For example, the use of pSenLys to screen mutant libraries of *C. glutamicum* for enhanced lysine production is not hampered by parallel sensitivity of pSenLys for histidine and arginine (Binder et al., 2012). The reason is, that the probability to achieve lysine overproducing mutants is much larger than the chance to get histidine or arginine overproducing mutants, because more mutations in specific combinations are necessary to provoke that. In return it is very difficult to screen for histidine or arginine producers in this setup, as observed by S. Binder (personal communication). The foregoing also applies to the Lrp/*brnF* based sensor, detecting methionine, leucine, isoleucine and valine (Mustafi et al., 2012). Even if methionine causes strongest sensor response, attempts to isolate mutant *C. glutamicum* cells with enhanced methionine production were not successful, because frequently occurring valine producers appeared as vast amounts of false-positives.

On the other hand, multiple specificities for several compounds of interest can be an advantage, enabling application of the sensor in different screening approaches. In the present work pSenLys was successfully used to isolate productive mutants of ArgB, HisG and LysC, key enzymes of arginine, histidine and lysine biosynthesis (Schendzielorz et al., 2013). Given

the targeted mutagenesis without affecting biosynthesis pathways for competing metabolites, multiple sensitivities of pSenLys did not hamper the screenings.

(5) In order to broaden the applicability of a sensor system, access to **specific variants for a broad range of substances** would be beneficial. Microorganisms possess a large number of natural TFs with many of them detecting biotechnological relevant molecules. Moreover, protein engineering and fine-tuning of sensor response offers possibilities to modify specificity and sensitivity of these TFs to meet individual needs (Collins et al., 2006; Tang and Cirino, 2011; Tang et al., 2013).

Aside from effector-specificities, function of a given sensor in different host-organisms would broaden the applicability. To address this point, the transferability of metabolite sensors from *C. glutamicum* to *E. coli* or vice versa was tested with pSenLys and pSenArg. These sensors are based on the orthologous regulator/exporter pairs LysG/LysE and ArgP/ArgO, which, as mentioned, share high sequence similarity and have in part the same function. Both sensors are functional in their host organisms. When *C. glutamicum* was transformed with pSenArg, constitutive fluorescence at a medium level was observed regardless, whether Ala-Ala, Arg-Ala, His-Ala or Lys-Ala was added. Similar results were obtained with *E. coli* cells carrying pSenLys. This observation is not consistent with experiments by Marbaniang et al., who observed, that LysG activates *lysE* expression in *E. coli,* induced by Arg-Ala, His-Ala or Lys-Ala, whereas ArgP or LysG do not cross-activate their orthologous targets *lysE* or *argO* (Marbaniang and Gowrishankar, 2012). The reconstitution of LysG/*lysE* regulation was not possible in this work with pSenLys in either *E. coli* DH5α or *E. coli* ER2566 (NEB). Different experimental setups could be the reason for that. In the work by Marbaniang et al. *lysG* is fused to the P_{ara} promoter, rendering *lysG* expression inducible by arabinose, while in this study, native P_{lysG} promoter was present in the sensor plasmid, which might be inactive in *E. coli*. Moreover, a larger *lysE* regulatory region (nucleotides -289 bp to +45 bp with respect to transcription start) was used in the fusions of P_{lysE} or P_{argO} with the reporter gene. As reporter gene *lacZ* was used to detect transcriptional activation via β-galactosidase.

Experiments with other sensors constructed in this study indicate, that a transfer of sensor-function from *C. glutamicum* to *E. coli* or vice versa is not possible in any of these cases (data not shown). This is in accordance with the fact, that there are no further reports of *in vivo* reconstitution of transcriptional activation between *C. glutamicum* and *E. coli* (Marbaniang and Gowrishankar, 2012), although many promoters from *C. glutamicum* are active in *E. coli* (Pátek et al., 2003).

Library Screening

Enzymes with key roles in biosynthesis of biotechnological products are often feedback inhibited by an intermediate or the final product of the corresponding pathway (Eggeling, L., Pfefferle, W. and Sahm, 2006; Ikeda et al., 2009). This renders them unsuitable for overproduction of desired substances and requires the availability of feedback resistant variants for the construction of producer strains. To date, nearly all known feedback resistant enzyme variants were derived from mutant strains, obtained by undirected mutation and selection. For example, a superior L-threonine producer of *E. coli* was constructed using three feedback resistant enzymes (lysC-T432I, thrA-S345F and tdh-S97F), which were all taken from classical mutant strains (Lee et al., 2007). Also a *C. glutamicum*

strain with improved L-lysine production was generated by introducing two mutations (pyc-P485S, lysC-T311I) derived from classical mutants (Becker et al., 2011). In a muconic acid producing strain of *Saccharomyces cerevisiae*, an already known allele of 3-deoxy-D-arabinoheptulosonate-7-phosphate (DAHP) synthase (aro4-K229L) was used to reduce feedback inhibition in the shikimate pathway (Curran et al., 2013). However, dependence on classical producer strains limits accessibility of feedback resistant enzymes and in some cases such enzymes, respectively mutant strains containing such enzymes, are not easily available. To overcome this problem the metabolite sensor pSenLys was used in the present work to derive a number of feedback resistant key enzymes of the arginine, lysine and histidine biosynthesis pathway of *C. glutamicum*.

Productive mutants of N-acetylglutamate kinase

The *argB*-encoded N-acetylglutamate kinase (NAGK) initiates the L-arginine biosynthesis pathway in *C. glutamicum*, catalyzing the transfer of a phosphate group from ATP to N-acetyl-L-glutamate. Enzymatic activity is strongly inhibited by L-arginine, preventing increased L-arginine formation (Ramón-Maiques et al., 2006; Xu et al., 2007). Several feedback resistant variants of ArgB were derived from mutant strains (Ikeda et al., 2009) or obtained by site-directed mutagenesis (Xu et al., 2012). In this work, additional feedback resistant NAGK-variants were identified and characterized *in vivo* and *in vitro*. Compared to wild-type enzyme, all analyzed mutants exhibit at least a 19.5-fold higher K_i for L-arginine, a higher K_m for the substrate N-acetyl-L-glutamate and with one exception, reduced k_{cat} values (Schendzielorz et al., 2013, Table 2).

In its native form, *C. glutamicum* NAGK homodimers assemble to ring-like hexamers via N-terminal α-helices. The mechanism of feedback inhibition by L-arginine relies on this hexameric structure. L-arginine is bound in the interdimeric junction between the N-terminal helix of one monomer and the C-terminal lobe of another, resulting in six arginine sites per hexamer. Upon arginine binding, orientation of the N-terminal helix is changed, provoking increased distance between the bodies of two adjacent dimers. This produces structural tension on the ring-like hexameric complex, resulting in an enlarged active center with increased distance between the ATP and NAG site (open form), which hampers catalysis (Ramón-Maiques et al., 2006). Given the fact, that arginine interacts with the N-helix and orientation of the N-helix influences catalytic activity, one could speculate, that some mutations obtained in this study affect feedback inhibition by altering orientation or flexibility of the N-helix, as also speculated by Xu et al. (2012).

The binding of arginine to the interdimeric junctions follows a cooperative kinetic. Presumably, binding of first arginine molecules lead to structural rearrangements, which provoke high-affinity states of other arginine binding sites. This theory is supported by the arginine- and substrate-free crystal structure of *Mycobacterium tuberculosis* NAGK, which exhibits five subunits in the closed, active form and one subunit in the open form, which is highly sensitivity for arginine (Ramón-Maiques et al., 2006). As mentioned above, one NAGK mutant (K47H) exhibits a higher k_{cat} than wildtype-enzyme. One speculative explanation is, that K47H stabilizes the orientation of the N-terminal helix by interactions with the amide backbone, and thereby lowers affinity for arginine in all of the six subunits. This favors the active, closed form for all six active centers, which may enhance overall catalytic activity.

In other cases, *in vitro* and *in vivo* performances of mutant NAGKs are not consistent. For example, the mutants ArgB-K47H-G122T and ArgB-K47H-G122T-T180P differ greatly regarding catalytic efficiency, but perform similarly with respect to *in vivo* product accumulation (Schendzielorz et al., 2013, Table 1/ Table 2). Obviously, *in vitro* conditions do not integrate the total cellular characteristics,

which are relevant for overproduction of the final product L-arginine. This emphasizes an advantage of *in vivo* screenings for the isolation of productive enzyme variants, as compared to the in silico design of enzymes.

Productive mutants of aspartate kinase

The aspartate kinase, encoded by *lysC*, catalyzes the initial step in lysine biosynthesis and is feedback inhibited by L-lysine in *C. glutamicum* (Shiio and Miyajima, 1969). Numerous mutations, conferring feedback resistance, are already known and in many cases covered by patents (Table 2), making them unavailable for competing projects. In this study, new productive variants were generated and characterized (Schendzielorz et al., 2013, Table 3).

Table 2: Overview of patented mutations in LysC (Eggeling and Bott, 2005)

A279T	A279V	S301F	S301Y	T308I	T311I	S317A	R320G	G345D	S381F	Q404E	G408R	Amino acid exchange / Accession number, patent
						X						E06825, WO9425605_1
X						X						E06826, WO9425605_2
						X		X				L16848
						X	X	X				L27125
X												E08178
	X											E08179
		X										E08180
				X								E08181
			X									X57226, EP0387527
										X	X	JP6261766_1
X										X	X	JP6261766_2
	X									X	X	JP6261766_3
		X								X	X	JP6261766_4
				X						X	X	JP6261766_5
					X							EP1108790

LysC is a heterotetramer, consisting of two catalytic α-fragments and two regulatory β-fragments (Yoshida et al., 2010). All known mutations, conferring feedback resistance, are solely located in the regulatory β-fragment (Chen et al., 2011; Jetten et al., 1995; Ohnishi et al., 2002; Shiio et al., 1970; Thierbach et al., 1990), while productive variants, identified in this study, contain mutations in both domains (Schendzielorz et al., 2013, Table S6). To confirm the influence of mutations in the catalytic α-fragment on enhanced lysine formation, the mutation N21D was introduced into the wildtype sequence. *C. glutamicum* cells, expressing LysC-N21D accumulated 16-fold more L-lysine in the culture supernatant than cells expressing LysC-WT under same conditions. When N21D is combined with T311I, a known mutation in the regulatory domain conferring feedback resistance (Ohnishi et al., 2002), product accumulation exceeds both single mutants. The surprising fact, why the single mutation N21D causes increased lysine formation, is not known. The identification of productive mutations in the catalytic domain, whose positive influence on product formation was not expected by

structural knowledge of the enzyme, underlines the advantage of undirected approaches in combination with HT-*in-vivo* screening systems.

Productive mutants of ATP phosphoribosyl transferase

The *hisG*-encoded ATP phosphoribosyl transferase controls histidine biosynthesis in *C. glutamicum* and is feedback inhibited by L-histidine (Mizukami et al., 1994). The crystal structure of *M. tuberculosis* HisG in complex with histidine is known (Cho et al., 2003). This enabled homology modeling of *C. glutamicum* HisG by SWISS-MODEL (Arnold et al., 2006) and assignment of residues, which may interact with histidine. Based on that, seven residues were selected for saturation by degenerate NNK codons, and five libraries were constructed with two of them covering two codons in parallel. By NNK saturation, all 20 amino acids are represented in 32 different codons, resulting in a library size of 1024 unique clones, when two codons are saturated in parallel. Those HisG-variants, causing strongest histidine accumulation, were isolated from the double-saturation library GT233 (Schendzielorz et al., 2013, Table 3). Another site, N216, has been proven to be relevant for enhanced histidine formation. Possibly, triple-saturation libraries including all three residues would gain access to even better performing HisG-variants. This library would contain nearly 33,000 clones, emphasizing the need for HT-screening techniques once more.

Crystal structure of LysG

Only a limited number of full-length LTTR structures is available and no structure of a full-length LTTR co-crystallized with its effector is reported so far, leaving structural mechanisms of effector-induced transcription initiation a matter of speculation. LysG was successfully crystallized without ligand and co-crystallized with L-arginine, L-histidine and L-lysine. Structural models were generated for LysG without ligand and LysG-Arg, since only in these cases sufficient electron density maps could be obtained (Schendzielorz and Syberg, 2013, Table 1).

The structural model of LysG conforms largely to known models for other LTTRs (Monferrer et al., 2010; Muraoka et al., 2003; Ruangprasert et al., 2010; Sainsbury et al., 2009; Taylor et al., 2012; Zhou et al., 2010), with an N-terminal DNA-binding domain (DBD), an α-helical linker (LH) and two C-terminal effector-binding domains (EBD-I, EBD-II) (Schendzielorz and Syberg, 2013, Figure 2). Four LysG molecules are present in the unit-cell, forming homodimers, while in each dimer two different forms of the protomer, a compact one and an extended one, are found (Schendzielorz and Syberg, 2013, Figure 2). Two dimers align to a tetramer (dimer of dimers), which was also observed for CbnR (Muraoka et al., 2003), ArgP (Zhou et al., 2010) and TsaR (Monferrer et al., 2010). Gelchromatography experiments with native LysG indicate, that a tetrameric assembly is also present in solution (Binder et al., 2012, Figure S1).

All four DBDs are exposed on one side of the tetramer, thereby facilitating their binding to the DNA. According to the current model, LTTRs bind via both homodimers at two distinct sites in the target promoter, the regulatory binding site (RBS), located at -35 to +20 bp, and the activation binding site (ABS), located -40 to -20 bp (Leveau et al., 1994; McFall et al., 1997, 1998; Ogawa et al., 1999; Wang and Winans, 1995a, 1995b; Wang et al., 1992). It is proposed, that in the un-induced state one dimer binds tightly to the RBS, while the second dimer binds loosely to the ABS. Interaction with an effector might result in enhanced binding of the second dimer to the ABS (Monferrer et al., 2010; Tropel and Meer, 2004) and exposition of interfaces for RNAP interaction, thereby activating transcription (Zhou et al., 2010). This model implies effector-induced structural changes of the dimeric or tetrameric LTTR-structure (Choi et al., 2001; Ezezika et al., 2007).

First insights into LTTR-effector interaction on the structural level were obtained with truncated versions of BenM and CatM of *Acinetobacter baylyi* (Ezezika et al., 2007). The effector domains of BenM and CatM were crystallized and soaked with the effectors benzoate and muconate. Both effectors were found to bind in a region between EBD-I and EBD-II, which was predicted as inducer binding cleft (IBC) (Akakura and Winans, 2002; Dangel et al., 2005; Lochowska et al., 2001; Schell, 1993; Smirnova et al., 2004; Stec et al., 2006; Tyrrell et al., 1997). Because the EBDs were crystallized without LH and DBD, influences of effector-induced EBD-reorientation on the full-length structure or subsequently on dimer and tetramer assembly remained still speculative.

Recently, crystals of TsaR were soaked with high concentrations of its effector *p*-toluenesulfonate (TSA) (Monferrer et al., 2010). Collected datasets revealed 11 TSA molecules in the asymmetric unit, thus 22 TSA molecules in the tetramer. Two of them are located in the assumed IBC of both, the closed and extended protomers, whose structure and orientation was not different from the effector-free ones. Thus, conclusions about structural outcomes of effector-binding and consequences on higher structural level were difficult to draw.

In the model of co-crystallized LysG-Arg, arginine does also bind in the proposed IBC between EBD-I and EBD-II (Schendzielorz and Syberg, 2013, Figure 10). Two arginine molecules were discovered in the tetramer, one of them in each IBC of the extended protomers. Arginine is mainly coordinated by negatively charged side chains of neighboring residues. By this it seems possible, that similar interactions will also coordinate lysine and histidine as effectors, which are proven to induce LysG-mediated transcriptional activation by physiological experiments (Bellmann et al., 2001; Vrljic et al., 1996).

Structural differences between the models for LysG and LysG-Arg are visible. In the arginine bound form, the side chains of two residues in the EBD, Asp124 and Glu125, are rotated to point towards the IBC, thereby coordinating the amide group of L-arginine. This results in tilting of α-helix 6, the second helix of the regulatory domain, by 8° (Schendzielorz and Syberg, 2013, Figure 8). The tilt opens up a possible interaction interface between α-helix 6 of the arginine-containing extended protomer and the HTH motif of the compact protomer. This enables a possible connection of effector interaction with the C-terminal part of LysG and structural changes in the N-terminal HTH-motif, which binds to the DNA. In fact, reorientation of the HTH-motif is not visible in our model for co-crystallized LysG-Arg. This could be explained by the absence of DNA in our model, which might be necessary for native orientation of DBDs, since DNA is an essential part of the higher-order complex, involved in the transcription initiation process. Co-crystallization of LysG with arginine and DNA would be an option to prove that. Moreover, crystallization conditions could influence the structure and result in non-native conformations of the DBD. Structural analysis of LysG-Arg in solution, for example by NMR, would avoid these effects.

These results do not support former models by Ezezika et al. and Monferrer et al., which propose effector-induced modulation of tetramer packing and subsequent changes in DBD distances. Instead, the now identified tilt of α-helix 6 might represent an information pathway to transmit presence or absence of effector at the EBD to the DBD.

References

Adrio, J.-L., and Demain, A.L. (2010). Recombinant organisms for production of industrial products. Bioeng Bugs *1*, 116–131.

Akakura, R., and Winans, S.C. (2002). Constitutive mutations of the OccR regulatory protein affect DNA bending in response to metabolites released from plant tumors. J Biol Chem *277*, 5866–5874.

Allen, M.S., Wilgus, J.R., Chewning, C.S., Sayler, G.S., and Simpson, M.L. (2007). A destabilized bacterial luciferase for dynamic gene expression studies. Syst Synth Biol *1*, 3–9.

An, G.H., Bielich, J., Auerbach, R., and Johnson, E.A. (1991). Isolation and characterization of carotenoid hyperproducing mutants of yeast by flow cytometry and cell sorting. Biotechnol. N *9*, 70–73.

Andersen, J.B., Sternberg, C., Poulsen, L.K., Bjorn, S.P., Givskov, M., and Molin, S. (1998). New unstable variants of green fluorescent protein for studies of transient gene expression in bacteria. Appl Env. Microbiol *64*, 2240–2246.

Aravind, L., Anantharaman, V., Balaji, S., Babu, M.M., and Iyer, L.M. (2005). The many faces of the helix-turn-helix domain: transcription regulation and beyond. FEMS Microbiol Rev *29*, 231–262.

Arnold, K., Bordoli, L., Kopp, J., and Schwede, T. (2006). The SWISS-MODEL workspace: a web-based environment for protein structure homology modelling. Bioinformatics *22*, 195–201.

Azuma, T., Harrison, G.I., and Demain, A.L. (1992). Isolation of a gramicidin S hyperproducing strain of Bacillus brevis by use of a fluorescence activated cell sorting system. Appl Microbiol Biotechnol *38*, 173–178.

Baumgart, M., Unthan, S., Rückert, C., Sivalingam, J., Grünberger, A., Kalinowski, J., Bott, M., Noack, S., and Frunzke, J. (2013). Construction of a Prophage-Free Variant of Corynebacterium glutamicum ATCC 13032 for Use as a Platform Strain for Basic Research and Industrial Biotechnology. Appl. Environ. Microbiol. *79*, 6006–6015.

Becker, J., and Wittmann, C. (2012). Bio-based production of chemicals, materials and fuels - Corynebacterium glutamicum as versatile cell factory. Curr Opin Biotechnol *23*, 631–640.

Becker, J., Zelder, O., Häfner, S., Schröder, H., and Wittmann, C. (2011). From zero to hero–Design-based systems metabolic engineering of Corynebacterium glutamicum for l-lysine production. Metab. Eng. *13*, 159–168.

Becker, S., Schmoldt, H.-U., Adams, T.M., Wilhelm, S., and Kolmar, H. (2004). Ultra-high-throughput screening based on cell-surface display and fluorescence-activated cell sorting for the identification of novel biocatalysts. Curr Opin Biotechnol *15*, 323–329.

Bellmann, A., Vrljic, M., Pátek, M., Sahm, H., Krämer, R., and Eggeling, L. (2001). Expression control and specificity of the basic amino acid exporter LysE of Corynebacterium glutamicum. Microbiology *147*, 1765–1774.

Benenson, Y. (2012). Synthetic biology with RNA: progress report. Curr Opin Chem Biol *16*, 278–284.

Binder, S., Schendzielorz, G., Stäbler, N., Krumbach, K., Hoffmann, K., Bott, M., and Eggeling, L. (2012). A high-throughput approach to identify genomic variants of bacterial metabolite producers at the single-cell level. Genome Biol *13*, R40.

Blokpoel, M.C.J., O'Toole, R., Smeulders, M.J., and Williams, H.D. (2003). Development and application of unstable GFP variants to kinetic studies of mycobacterial gene expression. J Microbiol Methods *54*, 203–211.

Brennan, R.G., and Matthews, B.W. (1989). The helix-turn-helix DNA binding motif. J Biol Chem *264*, 1903–1906.

Brune, I., Jochmann, N., Brinkrolf, K., Hüser, A.T., Gerstmeir, R., Eikmanns, B.J., Kalinowski, J., Pühler, A., and Tauch, A. (2007). The IclR-type transcriptional repressor LtbR regulates the expression of leucine and tryptophan biosynthesis genes in the amino acid producer Corynebacterium glutamicum. J Bacteriol *189*, 2720–2733.

Celis, R.T. (1999). Repression and activation of arginine transport genes in Escherichia coli K 12 by the ArgP protein. J Mol Biol *294*, 1087–1095.

Chen, Z., Meyer, W., Rappert, S., Sun, J., and Zeng, A.-P. (2011). Coevolutionary analysis enabled rational deregulation of allosteric enzyme inhibition in Corynebacterium glutamicum for lysine production. Appl Env. Microbiol *77*, 4352–4360.

Cho, E.J., Lee, J.-W., and Ellington, A.D. (2009). Applications of aptamers as sensors. Annu. Rev. Anal. Chem. *2*, 241–264.

Cho, Y., Sharma, V., and Sacchettini, J.C. (2003). Crystal structure of ATP phosphoribosyltransferase from Mycobacterium tuberculosis. J Biol Chem *278*, 8333–8339.

Choi, H., Kim, S., Mukhopadhyay, P., Cho, S., Woo, J., Storz, G., and Ryu, S.E. (2001). Structural basis of the redox switch in the OxyR transcription factor. Cell *105*, 103–113.

Collins, C.H., Leadbetter, J.R., and Arnold, F.H. (2006). Dual selection enhances the signaling specificity of a variant of the quorum-sensing transcriptional activator LuxR. Nat Biotechnol *24*, 708–712.

Curran, K.A., Leavitt, J.M., Karim, A.S., and Alper, H.S. (2013). Metabolic engineering of muconic acid production in Saccharomyces cerevisiae. Metab Eng *15*, 55–66.

Dangel, A.W., Gibson, J.L., Janssen, A.P., and Tabita, F.R. (2005). Residues that influence in vivo and in vitro CbbR function in Rhodobacter sphaeroides and identification of a specific region critical for co-inducer recognition. Mol Microbiol *57*, 1397–1414.

Desai, S.K., and Gallivan, J.P. (2004). Genetic screens and selections for small molecules based on a synthetic riboswitch that activates protein translation. J Am Chem Soc *126*, 13247–13254.

Diesveld, R., Tietze, N., Fürst, O., Reth, A., Bathe, B., Sahm, H., and Eggeling, L. (2008). Activity of exporters of Escherichia coli in Corynebacterium glutamicum, and their use to increase L-threonine production. J Mol Microbiol Biotechnol *16*, 198–207.

Dietrich, J.A., McKee, A.E., and Keasling, J.D. (2010). High-throughput metabolic engineering: advances in small-molecule screening and selection. Annu Rev Biochem *79*, 563–590.

Dietrich, J.A., Shis, D.L., Alikhani, A., and Keasling, J.D. (2013). Transcription factor-based screens and synthetic selections for microbial small-molecule biosynthesis. ACS Synth Biol *2*, 47–58.

Drepper, T., Huber, R., Heck, A., Circolone, F., Hillmer, A.-K., Büchs, J., and Jaeger, K.-E. (2010). Flavin mononucleotide-based fluorescent reporter proteins outperform green fluorescent protein-like proteins as quantitative in vivo real-time reporters. Appl Env. Microbiol *76*, 5990–5994.

Eggeling, L., and Bott, M. (2005). Handbook of Corynebacterium glutamicum. CRC 490 Press (Taylor & Francis Group, Boca Raton, Florida, USA).

Eggeling, L., Pfefferle, W., and Sahm, H. (2006). Amino Acids, in Basic Biotechnology (Cambridge: Cambridge University Press).

Ellington, A.D., and Szostak, J.W. (1990). In vitro selection of RNA molecules that bind specific ligands. Nature *346*, 818–822.

Ezezika, O.C., Haddad, S., Clark, T.J., Neidle, E.L., and Momany, C. (2007). Distinct effector-binding sites enable synergistic transcriptional activation by BenM, a LysR-type regulator. J Mol Biol *367*, 616–629.

Fiet, S. van S., Beilen, J.B. van, and Witholt, B. (2006). Selection of biocatalysts for chemical synthesis. Proc Natl Acad Sci U S *103*, 1693–1698.

Fouchet, P., Jan, S., Courtois, J., Courtois, B., Frelat, G., and Barbotin, J.. (1995). Quantitative single-cell detection of poly(β-hydroxybutyrate) accumulation in Rhizobium meliloti by flow cytometry. FEMS Microbiol. Lett. *126*, 31–35.

Gouveia, L., Marques, A.E., Silva, T.L. da, and Reis, A. (2009). Neochloris oleabundans UTEX 1185: a suitable renewable lipid source for biofuel production. J Ind Microbiol Biotechnol *36*, 821–826.

Gu, M.B., Mitchell, R.J., and Kim, B.C. (2004). Whole-cell-based biosensors for environmental biomonitoring and application. Adv Biochem Eng Biotechnol *87*, 269–305.

Hentschel, E., Will, C., Mustafi, N., Burkovski, A., Rehm, N., and Frunzke, J. (2013). Destabilized eYFP variants for dynamic gene expression studies in Corynebacterium glutamicum. Microb Biotechnol *6*, 196–201.

Hermann, T., and Patel, D.J. (2000). Adaptive recognition by nucleic acid aptamers. Science *287*, 820–825.

Huffman, J.L., and Brennan, R.G. (2002). Prokaryotic transcription regulators: more than just the helix-turn-helix motif. Curr Opin Struct Biol *12*, 98–106.

Ikeda, M., Mitsuhashi, S., Tanaka, K., and Hayashi, M. (2009). Reengineering of a Corynebacterium glutamicum L-arginine and L-citrulline producer. Appl Env. Microbiol *75*, 1635–1641.

Jetten, M.S., Follettie, M.T., and Sinskey, A.J. (1995). Effect of different levels of aspartokinase on the lysine production by Corynebacterium lactofermentum. Appl Microbiol Biotechnol *43*, 76–82.

Kennerknecht, N., Sahm, H., Yen, M.-R., Pátek, M., Jr, M.H.S., and Eggeling, L. (2002). Export of L-isoleucine from Corynebacterium glutamicum: a two-gene-encoded member of a new translocator family. J Bacteriol *184*, 3947–3956.

Kensy, F., Zang, E., Faulhammer, C., Tan, R.-K., and Büchs, J. (2009). Validation of a high-throughput fermentation system based on online monitoring of biomass and fluorescence in continuously shaken microtiter plates. Microb Cell Fact *8*, 31.

Keulen, G. van, Girbal, L., Bergh, E.R. van den, Dijkhuizen, L., and Meijer, W.G. (1998). The LysR-type transcriptional regulator CbbR controlling autotrophic CO2 fixation by Xanthobacter flavus is an NADPH sensor. J Bacteriol *180*, 1411–1417.

Kinoshita, S., Nakayama, K., and Kitada, S. (1958). L-lysine production using microbial auxotroph. J. Gen. Appl. Microbiol. *4*, 128–129.

Kruse, D., Krämer, R., Eggeling, L., Rieping, M., Pfefferle, W., Tchieu, J.H., Chung, Y.J., Saier, M.H.J., and Burkovski, A. (2002). Influence of threonine exporters on threonine production in Escherichia coli. Appl Microbiol Biotechnol *59*, 205–210.

Kulis-Horn, R.K., Persicke, M., and Kalinowski, J. (2013). Histidine biosynthesis, its regulation and biotechnological application in Corynebacterium glutamicum. Microb. Biotechnol. *Article first published online: 25 APR 2013*.

Kumar, M.D.P.D.; K.R.S.P.D.; C.S.R. (2012). Analysis of the Central and Eastern European Animal Feed Additives Market. Value-Added Feed Ingredients Drive Market Growth (331 E. Evelyn Ave. Suite 100 Mountain View, CA 94041: Frost & Sullivan).

Laishram, R.S., and Gowrishankar, J. (2007). Environmental regulation operating at the promoter clearance step of bacterial transcription. Genes Dev *21*, 1258–1272.

Lee, K.H., Park, J.H., Kim, T.Y., Kim, H.U., and Lee, S.Y. (2007). Systems metabolic engineering of Escherichia coli for L-threonine production. Mol Syst Biol *3*, 149.

Leveau, J.H., Vos, W.M. de, and Meer, J.R. van der (1994). Analysis of the binding site of the LysR-type transcriptional activator TcbR on the tcbR and tcbC divergent promoter sequences. J Bacteriol *176*, 1850–1856.

Liang, J.C., Bloom, R.J., and Smolke, C.D. (2011). Engineering biological systems with synthetic RNA molecules. Mol Cell *43*, 915–926.

Liang, J.C., Chang, A.L., Kennedy, A.B., and Smolke, C.D. (2012). A high-throughput, quantitative cell-based screen for efficient tailoring of RNA device activity. Nucleic Acids Res. *40*, e154.

Livshits, V.A., Zakataeva, N.P., Aleshin, V.V., and Vitushkina, M.V. (2003). Identification and characterization of the new gene rhtA involved in threonine and homoserine efflux in Escherichia coli. Res. Microbiol. *154*, 123–135.

Lochowska, A., Iwanicka-Nowicka, R., Plochocka, D., and Hryniewicz, M.M. (2001). Functional dissection of the LysR-type CysB transcriptional regulator. Regions important for DNA binding, inducer response, oligomerization, and positive control. J Biol Chem *276*, 2098–2107.

Marbaniang, C.N., and Gowrishankar, J. (2012). Transcriptional cross-regulation between Gram-negative and gram-positive bacteria, demonstrated using ArgP-argO of Escherichia coli and LysG-lysE of Corynebacterium glutamicum. J Bacteriol *194*, 5657–5666.

Marienhagen, J., and Bott, M. (2013). Metabolic engineering of microorganisms for the synthesis of plant natural products. J Biotechnol *163*, 166–178.

McFall, S.M., Klem, T.J., Fujita, N., Ishihama, A., and Chakrabarty, A.M. (1997). DNase I footprinting, DNA bending and in vitro transcription analyses of ClcR and CatR interactions with the clcABD promoter: evidence of a conserved transcriptional activation mechanism. Mol. Microbiol. *24*, 965–976.

McFall, S.M., Chugani, S.A., and Chakrabarty, A.M. (1998). Transcriptional activation of the catechol and chlorocatechol operons: variations on a theme. Gene *223*, 257–267.

Michener, J.K., and Smolke, C.D. (2012). High-throughput enzyme evolution in Saccharomyces cerevisiae using a synthetic RNA switch. Metab Eng *14*, 306–316.

Mizukami, T., Hamu, A., Ikeda, M., Oka, T., and Katsumata, R. (1994). Cloning of the ATP phosphoribosyl transferase gene of Corynebacterium glutamicum and application of the gene to L-histidine production. Biosci Biotechnol Biochem *58*, 635–638.

Monferrer, D., Tralau, T., Kertesz, M.A., Dix, I., Solà, M., and Usón, I. (2010). Structural studies on the full-length LysR-type regulator TsaR from Comamonas testosteroni T-2 reveal a novel open conformation of the tetrameric LTTR fold. Mol Microbiol *75*, 1199–1214.

Muraoka, S., Okumura, R., Ogawa, N., Nonaka, T., Miyashita, K., and Senda, T. (2003). Crystal structure of a full-length LysR-type transcriptional regulator, CbnR: unusual combination of two subunit forms and molecular bases for causing and changing DNA bend. J Mol Biol *328*, 555–566.

Mustafi, N., Grünberger, A., Kohlheyer, D., Bott, M., and Frunzke, J. (2012). The development and application of a single-cell biosensor for the detection of l-methionine and branched-chain amino acids. Metab Eng *14*, 449–457.

Nandineni, M.R., and Gowrishankar, J. (2004). Evidence for an arginine exporter encoded by yggA (argO) that is regulated by the LysR-type transcriptional regulator ArgP in Escherichia coli. J Bacteriol *186*, 3539–3546.

Nomura, Y., and Yokobayashi, Y. (2007). Reengineering a natural riboswitch by dual genetic selection. J Am Chem Soc *129*, 13814–13815.

Nonomura, A., and Coder, D. (1988). Improved Phycocatalysis of Carotene Production by Flow Cytometry and Cell Sorting. Biocatal. Biotransformation *1*, 333–338.

Ogawa, N., McFall, S.M., Klem, T.J., Miyashita, K., and Chakrabarty, A.M. (1999). Transcriptional activation of the chlorocatechol degradative genes of Ralstonia eutropha NH9. J Bacteriol *181*, 6697–6705.

Ohnishi, J., Mitsuhashi, S., Hayashi, M., Ando, S., Yokoi, H., Ochiai, K., and Ikeda, M. (2002). A novel methodology employing Corynebacterium glutamicum genome information to generate a new L-lysine-producing mutant. Appl Microbiol Biotechnol *58*, 217–223.

Paige, J.S., Wu, K.Y., and Jaffrey, S.R. (2011). RNA mimics of green fluorescent protein. Science *333*, 642–646.

Paige, J.S., Nguyen-Duc, T., Song, W., and Jaffrey, S.R. (2012). Fluorescence imaging of cellular metabolites with RNA. Science *335*, 1194.

Palmieri, L., Berns, D., Krämer, R., and Eikmanns, M. (1996). Threonine diffusion and threonine transport in Corynebacterium glutamicum and their role in threonine production. Arch. Microbiol. *165*, 48–54.

Pátek, M., Muth, G., and Wohlleben, W. (2003). Function of Corynebacterium glutamicum promoters in Escherichia coli, Streptomyces lividans, and Bacillus subtilis. J Biotechnol *104*, 325–334.

Peeters, E., Minh, P.N.L., Foulquié-Moreno, M., and Charlier, D. (2009). Competitive activation of the Escherichia coli argO gene coding for an arginine exporter by the transcriptional regulators Lrp and ArgP. Mol Microbiol *74*, 1513–1526.

Picossi, S., Belitsky, B.R., and Sonenshein, A.L. (2007). Molecular mechanism of the regulation of Bacillus subtilis gltAB expression by GltC. J Mol Biol *365*, 1298–1313.

Ramón-Maiques, S., Fernández-Murga, M.L., Gil-Ortiz, F., Vagin, A., Fita, I., and Rubio, V. (2006). Structural bases of feed-back control of arginine biosynthesis, revealed by the structures of two hexameric N-acetylglutamate kinases, from Thermotoga maritima and Pseudomonas aeruginosa. J Mol Biol *356*, 695–713.

Raser, J.M., and O'Shea, E.K. (2004). Control of stochasticity in eukaryotic gene expression. Science *304*, 1811–1814.

Ruangprasert, A., Craven, S.H., Neidle, E.L., and Momany, C. (2010). Full-length structures of BenM and two variants reveal different oligomerization schemes for LysR-type transcriptional regulators. J Mol Biol *404*, 568–586.

Saier, M.H. (2000). Families of transmembrane transporters selective for amino acids and their derivatives. Microbiology *146 (Pt 8)*, 1775–1795.

Sainsbury, S., Lane, L.A., Ren, J., Gilbert, R.J., Saunders, N.J., Robinson, C.V., Stuart, D.I., and Owens, R.J. (2009). The structure of CrgA from Neisseria meningitidis reveals a new octameric assembly state for LysR transcriptional regulators. Nucleic Acids Res *37*, 4545–4558.

Schell, M.A. (1993). Molecular biology of the LysR family of transcriptional regulators. Annu Rev Microbiol *47*, 597–626.

Schendzielorz, G., Dippong, M., Grünberger, A., Kohlheyer, D., Yoshida, A., Binder, S., Nishiyama, C., Nishiyama, M., Bott, M., and Eggeling, L. (2013). Taking Control over Control: Use of Product Sensing in Single Cells to Remove Flux Control at Key Enzymes in Biosynthesis Pathways. ACS Synth Biol *Publication Date (Web): July 5, 2013*.

Schröder, J., Maus, I., Ostermann, A.L., Kögler, A.C., and Tauch, A. (2012). Binding of the IclR-type regulator HutR in the histidine utilization (hut) gene cluster of the human pathogen Corynebacterium resistens DSM 45100. FEMS Microbiol. Lett. *331*, 136–143.

Shaner, N.C., Steinbach, P.A., and Tsien, R.Y. (2005). A guide to choosing fluorescent proteins. Nat Methods *2*, 905–909.

Shiio, I., and Miyajima, R. (1969). Concerted inhibition and its reversal by end products of aspartate kinase in Brevibacterium flavum. J Biochem *65*, 849–859.

Shiio, I., Miyajima, R., and Sano, K. (1970). Genetically desensitized aspartate kinase to the concerted feedback inhibition in Brevibacterium flavum. J Biochem *68*, 701–710.

Silva, T.L. da, Reis, A., Medeiros, R., Oliveira, A.C., and Gouveia, L. (2009). Oil production towards biofuel from autotrophic microalgae semicontinuous cultivations monitorized by flow cytometry. Appl Biochem Biotechnol *159*, 568–578.

Simic, P., Sahm, H., and Eggeling, L. (2001). L-threonine export: use of peptides to identify a new translocator from Corynebacterium glutamicum. J Bacteriol *183*, 5317–5324.

Smirnova, I.A., Dian, C., Leonard, G.A., McSweeney, S., Birse, D., and Brzezinski, P. (2004). Development of a bacterial biosensor for nitrotoluenes: the crystal structure of the transcriptional regulator DntR. J Mol Biol *340*, 405–418.

Stec, E., Witkowska-Zimny, M., Hryniewicz, M.M., Neumann, P., Wilkinson, A.J., Brzozowski, A.M., Verma, C.S., Zaim, J., Wysocki, S., and Bujacz, G.D. (2006). Structural basis of the sulphate starvation response in E. coli: crystal structure and mutational analysis of the cofactor-binding domain of the Cbl transcriptional regulator. J Mol Biol *364*, 309–322.

Stoltenburg, R., Reinemann, C., and Strehlitz, B. (2007). SELEX–a (r)evolutionary method to generate high-affinity nucleic acid ligands. Biomol Eng *24*, 381–403.

Stolz, M., Peters-Wendisch, P., Etterich, H., Gerharz, T., Faurie, R., Sahm, H., Fersterra, H., and Eggeling, L. (2007). Reduced folate supply as a key to enhanced L-serine production by Corynebacterium glutamicum. Appl Env. Microbiol *73*, 750–755.

Suess, B., Fink, B., Berens, C., Stentz, R., and Hillen, W. (2004). A theophylline responsive riboswitch based on helix slipping controls gene expression in vivo. Nucleic Acids Res *32*, 1610–1614.

Tang, M. (2008). The mean and noise of stochastic gene transcription. J Theor Biol *253*, 271–280.

Tang, S.-Y., and Cirino, P.C. (2011). Design and Application of a Mevalonate-Responsive Regulatory Protein. Angew. Chem. Int. Ed. *50*, 1084–1086.

Tang, S.-Y., Qian, S., Akinterinwa, O., Frei, C.S., Gredell, J.A., and Cirino, P.C. (2013). Screening for Enhanced Triacetic Acid Lactone Production by Recombinant Escherichia coli Expressing a Designed Triacetic Acid Lactone Reporter. J. Am. Chem. Soc. *135*, 10099–10103.

Tavori, H., Kimmel, Y., and Barak, Z. (1981). Toxicity of leucine-containing peptides in Escherichia coli caused by circumvention of leucine transport regulation. J Bacteriol *146*, 676–683.

Taylor, J.L., Silva, R.S.D., Kovacikova, G., Lin, W., Taylor, R.K., Skorupski, K., and Kull, F.J. (2012). The crystal structure of AphB, a virulence gene activator from Vibrio cholerae, reveals residues that influence its response to oxygen and pH. Mol Microbiol *83*, 457–470.

Thierbach, G., Kalinowski, J., Bachmann, B., and Pühler, A. (1990). Cloning of a DNA fragment fromCorynebacterium glutamicum conferring aminoethyl cysteine resistance and feedback resistance to aspartokinase. Appl. Microbiol. Biotechnol. *32*, 443–448.

Tombolini, R., Unge, A., Davey, M.E., de Bruijn, F.J., and Jansson, J.K. (1997). Flow cytometric and microscopic analysis of GFP-tagged Pseudomonas fluorescens bacteria. FEMS Microbiol. Ecol. *22*, 17–28.

Triccas, J.A., Pinto, R., and Britton, W.J. (2002). Destabilized green fluorescent protein for monitoring transient changes in mycobacterial gene expression. Res Microbiol *153*, 379–383.

Tropel, D., and Meer, J.R. van der (2004). Bacterial transcriptional regulators for degradation pathways of aromatic compounds. Microbiol Mol Biol Rev *68*, 474–500, table of contents.

Trötschel, C., Deutenberg, D., Bathe, B., Burkovski, A., and Krämer, R. (2005). Characterization of methionine export in Corynebacterium glutamicum. J Bacteriol *187*, 3786–3794.

Tsien, R.Y. (1998). The green fluorescent protein. Annu Rev Biochem *67*, 509–544.

Tsyrenzhapova, I.S., Doroshenko, V.G., Aĭrikh, L.G., Mironov, A.S., and Mashko, S.V. (2009). [Gene yddG of Escherichia coli encoding the putative exporter of aromatic amino acids: constitutive transcription and dependence of the expression level on the cell growth rate]. Genetika *45*, 601–609.

Tuerk, C., and Gold, L. (1990). Systematic evolution of ligands by exponential enrichment: RNA ligands to bacteriophage T4 DNA polymerase. Science *249*, 505–510.

Tyrrell, R., Verschueren, K.H., Dodson, E.J., Murshudov, G.N., Addy, C., and Wilkinson, A.J. (1997). The structure of the cofactor-binding fragment of the LysR family member, CysB: a familiar fold with a surprising subunit arrangement. Structure *5*, 1017–1032.

Uchiyama, T., and Miyazaki, K. (2010). Product-induced gene expression, a product-responsive reporter assay used to screen metagenomic libraries for enzyme-encoding genes. Appl Env. Microbiol *76*, 7029–7035.

Ukibe, K., Katsuragi, T., Tani, Y., and Takagi, H. (2008). Efficient screening for astaxanthin-overproducing mutants of the yeast Xanthophyllomyces dendrorhous by flow cytometry. FEMS Microbiol Lett *286*, 241–248.

Vitreschak, A.G., Rodionov, D.A., Mironov, A.A., and Gelfand, M.S. (2004). Riboswitches: the oldest mechanism for the regulation of gene expression? Trends Genet *20*, 44–50.

Vrljic, M., Sahm, H., and Eggeling, L. (1996). A new type of transporter with a new type of cellular function: L-lysine export from Corynebacterium glutamicum. Mol Microbiol *22*, 815–826.

Wang, L., and Winans, S.C. (1995a). High angle and ligand-induced low angle DNA bends incited by OccR lie in the same plane with OccR bound to the interior angle. J Mol Biol *253*, 32–38.

Wang, L., and Winans, S.C. (1995b). The sixty nucleotide OccR operator contains a subsite essential and sufficient for OccR binding and a second subsite required for ligand-responsive DNA bending. J Mol Biol *253*, 691–702.

Wang, L., Helmann, J.D., and Winans, S.C. (1992). The A. tumefaciens transcriptional activator OccR causes a bend at a target promoter, which is partially relaxed by a plant tumor metabolite. Cell *69*, 659 – 667.

Weigand, J.E., and Suess, B. (2007). Tetracycline aptamer-controlled regulation of pre-mRNA splicing in yeast. Nucleic Acids Res *35*, 4179–4185.

Win, M.N., and Smolke, C.D. (2007). A modular and extensible RNA-based gene-regulatory platform for engineering cellular function. Proc Natl Acad Sci U S *104*, 14283–14288.

Win, M.N., and Smolke, C.D. (2008). Higher-order cellular information processing with synthetic RNA devices. Science *322*, 456–460.

Xu, M., Rao, Z., Dou, W., Jin, J., and Xu, Z. (2012). Site-directed mutagenesis studies on the L-arginine-binding sites of feedback inhibition in N-acetyl-L-glutamate kinase (NAGK) from Corynebacterium glutamicum. Curr Microbiol *64*, 164–172.

Xu, Y., Labedan, B., and Glansdorff, N. (2007). Surprising arginine biosynthesis: a reappraisal of the enzymology and evolution of the pathway in microorganisms. Microbiol Mol Biol Rev *71*, 36–47.

Yoshida, A., Tomita, T., Kuzuyama, T., and Nishiyama, M. (2010). Mechanism of concerted inhibition of alpha2beta2-type hetero-oligomeric aspartate kinase from Corynebacterium glutamicum. J Biol Chem *285*, 27477–27486.

Zakataeva, N.P., Aleshin, V.V., Tokmakova, I.L., Troshin, P.V., and Livshits, V.A. (1999). The novel transmembrane Escherichia coli proteins involved in the amino acid efflux. FEBS Lett *452*, 228–232.

Zhang, X.-X., and Rainey, P.B. (2007). Genetic analysis of the histidine utilization (hut) genes in Pseudomonas fluorescens SBW25. Genetics *176*, 2165–2176.

Zhou, X., Lou, Z., Fu, S., Yang, A., Shen, H., Li, Z., Feng, Y., Bartlam, M., Wang, H., and Rao, Z. (2010). Crystal structure of ArgP from Mycobacterium tuberculosis confirms two distinct conformations of full-length LysR transcriptional regulators and reveals its function in DNA binding and transcriptional regulation. J Mol Biol *396*, 1012–1024.

Zittrich, S., and Krämer, R. (1994). Quantitative discrimination of carrier-mediated excretion of isoleucine from uptake and diffusion in Corynebacterium glutamicum. J Bacteriol *176*, 6892–6899.

Appendix

(1) Supplemental Material**:** **Schendzielorz G**, Dippong M, Grünberger A, Kohlheyer D, Yoshida A, Binder S, Nishiyama C, Nishiyama M, Bott M, Eggeling L. Taking control over control: Use of product sensing in single cells to remove flux control at key enzymes in biosynthesis pathways.

(2) Supplemental Material**:** Binder S, **Schendzielorz G**, Stäbler N, Krumbach K, Hoffmann K, Bott M, Eggeling L. A high-throughput approach to identify genomic variants of bacterial metabolite producers at the single-cell level.

(3) Supplemental Material**:** Siedler S, **Schendzielorz G**, Binder S, Eggeling L, Bringer S, Bott M. SoxR as single-cell biosensor for NADPH-consuming enzymes in *Escherichia coli*.

(4) Supplemental Material**:** Grünberger A, Paczia N, Probst C, **Schendzielorz G**, Eggeling L, Noack S, Wiechert W, Kohlheyer D. A disposable picolitre bioreactor for cultivation and investigation of industrially relevant bacteria on the single cell level.

(5) Supplemental Material**:** Grünberger A, van Ooyen J, Paczia N, Rohe P, **Schendzielorz G**, Eggeling L, Wiechert W, Noack S. Beyond growth rate 0.6: *Corynebacterium glutamicum* cultivated in highly diluted environments.

Supporting Information to

Taking control over control: Use of product sensing in single cells to remove flux control at key enzymes in biosynthesis pathways

by Schendzielorz et al.

Supplementary Video S1

Supplementary Figure S1

Exogenous-Arg-Ala-dose response (red squares) and Ala-Ala-dose response (black circles) of *C. glutamicum* carrying pSenLys-Spc.

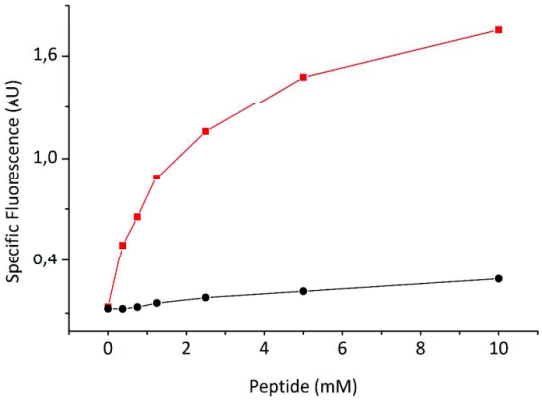

Supplementary Figure S2:
The microfluidic single cell chemostat used in this study is intended for long-term growth coupled metabolic studies. The device contains several hundred (1 µm x 1 µm x 20 µm) growth channels that allow for high-throughput single cell cultivation under environmental constant conditions. Using time-lapse-microscopy, growth coupled fluorescence studies on single cell level can be performed. In comparison to cultivation boxes, where only 8 to 9 generations can be followed (Grünberger *et al.*, 2013), here growth can be studied over many generations (here over 30) at constant conditions. During the seeding phase (Figure 1A), single cells are trapped within the channels. After a sufficient amount of cells is trapped, continuous growth is initiated by constant supply of medium of interest (Figure 1B). During the experiment cells are growing and excess cells are pushed out of the channel system which are removed with the medium flow. This procedure can be maintained for up to several days, depending on organism and experimental aim.

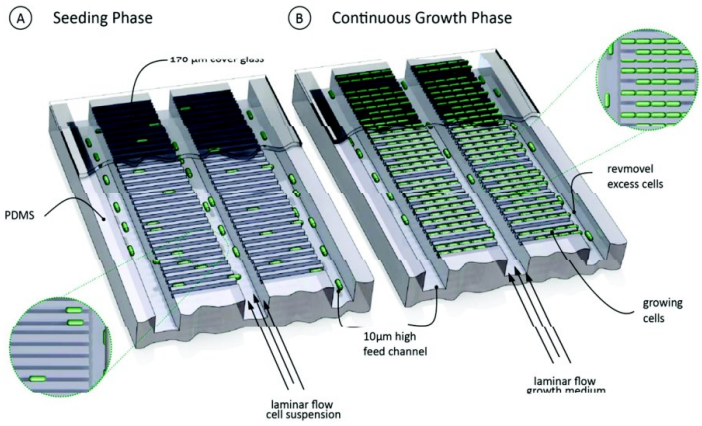

Supplementary Figure S3:
Plasmids constructed and used in this study.

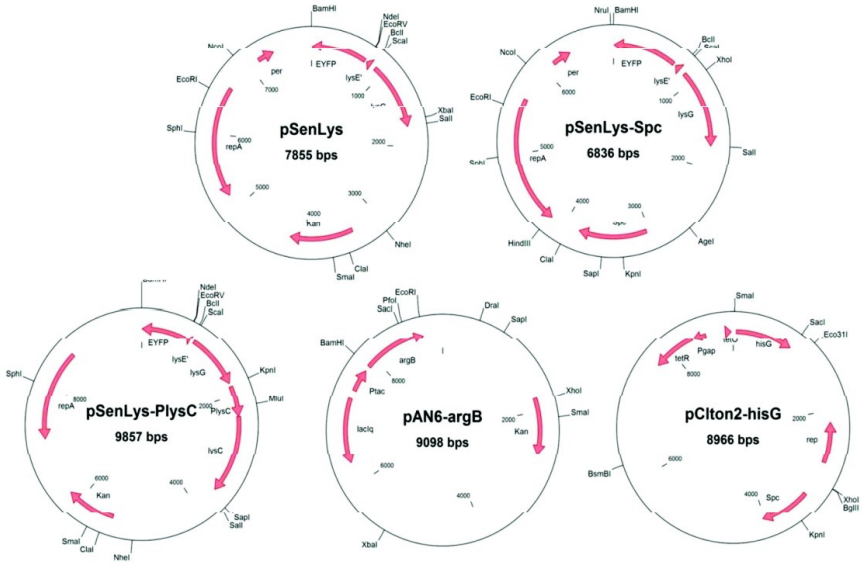

Supplementary Figure S4:

Results from isothermal titration calorimetry experiments with different ArgB proteins and L-arginine. (a) Wild-type ArgB; (b) ArgB-K47H; (c) ArgB-K47H-V65A, first peak from size exclusion chromatography (see Figure 5); (d) ArgB-K47H-V65A, second peak from size exclusion chromatography; (e) ArgB-K47H-G122T-T180P. Best fitting results for (a) and (b) were achieved with a sequential binding model and six binding sites using Origin 7G software. In case of (c), (d) and (e), no heat exchange was detectable.

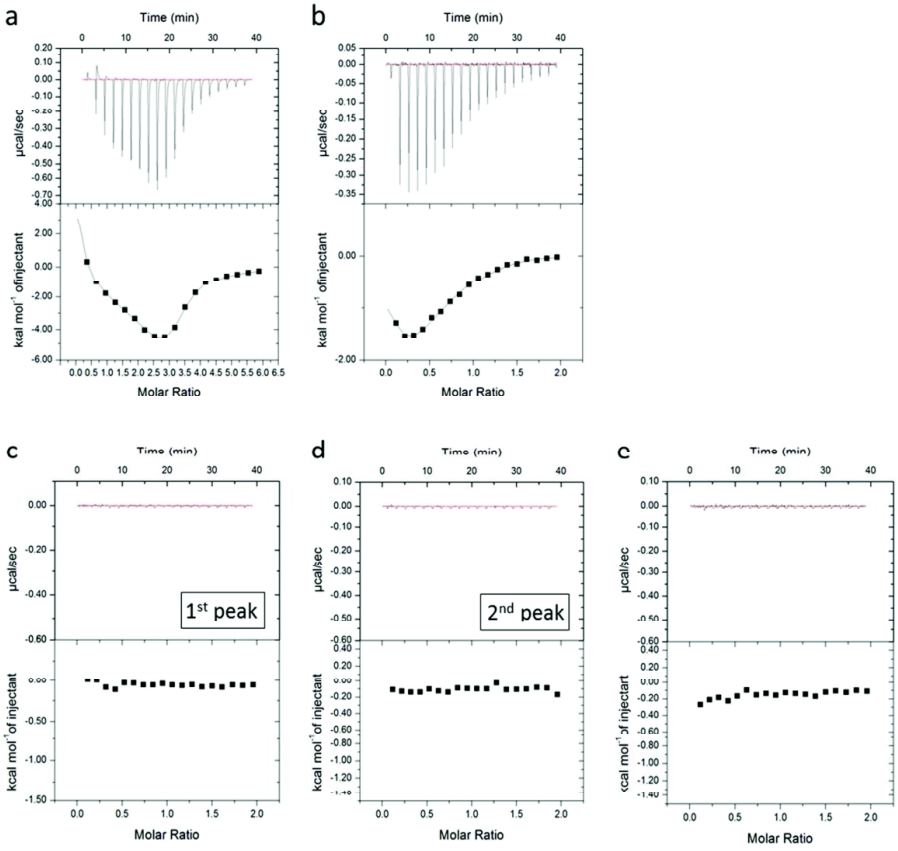

Supplementary Figure S5:

ClustalW alignment of ArgB from *C. glutamicum* (UniProt ID: A4QDZ0) with homologs of known structure such as ArgB from *M. tuberculosis* (PDB ID: 2AP9), *P. aeruginosa* (2BUF), *A. thaliana* (2RD5), and *T. maritima* (2BTY). Residues aligning with K47 from *C. glutamicum* are shaded in gray and are shown with highlighted helices αN and αA (green) as well as the β1 strand (cyan).

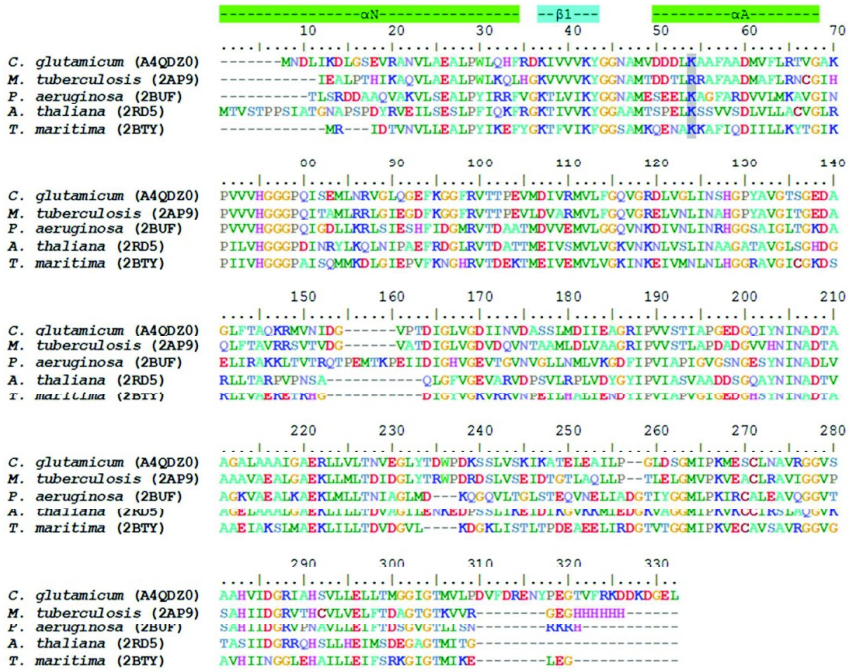

Supplementary Figure S6:

Inhibition kinetics of selected HisG and LysC muteins, obtained from activity assays with isolated protein. (a) Relative activity of HisG muteins in presence of L-histidine: black squares, wild-type enzyme; blue triangles, HisG-GT233HQ; red circles, HisG-N216I; green triangles, HisG-N216R. (b) Relative activity of LysC muteins in presence of L-lysine (plus 10 mM L-threonine): black squares, wild-type enzyme; green triangles, LysC-c88; red circles, LysC-c77; blue triangles, LysC-c90.
The sp A for the respective enzyme without allosteric regulator was as follows (in µmol min^{-1} mg^{-1}): HisG-WT=1.59±0.04; HisG-GT233HQ=0.61±0.03; HisG-N216I=1.68±0.04; HisG-N216R=1.56±0.04; LysC-WT=1.17±0.03; LysC-c88=1.40±0.03; LysC-c77=1.09±0.03; LysC-c90=2.29±0.13.

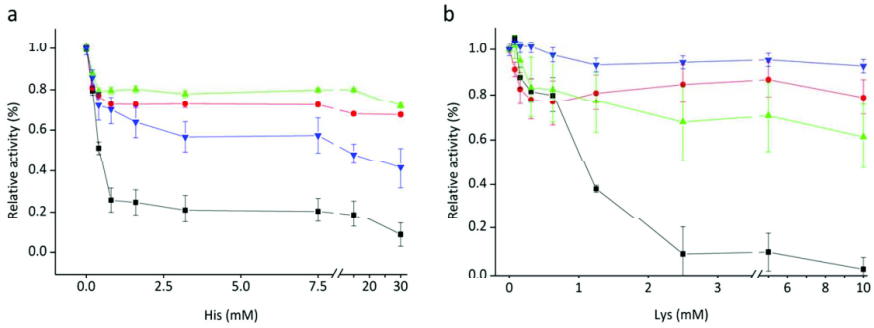

Supplementary Table S1:

Nucleotide and amino acids exchanges in the isolated ArgB muteins.

ArgB 14	ArgB 88	ArgB 79	ArgB 37	ArgB 39	ArgB 18	ArgB 59	Nucleotide exchange	Wild-type codon	Mutant codon	Mutation
x						x	a139g	aag	gag	K47E
					x		c176a	acc	aac	T59N
x							t194c	gtg	gcg	V65A
				x			a280t	acc	tcc	T94S
					x		a301g	att	gtt	I101V
	x	x					t329c	gtc	gcc	V110A
	x						g365c	ggc	gcc	G122A
				x			a430g	aac	gac	N144D
			x			x	a538g	acg	gcg	T180A
			x			x	t543c	att	atc	silent
	x						t566c	att	act	I189T
		x				x	t569g	tac	tgc	Y190C
			x			x	a591g	gca	gcg	silent
			x		x		c663t	acc	act	silent
					x		a674g	gat	ggt	D225G
x	x		x				c712t	ctg	ttg	silent
						x	t875a	gtg	gag	V292E

Supplementary Table S2:

Primer sets for site-specific saturation of *argB*.

Residue	Saturated codon	Primer	Sequence
K47	AAG139NNK	fw	CAT GGT GGA TGA TGA TCT CNN KGC TGT TTT TGC TGC CGA C
		rv	GTC GGC AGC AAA AAC AGC MNN GAG ATC ATC ATC CAC CAT G
V65	GTG193NNK	fw	GGG CGC AAA ACC ANN KGT GGT GCA CGG TGG
		rv	CCA CCG TGC ACC ACM NNT GGT TTT GCG CCC
V110	GTC328NNK	fw	GGT GCT CTT TGG TCA GNN KGG TCG CGA TTT AGT TG
		rv	CAA CTA AAT CGC GAC CMN NCT GAC CAA AGA GCA CC
G122	GGC364NNK	fw	GTT TGA TCA ACT CTC ATN NKC CTT ACG CTG TGG GAA C
		rv	GTT CCC ACA GCG TAA GGM NNA TGA GAG TTG ATC AAA C
T180	ACG538NNK	fw	CAT TCC TGT GGT CTC TNN KAT TGC TCC AGG CGA AG
		rv	CTT CGC CTG GAG CAA TMN NAG AGA CCA CAG GAA TG
I189	ATT565NNK	fw	CAG GCG AAG ACG GCC AGN NKT ACA ACA TTA ACG CCG
		rv	CGG CGT TAA TGT TGT AMN NCT GGC CGT CTT CGC CTG
Y190	TAC568NNK	fw	GCG AAG ACG GCC AGA TTN NKA ACA TTA ACG CCG ATA C
		rv	GTA TCG GCG TTA ATG TTM NNA ATC TGG CCG TCT TCG C

Supplementary Table S3:
Mutations and L-arginine accumulation in culture supernatants for clones isolated from saturation libraries. From each library, 20 cells were sorted and 4 of them were selected for detailed analysis. In the case where only one allele for one position is given all 4 selected clones were identical.

Clone	Wildtype Codon	Mutant Codon	Mutation	Arg (mM)	+/-
argB47-b5	aag	gag	K47E	1.2	0.02
argB47-c4	aag	acg	K47T	3.5	0.19
argB47-c8	aag	cat	K47H	5.5	0.24
argB65-a8	gtg	gca	V65A	4.8	0.05
argB110-e4	gtc	cgt	V110R	1.4	0.20
argB122-a5	ggc	acg	G122T	11.5	0.25
argB180-a4	acg	cct	T180P	2.1	0.08
argB189-c11	att	nd	nd	0.0	0.00
argB190-g10	tac	nd	nd	0.0	0.00

Supplementary Table S4:
Elution volume of ArgB proteins separated by a Superdex 200 10/300 GL column (GE Healthcare) and calculated molecular masses.

ArgB protein	± 10 mM L-Arginine	Elution volume (ml)	Calculated molecular masses (kDa)
WT	-	12.26	231.52
WT	+	12.30	226.75
K47H	-	12.00	265.10
K47H	+	12.52	202.20
K47H-V65A	-	11.97; 7.59	269.28; ND
K47A-V65A	+	13.35; 7.56	131.22; ND
K47H-G122T-T180P	-	7.84	ND
K47H-G122T-T180P	+	12.34	222.07
K47H-V65A-T180P	-	11.95	272.10
K47H-V65A-T180P	+	12.17	242.64

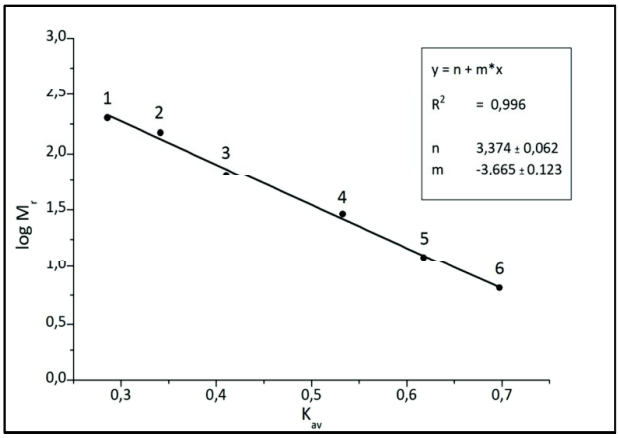

Calibration of Superdex 10/300 GL column. Semilogarithmic plot of molecular weight (M_r) against K_{av} (V_0=7.8 ml; V_t=24 ml). Protein standards: 1, 200 kDa; 2, 150 kDa; 3, 66 kDa; 4, 29 kDa; 5, 12.4 kDa; 6, 6.5 kDa.

Supplementary Table S5:

Primer sets for site-specific saturation of *hisG*.

Residue in *M. tuber.*	**Equivalent residue in *C. glut.***	**Saturated codons in Cg-HisG sequence**	**Primer**	**Sequence**
D218	N216	AAC(643)NNK	fw	CTT CCT CAT GCT GGA TTA CNN KGT CGA CCG CGA CAA CCT G
			rv	CAG GTT GTC GCG GTC GAC MNN GTA ATC CAG CAT GAG GAA G
LE234	LS231	TTATCC(691)NNKNNK	fw	CCA CTG CAG TAA CCC CAG GCN NKN NKG GCC CAA CGG TAT CCC CAC
			rv	GTG GGG ATA CCG TTG GGC CMN NMN NGC CTG GGG TTA CTG CAG TGG
SPT236	GPT233	GGCCCAACG(697)NNKCCANNK	fw	GTA ACC CCA GGC TTA TCC NNK CCA NNK GTA TCC CCA CTG GCA CG
			rv	CGT GCC AGT GGG GAT ACM NNT GGM NNG GAT AAG CCT GGG GTT AC
L253	M250	ATG(748)NNK	fw	GTT GCT GTA CGC GCC NNK GTG CCA CGC AGG TCA G
			rv	CTG ACC TGC GTG GCA CMN NGG CGC GTA CAG CAA C
A273	A270	GCC(808)NNK	fw	CTG GAC TCG GCG CTG AAN NKA TCC TGG CTT CTG AAA TC
			rv	GAT TTC AGA AGC CAG GAT MNN TTC AGC GCC GAG TCC AG

Supplementary Table S6:

Nucleotide and amino acid exchanges in isolated *lysC* alleles.

Position	Mutation	Nucleotide exchange	Wild-type codon	Mutant codon
20	R20S	a60c	aga	agc
21	N21D	a61g	aac	gac
24	E24G	a71g	gaa	gga
69	L69F	c205t	ctc	ttc
78	N78S	a233g	aac	agc
123	E123E	a369g	gaa	gag
124	A124P	g370c	gca	cca
125	L125L	c375a	ctc	cta
141	K141K	a423g	aaa	aag
159	V159G	t476g	gtt	ggt
186	I186V	a556g	atc	gtc
211	I211V	a631g	att	gtt
227	L227P	t680c	ctt	cct
235	N235D	a703g	aat	gat
278	E278G	a833g	gag	ggg
280	A280V	c839t	gcg	gtg
311	T311I	c932t	acc	atc
328	K328E	a982g	aag	gag
337	N337S	a1010g	aat	agt
341	D341N	g1021a	gac	aac
350	V350A	t1049c	gtg	gcg
365	M365K	t1094a	atg	aag
391	E391G	a1172g	gaa	gga
394	L394L	c1180t	ctg	ttg
399	R399L	g1196t	cgt	ctt

Supplementary Table S7:

Nucleotide and amino acid exchanges in isolated *hisG* alleles.

Mutein	Mutation	Nucleotide exchange	Mutation	Nucleotide exchange
HisG-WT				
HisG-GT233-3	G233H	ggc742cat	T235Q	acg748cag
HisG-GT233-8	G233S	ggc742agt	T235R	acg748agg
HisG-GT233-4	G233V	ggc742gtg	T235R	acg748cgt
HisG-GT233-5	G233I	ggc742att	T235V	acg748gtt
HisG-GT233-1	G233R	ggc742cgg	T235R	acg748agg
HisG-GT233-10	G233L	ggc742ctt		
HisG-GT233-6	G233H	ggc742cat	T235F	acg748ttt
HisG-GT233-11	G233P	ggc742cct	T235L	acg748ctg
HisG-GT233-7	G233R	ggc742cgt		
HisG-GT233-2	G233S	ggc742tcg	T235H	acg748agg
HisG-N216-1	N216I	aac688att		
HisG-N216-3	N216R	aac688cgt		

Supplemental Material to

A high-throughput approach to identify genomic variants of bacterial metabolite producers at the single-cell level.

By Binder et al.

Tables and Figures

The file contains detailed data on strains and sorting performance as follows:

Table S1. Strains and plasmids

Strain or plasmid	Description	Reference
WT *C. glutamicum*	WT strain ATCC 13032, biotin-auxotroph	This laboratory
C. glutamicum DM1132	WT strain ATCC 13032, biotin-auxotroph	Evonik laboratory
C. glutamicum DM1728	*pyc*(P458S), *hom*(V59A)	[1]
C. glutamicum DM1730	*pyc*(P458S), *hom*(V59A), *lysC*(T311I), Δ*pck*	Evonik laboratory
C. glutamicum DM1800	*pyc*(P458S), *lysC*(T311I)	[1]
C. glutamicum DM1919	*pyc*(P458S), *hom*(V59A), 2 copies of *lysC*(T311I), Δ*pck*	Evonik laboratory
C. glutamicum DM1920	*pyc*(P458S), *hom*(V59A), 2 copies of *lysC*(T311I), Δ*pck*, 2 copies of *lysE* derived from WT *C. glutamicum*	Evonik laboratory
C. glutamicum DM1933	Δ*pck, pyc*(P458S), *hom*(V59A), 2 copies of *lysC*(T311I), 2 copies of *asd*, 2 copies of *dapA*, 2 copies of *dapB*, 2 copies of *ddh*, 2 copies of *lysA*, 2 copies of *lysE* derived from WT *C. glutamicum*	[2]
C. glutamicum-Ser4	ATCC13032 Δ*sda*AΔ*pab*ABC pserAfbrCB	[2]
C. glutamicum-Cys3	ATCC13032 Δ*sda*AΔ*pab*ABCΔ*aec*D pserAfbrCB	This laboratory
E. coli DH5α	F- endA1 glnV44 thi-1 recA1 relA1 gyrA96 deoR nupG Φ80dlacZΔM15 Δ(lacZYA-argF)U169, hsdR17(rK- mK+), λ–	[3]
pK19mobsacB	Km^r, Suc^r, mobilizable (*oriT*), *oriV*	[4]
pSenLys	Encodes *C. glutamicum* LysG, and its target promoter of *lysE* with a transcriptional fusion to *eyfp*	HE583184
pSenArg	Encodes *E. coli* ArgP, and its target promoter of *argO* with a transcriptional fusion to *eyfp*	HE583185
pSenSer	Encodes *C. glutamicum* NCgl0581, and its target promoter of NCgl0580 with a transcriptional fusion to *eyfp*	HE583186
pSenOAS	Encodes *C. glutamicum* CysR, and its target promoter of *cysI* with a transcriptional fusion to *eyfp*	HE583187

The regulatory units of the pSen series of vectors were synthesized (LifeTechnologies GmbH, Frankfurter-Str.129b, 64293 Darmstadt, Germany) and cloned into pJC1. Full sequences have been deposited at EMBL.

Table S2. Quality assessment of sorting cells carrying pSenLys

Sorting criteria	Viability			Verified strain			Sorting specificity
	Sorted in total	Grown		WT	DM1728	DM1919	
P1 (ATCC13032)	432	386	89.4 (%)	99.4	0.6	0	99.4 (%)
P2 (DM1728)	288	257	89.2 (%)	3.1	94.8	2.1	94.8 (%)
P3 (DM1919)	288	244	84.7 (%)	4.2	6.2	89.6	89.6 (%)
Average			87.8 (%)				94.6 (%)

Sorting criteria	Viability			Verified strain		Sorting specificity
	Sorted in total	Grown (%)		WT	DM1728	
P2 (DM1728)	200	184	92.0 (%)	7.3	92.7	92.7 (%)

The upper part of the Table shows the result of sorting the mixture of three strains using gates P1-P3. Viability of sorted cells was determined by counting cfus grown up after spotting single cells on BHI petri dishes and incubating for 48 hrs at 30°C. Strains were verified by cultivating 96 clones in a microtiter plate containing minimal medium CGXII with 4% (w/v) glucose and quantification of their L-lysine forming capability after 48 hrs.

The lower part of the Table shows the result of sorting DM1728 out of 10,000 wild type cells, both carrying pSenLys. Determination of viability and L-lysine formation was as above.

Table S3. L-lysine formation with mutations introduced by reverse engineering

Mutation	**Recombinant strain**	**Lysine (mM)**	**Isolated mutant**	**Lysine (mM)**
thrB S102F	Lys016	0.4	K016	2.1
hom V211F	Lys039	6.3	K039	10.9
hom A364V	Lys049	1.1	K049	9.6
lysC H357Y	Lys096	0.9	K096	2.3

In the recombinant strains the single mutation given in the left column was introduced in the wild type genome ATCC13032 by allelic exchange as described [4]. L-lysine accumulations were determined in SK cultivations and the L-lysine formed determined after 48 hrs. For comparison L-lysine accumulations are shown for the original clones from which the specific mutations were derived by targeted sequencing.

Table S4. Statistical analysis of whole-genome sequencing

	Strain K051	
Description	**value**	
Number of sequenced reads	20,156,524	
Avg. length of sequenced read [bp]	51.0	
Number of reads after trimming	19,908,254	
Avg. length of reads after trimming [bp]	48.1	
Number of paired reads after trimming used for mapping	19,664,448	
Number of reads mapped to reference	17,877,215	
Coverage (# mapped reads * avg. length/3301500)	260.5	
SNPs in total	268	100 %
Transitions	268	100 %
SNPs leading to amino acid exchange	171	63.8 %
Silent mutations	65	24.3 %
Intergenic SNPs	28	10.4 %
Introduced stop-codons	4	1.5 %

Sequence reads were generated on an Illumina HiSeq 2000 and performed at GATC (GATC Biotech AG, Jakob-Stadler-Platz 7, 78467 Konstanz, Germany). Trimming and mapping was done using the CLC Genomics Work-bench Version 4.7.2 software of CLC bio (Finlandsgade 10-12, Katrinebjerg , 8200 Aarhus N, Denmark).

Table S5. Growth rates of *murE* mutants

Strain	μ h^{-1}
DM1132 (WT)	0.49 ± 0.11
DM1728	0.46 ± 0.16
DM1730	0.43 ± 0.11
DM1800	0.43 ± 0.16
DM1933	0.37 ± 0.13
DM1132 (L121F)	0.45 ± 0.09
DM1728 (L121F)	0.43 ± 0.20
DM1730 (L121F)	0.40 ± 0.11
DM1800 (L121F)	0.43 ± 0.19
DM1933 (L121F)	0.35 ± 0.14
DM1132 (G81E)	0.39 ± 0.12
DM1728 (G81E)	0.36 ± 0.16
DM1730 (G81E)	0.41 ± 0.10
DM1800 (G81E)	0.45 ± 0.18
DM1933 (G81E)	0.31 ± 0.21

Strains were pregrown for 8 hrs on complex medium BHI, followed by growth overnight in minimal medium CGXII-glucose, and this used to inoculate cultures in a new CGXII-glucose to determine growth rates. Cultivations were done in microtiter plates and growth was recorded from three parallel cultures.

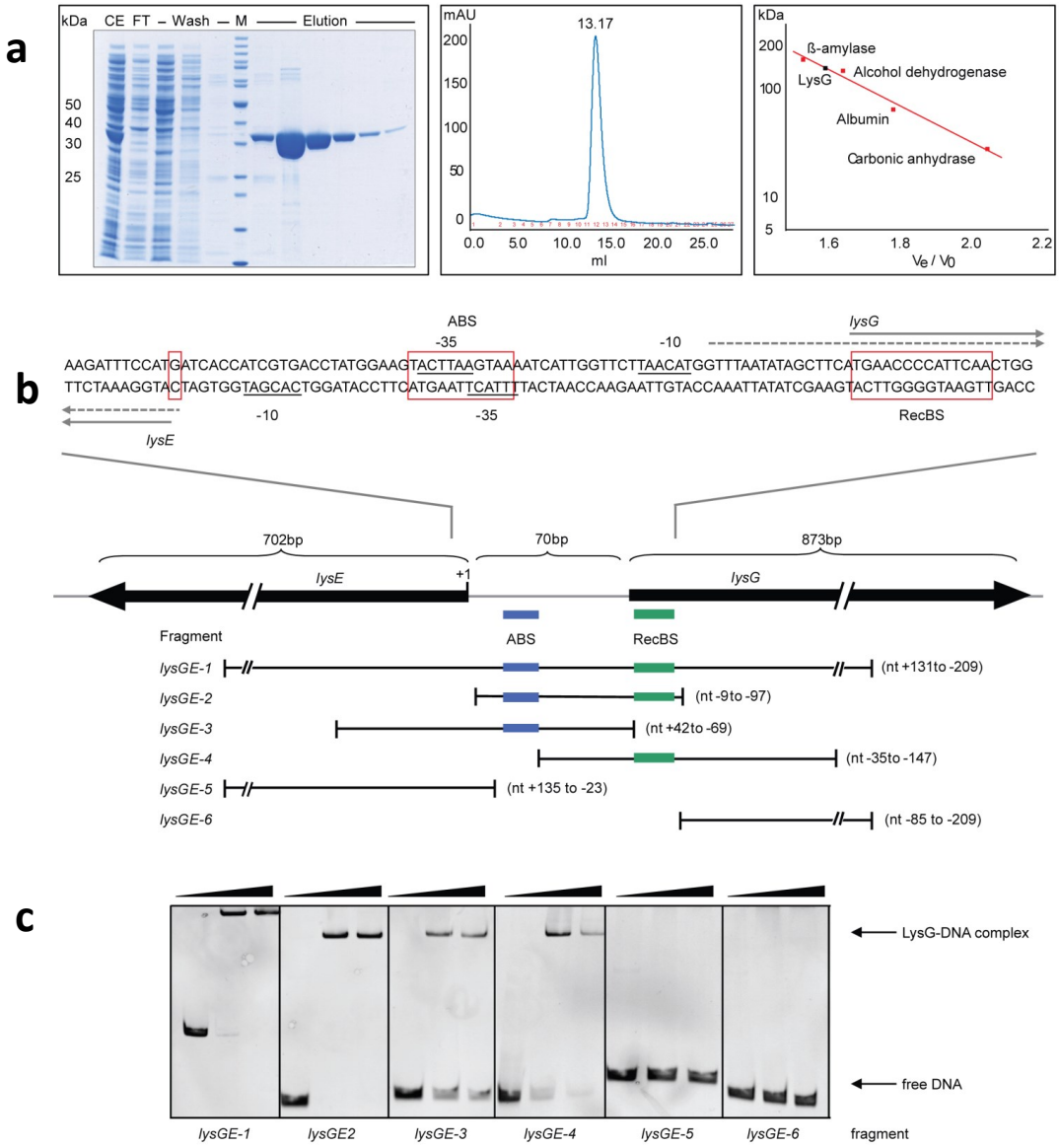

Figure S1. Isolation of LysG and characterization of LysG binding site. (**a**) Isolation of His-LysG and gel filtration analysis of LysG devoid of tag together with the calibration curve used for molecular mass determination. LysG eluted with an apparent molecular mass of ~140 kDa. Since the LysG monomer has a molecular mass of 32 kDa, LysG in solution forms a homotetramer similar to other LTTR-type regulators such as CbnR of *Ralstonia eutropha* [5] or CysB of *Escherichia coli* [6]. (**b**) Overview on *lysGE* organization with the intergenic region on top. The relative position of DNA fragments *lysGE*-1 to *lysGE*-6 are given and the location of the activation binding site (ABS) in blue and the recognition binding site (RecBS) in green. (**c**) Electrophoretic mobility shift assays showing binding of fragments 1-4 to LysG. In each panel (from left to right) no LysG was added, added in a 20-fold excess, and 50-fold excess.

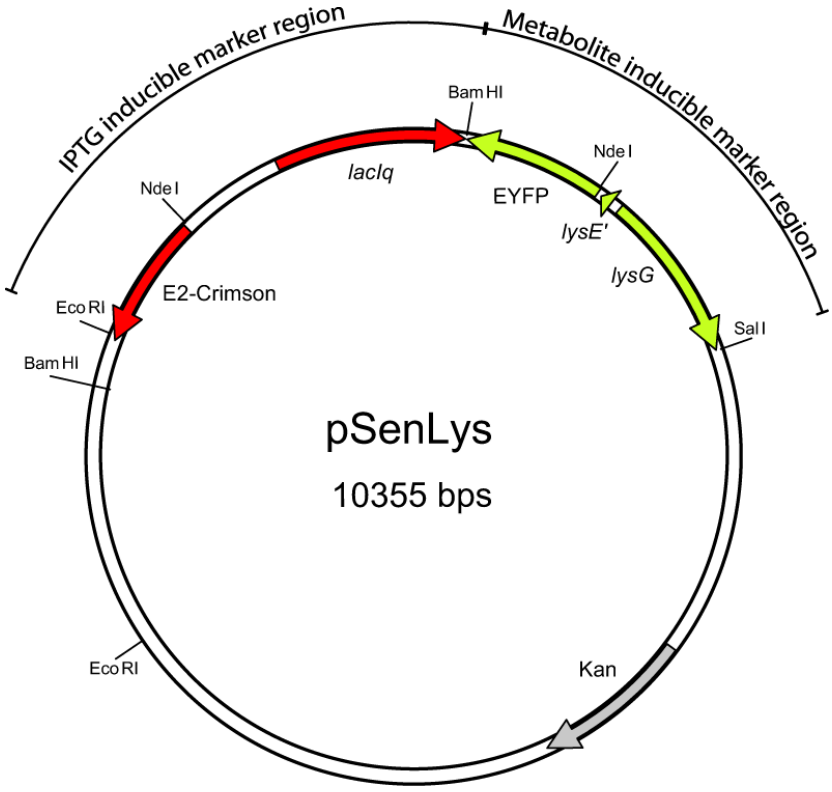

Figure S2. Vector pSenLys and general configuration of sensor plasmid. The vector pSenLys is a shuttle vector replicating in both *C. glutamicum* and *E. coli*. It carries the metabolite inducible marker region encoding the L-lysine sensing transcriptional regulator LysG. In presence of L-lysine LysG drives transcription of *lysE*, which is fused with *eyfp,* resulting in green fluorescence. pSenLys also carries the IPTG inducible marker region encoding the LacIq repressor which, in the presence of IPTG, diffuses from the tac promoter region in front of E2-Crimson, resulting in red fluorescence. The system permits the selection of viable cells that are capable of protein synthesis.

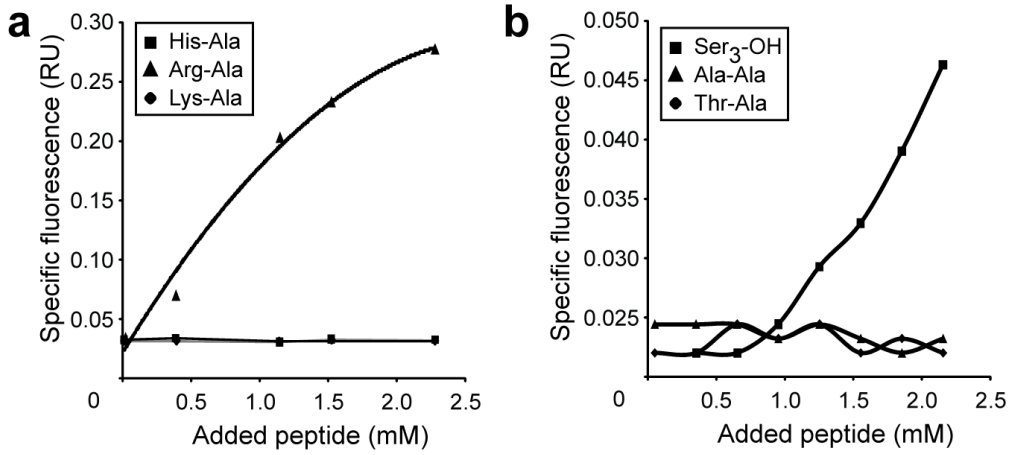

Figure S3. Peptide-dose response with *E. coli* pSenArg and *C. glutamicum* pSenSer. (**a**) *E. coli* pSenArg was cultivated in minimal medium and the specific peptide added at the given concentration. Addition of Arg-Ala results in fluorescent cultures, but this is not the case with His-Ala or Lys-Ala. (**b**) *C. glutamicum* pSenSer was cultivated in minimal medium and peptides added as shown. Ser-Ser-Ser results in fluorescent cultures, but this is not the case with Ala-Ala or Thr-Ala. In all cases Ala-Ala was included to give a total peptide concentration of 3 mM.

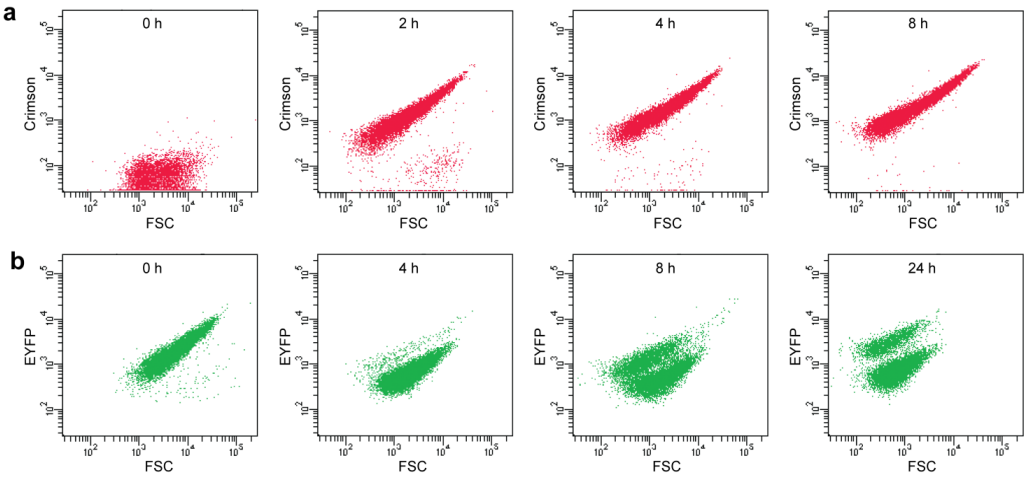

Figure S4. Development of Crimson and EYFP signals in mixtures of equal numbers of ATCC13032 and DM1728. To simulate the transfer of the mutant glycerol stock into minimal medium, the two cell types grown on BHI were mixed, glycerol was added and cells frozen. (**a**) Cells from the stock were diluted in minimal medium plus 0.1 mM IPTG. At the beginning of cultivation and 2, 4, and 8 hrs later, cells were assayed by flow cytometry for development of the Crimson signal. After 2 hrs, the majority of cells expressed Crimson, indicating active protein synthesis and thus living cells. (**b**) Cells were diluted as above and assayed at the beginning of culture and 4, 8, and 24 hrs later by flow cytometry for the EYFP signal. All cells derived from the complex medium exhibited high levels of fluorescence. After 4 hrs the majority showed reduced fluorescence, and after 8 hrs the signals specific for the two populations are apparent.

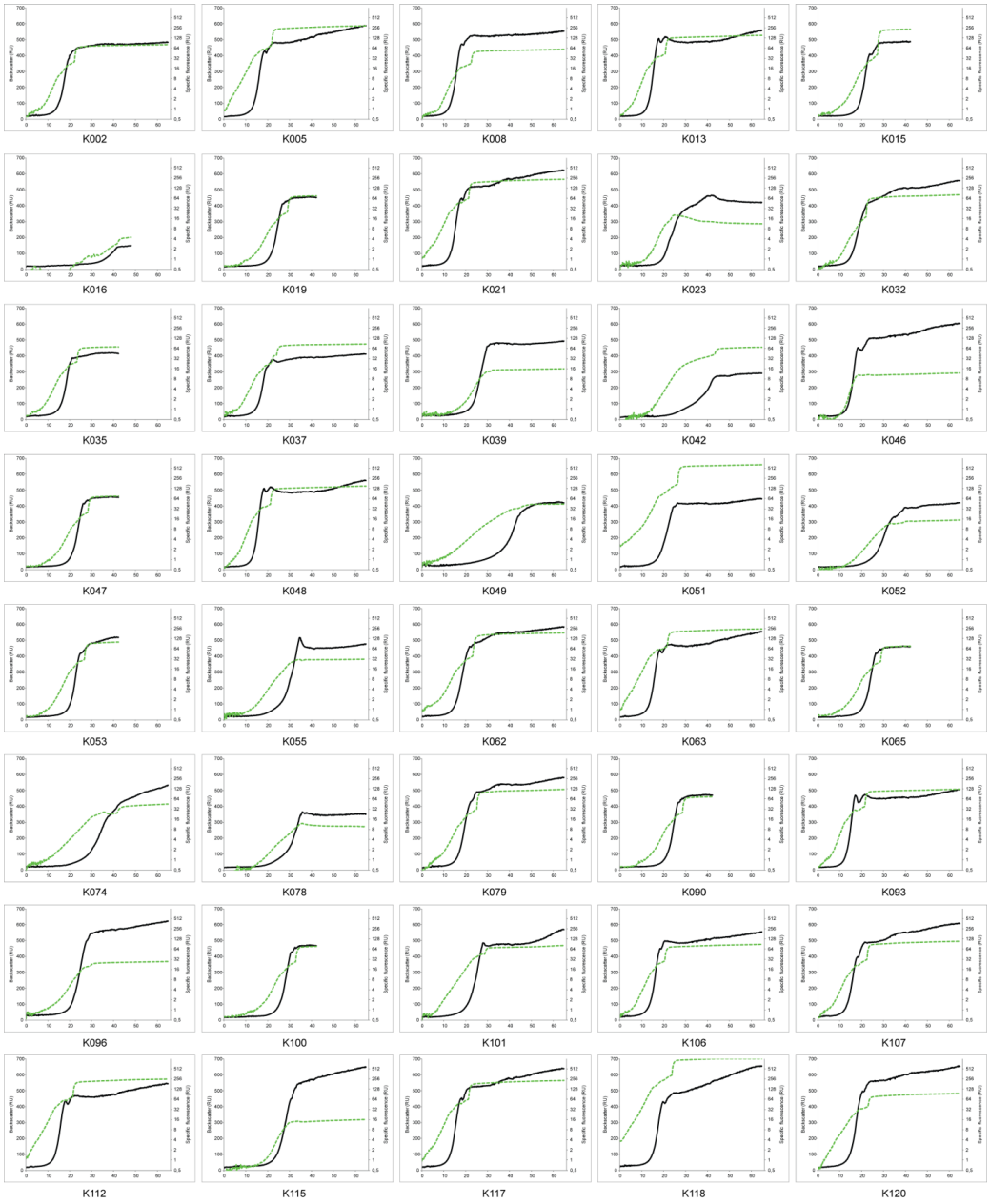

Figure S5. Growth curves and fluorescence for 40 mutant cultures. The BioLektor cultivation system was used (see Methods section) to follow the growth of 40 mutants in 0.75 ml cultures as measured by the backward scatter (black curve) and fluorescence at λ_{ex} 485 nm and λ_{em} 520 nm (green curve). Numbering of the different mutants is as given in Figure 4 of the main text.

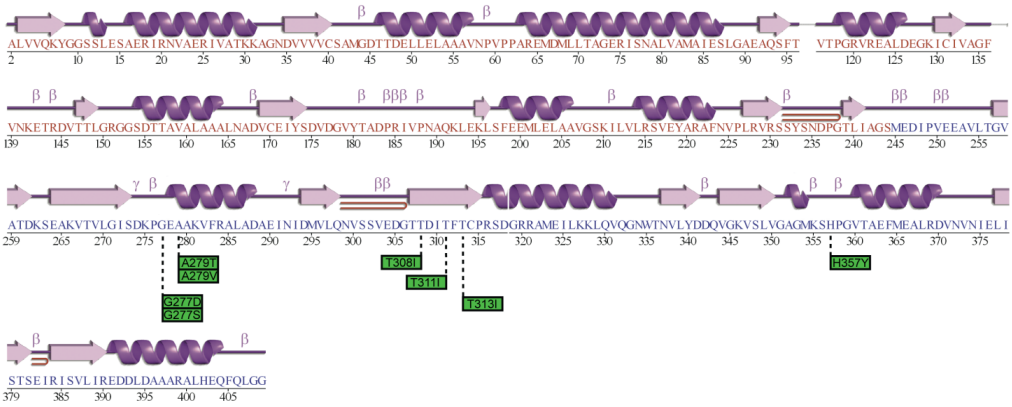

Figure S6. Structural presentation of LysC with the localization of mutations identified.

REFERENCES

1. Blombach B, Hans S, Bathe B, Eikmanns BJ: **Acetohydroxyacid synthase, a novel target for improvement of L-lysine production by Corynebacterium glutamicum.** *Appl Environ Microbiol* 2009, **75:**419-427.

2. Stolz M, Peters-Wendisch P, Etterich H, Gerharz T, Faurie R, Sahm H, Fersterra H, Eggeling L: **Reduced folate supply as a key to enhanced L-serine production by Corynebacterium glutamicum.** *Appl Environ Microbiol* 2007, **73:**750-755.

3. Grant SG, Jessee J, Bloom FR, Hanahan D: **Differential plasmid rescue from transgenic mouse DNAs into Escherichia coli methylation-restriction mutants.** *Proc Natl Acad Sci U S A* 1990, **87:**4645-4649.

4. Schäfer A, Tauch A, Jäger W, Kalinowski J, Thierbach G, Pühler A: **Small mobilizable multi-purpose cloning vectors derived from the Escherichia coli plasmids pK18 and pK19: selection of defined deletions in the chromosome of Corynebacterium glutamicum.** *Gene* 1994, **145:**69-73.

5. Ogawa N, McFall SM, Klem TJ, Miyashita K, Chakrabarty AM: **Transcriptional activation of the chlorocatechol degradative genes of Ralstonia eutropha NH9.** *J Bacteriol* 1999, **181:**6697-6705.

6. van der Ploeg JR, Iwanicka-Nowicka R, Kertesz MA, Leisinger T, Hryniewicz MM: **Involvement of CysB and Cbl regulatory proteins in expression of the tauABCD operon and other sulfate starvation-inducible genes in Escherichia coli.** *J Bacteriol* 1997, **179:**7671-7678.

Supplemental information to Siedler et al.:

SoxR as Single-Cell Biosensor for NADPH-Consuming Enzymes in *Escherichia coli*

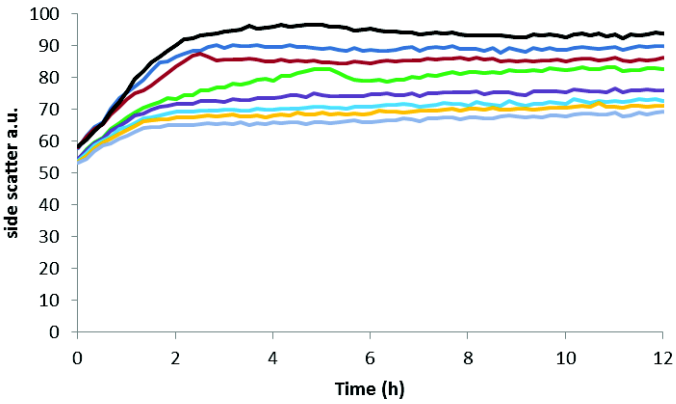

Figure S1: Growth of *E. coli* carrying pSenSox during biotransformation of 10 mM (dark blue), 20 mM (brown), 30 mM (green), 40 mM (purple), 50 mM (light blue), 60 mM (yellow) and 70 mM (grey) MAA to MHB via the NADPH-dependent alcohol dehydrogenase *Lb*Adh. In black a control without MAA is shown. The cultures were grown in a Biolector instrument (m2p-labs GmbH, Baesweiler, Germany) and growth was followed by measuring the side scatter in arbitrary units (a.u.).

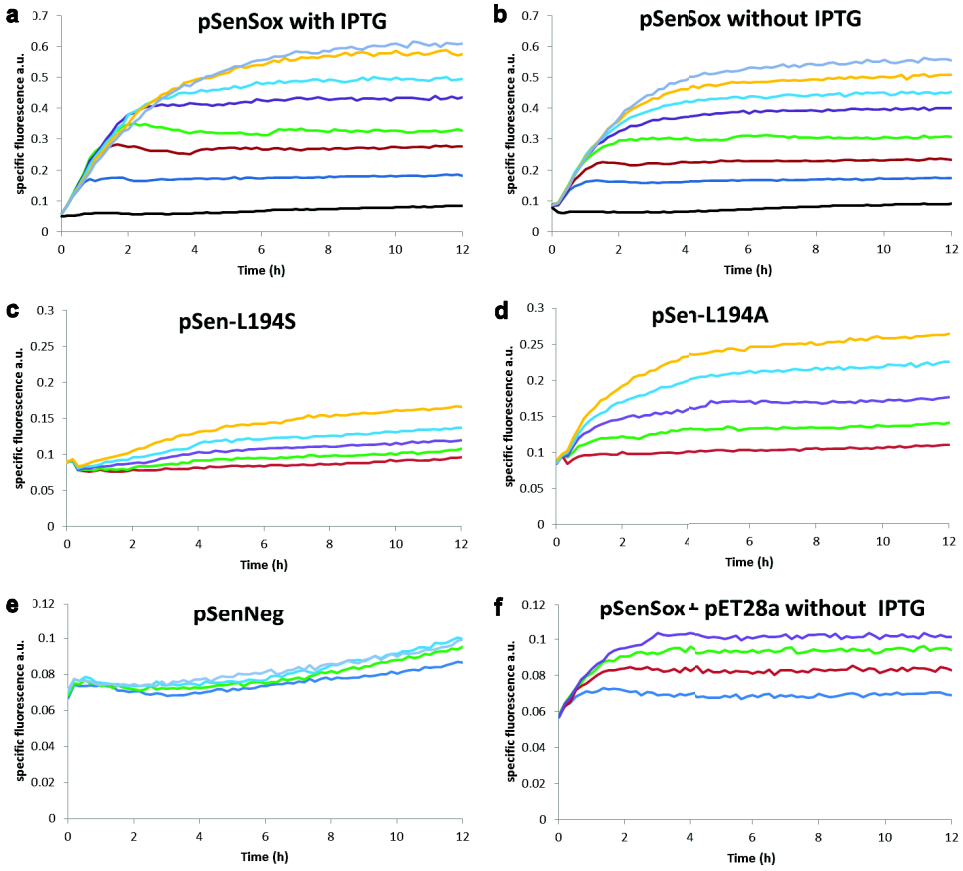

Figure S2: Specific fluorescence of *E. coli* BL21(DE3) carrying the indicated plasmids during reductive biotransformation of 10 mM (dark blue), 20 mM (brown), 30 mM (green), 40 mM (purple), 50 mM (light blue), 60 mM (yellow), or 70 mM (grey) MAA to MHB with the NADPH-dependent alcohol dehydrogenase *Lb*Adh. In black a control without MAA is shown. (a) Cells with pSenSox, IPTG was added to 1 mM. In order to allow reproducible expression, plasmid pSenSox carries no *lacI* gene, but *E. coli* BL21(DE3) possesses a chromosomal copy of *lacI*. IPTG was used to maximize *Lb*ADH expression. (b) Cells with pSenSox, but without IPTG addition. (c) Cells with pSen-L194S, which have a strongly reduced LbAdh activity (0.7 U/mg protein instead of 6.3 U/mg for wild-type *Lb*Adh). (d) Cells with pSen-L194A, which have a reduced LbAdh activity (2.7 U/mg protein instead of 6.3 U/mg for wild-type *Lb*Adh). (e) Cells with pSenNeg, which have only background Adh activity (0.03 U/mg). (f) Cells with pSenSox and pET28a. Expression of *lacI* from pET28a carries leads to inhibition of *Lbadh* expression and a very low *Lb*Adh activity of 0.5 U/mg.

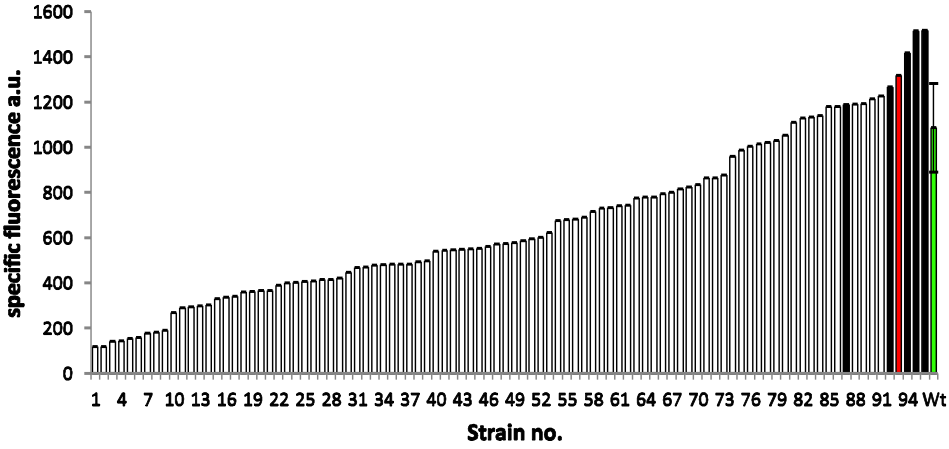

Figure S3: Specific fluorescence distribution of 96 clones of the *Lb*Adh mutant library isolated by FACS due to their increased fluorescence after 3 h of biotransformation with 4-methyl-2-pentanone (4M2P). Biotransformation was conducted in 96-well plates and specific fluorescence was measured 3 hours after addition of 20 mM 4M2P. The result for the clone with wild-type *Lb*Adh (Wt) is shown in green. The *Lb*Adh-A93M mutant selected in this screen is shown in red and five additional clones that were analyzed for *in vitro* Adh activity (Table S1) are shown in black.

Table S1. Enzyme activities of wild-type *Lb*Adh and mutated variants for NADPH-dependent reduction of the substrate 4-methyl-2-pentanone.

Enzyme[a]	Activity[b] U/ mg
*Lb*Adh	1.90 ± 0.07
86	0.98 ± 0.03
92	n.a.
A93M	2.59 ± 0.31
94	1.75 ± 0.19
95	n.a.
96	1.76 ± 0.09

[a]Enzyme activities were determined with crude extracts of the respective strains carrying either pSenSox or pSen-derivative. [b]Mean values and standard deviation from two replicates are given. n.a. no activity

Electronic Supplementary Material (ESI) for Lab on a Chip

A disposable picoliter bioreactor for cultivation and investigation of industrially relevant bacteria on single cell level

*Alexander Grünberger, Nicole Paczia, Christopher Probst, Georg Schendzielorz, Lothar Eggeling Stephan Noack, Wolfgang Wiechert and Dietrich Kohlheyer**

Institute of Bio and Geo Sciences IBG-1: Biotechnology, Forschungszentrum Jülich GmbH (Juelich Research Center) Wilhelm-Johnen-Str, D-52428 Juelich, Germany

**Corresponding author: Dr. Dietrich Kohlheyer, e-mail: d.kohlheyer@fz-juelich.de*

Supplementary Materials

Bacteria Strains

For proof of principle growth experiments, *E. coli* BL 21 and *C. glutamicum* ATCC130332 was used. For reactor comparison studies, *C. glutamicum* DM 1800 was used. For combined growth and L-arginine production studies, *C. glutamicum* wild type strain was transformed with plasmid pSenLysTKP-argB(fbr), containing a feedback resistant mutant of *argB* (coding for N-acetylglutamate kinase) and a metabolite sensor cassette, enabling EYFP expression in response to enhanced intracellular L-arginine concentration (Binder2012, in submission).

Media and Biological Sample Preparation

BHI medium (Becton-Dickinson/237500-Bacto Brain Heart Infusion) was used for *C. glutamicum* to prepare starter cultures for microfluidic experiments. *E. coli* BL 21 starter cultures were cultured in LB medium, containing 5 g yeast extract, 10 g peptone and 10 g NaCl per liter.

20 ml of sterile BHI medium (autoclaved and sterile filtered to prevent particles) were transferred into 100 ml culture flasks (Erlenmeyer shape, triple battled) and was inoculated with a single colony of *C. glutamicum* from BHI agar plates, containing no antibiotics. These cultures were incubated on an Incubator (Inforce) at 150 rpm at 30°C 10 hours. New culture using CGXII was started and cells were resuspended in new medium and transferred to the new culture starting optical density of 0.05 for adaption to the medium overnight. This step was done, that *C. glutamicum* could adapt to the new medium. The main culture was harvested in exponential phase (OD ~ 1-4) and washed with fresh sterile filtered medium prior to inoculation of the microfluidic system. For *E. coli* the same procedure was applied, using LB- medium for preculture. *E. coli* was directly transferred to chip after the first preculture.

Microfluidic experiments

For proof of principle experiments with *E. coli* BL 21 LB medium was used. The chip was flushed with Pluronic F-127 (Invitrogen) for 2 hours before culturing *E. coli*, to prevent undesired adhesion. No anti-adhesion additive was added to the medium. For microfluidic experiments with *C. glutamicum* ATCC130332 and DM 1800 CGXII medium [34] was used. The medium was adjusted to pH of 7.0 with sodium hydroxide. For artificial stationary phase CGXII medium without glucose was used. For microfluidic experiments with *C. glutamicum* the microfluidic chip was not coated before. Again, medium was not supplemented with any anti-adhesion detergence, to prevent unknown interaction between detergence and colony growth. No active biofilm control was necessary, since experiments

were finished before wall attachment and growth leads to formation of microcolonies that clog fluidic channels in average after 24-48 hours.

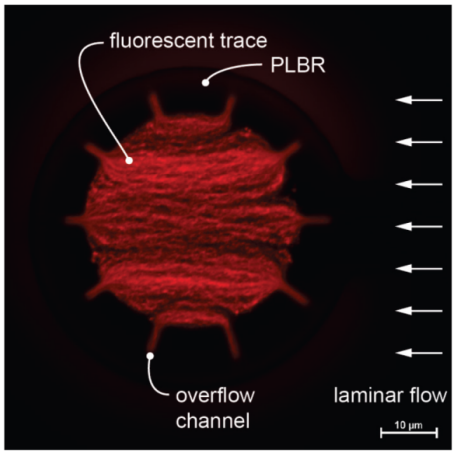

Figure S1 Image showing the flow pattern of fluorescently labeled latex beads with 200nm diameter through a single PLBR. The PLBR chip was coated with a 0.1% Pluoronic F68 solution for 60 minutes at a total flow-rate of 700 nl/min to minimize bead adhesion to the chip material. Red fluorescent latex beads (FluoSpheres® Carboxylate-Modified Microspheres, 0.2 µm, Red Fluorescent (580/605) 2% Solids, Molecular Probes) were diluted 100 times and flushed through the microfluidic device at 10 nl/min per PLBR channel each. Image exposure time was 10 s. Fluorescent bead trajectories clearly show flow through the PLBR device.

Lab-Scale Cultivation

Cultivation conditions

For cultivation of *C. glutamicum* DM 1800 the defined minimal medium CGXII [34] was used containing per liter of distilled water: 20 g $(NH_4)_2SO_4$, 1 g K_2HPO_4, 1 g KH_2PO_4, 5 g Urea, 10 g D-glucose, 13.25 mg $CaCl_2$*$2H_2O$, 0.25 g $MgSO_4$*$7H_2O$, 1 mg $FeSO_4$*$7H_2O$, 1 mg $MnSO_4$*H_2O, 0.02 mg $NiCl_2$*$6H_2O$, 0.313 mg $CuSO_4$*$5H_2O$, 1 mg $ZnSO_4$*$7H_2O$. The medium was adjusted to pH of 7.0 with sodium hydroxide. The medium contained additionally 3 ml of 10 % (v/v) AF 204 (Sigma) and 1 mL of a 0.2 g/L biotin stock solution per liter witch were added after sterilization. Cryocultures of the two strains were stored at -80°C in CGXII medium containing 20 % (v/v) glycerol.

For batch-cultivation a 1.5 L bioreactor (DASGIP AG, Jülich) with a working volume of 1 L was prepared and inoculated directly with 2 mL of cryoculture. To increase reproducibility no pre-cultivation was performed. All cultivations were carried out at constant air flow (1 vvm) and 30°C. The pH was maintained at 7.0 by adding 4 M NaOH and 4 M HCl, respectively. Aerobic process conditions (dissolved oxygen > 30 %) were ensured via stirrer speed control (200-1200 rpm). During cultivation dissolved oxygen (Visiferm DO 225, Hamilton), pH (405-DPAS-SC-K80/225, Mettler Toledo) and exhaust gas concentrations of carbon dioxide and oxygen (GA4, DASGIP AG Jülich) were measured online.

Offline-Analysis

Cell number and size were monitored offline via coulter counter equipped with a 45 µm capillary (CASY® 1 Modell TT, Roche Diagnostics). For analysis a cell suspension volume of 2 ml was sucked into a 5 ml plastic syringe and dropped to withdrawal the dead volume of the sample port. After that 1 ml was sucked into a fresh 2 ml plastic syringe. The cell suspension was diluted with isotonic dilution liquid (CASY®ton, Roche Diagnostics) into the detection range of the coulter counter and measured as triplicates.

Supplemental Videos

Video S1 Time lapse movie showing the cultivation of E. coli BL21 inside a PLBR. A single E. coli cell was seeded into the PLBR and complex LB growth medium was infused. After 2.5 hours of cultivation at T=37°C a microcolony of app. 30 cells was formed. After 3.5 hours of cultivation the overflow phase was reached. Cells were pushed continuously out of the PLBR maintaining a constant density. The overflow channels have different lengths due to a slight misalignment during the two layer photolithography process. The functionality was not affected by this misalignment.

Video S2 Time-lapse movie showing the growth and production of C. glutamicum pSenLysTKP-argB(fbr) during PLBR cultivation. The strain contains a metabolite sensor enabling EYFP expression in response to enhanced intracellular L-arginine concentration. The seeded mother cell starts to emit fluorescence after 12 hours indicating production of L-arginine. While undergoing a change to maximum cell growth EYFP emission declined.

Supplementary Information

Beyond growth rate 0.6: *C. glutamicum* cultivated in highly diluted environments

Alexander Grünberger[1], Jan van Ooyen[2], Nicole Paczia[1], Peter Rohe[1], Georg Schiendzielorz[2], Lothar Eggeling[2], Wolfgang Wiechert[1], Dietrich Kohlheyer[1], Stephan Noack*[1]

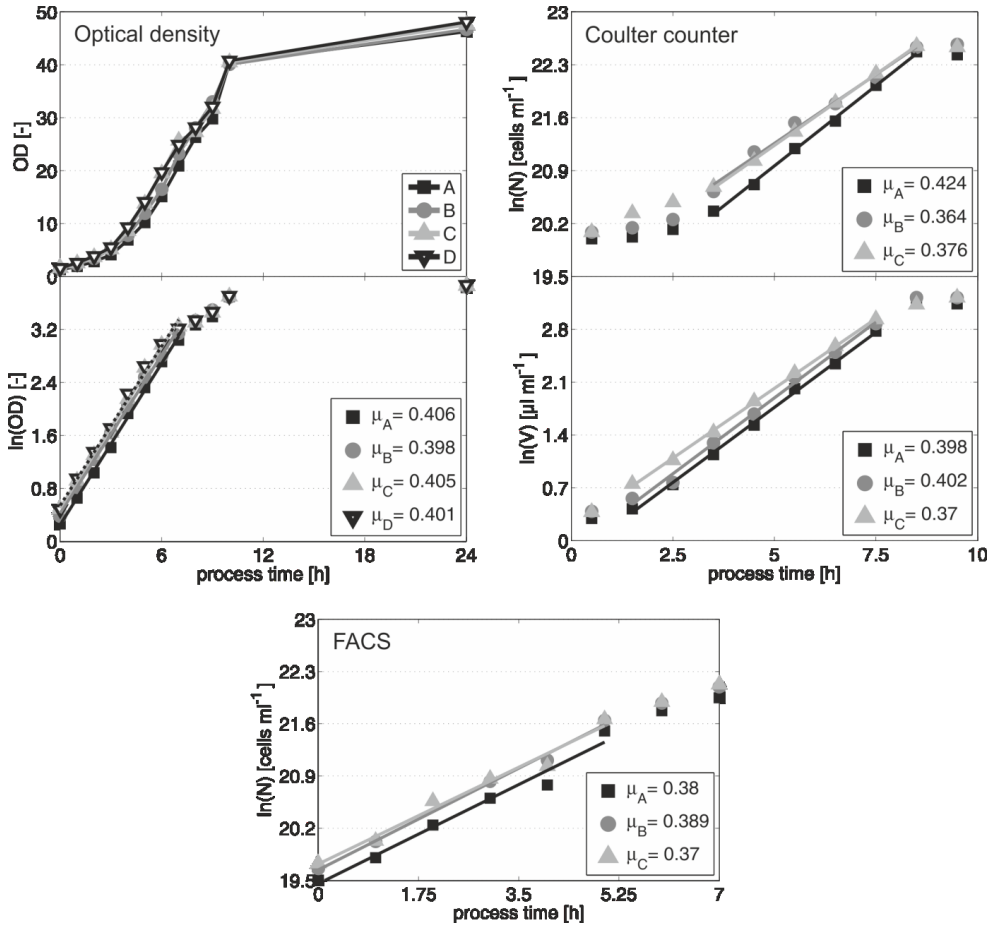

Figure S1: Growth of *C. glutamicum* wild type in bioreactor batch-cultivations on CGXII glucose medium. Maximum growth rates were determined based on optical density, cell number and cell volume via Coulter counter and cell number via FACS.

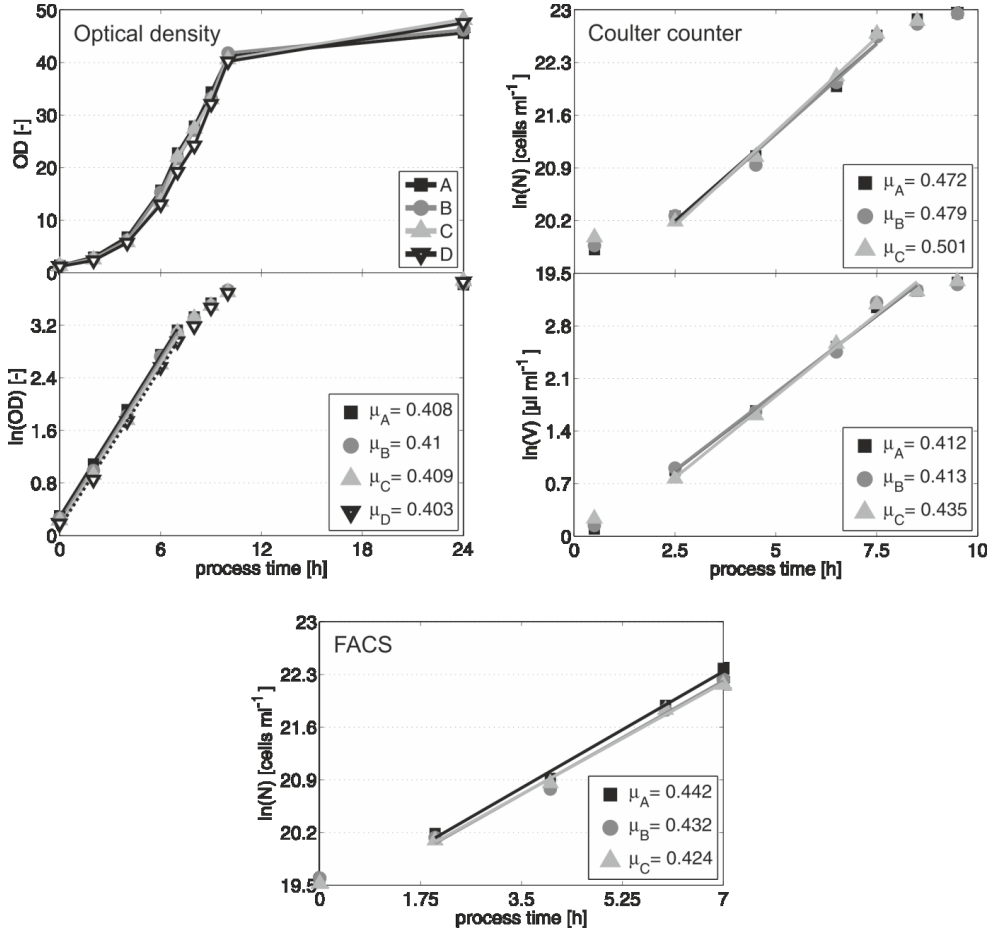

Figure S2: Growth of *C. glutamicum* wild type in shake flasks on CGXII glucose medium. Maximum growth rates were determined based on optical density, cell number and cell volume via Coulter counter and cell number via FACS.

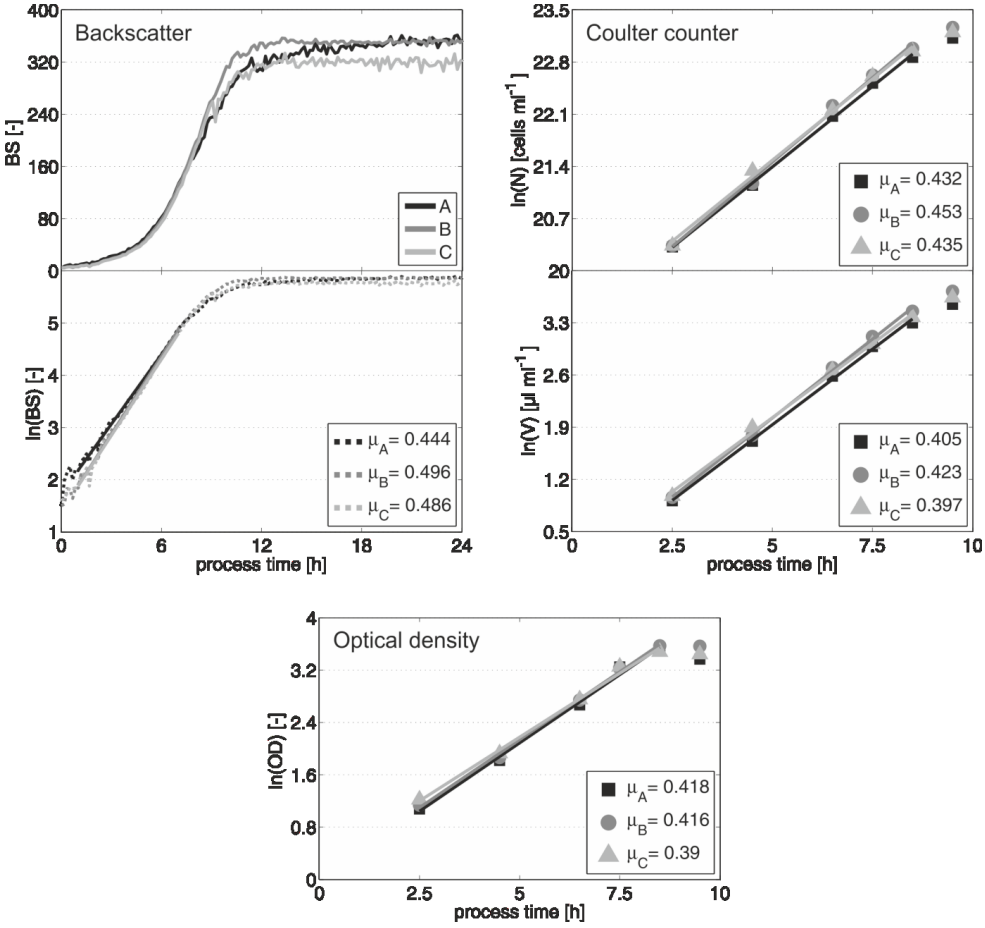

Figure S3: Growth of *C. glutamicum* wild type in microtiter plates on CGXII glucose medium. Maximum growth rates were determined based on backscatter, cell number and cell volume via Coulter counter and optical density.

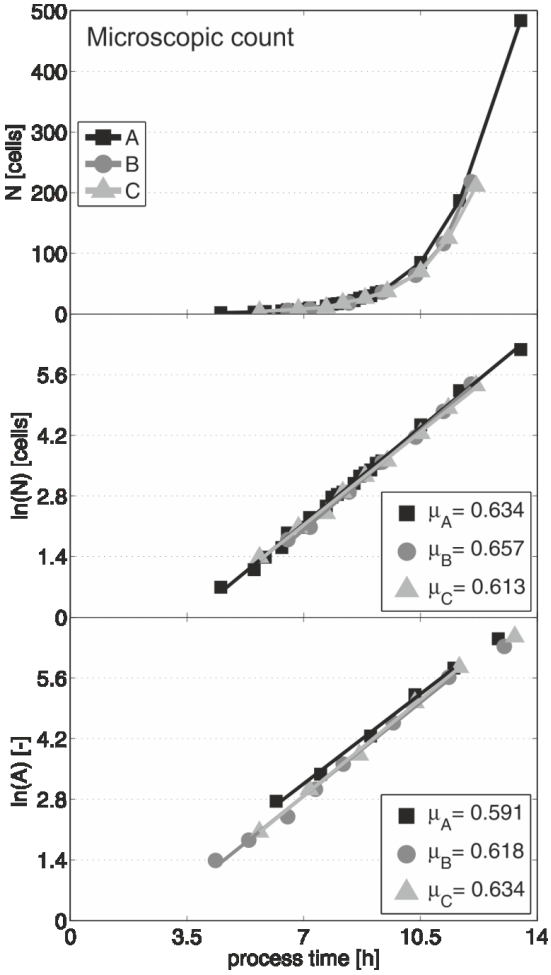

Figure S4: Growth of *C. glutamicum* wild type under PLBR conditions on CGXII glucose medium. Maximum growth rates were determined based on cell number and cell size via microscopic count.

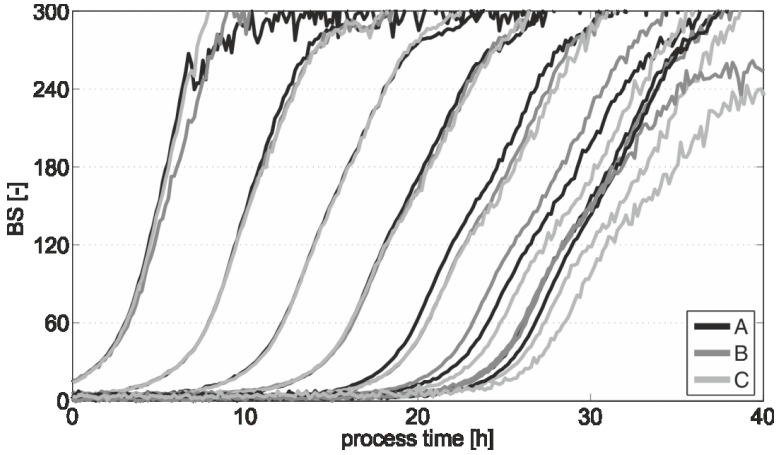

Figure S5: Growth of *C. glutamicum* wild type in microtiter plates on CGXII glucose medium applying different inoculum concentrations. Log-dilution series were generated from three reference cultures and grown in parallel.

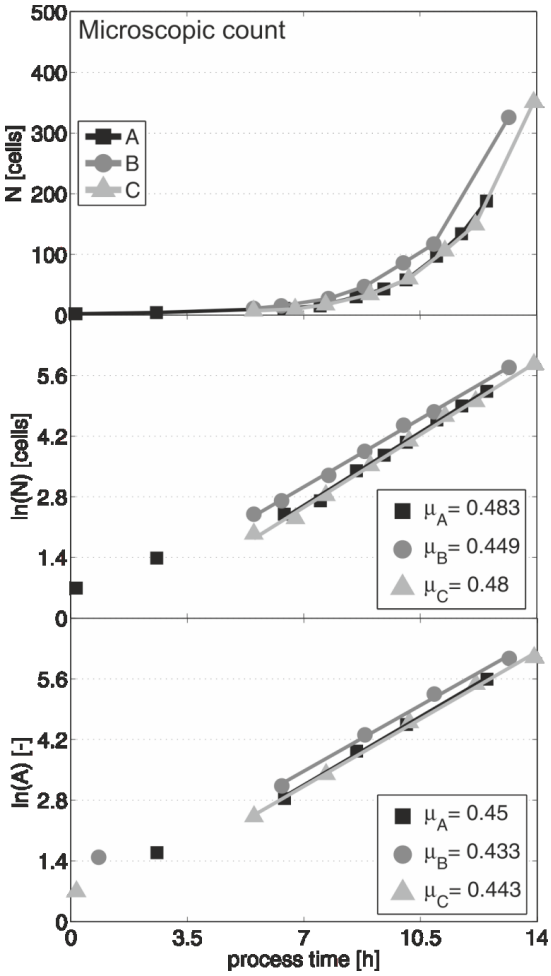

Figure S6: Growth of *C. glutamicum* wild type under PLBR conditions on cell-free supernatant from shaking flask cultivation. Maximum growth rates were determined based on cell number and cell size via microscopic count.

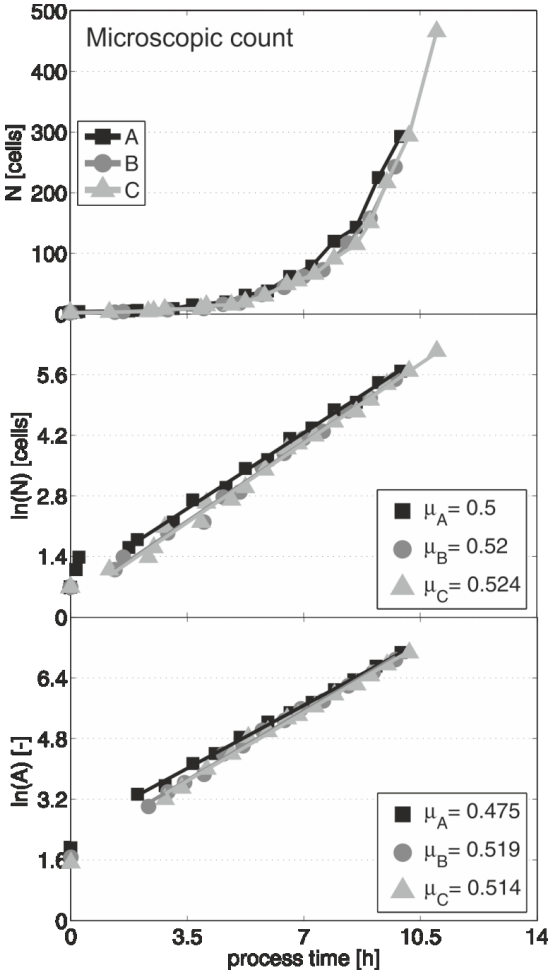

Figure S7: Growth of *C. glutamicum* wild type under PLBR conditions on CGXII glucose medium supplemented with 5 mM acetate. Maximum growth rates were determined based on cell number and cell size via microscopic count.

Danksagung

Ich danke meinem Doktorvater Prof. Dr. Michael Bott für seine wissenschaftliche Unterstützung und die außergewöhnliche Möglichkeit, viele, über die Wissenschaft hinausgehende, berufliche Erfahrungen sammeln zu dürfen.

Frau Prof. Dr. Martina Pohl danke ich für die Übernahme des Zweitgutachtens.

Herzlichen Dank Lothar für die perfekte Betreuung meiner Arbeit, jede Menge Motivation, und viele fachliche und persönliche Impulse, die ich langfristig mitnehmen werde.

Vielen Dank Stephan für die effektive, schlagkräftige und ehrliche Zusammenarbeit.

Danke an Karin, Martin, Alex, Solvej, Sabine, Sabrina, Philana, Jan, Sascha, Micha, Jenny, Katharina, Marcus, Hoffi, Norma und Falk für die gute Zusammenarbeit und tolle Stimmung im Team.

Ich danke Iris Heitzer für literarisch atemberaubende Schriftwechsel, Frau Lauer, Frau Böckmann, Frau Bräker und Frau Dreßen-Combach für ihre allzeit freundliche Hilfe und Iris Eggeling für ihren Rat bei verwaltungstechnischen Dingen, die einen Forscher regelmäßig überfordern.

Jan Marienhagen und Janko Potzkei danke ich für die beste Stellenempfehlung meines Lebens.

Michael Raulf, Klaus-Dieter Schmidt, Marie Eckert, Gerhard Straub und Robert Wittbrodt danke ich für entscheidende Unterstützung in schwieriger Zeit, die daher sehr kurz blieb.

Meiner Freundin Katharina danke ich wie vereinbart dafür, dass sie meine Arbeit möglichst wenig behindert hat.

Meinen Eltern danke ich für alles, was durch Obiges ergänzt wurde.

Band / Volume 58
Prozessnahe Hochdurchsatzoptimierung der heterologen Proteinproduktion in alternativen Wirtsorganismen
P. Rohe (2012), 165 pp
ISBN: 978-3-89336-834-1

Band / Volume 59
Validation and characterisation of novel cellular ligands of membrane-associated HIV-1 Nef
E.C.Kammula (2012), 151 pp
ISBN: 978-3-89336-839-6

Band / Volume 60
Untersuchungen zur Membranintegrität während der Tat-abhängigen Proteintranslokation in *Escherichia coli*
S. Fleckenstein (2013), VI, 160 pp
ISBN: 978-3-89336-841-9

Band / Volume 61
Characterization of Novel Amyloid-β Peptide (Aβ) Binding Ligands
S. Dornieden (2013), vii, 129 pp
ISBN: 978-3-89336-844-0

Band / Volume 62
Regulatorische Aspekte der Expression und Sekretion heterologer Proteine in *Corynebacterium glutamicum*
A. R. Chattopadhyay (2013), VIII, 195 pp
ISBN: 978-3-89336-845-7

Band / Volume 63
***Gluconobacter oxydans* strain development: Studies on central carbon metabolism and respiration**
J. Richhardt (2013), III, 181 pp
ISBN: 978-3-89336-851-8

Band / Volume 64
Metabolic Engineering von *Corynebacterium glutamicum* für die Produktion einer Dicarbonsäure
A. Otten (2013), 98 pp
ISBN: 978-3-89336-860-0

Band / Volume 65
Rapid Development of Small-Molecule producing Microorganisms based on Metabolite Sensors
S. Binder (2013), 138 pp
ISBN: 978-3-89336-872-3

Band / Volume 66
Increasing the NADPH supply for whole-cell biotransformation and development of a novel biosensor
S. Solvej (2013), 130 pp
ISBN: 978-3-89336-900-3

Band / Volume 67
Expression, purification and biophysical characterization of human Presenilin 2
G. Yang (2013), 159 pp
ISBN: 978-3-89336-928-7

Band / Volume 68
Modifikationen der Atmungskette in *Corynebacterium glutamicum* und Rolle des Flavohämoproteins Hmp
L. Platzen (2013), IV, 119 pp
ISBN: 978-3-89336-931-7

Band / Volume 69
L-Cystein-Bildung mit *Corynebacterium glutamicum* und optische Sensoren zur zellulären Metabolitanalyse
K. Hoffmann (2014),vi, 83 pp
ISBN: 978-3-89336-939-3

Band / Volume 70
Metabolic engineering of *Corynebacterium glutamicum* for production of the adipate precursor 2-oxoadipate
M. Spelberg (2014), 118 pp
ISBN: 978-3-89336-954-6

Band / Volume 71
Design and application of metabolite sensors for the FACS-based isolation of feedback-resistant enzyme variants
G. Schendzielorz (2014), 128 pp
ISBN: 978-3-89336-955-3

Gesundheit / Health
Band / Volume 71
ISBN 978-3-89336-955-3

JÜLICH
FORSCHUNGSZENTRUM